Characterizing the biochemical interactions between Arabidopsis CRINKLY4 (ACR4), the catalytic subunit of PP2A phosphatase and Arabidopsis CRINKLY4 related kinase (CRK1)

by

Priyanka Sandal

A dissertation submitted to the graduate faculty

in partial fulfillment of the requirements for the degree of

DOCTOR OF PHILOSOPHY

Major: Biochemistry

Program of Study Committee:
A. Gururaj Rao, Major Professor
Amy Andreotti
Scott Nelson
Phil Becraft
Anumantha Kanthasamy

The student author, whose presentation of the scholarship herein was approved by the program of study committee, is solely responsible for the content of this dissertation. The Graduate College will ensure this dissertation is globally accessible and will not permit alterations after a degree is conferred.

Iowa State University

Ames, Iowa

2017

TABLE OF CONTENTS

ACKNOWLEDGMENTS

I would like to extend my heart-felt thanks to my mentor Dr. Guru Rao for his never-ending support and invaluable guidance throughout my graduate career. From him, I have learnt to critically analyze data, pay attention to detail and think outside of the box. He has displayed patience, trust and provided constant encouragement towards the fulfillment of my research study. Under his guidance, I have flourished both as a person and a researcher. I could not have imagined having a better advisor and mentor for my Ph.D. study.

Besides my advisor, I would like to express my gratitude towards my committee members: Dr. Amy Andreotti, Dr. Scott Nelson, Dr. Phil Becraft and Dr. Anumantha Kanthasamy for being extremely accommodating and supportive. They have made themselves available from time to time and provided their research expertise during my years of Ph.D.

I would like to thank my co-worker in the lab, Dr. Shweta Shah. You have been my go-to person whenever I needed help and guidance and I am extremely thankful for your support and valuable insights. Thank you, Dr. Matthew Meyer, for being available on emails and phones to solve my queries.

The past six years of hard-work and dedication would not have been possible without the constant support, confidence and love of my parents Chanchal and Dilbagh Singh Sandal and my younger siblings Komal and Akshay. My best friends, Aparajita and Khushbu, you both have literally sailed with me through the ups and downs and given me

the encouragement to push my limits. My dear friend Kiran, you have been my companion from day 1 at Iowa State University. I am immensely lucky to find a friend like you, who has helped both inside and outside of laboratory. I owe you big time!

Lastly, I would like to express my infinite gratitude towards my husband Karan Verlani. Your love, time, encouragement and everlasting belief has allowed me to pull through some of the toughest times of my research career. Thank you for being there always. I couldn't have done it without you.

ABSTRACT

Plant growth and development, much like in animals, is a highly-coordinated process of cell division and differentiation which generate new cell types and tissues. Receptor kinases respond to extra-cellular cues and mediate appropriate downstream gene expression through *auto* and *trans*-phosphorylation events. *Arabidopsis* CRINKLY4 (ACR4) is a plasma membrane localized receptor-like kinase that plays an important role in formative cell division and stem cell differentiation in root tip and initiates lateral root development in *Arabidopsis*. The *Arabidopsis* genome also encodes four homologs of ACR4, referred to as *Arabidopsis* CRINKLY4 Related (AtCRR) proteins. ACR4 and its homologs have equivalent architecture, comprised of an extracellular ligand binding domain, a transmembrane helix, and an intracellular kinase domain. Cell biology, genetic and *in vitro* biochemical studies have indicated potential interaction partners within the ACR4 family. However, very little is known of the ACR4 mediated network of interactions and the molecular mechanism of its regulation.

In this dissertation, we report the identification of the catalytic subunit of Protein Phosphatase 2A-3 isoform (PP2A3c) as the first known substrate for the kinase activity of ACR4 and ACR4-homolog CRK1. We provide evidence of a regulatory reciprocal interaction between the catalytic subunit of PP2A3c and ACR4, with PP2A3c serving the dual role as a substrate for ACR4 kinase and as a regulatory phosphatase in modulating kinase activity. To further advance *in vitro* biochemical and biophysical studies on the regulation of phosphatase activity, we describe expression and purification of MBP-tagged PP2A3c in *E. coli.* We demonstrate slow activation of phosphatase activity of PP2A3c over

time and further demonstrate the ability of the PP2A chaperone, PTPA, to more rapidly activate phosphatase activity *in trans*, in the presence of ATP. We provide a biochemical context to these results and the usefulness of our system in investigating the role of post-translational modifications. Additionally, we have characterized the biochemical properties of the recombinantly expressed intracellular kinase domain of the ACR4 homolog, CRK1. The *in-planta* expression of this RLK in the cells of the root tip overlaps the expression pattern of ACR4 and PP2A and we demonstrate that PP2A3c is also a substrate for CRK1. Mass spectrometry analysis confirmed >30 sites of phosphorylation at Serine, Threonine and Tyrosine residues, spanning the entire intracellular domain of CRK1. Mutagenesis experiments identified phosphorylation sites within the activation loop that had both positive and negative effects on the kinase activity of CRK1. Finally, we describe the generation of a highly specific monoclonal antibody to the kinase domain of ACR4.

CHAPTER 1: GENERAL INTRODUCTION

In response to extra-cellular stimuli both plant and animal cells have developed mechanisms to cope with the extremes of environmental changes. Cells utilize diverse enzymes to modulate cellular activities and maintain homeostasis. Reversible protein phosphorylation, mediated by kinases and phosphatases, is one of the major molecular mechanisms that regulate protein function and maintain the cellular well-being in response to the external cues. Phosphorylation is a covalent post-translational modification in which protein kinases catalyze the transfer of γ phosphate group from ATP to the hydroxyl group of serine, threonine and tyrosine residues on its substrate and protein phosphatases hydrolyze the phospho-ester bond to generate free phosphate and dephosphorylated protein. In eukaryotic cells, the occurrence of phosphorylation is most commonly seen on serine (84-86%) followed by threonine (10-20%) and tyrosine 2–4% [1,2,3,4,5].

Almost, one-third of the cellular activities such as cell cycle progression, metabolic activity, ion-transport, developmental growth and, stress response is regulated by reversible phosphorylation [6,7]. Phosphorylation regulates protein function by triggering an allosteric conformational change, disruption and/or creation of interaction sites for other proteins [8,9,10], regulation of the sub cellular localization and turnover of its target. Protein phosphorylation and dephosphorylation, is by far the most prevalent and extensively studied post-translational modification amongst ≤200 different post-translational modifications (PTM) including but not limited to ubiquitination, methylation and acetylation[11]. The rapid reversible nature, small metabolic cost and the ability to regulate function of target proteins [12], are important attributes of these protein modifications. As in mammalian systems, receptor like kinases (RLK) in plants mediate

downstream signal transduction which guide a host of cellular responses such as cell growth, proliferation and differentiation [13,14].

Dissertation Organization

This dissertation is organized into six chapters. Chapter 1 briefly reviews the current state of knowledge of plant receptor-like kinases in general, the role of ACR4 and homologs and the emerging importance of PP2A as a major regulator of receptor function. Chapter 2 has been published in the Proceedings of the National Academy of Sciences, USA [15] in a collaborative study and my contribution as a first author is summarized. This paper for the first time describes the characterization of PP2A3c as a substrate for ACR4 and a regulator of formative cell division in the Arabidopsis root. Chapter 3 is a manuscript that has been prepared for publication and describes the expression and purification of MBP-tagged PP2A3c and the activation of phosphatase activity *in trans* via the protein chaperone PTPA. Chapter 4 is prepared as a manuscript describing the characterization of the SUMO-tagged intracellular kinase domain of the ACR4 homolog, CRK1. This includes characterization of basic kinetic properties, the role of phosphorylation sites in the activation loop through mutagenesis studies and interaction with PP2A3c. Chapter 5 describes the path to the generation of a monoclonal antibody to the kinase domain of ACR4 and its value as a reagent for *in vivo* biological studies. Lastly, Chapter 6 is a general conclusion that draws together the work described in the previous chapters and outlines potential future directions.

Literature Review

Plant receptor-like kinase (RLK)

Plant RLKs represent one of the largest family of plant kinases [16] with more than 600 RLKs present in the *Arabidopsis* genome representing 2.5% of the known coding sequences *[14]* and 60% of the total kinases encoded [17]. Unlike animals, the absence of an "immune system" and the inability to be mobile, has led to the development of strategies to combat diverse environmental challenges and attacks by pathogens and insects. The Leucine Rich Repeat domain (LRR)- RLKs represent the largest group of plant receptors with more than 200 members [18]. The LRR-RLKs interact with a wide array of proteins allowing for combinatorial variations in signal response specificity. Importantly, RLK mediated signaling plays a cardinal role in pathogen recognition followed by activation of plant defense mechanisms and developmental control [19].

Architecturally, plant RLKs much like animal RTKs, are single transmembrane signaling protein, includes an extracellular ligand domain, a transmembrane domain and an intracellular protein kinase domain [16,20]. The extracellular domain perceives the extracellular ligand and the intracellular kinase domain mediates signal transduction [21]. The intracellular kinase domain further undergoes *auto/trans*-phosphorylation to form an active complex which elicits an amplified extracellular signal intracellularly by recruiting and phosphorylating the cytoplasmic downstream protein target [22,23,24,25]. The phosphorylated effector proteins can then affect gene transcription within the nucleus. Plant RLKs activate diverse signal transduction pathways, including those that control hormonal responses [26,27,28,29,30,31], flower development [32,33], innate immunity against bacterial pathogens [34], self-incompatibility [35], and root nodule formation

[36,37,38,39,40,41]. RLKs such as CLAVATA1, Brassinosteroid- insensitive 1(BRI1) and erecta regulate the development process [14,42], FLS2 and Xa21 mediate plant defense [14,42], HAESA regulates floral organ abscission and SYMRK manages root symbiosis with nitrogen-fixing bacteria or phosphate-acquiring arbuscular mycorrhizal fungi [21].

Brassinosteriod-insensitive1 (BRI1) is one of the best characterized RLKs and serves as an ideal paradigm of our understanding of receptor activation and regulation in plants. Brassinosteriod, a steroid hormone acts as a ligand to BRI1, which on binding activates the hetero-dimerization of BRI1 with its co-receptor BAK1, and initiates intracellular signaling cascade involving recruitment and activation of membrane-localized kinases BSK1 and BSK2 [43], a protein phosphatase BSU1 [43,44], the cytoplasmic kinase BIN2 [45], and transcription factors BZR1 and 2 [45,46,47]. However, in the absence of BR stimulation, BRI activity is auto-regulated by inactive homo-dimerization [48,49] and interaction with inactive kinase inhibitor (BK1)[50]. In presence of low BR, BIN2 kinase phosphorylates and inactivates BZR1 transcription factor which in-turn inhibits the plant growth. However, a recent study describes the PP2A mediated dephosphorylation of the phosphorylated BZR1 [51,52] and highlights the earlier reports regarding the regulation of BR signaling by PP2A phosphatase activity [51,52]. In *Arabidopsis*, the initiation of BR mediated BRI1 signaling increased mRNA expression levels of sbiI (suppressor of bri1) which encodes a Leucine Carboxy-Methyl Transferase (LCMT), known to methylate PP2A and control its membrane associated localization. The degradation of the BRI1 by PP2A mediated dephosphorylation, requires its association with BRI1 on the membrane, which is driven by methylation of PP2A via *sbiI* (LCMT). Hence, PP2A is hypothesized to inactivate the BRI1 signaling by means of internalization [53].

Arabidopsis Crinkly4 (ACR4)

Arabidopsis CRINKLY4 (ACR4, At3g59420) is an ortholog of maize CRINKLY 4 ZmCR4. ZmCR4 encodes gene for proper differentiation of epidermal tissues in aerial organs of plant. It regulates the epidermal cell specification and morphology in leaves and kernel [54,55]. ACR4 is important for the overall development of plant and thus is globally expressed in the plant. In aerial organs, ACR4 is present in the L1 layer of shoot apical meristem, ovule integuments, and epidermal layer of leaves [56,57,58] and, in roots, it is expressed in the quiescent center (QC), underlying columella cells and the flanking cells of the lateral root cap [57,59,60].

The root and shoot system of plants originate from the root apical meristem (RAM) and the shoot apical meristem (SAM) respectively. On embryogenesis, pollen sperm cell fertilizes the female gametophyte [61] followed by post embryonic stages of development, where two polar stem cells niche flourish into the root and shoot apical meristem [62,63]. Root apical meristem (RAM) has a centrally located quiescent center (QC), composed of rarely dividing cells which signal to maintain a strict control of stem cell population in the undifferentiated state. Stem cell division give rise to daughter cells distal to quiescent center and the surrounding mature differentiated cells then stimulate daughter cells to differentiate into appropriate cell type [64,65]. Columella cells (CC) originate from differentiation of columella stem cells (CSC) present below the quiescent center. The CSCs differentiation leads the daughter cells to differentiate into columella cells, at a proper signal from underlying CCs [60,64,66,67].

ACR4 mediates columella stem cell differentiation in the root apical meristem (RAM) and is essential for proper lateral root formation. The RLK mediates the

differentiation of columella stem cells (CSC) into columella cells (CC) which when disrupted cause proliferation and disorganization of CCs in the root tip [59,60]. Additionally, double and triple mutants within ACR4 family have displayed increased lateral root meristems suggesting functional redundancy within ACR4 family of RLKs [56,59].

ACR4 is a single transmembrane RLK with the extracellular domain (ECD) ligand binding domain, made of 39 amino acid long seven repeat regions, followed by three cysteine-rich regions similar to the tumor necrosis factor receptor (TNFR) ligand binding domain. The single alpha helical transmembrane domain connects the ECD to the intracellular domain (ICD). The ICD of ACR4 is composed of juxta membrane (JMD) and the C-terminal (CTD) subdomains, flanking the core kinase domain (KD). The intracellular domain of ACR4 has been demonstrated to possess intrinsic kinase activity [56,57,58]. *In vitro* biochemical/biophysical studies of ACR4 have provided valuable insights to the properties of the kinase domain [68]. Investigation of specific phosphorylation sites in the JMD domain by means of phage display and peptide binding assay suggested a model for potential phosphorylation dependent *intra-molecular* interaction between phosphorylated JMD peptide and kinase domain through a 'LXXLL' motif [69] and potential *inter-molecular* interaction between ACR4 and its homologs CRRs by the same motif [70].]

Homologs of ACR4

Arabidopsis genome encodes four homologs of ACR4, designated as AtCRR1(At3g09780), AtCRR2 (At2g39180), AtCRR3 (At3g55950) and AtCRK1 (At5g47850), that share sequence similarly and architectural features analogous to ACR4 [56,57,58] (Figure 1). Amongst the four homologs, AtCRK1 and AtCRR3 are kinase

active, but lack the TNFR like repeats in the extracellular domain. AtCRR1 and AtCRR2 are intrinsically dead kinases owing to the absence the domain VIII in activation loop [56]. *acr4* knockout plants showed similar phenotypic effects like cr4 mutant with developmental defects in integuments and seed coat but with no evident defects in embryo morphology, suggesting functional redundancy amongst the CRR family members [57].

Meyer et al [70] have previously demonstrated the intermolecular interactions between the intracellular domains of ACR4 and the homologs and also used the mRNA co-expression analysis tool within CORNET 2 (https://cornet.psb.ugent.be/) [71,72] to show overlapping and comparable mRNA expression levels of the groups of RLKs in the quiescent center, lateral root cap, root tip, root cortex and columella root cap cells, consequently spanning the entire RAM. The co-expression of these genes is a strong indicator of potential overlapping function and *in vivo* interaction. CRRs may have the ability to compensate for the loss of ACR4 function in lateral root initiation with significantly enhanced density of lateral roots in acr4/crr triple mutant background much different from acr4 single mutant plant [60]. Additionally, hetero-dimerization of ACR4 and CLAVATA1 (CLV1) has been reported to regulate the maintenance of root meristem and collectively restrict root stemness at the root tip [73]. CLV1 is an essential RLK, required for shoot stemness maintenance and a recent study described its ability to moderate root stemness in *Arabidopsis* through homo- and heteromeric interaction with ACR4. Thus, heteromeric interaction of multiple RLKs driving a common signaling cascade, may be more common than the simplistic model of single receptor-single ligand driven downstream signaling.

Kinase domain structure and regulation

Kinase enzyme catalyzes the transfer of γ phosphate from adenosine tri-phosphate (ATP) molecule to serine, threonine and tyrosine amino acid in a specific substrate. Structurally the kinase domain folds into an N-terminal lobe predominantly composed of β- sheet and a C-terminal α-alpha lobe as described in the crystal structure of cyclic AMP dependent kinase [74,75,76]. The N and C terminal lobes create a pocket for active site of the kinase (Figure 2). The catalytic domain of kinase is subdivided into 11 distinct subdomains (Figure 3) with about 10 highly conserved residues/ motifs which contribute towards the kinase activity and stability. The β strands 1 & 2 in N-lobe host a Gly rich P – loop which stabilizes the α and β phosphates of the bound ATP molecule. The conserved Lys in β strand 3 also helps to stabilize the α & β phosphates of ATP and form a salt bridge with invariant Glu residue in helix-C. C lobe is comprised of catalytic loop and activation loop. The catalytic loop present in the C lobe harbors HRD motif in which the aspartic acid functions as a catalytic base for the phospho-transfer reaction and chelates the Mg^{2+} ion bridging the α and γ phosphate of the incoming ATP molecule. Mutation or loss of this aspartate causes complete inactivity of the kinase. Downstream to catalytic loop is the activation loop with two conserved DFG and APE/DPE motifs, which serve as hinge points for activation loop movement. The aspartic acid in DFG chelates Mg^{2+} ion and stabilizes β and γ phosphates of ATP. The APE/DPE motif act towards structural stability of the C-lobe [76,77,78]. These conserved motifs and regions synchronize towards efficient phosphate transfer from ATP to the substrate molecule.

Protein phosphatases: Regulators of protein kinases

Kinases and phosphatases mediate reversible protein phosphorylation and serve as an on-off switch controlling the cellular activities in eukaryotic cells [79]. Protein phosphatases are classified into five classes based on the primary sequence and catalytic mechanism: 1) PPP- Phospho-protein phosphatases, 2) PPM or PP2C- Metallo-dependent protein phosphatases, 3) PTP–phospho-tyrosine phosphatase, 4) Aspartate dependent phosphatases and, 5) DSP- Dual specificity phosphatases [5,80]. PPP and PP2C family of phosphatases comprise the largest family of well-studied phosphatases, catalyze dephosphorylation at serine & threonine residues, and are responsible for catalyzing about 90% of the dephosphorylation reaction in eukaryotes [80,81]. PPP family is further divided into nine sub-classes: PP1 (protein phosphatase type one), PP2A (protein phosphatase 2A), PP4, PP5, PP6, PP7, SLP (*Shewanella*-like protein) phosphatase, and PPKL (protein phosphatase with Kelch-like repeat domains) [5]. Catalytically each member of the PPP family displays identical mechanism owing to the presence of highly conserved catalytic subunit throughout eukaryotes.

Phosphatases in the PPP family conduct variety of biological and cellular functions in plants. PP1 along with its interactors mediate cell cycle regulation, cell division and patterning, cell differentiation, embryo development and cytokinin production. Protein phosphatase 2A (PP2A) has important role in growth and development [82,83], cytoskeleton structure formation [84], auxin transport [85,86], biotic and abiotic stress signaling [87], acid and ethylene signaling [88,89,90], light and abscisic acid (ABA) signaling, stomatal opening, and most notably, in brassinosteroid (BR) signaling [91]. PP6 is involved in ABA signaling and maintenance of cell polarity, PP5 has roles in disease resistance, thermo-tolerance and light detection. PP7 has been involved in light sensing

and so far, no defined role is reported for PP4 in plants [5,81]. In humans, deregulation of PP2A has been associated with many debilitating diseases such as cancer [92,93,94,95], Alzheimer's [96,97,98] and heart failure [94,99].

Protein phosphatase 2A: Structure, regulation and activation

PP2A phosphatase is a heterotrimeric holoenzyme, comprised of highly conserved ~ 36 kDa Catalytic 'C' subunit regulated by a ~65 kDa structural scaffold 'A' subunit, and together form the PP2A core protein (Figure 4A). This further interacts with a variable 'B' subunit which determines its substrate specificity and cellular localization. The sequence of 'C' and 'A' subunit is highly conserved through eukaryotes (Figure 5).

In *Arabidopsis,* the phosphatases and kinases are disproportionately represented with ~150 protein phosphatases for ~1050 protein kinases [100,101]. Members of the PPP family have developed strategies to compensate for this disproportionality between kinase and phosphatases through specific interaction of catalytic subunit with varying regulatory subunits, specifically varying B subunits. This not only confers specificity towards its substrates but also allows for enormous substrate diversity. *Arabidopsis* has five genes for the catalytic C subunit (c1-5), three genes for 'A' subunit (A1-3) where A1/RCN1 is encoded by the gene ROOT CURLS IN NAPHTHYLPHTHALAMIC ACID1 [85] and seventeen genes encoding for 'B' subunits [102], making a total of 255 possible combinations just within the PP2A subclass of PPP phosphatases.

Crystal structure of heterotrimeric human PP2A [103,104,105] (Figure 4B) along with biochemical analysis have provided significant mechanistic understanding of PP2A function and assembly and, serves as framework for future studies amongst other eukaryotic phosphatases. In mammalian cells, A/PR65 & C subunit each has two

isoforms α and β which share high sequence similarity, with α isoform present at higher abundance than β isoform [106,107,108,109]. The variable B subunit is subdivided into four families: B (PR55), B' (B56 or PR61), B'' (PR72) and B''' (PR93/PR110). The scaffolding A subunit contains 15 HEAT (huntingtin-elongation-A subunit-TOR) repeats made of conserved 39 amino acid residues. Each HEAT repeat consists of parallel α helices connected by an intra-repeat loop, and adjacent repeats are connected by inter-repeat loops. The catalytic subunit forms a compact ellipsoidal structure and recognizes one end of the elongated A subunit. B (PR61/B56γ1) subunit interact with the AC dimer on significant bending of HEAT repeats 12-15 towards the amino terminus of A subunit, which creates an interface of A-C interaction from HEAT repeat 2-7. A & B do not form a stable complex due to a relatively loose interacting interface. The B subunit has an elongated super helical structure comprised of 18 α helices, which fold like pseudo HEAT repeats, despite the lack of canonical HEAT repeat sequence. The B and C subunit dock on the apical side of the horse shoe A subunit and make extensive contacts between each other. In addition to these interactions, C subunit contains a highly-conserved C–terminal tail which docks on the interface of A and C subunit and reported to regulate the recruitment of B subunit by means of methylation of conserved carboxy- terminal leucine [110,111,112,113,114].

The active site of PP2Ac is structurally conserved throughout eukaryotes and is formed by protein loops connecting two central β sheets flanked by α helices. Six highly conserved residues on these loops, two aspartates (D), one asparagine (N) and, three histidines (H) coordinate the two catalytic metal ions and a catalytic water molecule. Incoming phosphorylated residues is coordinated by one conserved histidine and two arginine (R) residues. Dephosphorylation reaction proceeds through an Sn2 mechanism,

where activated water molecule carries out a nucleophilic attack on the incoming phosphate group attached to a Ser/Thr residue [115] (Figure 6). The active site conformation and its protein fold are reported to be highly dynamic in nature. This is one of the reasons why all the crystal structures solved till date require potent inhibitors such as microcystin LR or okadaic acid for stabilization of the active site [104,105,116].

Regulation of PP2Ac activity by post-translational modifications

PP2A activity and holoenzyme assembly is highly-regulated by means of two important covalent post-translational modifications that occur on the conserved C-terminal tail "T^{304}DPYGL^{309}" of PP2A catalytic subunit namely: Phosphorylation at T304 and Y307 [117] and, carboxy-methylation at C terminal Leu 309 [94,118].

Phosphorylation of Thr-304 & Try-307 residues in the conserved C-terminal tail is reported to be inhibitory to phosphatase activity [96,119,120]. Phosphorylation of these sites are regulated by PTB1, $p60^{v\text{-}src}$ and $P56^{lck}$ kinases [98,119,121,122]. The effect of the phosphorylation is generally thought to be inhibitory both in an *in vivo* and *in vitro* set up [122] although there are a few reports that suggest otherwise [96,119,123].

Carboxy-methylation is a reversible mechanism controlled by Leucine Carboxy-Methyl transferase (LCMT-1) and Phospho-Methyl Esterase (PME-1) [104,124]. The role of carboxy-leucine methylation towards phosphatase activity and holoenzyme assembly has been an open-ended question with contradictory results been reported by various groups. Structural studies on mammalian PP2A has revealed the environment of C-terminal leucine to be highly negatively charged, formed by three glutamic acid and one aspartic acid residue contributed by A subunit and an aspartic acid from C subunit. It is speculated that in the absence of C-terminal carboxy- methylation, the negative charge-

charge repulsion does not favor the docking of C-terminal tail in this region and prevents binding of B subunit to the AC core enzyme [103]. In the crystal structure of PP2Ac with B/PR55 regulatory subunits, the interaction of PP2Ac with B/PR55 is suggested to be independent of methylation, with no indication of methylated C-tail present at docking site of C and B subunit [105,125]. On the other hand, methylation was reported to be important for PP2A core enzyme to interact with B'/PR61 and B''/PR71 subunits [104,110,111,112,114,126,127]. However, *in vivo,* methylation of C-terminal leucine has been shown to be unequivocally critical for stable heterotrimeric PP2A assembly [93,118,128]. LCMT-1 binds directly to the active site residues and requires active conformation of PP2Ac subunit for methylation. Active PP2Ac selectively undergoes methylation and assembles into the holoenzyme, thereby minimizing the unregulated phosphatase activity of free C subunit [124]. PME-1 in addition to demethylation, also mediates PP2A inactivation by eviction of metal ions at the active site [104]. Methylation level of PP2A fluctuates throughout the cell cycle and knockdown studies describe LCMT-1 to be essential for cellular functions, indicating that regulation of PP2Ac methylation and holoenzyme assembly is required for cell cycle regulation [94,114]. In *Arabidopsis*, LCMT-1 was reported to negatively regulate BRI1 signaling [52]. In melanoma tumor cells, methylation of PP2A was shown to tightly regulate the phosphatase activity [129] whereas, in a study reported by Ikehara et al [125], alanine and deletion mutants of Leu 309 exhibited phosphatase activity indicating methylation to be irrelevant for phosphatase activity.

Biogenesis of active PP2Ac by PTPA (Phosphatase Two A Protein Activator)

The function and complete biogenesis of active PP2A heterotrimeric complex relies on proper activation of PP2A catalytic subunit (PP2Ac). Biochemical and structural studies

on mammalian PP2A has provided extensive understanding to a potential linear path towards generation of active PP2A *in-vivo*. Activation of PP2Ac facilitates carboxyl-methylation of the C-terminal leucine and stable association of A subunit to form PP2A core AC dimer [6,124,130]. In a cellular environment, promiscuous activity of PP2A catalytic subunit (PP2Ac) is kept under control by interaction with stable latency factor α4 [131], and/or PME-1 [95,128,132], which preferentially binds to partially folded PP2Ac by making contacts with both surface residues and inner structures of unfolded active site. (Figure 7)

PTPA, a phospho tyrosyl phosphatase activator/ phosphatase two A protein activator, is an essential protein involved in regulation of PP2A. PTPA is reported to possess an ATP –dependent activation energy [133,134] and a peptidyl-prolyl isomerase activity [135]. Together they drive activation of an inactive PP2A catalytic subunit. Crystal structure of PP2A-PTPA-ATPγS provide valuable insights to PTPA mediated activation of PP2A. The binding of PTPA stabilizes the inactive apo-PP2Ac conformation, orients phosphoryl groups of ATP molecule to PP2A active site, which selectively enhances binding and proper orientation of Mg^{2+} metal ions into the active site of PP2Ac, driving ATP hydrolysis and acquisition of phospho-serine/threonine activity. [133]. The structure reveals that the ATP hydrolysis requires both PP2A and PTPA to form an ATP binding pocket. PTPA is suggested to stabilize the dynamic and conformationally flexible active site of PP2Ac to a conformation suitable for phosphatase activation and methylation by LCMT-1[124]. Additionally, PTPA also interacts with the C-terminal tail of PP2Ac, phosphorylation of C-terminal tail at Ty307 and methylation at Leu309 was shown to abrogate this interaction with no effect observed when Thr304 is phosphorylated [117].

PTPA is also reported to have Peptidyl – Prolyl *cis/trans* isomerase (PPIase) activity which induces a reversible conformational change in PP2Ac at Proline190 [135]. Other PPIases such as cyclophilins or FKBPs cannot activate PP2A and underline the specificity of PTPA towards PP2A isomerization. The isomerization and activation energy of PTPA are correlated, since both are stimulated in the presence of Mg^{2+} and ATP. Proline isomerization is a rate –limiting step in protein folding and peptidyl prolyl isomerases catalyze the intrinsically slow proline isomerization property of proteins to much rapid extend [136]. Conformational switch due to *trans-cis* isomerization at the conserved proline in SAPNY motif is recently reported for human calcineurin, another serine/threonine PPP phosphatase [137]. Additionally, *in-vivo,* PTPA was shown to activate PP2A by reducing the level of inhibitory Y307 phosphorylation by upregulating a protein tyrosine phosphatase PTPB1 [138].

Role of PP2A in root development

In addition to the role of ACR4 RLK, recent gene knock out studies in plants have characterized the function of PP2A enzymes in root development [139,140,141]. Severe developmental defects including impaired root development, lethality in seedling are reported in pp2a3c and pp2a4c double mutant plants. PP2A3c and PP2A4c have redundant functions and control embryo patterning, root development and auxin flux processes. Different combinations of pp2a3c and pp2a4c null alleles showed dosage sensitive defect in the distal root meristem, ectopic QC division, abnormal cell division planes and unclear delimitation of the stem cell niche (SCN) along with dosage- sensitive defects in embryo patterning and development [139]. Additionally, PP2A-5c isoform is shown to positively regulate plant responses towards high salt concentration with pp2a5c mutant plant

exhibiting diminished root and vegetative growth, and over-expression of pp2a5c triggering improved growth under high salt concentrations [140]. The regulatory role of PP2A regulatory subunit has also been reported with PP2A-B55 and PP2A-b'γ antagonistically regulating the flowering time [142]. PP2A-A1/RCN1 (ROOT CURLING ON NPA1), PP2A-A2 and PP2A-A3, display dosage dependent sensitivity towards primary root meristem development, with rcn1 knockout affecting root-tip organization, abnormality in QC and columella cell number [82].

Scope of the Thesis

ACR4 has been described as a major RLK with assigned role in root development. However, little is known of the signaling pathway, its interacting partners and the mechanism of its regulation. In-silico analysis, co-expression studies and biochemical analysis provide the basis for investigating the *in vitro* interaction and regulation between these co-expressed proteins: ACR4, ACR4 homolog- CRK1 and PP2A3c phosphatase and thus contribute towards advancing our knowledge of ACR4 mediated interactions in planta in the root meristem. Insights to PP2A function, holoenzyme assembly, activation and regulation have been obtained from biochemical investigations and structural studies on recombinant expression of protein in eukaryotic expression system, specifically insect cell–baculovirus expression system [103,143,144,145]. This study offers the E. coli platform as an alternative for recombinant expression of PP2A catalytic subunit and specifically investigating the role of post-translational modifications. Lastly, we describe the production and characterization of a purified monoclonal antibody, highly specific against ACR4 kinase, with no detectable cross-reactivity within ACR4 homologs, thus offering an invaluable reagent for *in planta* and *in vitro* studies centered on ACR4 RLK.

References

1. Humphrey SJ, James DE, Mann M (2015) Protein Phosphorylation: A Major Switch Mechanism for Metabolic Regulation. Trends Endocrinol Metab 26: 676-687.
2. Nakagami H, Sugiyama N, Mochida K, Daudi A, Yoshida Y, et al. (2010) Large-scale comparative phosphoproteomics identifies conserved phosphorylation sites in plants. Plant Physiol 153: 1161-1174.
3. Nguyen TH, Brechenmacher L, Aldrich JT, Clauss TR, Gritsenko MA, et al. (2012) Quantitative phosphoproteomic analysis of soybean root hairs inoculated with Bradyrhizobium japonicum. Mol Cell Proteomics 11: 1140-1155.
4. Sugiyama N, Nakagami H, Mochida K, Daudi A, Tomita M, et al. (2008) Large-scale phosphorylation mapping reveals the extent of tyrosine phosphorylation in Arabidopsis. Mol Syst Biol 4: 193.
5. Uhrig RG, Labandera AM, Moorhead GB (2013) Arabidopsis PPP family of serine/threonine protein phosphatases: many targets but few engines. Trends Plant Sci 18: 505-513.
6. Hombauer H, Weismann D, Mudrak I, Stanzel C, Fellner T, et al. (2007) Generation of active protein phosphatase 2A is coupled to holoenzyme assembly. PLoS Biol 5: e155.
7. Graves JD, Krebs EG (1999) Protein phosphorylation and signal transduction. Pharmacol Ther 82: 111-121.
8. Pawson T (1995) Protein Modules and Signaling Networks. Nature 373: 573-580.
9. Johnson LN, O'Reilly M (1996) Control by phosphorylation. Curr Opin Struct Biol 6: 762-769.
10. Johnson LN, Snape P, Martin JL, Acharya KR, Barford D, et al. (1993) Crystallographic binding studies on the allosteric inhibitor glucose-6-phosphate to T state glycogen phosphorylase b. J Mol Biol 232: 253-267.
11. Walsh G, Jefferis R (2006) Post-translational modifications in the context of therapeutic proteins. Nat Biotechnol 24: 1241-1252.
12. Cohen P (2002) The origins of protein phosphorylation. Nature Cell Biology 4: E127-E130.
13. Lemmon MA, Schlessinger J (2010) Cell Signaling by Receptor Tyrosine Kinases. Cell 141: 1117-1134.
14. Shiu SH, Bleecker AB (2001) Receptor-like kinases from Arabidopsis form a monophyletic gene family related to animal receptor kinases. Proc Natl Acad Sci U S A 98: 10763-10768.
15. Shiu SH, Karlowski WM, Pan R, Tzeng YH, Mayer KF, et al. (2004) Comparative analysis of the receptor-like kinase family in Arabidopsis and rice. Plant Cell 16: 1220-1234.
16. Shiu SH, Bleecker AB (2003) Expansion of the receptor-like kinase/Pelle gene family and receptor-like proteins in Arabidopsis. Plant Physiol 132: 530-543.
17. Afzal AJ, Wood AJ, Lightfoot DA (2008) Plant receptor-like serine threonine kinases: roles in signaling and plant defense. Mol Plant Microbe Interact 21: 507-517.
18. Cock JM, Vanoosthuyse V, Gaude T (2002) Receptor kinase signalling in plants and animals: distinct molecular systems with mechanistic similarities. Curr Opin Cell Biol 14: 230-236.

19. Shiu SH, Li WH (2004) Origins, lineage-specific expansions, and multiple losses of tyrosine kinases in eukaryotes. Mol Biol Evol 21: 828-840.
20. Parniske M (2004) Molecular genetics of the arbuscular mycorrhizal symbiosis. Curr Opin Plant Biol 7: 414-421.
21. Trotochaud AE, Hao T, Wu G, Yang Z, Clark SE (1999) The CLAVATA1 receptor-like kinase requires CLAVATA3 for its assembly into a signaling complex that includes KAPP and a Rho-related protein. Plant Cell 11: 393-406.
22. Clark SE (2001) Cell signalling at the shoot meristem. Nature Reviews Molecular Cell Biology 2: 276-284.
23. Rojo E, Sharma VK, Kovaleva V, Raikhel NV, Fletcher JC (2002) CLV3 is localized to the extracellular space, where it activates the Arabidopsis CLAVATA stem cell signaling pathway. Plant Cell 14: 969-977.
24. Trotochaud AE, Jeong S, Clark SE (2000) CLAVATA3, a multimeric ligand for the CLAVATA1 receptor-kinase. Science 289: 613-617.
25. Li JM, Chory J (1997) A putative leucine-rich repeat receptor kinase involved in brassinosteroid signal transduction. Cell 90: 929-938.
26. Matsubayashi Y, Ogawa M, Morita A, Sakagami Y (2002) An LRR receptor kinase involved in perception of a peptide plant hormone, phytosulfokine. Science 296: 1470-1472.
27. Montoya T, Nomura T, Farrar K, Kaneta T, Yokota T, et al. (2002) Cloning the tomato curl3 gene highlights the putative dual role of the leucine-rich repeat receptor kinase tBRI1/SR160 in plant steroid hormone and peptide hormone signaling. Plant Cell 14: 3163-3176.
28. Scheer JM, Ryan CA (2002) The systemin receptor SR160 from Lycopersicon peruvianum is a member of the LRR receptor kinase family. Proceedings of the National Academy of Sciences of the United States of America 99: 9585-9590.
29. Szekeres M (2003) Brassinosteroid and systemin: two hormones perceived by the same receptor. Trends Plant Sci 8: 102-104.
30. Yin YH, Wu DY, Chory J (2002) Plant receptor kinases: Systemin receptor identified. Proceedings of the National Academy of Sciences of the United States of America 99: 9090-9092.
31. Stone JM, Trotochaud AE, Walker JC, Clark SE (1998) Control of meristem development by CLAVATA1 receptor kinase and kinase-associated protein phosphatase interactions. Plant Physiol 117: 1217-1225.
32. Williams RW, Wilson JM, Meyerowitz EM (1997) A possible role for kinase-associated protein phosphatase in the Arabidopsis CLAVATA1 signaling pathway. Proc Natl Acad Sci U S A 94: 10467-10472.
33. Gomez-Gomez L, Bauer Z, Boller T (2001) Both the extracellular leucine-rich repeat domain and the kinase activity of FLS2 are required for flagellin binding and signaling in arabidopsis. Plant Cell 13: 1155-1163.
34. Braun DM, Stone JM, Walker JC (1997) Interaction of the maize and Arabidopsis kinase interaction domains with a subset of receptor-like protein kinases: implications for transmembrane signaling in plants. Plant J 12: 83-95.
35. Downie JA, Walker SA (1999) Plant responses to nodulation factors. Curr Opin Plant Biol 2: 483-489.

36. Endre G, Kereszt A, Kevei Z, Mihacea S, Kalo P, et al. (2002) A receptor kinase gene regulating symbiotic nodule development. Nature 417: 962-966.
37. Krusell L, Madsen LH, Sato S, Aubert G, Genua A, et al. (2002) Shoot control of root development and nodulation is mediated by a receptor-like kinase. Nature 420: 422-426.
38. Nishimura R, Hayashi M, Wu GJ, Kouchi H, Imaizumi-Anraku H, et al. (2002) HAR1 mediates systemic regulation of symbiotic organ development. Nature 420: 426-429.
39. Spaink HP (2002) Plant-microbe interactions: a receptor in symbiotic dialogue. Nature 417: 910-911.
40. Stracke S, Kistner C, Yoshida S, Mulder L, Sato S, et al. (2002) A plant receptor-like kinase required for both bacterial and fungal symbiosis. Nature 417: 959-962.
41. Tichtinsky G, Vanoosthuyse V, Cock JM, Gaude T (2003) Making inroads into plant receptor kinase signalling pathways. Trends in Plant Science 8: 231-237.
42. Tang W, Kim TW, Oses-Prieto JA, Sun Y, Deng Z, et al. (2008) BSKs mediate signal transduction from the receptor kinase BRI1 in Arabidopsis. Science 321: 557-560.
43. Mora-Garcia S, Vert G, Yin Y, Cano-Delgado A, Cheong H, et al. (2004) Nuclear protein phosphatases with Kelch-repeat domains modulate the response to brassinosteroids in Arabidopsis. Genes Dev 18: 448-460.
44. Li J, Nam KH (2002) Regulation of brassinosteroid signaling by a GSK3/SHAGGY-like kinase. Science 295: 1299-1301.
45. He JX, Gendron JM, Sun Y, Gampala SSL, Gendron N, et al. (2005) BZR1 is a transcriptional repressor with dual roles in brassinosteroid homeostasis and growth responses. Science 307: 1634-1638.
46. Yin YH, Vafeados D, Tao Y, Yoshida S, Asami T, et al. (2005) A new class of transcription factors mediates brassinosteroid-regulated gene expression in Arabidopsis. Cell 120: 249-259.
47. Russinova E, Borst JW, Kwaaitaal M, Cano-Delgado A, Yin YH, et al. (2004) Heterodimerization and endocytosis of Arabidopsis brassinosteroid receptors BRI1 and AtSERK3 (BAK1). Plant Cell 16: 3216-3229.
48. Wang XL, Li XQ, Meisenhelder J, Hunter T, Yoshida S, et al. (2005) Autoregulation and homodimerization are involved in the activation of the plant steroid receptor BRI1. Developmental Cell 8: 855-865.
49. Wang XL, Chory J (2006) Brassinosteroids regulate dissociation of BKI1, a negative regulator of BRI1 signaling, from the plasma membrane. Science 313: 1118-1122.
50. Tang W, Yuan M, Wang R, Yang Y, Wang C, et al. (2011) PP2A activates brassinosteroid-responsive gene expression and plant growth by dephosphorylating BZR1. Nature Cell Biology 13: 124-131.
51. Wu G, Wang X, Li X, Kamiya Y, Otegui MS, et al. (2011) Methylation of a phosphatase specifies dephosphorylation and degradation of activated brassinosteroid receptors. Sci Signal 4: ra29.
52. Di Rubbo S, Irani NG, Russinova E (2011) PP2A phosphatases: the "on-off" regulatory switches of brassinosteroid signaling. Sci Signal 4: pe25.
53. Becraft PW, Stinard PS, McCarty DR (1996) CRINKLY4: A TNFR-like receptor kinase involved in maize epidermal differentiation. Science 273: 1406-1409.
54. Jin P, Guo T, Becraft PW (2000) The maize CR4 receptor-like kinase mediates a growth factor-like differentiation response. Genesis 27: 104-116.

55. Cao X, Li K, Suh SG, Guo T, Becraft PW (2005) Molecular analysis of the CRINKLY4 gene family in Arabidopsis thaliana. Planta 220: 645-657.
56. Gifford ML, Dean S, Ingram GC (2003) The Arabidopsis ACR4 gene plays a role in cell layer organisation during ovule integument and sepal margin development. Development 130: 4249-4258.
57. Watanabe M, Tanaka H, Watanabe D, Machida C, Machida Y (2004) The ACR4 receptor-like kinase is required for surface formation of epidermis-related tissues in Arabidopsis thaliana. Plant J 39: 298-308.
58. De Smet I, Vassileva V, De Rybel B, Levesque MP, Grunewald W, et al. (2008) Receptor-like kinase ACR4 restricts formative cell divisions in the Arabidopsis root. Science 322: 594-597.
59. Stahl Y, Wink RH, Ingram GC, Simon R (2009) A signaling module controlling the stem cell niche in Arabidopsis root meristems. Curr Biol 19: 909-914.
60. Ma H, Sundaresan V (2010) Development of Flowering Plant Gametophytes. Plant Development 91: 379-412.
61. De Smet I, Voss U, Jurgens G, Beeckman T (2009) Receptor-like kinases shape the plant. Nature Cell Biology 11: 1166-1173.
62. Scheres B (2007) Stem-cell niches: nursery rhymes across kingdoms. Nature Reviews Molecular Cell Biology 8: 345-354.
63. van den Berg C, Willemsen V, Hendriks G, Weisbeek P, Scheres B (1997) Short-range control of cell differentiation in the Arabidopsis root meristem. Nature 390: 287-289.
64. Sarkar AK, Luijten M, Miyashima S, Lenhard M, Hashimoto T, et al. (2007) Conserved factors regulate signalling in Arabidopsis thaliana shoot and root stem cell organizers. Nature 446: 811-814.
65. Blancaflor EB, Masson PH (2003) Plant gravitropism. Unraveling the ups and downs of a complex process. Plant Physiol 133: 1677-1690.
66. Perrin RM, Young LS, Murthy UMN, Harrison BR, Wang Y, et al. (2005) Gravity signal transduction in primary roots. Ann Bot 96: 737-743.
67. Meyer MR, Lichti CF, Townsend RR, Rao AG (2011) Identification of in vitro autophosphorylation sites and effects of phosphorylation on the Arabidopsis CRINKLY4 (ACR4) receptor-like kinase intracellular domain: insights into conformation, oligomerization, and activity. Biochemistry 50: 2170-2186.
68. Meyer MR, Shah S, Rao AG (2013) Insights into molecular interactions between the juxtamembrane and kinase subdomains of the Arabidopsis Crinkly-4 receptor-like kinase. Archives of Biochemistry and Biophysics 535: 101-110.
69. Meyer MR, Shah S, Zhang J, Rohrs H, Rao AG (2015) Evidence for intermolecular interactions between the intracellular domains of the arabidopsis receptor-like kinase ACR4, its homologs and the Wox5 transcription factor. PLoS One 10: e0118861.
70. De Bodt S, Carvajal D, Hollunder J, Van den Cruyce J, Movahedi S, et al. (2010) CORNET: a user-friendly tool for data mining and integration. Plant Physiol 152: 1167-1179.
71. De Bodt S, Hollunder J, Nelissen H, Meulemeester N, Inze D (2012) CORNET 2.0: integrating plant coexpression, protein-protein interactions, regulatory interactions, gene associations and functional annotations. New Phytol 195: 707-720.

72. Stahl Y, Grabowski S, Bleckmann A, Kuhnemuth R, Weidtkamp-Peters S, et al. (2013) Moderation of Arabidopsis root stemness by CLAVATA1 and ARABIDOPSIS CRINKLY4 receptor kinase complexes. Curr Biol 23: 362-371.
73. Knighton DR, Zheng JH, Ten Eyck LF, Ashford VA, Xuong NH, et al. (1991) Crystal structure of the catalytic subunit of cyclic adenosine monophosphate-dependent protein kinase. Science 253: 407-414.
74. Knighton DR, Zheng JH, Ten Eyck LF, Xuong NH, Taylor SS, et al. (1991) Structure of a peptide inhibitor bound to the catalytic subunit of cyclic adenosine monophosphate-dependent protein kinase. Science 253: 414-420.
75. Zheng J, Knighton DR, ten Eyck LF, Karlsson R, Xuong N, et al. (1993) Crystal structure of the catalytic subunit of cAMP-dependent protein kinase complexed with MgATP and peptide inhibitor. Biochemistry 32: 2154-2161.
76. Hanks SK, Hunter T (1995) Protein kinases 6. The eukaryotic protein kinase superfamily: kinase (catalytic) domain structure and classification. FASEB J 9: 576-596.
77. Nolen B, Taylor S, Ghosh G (2004) Regulation of protein kinases: Controlling activity through activation segment conformation. Molecular Cell 15: 661-675.
78. Hunter T (1995) Protein kinases and phosphatases: the yin and yang of protein phosphorylation and signaling. Cell 80: 225-236.
79. Moorhead GB, De Wever V, Templeton G, Kerk D (2009) Evolution of protein phosphatases in plants and animals. Biochem J 417: 401-409.
80. Lillo C, Kataya AR, Heidari B, Creighton MT, Nemie-Feyissa D, et al. (2014) Protein phosphatases PP2A, PP4 and PP6: mediators and regulators in development and responses to environmental cues. Plant Cell Environ 37: 2631-2648.
81. Blakeslee JJ, Zhou HW, Heath JT, Skottke KR, Barrios JA, et al. (2008) Specificity of RCN1-mediated protein phosphatase 2A regulation in meristem organization and stress response in roots. Plant Physiol 146: 539-553.
82. Zhou HW, Nussbaumer C, Chao Y, DeLong A (2004) Disparate roles for the regulatory A subunit isoforms in Arabidopsis protein phosphatase 2A. Plant Cell 16: 709-722.
83. Camilleri C, Azimzadeh J, Pastuglia M, Bellini C, Grandjean O, et al. (2002) The Arabidopsis TONNEAU2 gene encodes a putative novel protein phosphatase 2A regulatory subunit essential for the control of the cortical cytoskeleton. Plant Cell 14: 833-845.
84. Garbers C, DeLong A, Deruere J, Bernasconi P, Soll D (1996) A mutation in protein phosphatase 2A regulatory subunit A affects auxin transport in Arabidopsis. EMBO J 15: 2115-2124.
85. Michniewicz M, Zago MK, Abas L, Weijers D, Schweighofer A, et al. (2007) Antagonistic regulation of PIN phosphorylation by PP2A and PINOID directs auxin flux. Cell 130: 1044-1056.
86. Pais SM, Tellez-Inon MT, Capiati DA (2009) Serine/threonine protein phosphatases type 2A and their roles in stress signaling. Plant Signal Behav 4: 1013-1015.
87. Kwak JM, Moon JH, Murata Y, Kuchitsu K, Leonhardt N, et al. (2002) Disruption of a guard cell-expressed protein phosphatase 2A regulatory subunit, RCN1, confers abscisic acid insensitivity in Arabidopsis. Plant Cell 14: 2849-2861.
88. Larsen PB, Cancel JD (2003) Enhanced ethylene responsiveness in the Arabidopsis eer1 mutant results from a loss-of-function mutation in the protein phosphatase 2A A regulatory subunit, RCN1. Plant J 34: 709-718.

89. Pernas M, Garcia-Casado G, Rojo E, Solano R, Sanchez-Serrano JJ (2007) A protein phosphatase 2A catalytic subunit is a negative regulator of abscisic acid signalling. Plant J 51: 763-778.
90. Kim TW, Guan S, Sun Y, Deng Z, Tang W, et al. (2009) Brassinosteroid signal transduction from cell-surface receptor kinases to nuclear transcription factors. Nature Cell Biology 11: 1254-1260.
91. Arroyo JD, Hahn WC (2005) Involvement of PP2A in viral and cellular transformation. Oncogene 24: 7746-7755.
92. Mumby M (2007) PP2A: unveiling a reluctant tumor suppressor. Cell 130: 21-24.
93. Janssens V, Goris J, Van Hoof C (2005) PP2A: the expected tumor suppressor. Curr Opin Genet Dev 15: 34-41.
94. Van Hoof C, Janssens V, Dinishiotu A, Merlevede W, Goris J (1998) Functional analysis of conserved domains in the phosphotyrosyl phosphatase activator. Molecular cloning of the homologues from Drosophila melanogaster and Saccharomyces cerevisiae. Biochemistry 37: 12899-12908.
95. Liu R, Zhou XW, Tanila H, Bjorkdahl C, Wang JZ, et al. (2008) Phosphorylated PP2A (tyrosine 307) is associated with Alzheimer neurofibrillary pathology. J Cell Mol Med 12: 241-257.
96. Sontag E, Nunbhakdi-Craig V, Sontag JM, Diaz-Arrastia R, Ogris E, et al. (2007) Protein phosphatase 2A methyltransferase links homocysteine metabolism with tau and amyloid precursor protein regulation. J Neurosci 27: 2751-2759.
97. Sontag E, Hladik C, Montgomery L, Luangpirom A, Mudrak I, et al. (2004) Downregulation of protein phosphatase 2A carboxyl methylation and methyltransferase may contribute to Alzheimer disease pathogenesis. J Neuropathol Exp Neurol 63: 1080-1091.
98. Virshup DM (2000) Protein phosphatase 2A: a panoply of enzymes. Curr Opin Cell Biol 12: 180-185.
99. Kerk D, Templeton G, Moorhead GB (2008) Evolutionary radiation pattern of novel protein phosphatases revealed by analysis of protein data from the completely sequenced genomes of humans, green algae, and higher plants. Plant Physiol 146: 351-367.
100. Lehti-Shiu MD, Shiu SH (2012) Diversity, classification and function of the plant protein kinase superfamily. Philosophical Transactions of the Royal Society B-Biological Sciences 367: 2619-2639.
101. Farkas I, Dombradi V, Miskei M, Szabados L, Koncz C (2007) Arabidopsis PPP family of serine/threonine phosphatases. Trends Plant Sci 12: 169-176.
102. Cho US, Xu W (2007) Crystal structure of a protein phosphatase 2A heterotrimeric holoenzyme. Nature 445: 53-57.
103. Xing Y, Xu Y, Chen Y, Jeffrey PD, Chao Y, et al. (2006) Structure of protein phosphatase 2A core enzyme bound to tumor-inducing toxins. Cell 127: 341-353.
104. Xu Y, Xing Y, Chen Y, Chao Y, Lin Z, et al. (2006) Structure of the protein phosphatase 2A holoenzyme. Cell 127: 1239-1251.
105. Arino J, Woon CW, Brautigan DL, Miller TB, Jr., Johnson GL (1988) Human liver phosphatase 2A: cDNA and amino acid sequence of two catalytic subunit isotypes. Proc Natl Acad Sci U S A 85: 4252-4256.

106. Green DD, Yang SI, Mumby MC (1987) Molecular cloning and sequence analysis of the catalytic subunit of bovine type 2A protein phosphatase. Proc Natl Acad Sci U S A 84: 4880-4884.
107. Hemmings BA, Adams-Pearson C, Maurer F, Muller P, Goris J, et al. (1990) alpha- and beta-forms of the 65-kDa subunit of protein phosphatase 2A have a similar 39 amino acid repeating structure. Biochemistry 29: 3166-3173.
108. Stone SR, Hofsteenge J, Hemmings BA (1987) Molecular cloning of cDNAs encoding two isoforms of the catalytic subunit of protein phosphatase 2A. Biochemistry 26: 7215-7220.
109. Bryant JC, Westphal RS, Wadzinski BE (1999) Methylated C-terminal leucine residue of PP2A catalytic subunit is important for binding of regulatory Balpha subunit. Biochem J 339 (Pt 2): 241-246.
110. Kloeker S, Bryant JC, Strack S, Colbran RJ, Wadzinski BE (1997) Carboxymethylation of nuclear protein serine/threonine phosphatase X. Biochem J 327 (Pt 2): 481-486.
111. Tolstykh T, Lee J, Vafai S, Stock JB (2000) Carboxyl methylation regulates phosphoprotein phosphatase 2A by controlling the association of regulatory B subunits. EMBO J 19: 5682-5691.
112. Wei H, Ashby DG, Moreno CS, Ogris E, Yeong FM, et al. (2001) Carboxymethylation of the PP2A catalytic subunit in Saccharomyces cerevisiae is required for efficient interaction with the B-type subunits Cdc55p and Rts1p. J Biol Chem 276: 1570-1577.
113. Yu XX, Du XX, Moreno CS, Green RE, Ogris E, et al. (2001) Methylation of the protein phosphatase 2A catalytic subunit is essential for association of B alpha regulatory subunit but not SG2NA, striatin, or polyomavirus middle tumor antigen. Molecular Biology of the Cell 12: 185-199.
114. Shi Y (2009) Serine/threonine phosphatases: mechanism through structure. Cell 139: 468-484.
115. Wlodarchak N, Xing Y (2016) PP2A as a master regulator of the cell cycle. Crit Rev Biochem Mol Biol 51: 162-184.
116. Low C, Quistgaard EM, Kovermann M, Anandapadamanaban M, Balbach J, et al. (2014) Structural basis for PTPA interaction with the invariant C-terminal tail of PP2A. Biol Chem 395: 881-889.
117. Lee JA, Pallas DC (2007) Leucine carboxyl methyltransferase-1 is necessary for normal progression through mitosis in mammalian cells. J Biol Chem 282: 30974-30984.
118. Chen J, Martin BL, Brautigan DL (1992) Regulation of protein serine-threonine phosphatase type-2A by tyrosine phosphorylation. Science 257: 1261-1264.
119. Evans DR, Hemmings BA (2000) Important role for phylogenetically invariant PP2Acalpha active site and C-terminal residues revealed by mutational analysis in Saccharomyces cerevisiae. Genetics 156: 21-29.
120. Chen J, Parsons S, Brautigan DL (1994) Tyrosine phosphorylation of protein phosphatase 2A in response to growth stimulation and v-src transformation of fibroblasts. J Biol Chem 269: 7957-7962.
121. Damuni Z, Xiong H, Li M (1994) Autophosphorylation-activated protein kinase inactivates the protein tyrosine phosphatase activity of protein phosphatase 2A. FEBS Lett 352: 311-314.

122. Ogris E, Gibson DM, Pallas DC (1997) Protein phosphatase 2A subunit assembly: the catalytic subunit carboxy terminus is important for binding cellular B subunit but not polyomavirus middle tumor antigen. Oncogene 15: 911-917.
123. Stanevich V, Jiang L, Satyshur KA, Li Y, Jeffrey PD, et al. (2011) The structural basis for tight control of PP2A methylation and function by LCMT-1. Mol Cell 41: 331-342.
124. Ikehara T, Ikehara S, Imamura S, Shinjo F, Yasumoto T (2007) Methylation of the C-terminal leucine residue of the PP2A catalytic subunit is unnecessary for the catalytic activity and the binding of regulatory subunit (PR55/B). Biochem Biophys Res Commun 354: 1052-1057.
125. Wei HJ, Ashby DG, Moreno CS, Ogris E, Yeong FM, et al. (2001) Carboxymethylation of the PP2A catalytic subunit in Saccharomyces cerevisiae is required for efficient interaction with the B-type subunits CDC55p and RTS1p. Journal of Biological Chemistry 276: 1570-1577.
126. Wu J, Tolstykh T, Lee J, Boyd K, Stock JB, et al. (2000) Carboxyl methylation of the phosphoprotein phosphatase 2A catalytic subunit promotes its functional association with regulatory subunits in vivo. EMBO J 19: 5672-5681.
127. Longin S, Jordens J, Martens E, Stevens I, Janssens V, et al. (2004) An inactive protein phosphatase 2A population is associated with methylesterase and can be re-activated by the phosphotyrosyl phosphatase activator. Biochem J 380: 111-119.
128. Guenin S, Schwartz L, Morvan D, Steyaert JM, Poignet A, et al. (2008) PP2A activity is controlled by methylation and regulates oncoprotein expression in melanoma cells: A mechanism which participates in growth inhibition induced by chloroethylnitrosourea treatment. International Journal of Oncology 32: 49-57.
129. Sablina AA, Hector M, Colpaert N, Hahn WC (2010) Identification of PP2A complexes and pathways involved in cell transformation. Cancer Res 70: 10474-10484.
130. Jiang L, Stanevich V, Satyshur KA, Kong M, Watkins GR, et al. (2013) Structural basis of protein phosphatase 2A stable latency. Nat Commun 4: 1699.
131. Fellner T, Lackner DH, Hombauer H, Piribauer P, Mudrak I, et al. (2003) A novel and essential mechanism determining specificity and activity of protein phosphatase 2A (PP2A) in vivo. Genes Dev 17: 2138-2150.
132. Guo F, Stanevich V, Wlodarchak N, Sengupta R, Jiang L, et al. (2014) Structural basis of PP2A activation by PTPA, an ATP-dependent activation chaperone. Cell Res 24: 190-203.
133. Cayla X, Goris J, Hermann J, Hendrix P, Ozon R, et al. (1990) Isolation and characterization of a tyrosyl phosphatase activator from rabbit skeletal muscle and Xenopus laevis oocytes. Biochemistry 29: 658-667.
134. Jordens J, Janssens V, Longin S, Stevens I, Martens E, et al. (2006) The protein phosphatase 2A phosphatase activator is a novel peptidyl-prolyl cis/trans-isomerase. J Biol Chem 281: 6349-6357.
135. Fischer G, Bang H, Mech C (1984) [Determination of enzymatic catalysis for the cis-trans-isomerization of peptide binding in proline-containing peptides]. Biomed Biochim Acta 43: 1101-1111.
136. Guasch A, Aranguren-Ibanez A, Perez-Luque R, Aparicio D, Martinez-Hoyer S, et al. (2015) Calcineurin Undergoes a Conformational Switch Evoked via Peptidyl-Prolyl Isomerization. PLoS One 10: e0134569.

137. Luo Y, Nie YJ, Shi HR, Ni ZF, Wang Q, et al. (2013) PTPA activates protein phosphatase-2A through reducing its phosphorylation at tyrosine-307 with upregulation of protein tyrosine phosphatase 1B. Biochim Biophys Acta 1833: 1235-1243.
138. Ballesteros I, Dominguez T, Sauer M, Paredes P, Duprat A, et al. (2013) Specialized functions of the PP2A subfamily II catalytic subunits PP2A-C3 and PP2A-C4 in the distribution of auxin fluxes and development in Arabidopsis. Plant J 73: 862-872.
139. Hu R, Zhu Y, Wei J, Chen J, Shi H, et al. (2017) Overexpression of PP2A-C5 that encodes the catalytic subunit 5 of protein phosphatase 2A in Arabidopsis confers better root and shoot development under salt conditions. Plant Cell Environ 40: 150-164.
140. Heidari B, Nemie-Feyissa D, Kangasjarvi S, Lillo C (2013) Antagonistic regulation of flowering time through distinct regulatory subunits of protein phosphatase 2A. PLoS One 8: e67987.
141. Ikehara T, Nakashima S, Nakashima J, Kinoshita T, Yasumoto T (2016) Efficient production of recombinant PP2A at a low temperature using a baculovirus expression system. Biotechnol Rep (Amst) 11: 86-89.
142. Ikehara T, Shinjo F, Ikehara S, Imamura S, Yasumoto T (2006) Baculovirus expression, purification, and characterization of human protein phosphatase 2A catalytic subunits alpha and beta. Protein Expr Purif 45: 150-156.
143. Kamibayashi C, Estes R, Lickteig RL, Yang SI, Craft C, et al. (1994) Comparison of heterotrimeric protein phosphatase 2A containing different B subunits. J Biol Chem 269: 20139-20148.
144. Czyzewicz N, Nikonorova N, Meyer MR, Sandal P, Shah S, et al. (2016) The growing story of (ARABIDOPSIS) CRINKLY 4. J Exp Bot 67: 4835-4847.
145. Egloff MP, Johnson DF, Moorhead G, Cohen PTW, Cohen P, et al. (1997) Structural basis for the recognition of regulatory subunits by the catalytic subunit of protein phosphatase 1. Embo Journal 16: 1876-1887.
146. Magnúsdóttir A (2008) Structural studies on PP2A and Methods in Protein Production

Figures

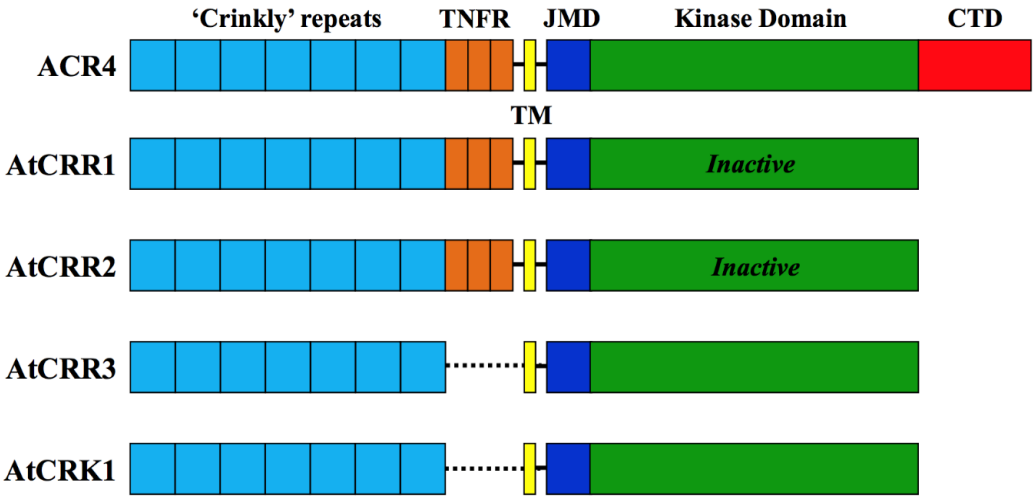

Figure 1: Diagram of conserved architecture ACR4 Receptor-like kinase family. Extracellular region consists of the 'Crinkly' repeats (light blue) and TNFR-like domain (orange). Intracellular region comprises of the juxta membrane domain (blue), kinase domain (green), and C-terminal domain (red). A transmembrane helix (yellow) connects the extracellular and intracellular portions of the protein. AtCRRs lack the CTD domain, TNFR-like domains are absent in AtCRR3 and AtCRK1. AtCRR1 and AtCRR2 are kinase inactive RLKs. *Diagram courtesy: Matthew Meyer*

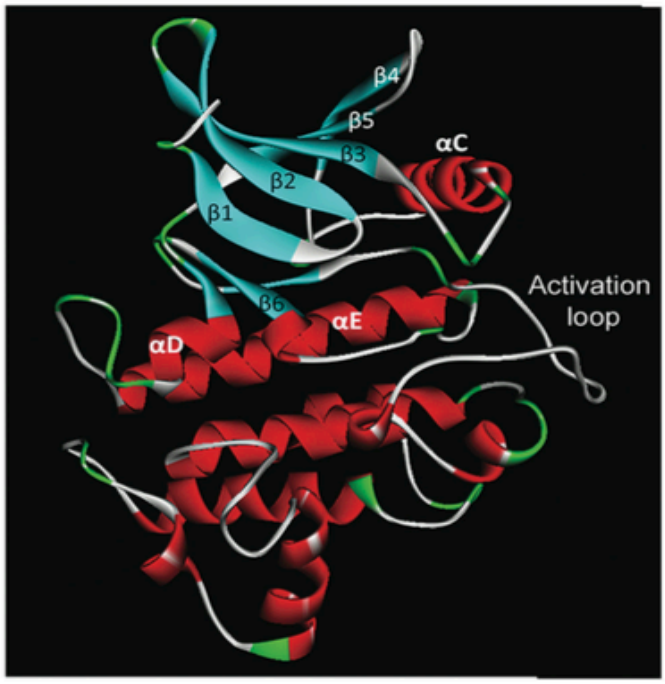

Figure 2: Structural organization of a kinase domain. The diagram represents a homology model of ACR4 kinase domain modeled after Interleukin-1 kinase domain. Kinase domain has a bilobal structure with N-lobe primarily composed of β sheet (blue) and C-lobe predominantly composed of α helical structure (red) [68,146].

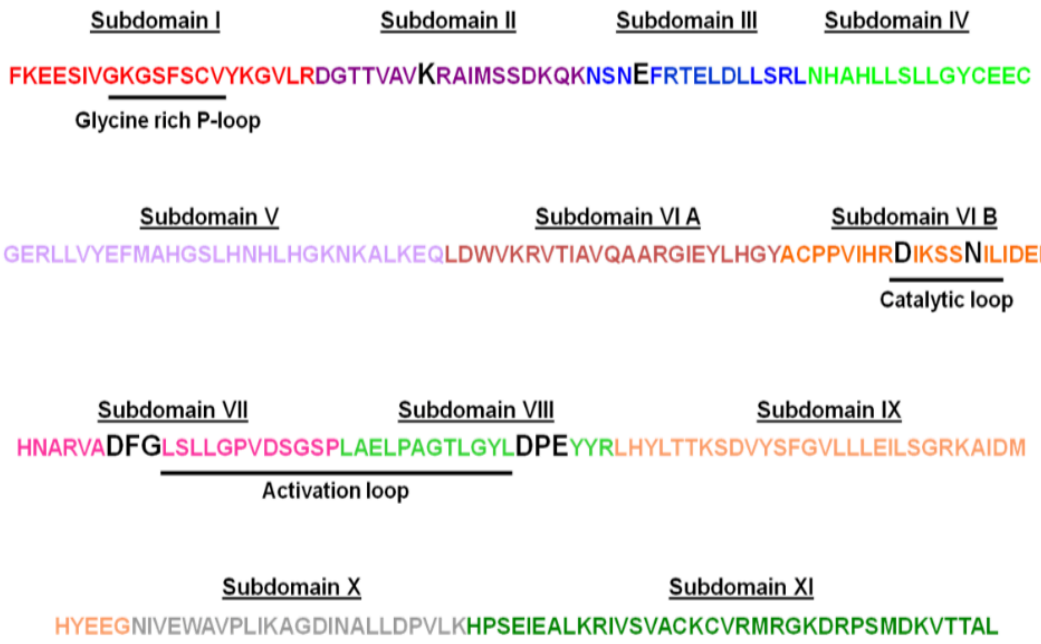

Figure 3: Diagram of ACR4 kinase subdomains. Each subdomain is represented in a different color. Catalytically important residues are highlighted in black (bold). Regions involved in kinase activation and catalysis are underlined in black (adapted from[68,146]

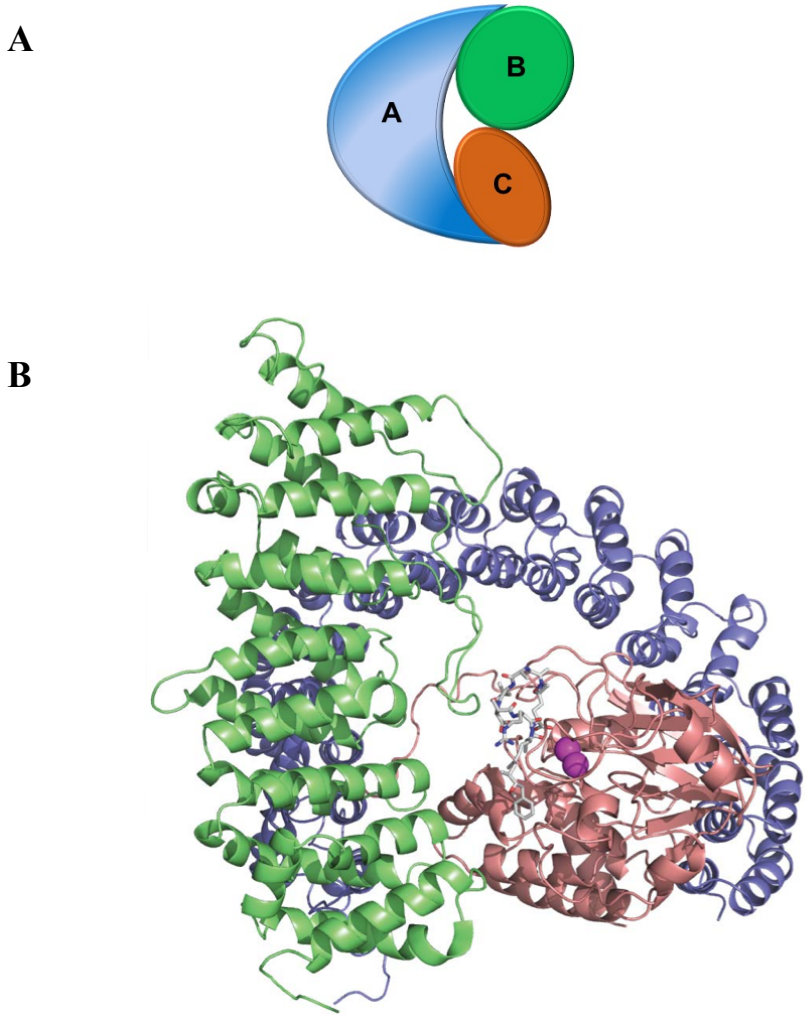

Figure 4: Overall structure of the heterotrimeric PP2A holoenzyme. **(A)** Simplistic cartoon of the heterotrimeric PP2A holoenzyme, with conserved A and C subunit and variable B regulatory subunit. **(B)** Crystal structure of human PP2A holoenzyme composed of Aα–B56c1–Cα with the scaffold Aα subunit (green), catalytic Cα subunit (blue) and, regulatory B56c1 subunit (orange) illustrated in the cartoon. Also present are two metal ions (purple) in the active site of C subunit and PP2A inhibitor microcystin is represented in sticks (adapted from [103]).

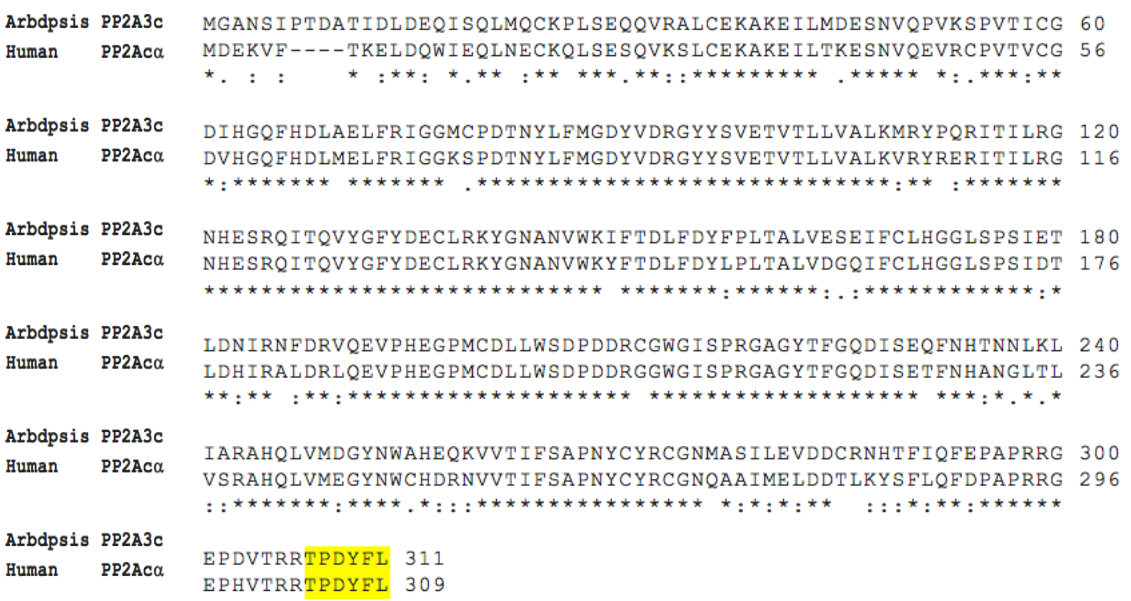

Figure 5: Multiple sequence alignment of the catalytic subunit sequence of *Arabidopsis* PP2A-3 isoform and Human PP2Ac α isoform. ∗ Indicate identical amino acid and : indicate similarity between amino acids. Highlighted yellow represents the carboxy-terminal conserved tail.

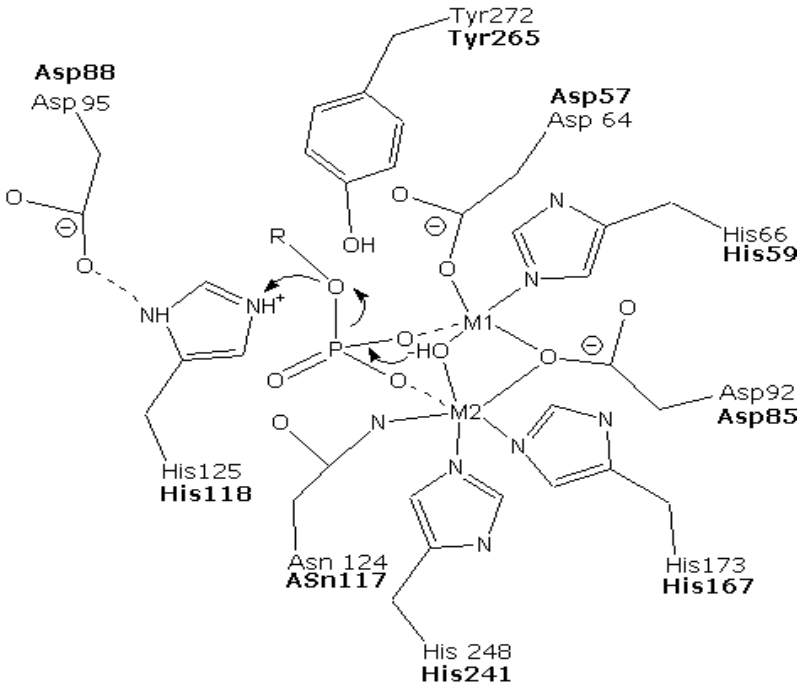

Figure 6: Diagram depicts the catalysis at the conserved active site of PPP phosphatase. Shown is the active site of PP1 [147] and the bold amino acids represent the corresponding conserved residues in PP2A. M1 and M2 are the two chelated metal ions at the active site coordinating the nucleophilic attack on the incoming phosphate group by the water molecule (adapted from [148]).

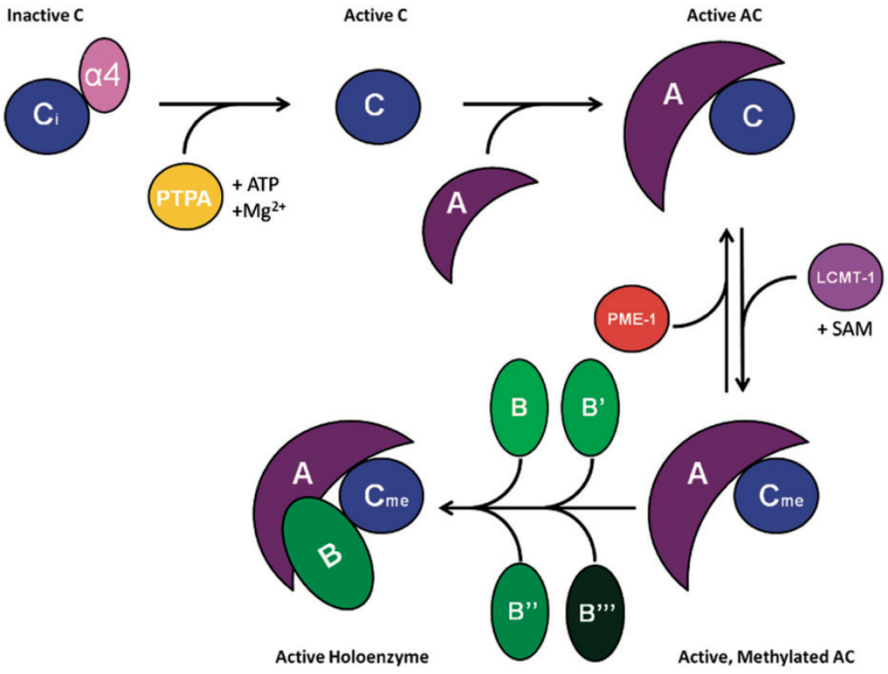

Figure 7: Schematic of a potential linear array towards biogenesis of active heterotrimeric PP2A. Shown is a mammalian PP2A holoenzyme. Inactive PP2Ac is regulated by α4. PTPA in presence of catalytic Mg^{2+} ions, and ATP activate the C subunit, which binds to scaffold A subunit. Activated AC core enzyme is reversibly methylated by LCMT-1and PME-1. Methylation then allows the interaction of one of the substrate specific regulatory B subunit forming the completely active heterotrimeric PP2A holoenzyme (adapted from [116])

CHAPTER 2: PP2A-3 INTERACTS WITH ACR4 AND REGULATES FORMATIVE CELL DIVISION IN THE ARABIDOPSIS ROOT

A paper published in the journal of Proceedings of National Academy of Sciences

[1]K.Y., P.S. and E.L.W. contributed equally to this work.

Kun YUE[a,b,1], Priyanka SANDAL[c,1], Elisabeth L. WILLIAMS[d,1], Evan MURPHY[d], Elisabeth STES[a,b,e,f], Natalia NIKONOROVA[a,b], Priya RAMAKRISHNA[d], Nathan CZYZEWICZ[d], Laura MONTERO MORALES[a,b], Robert KUMPF[a,b], Zhefeng LIN[d], Brigitte VAN DE COTTE[a,b], Mudassar IQBAL[g,#], Michiel VAN BEL[a,b], Eveline VAN DE SLIJKE[a,b], Matthew R. MEYER[h], Astrid GADEYNE[a,b], Cyril ZIPFEL[i], Geert DE JAEGER[a,b], Marc VAN MONTAGU[a,b,3], Daniël VAN DAMME[a,b], Kris GEVAERT[e,f], A. Gururaj RAO[c,2],Tom BEECKMAN[a,b,2], and Ive DE SMET[a,b,d,j,2,3]

[a]Department of Plant Systems Biology, VIB, B-9052 Ghent, Belgium.

[b]Department of Plant Biotechnology and Bioinformatics, Ghent UniversityB-9052 Ghent, Belgium.

[c]Roy J. Carver Department of Biochemistry, Biophysics and Molecular Biology, Iowa State University, Ames, Iowa 50011, United States.

[d]Division of Plant and Crop Sciences, School of Biosciences, University of Nottingham, Loughborough LE12 5RD, United Kingdom.

[e]Department of Medical Protein Research, VIB, B-9000 Ghent, Belgium

[f]Department of Biochemistry, Ghent University, B-9000 Ghent, Belgium

[g]Multidisciplinary Centre for Integrative Biology, School of Biosciences, University of Nottingham, Loughborough LE12 5RD, United Kingdom

[h]Department of Medicine, Washington University, School of Medicine, St. Louis, MO 63130, United States.

[i]The Sainsbury Laboratory, Norwich Research Park, Norwich, United Kingdom.

[j]Centre for Plant Integrative Biology, University of Nottingham, Loughborough LE12 5RD, United Kingdom

My Contributions

I contributed towards this study as a joint-first author, which involved performing all the *in-vitro* biochemical experiments. Mentioned below are my contributions towards this study:

1) Recombinantly cloned and established the protocol for expression and purification of catalytic subunit of *Arabidopsis* PP2A3c in *E. coli* system (Figure S11-S12)

2) Established the interaction between ICD of ACR4 and PP2A3c via *in vitro* studies such as pull down assays, overlay assays (Figure S3, B-E) and gel-filtration studies (Figure S3, F- K)

3) Performed radioactive kinase assay which provided the primary evidence of PP2A3c as a downstream substrate for ACR4 (Figure 3A, Figure S8)

4) Established the reciprocal regulatory interaction between ACR4 and PP2A3c, by performing a radioactive phosphatase assay and a non-radioactive Pro-Q-Diamond total phospho-stain assay, using human PP2Ac as a surrogate phosphatase (Figure 4A)

Other than performing the above definitive experiments which provided the basis for the *in-planta* studies, I have intellectually contributed towards analyzing the results and building up a model for the reciprocal interaction between ACR4 and PP2A3c, and, provided significant input towards corroborating the findings from all researchers towards development and writing of this paper.

Abstract

In plants, the generation of new cell types and tissues depends on coordinated and oriented formative cell divisions**.** The plasma membrane-localized receptor kinase ARABIDOPSIS CRINKLY 4 (ACR4) is part of a mechanism controlling formative cell divisions in the *Arabidopsis* root. Despite its important role in plant development, very little is known about the molecular mechanism ACR4 is affiliated to and its network of interactions. Here, we used various complementary proteomic approaches to identify ACR4-interacting protein candidates that are likely novel regulators of formative cell divisions and that could pave the way to unraveling the molecular basis behind ACR4-mediated signaling. We identified PROTEIN PHOSPHATASE 2A-3 (PP2A-3), a catalytic subunit of PP2A holoenzymes, as a novel regulator of formative cell divisions and as the first described substrate of ACR4. Our *in vitro* data argue for the existence of a tight post-translational regulation in the associated biochemical network through reciprocal regulation between ACR4 and PP2A-3 at the phosphorylation level.

Significance Statement

Plant growth and development are mediated through a wide range of proteins, including receptor kinases and phosphatases. The receptor kinase ACR4 is part of a mechanism controlling formative cell divisions in the *Arabidopsis* root. However, the regulation of ACR4 signaling and how it affects cell divisions remains completely unknown. We discovered that ACR4 phosphorylates the PP2A-3 catalytic subunit of the PP2A phosphatase holoenzyme, and that PP2A dephosphorylates ACR4. These data exposed a tightly regulated point in the associated biochemical network regulating formative cell divisions in plant roots.

Abbreviations

ACR4, *Arabidopsis* CRINKLY 4; AEBSF, 4-(2-Aminoethyl) benzenesulfonyl fluoride hydrochloride; ACN, acetonitrile; BRI1, brassinosteroid insensitive 1; BAK1, brassinosteroid associated kinase 1; CCR, crinkly4-related; CLE40, clavata3/embryo surrounding region 40*;* CLV, CLAVATA1; CORNET 2.0, Correlation network; DMSO, dimethyl sulfoxide; DTT, Dithiothreitol; FA, formic acid; FH6, formin homolog 6; eFP, electronic fluorescent pictographic; GO, Gene Ontology; GFP, green fluorescent protein; GST, glutathione s-transferase; HA, hemagglutinin; HTPA, hydroxy-tetrahydrodipicolinate; ICD, intracellular domain; $mACR4^{ICD}$, inactive mutant; MALDI, matrix assisted laser desorption ionization; PP2A, protein phosphatase A; PVDF, polyvinylidene fluoride; PTB, polypyrimidine-tract binding protein; RT, room temperature; *rcn,* root curls in naphthylphthalamic acid1; TAP, tandem affinity purification; TOF, time of flight; WOX5, wuschel related homeobox 5, Y2H- yeast two hybrid, YFP, yellow fluorescent protein.

Introduction

Plants rely on coordinated formative cell division for the formation of new cell types and tissues (1). For example, in the *Arabidopsis* root, the development of columella cells requires a tight coordination of formative cell division and differentiation (1). In the primary root apical meristem, columella stem cells − upon formative cell division − give rise to new stem cells and daughter cells that will differentiate (2) (Figure. S1 A). Several plant hormones and proteins that play a role in this process have been identified, and small regulatory networks have been proposed (3-11). However, our knowledge on the

mechanisms and signaling networks mediating formative cell divisions is sparse and is largely derived from transcriptional data (12).

Reversible protein phosphorylation represents a major mechanism regulating cell signaling (13), and several kinases have been shown to play a role in primary root development (5, 6, 14). For example, the evolutionarily conserved plasma membrane-localized receptor-like kinase *Arabidopsis* CRINKLY 4 (ACR4) marks the plasma membrane in the primary root tip columella and is part of a mechanism controlling formative cell divisions in the *Arabidopsis* root (5, 15, 16). ACR4 possesses an extracellular ligand binding domain, a transmembrane helix, and an intracellular domain that contains the juxta membrane and the C-terminal subdomains, which flank the core kinase domain with serine/threonine kinase activity (Figure 1 A). The intracellular juxta membrane domain is a likely recruitment site for interacting proteins and essential to facilitate downstream signaling (17, 18). ACR4 is expressed throughout plant development in specific cells and tissues, such as protoderm, columella and stage I lateral roots, and ACR4 preferentially localizes at plasmodesmata (15, 19-21). In addition to its primary and lateral root phenotypes, *Arabidopsis* loss-of-function *acr4* mutants are affected in maintaining epidermal cell identity, including disorganized cell layers in the ovule integument (19, 21). Although ACR4 was the first receptor kinase to be assigned a role in root development (5), our knowledge about its signaling pathway in the root remains limited (15, 22).

In addition to post-translational modifications such as phosphorylation, developmental programs and cellular functions largely rely on interactions between proteins, forming complex networks to control biological processes (23). While membrane

proteins play a crucial role in many biological processes, knowledge of the *in-planta* membrane interactome is limited (23). Notwithstanding the recent progress with respect to global analyses of membrane protein interactions, so far ACR4 was not represented in a membrane-linked *Arabidopsis* interactome (24). Therefore, the objective of this study was to use ACR4-centered, protein-focused systems biology approaches to gain insight into the ACR4 signaling cascade and to identify new potential regulators of formative cell division.

Results and Discussion

Mapping putative ACR4 interactions.

To identify novel regulators of formative cell division in *Arabidopsis*, we combined *in silico*, tandem affinity purification (TAP), yeast two-hybrid (Y2H), and phage display approaches to define potential ACR4-interacting proteins. Given the technical difficulties associated with plasma membrane proteins, we focused on intracellular ACR4 domains for our *in vitro* and *in vivo* studies (Figure. 1 A). We first interrogated available protein-protein interaction (PPI) databases for experimental and predicted interactions by applying the PPI tool within CORNET 2.0 (25) to ACR4 (AT3G59420). This resulted in a network with 85 nodes which mainly lacked experimental validation (Figure. S2 and SI Appendix). Second, we applied a TAP approach to *Arabidopsis* cell suspension cultures expressing the N- or C-terminally tagged ACR4 intracellular kinase domain (Figure. 1 A and Figure. S3). This analysis resulted in 4 putative ACR4-interacting proteins, of which 2 occurred in at least 2 biological replicates and in both assays with N- and C-terminally tagged ACR4 intracellular kinase domain, and were not present in any *in house* background list, namely 4-HYDROXY-TETRAHYDRODIPICOLINATE REDUCTASE 1 (HTPA REDUCTASE 1/DAPB1; AT2G44040) and HTPA REDUCTASE 2/DAPB2 (AT3G59890) (SI

Appendix). Based on TAP data alone, two other candidates, PROTEIN PHOSPHATASE 2A-3 (PP2A-3; AT2G42500) and PP2A-4 (AT3G58500), could not be conclusively identified as *bona fide* ACR4-interacting proteins as they were only detected in one technical repeat. Third, we applied a conventional high throughput Y2H assay to screen for potential interactions with the ACR4 intracellular domain (Figure. 1 A). This revealed 4 potential ACR4-interacting proteins with high confidence (SI Appendix). Finally, we screened a synthetic 15-mer peptide encompassing the Ser^{475} phosphorylation site within the intracellular juxta membrane domain of ACR4 (Figure. 1 A) against a 21-amino acid phage-peptide library (26, 27). When the resulting consensus binding motifs for the phosphorylated peptide were queried against the *Arabidopsis* protein database, over 4000 potential ACR4-interacting proteins were identified (SI Appendix). Taken together, our complementary approaches identified several putative ACR4-interacting proteins, but when we searched for overlap between the different approaches this was limited to absent (SI Appendix). This could mean that different approaches yielded different subsets of putative ACR4-interacting proteins or that we picked a large number of likely false-positives. *In silico* quality assessment of putative ACR4 interactions. To increase the confidence in the potential ACR4-interacting proteins listed in *SI Appendix* and to select candidates for functional analyses, we performed in depth *in silico* quality assessment. Correlated gene expression is an indicator of co-functionality of genes incommon pathways and processes (28), and interacting proteins are often significantly co-expressed. First, we used CORNET 2.0 (25) to globally explore co-expression of ACR4 and genes encoding potential ACR4-interacting proteins, which showed some co-expression (Pearson correlation coefficient > 0.55) between ACR4 and some CORNET (2/85) and phage

display hits (44/4402) (*SI Appendix*). Second, to further support potential PPIs in the root tip and during lateral root initiation, we used available cell- and tissue-specific transcript profiling datasets (5, 29). Visualization of root tip *in silico* expression patterns for TAP (3/4) and Y2H candidates (2/4) through the BAR Arabidopsis eFP Browser (30), revealed distinct expression patterns that, at least partially, overlapped with the *ACR4* expression domain (Figure. S2). In addition, some of the CORNET (8/85) and PHAGE DISPLAY candidates (360/4402) were – similar to *ACR4* – also transcriptionally differentially regulated in a transcriptome study of pericycle cells undergoing lateral root initiation (5) (*SI Appendix*). Based on the above observations, we generated a priority list for CORNET, TAP, Y2H and PHAGE DISPLAY hits, narrowing down the number of candidates from 4495 to 525 (*SI Appendix*). Next, to globally assess interactions between ACR4 and potential interacting proteins, we used the PPI tool within CORNET 2.0 (25). Indeed, several of the CORNET, Y2H, TAP and prioritized PHAGE DISPLAY hits are connected with ACR4 and with each other in predicted and experimentally validated protein-protein interaction networks focusing on pairwise interactions (*SI Appendix*). To gain insight in the molecular functions represented in this protein-protein interaction network, we determined that several statistically overrepresented Gene Ontology (GO) categories with respect to biological process (5%) and molecular function (5%) were related to phosphorylation (*SI Appendix*), which is in agreement with the fact that ACR4 is a receptor kinase. Taken together, through our *in-silico* assessment we increased the confidence in a subset of potential ACR4-interacting proteins (*SI Appendix*). However, our dataset is not necessarily comprehensive, as, for example, WUSCHEL RELATED HOMEOBOX 5 (WOX5),

CRINKLY4-RELATED (CCR) proteins, and CLAVATA1 (CLV1), which were shown to interact with ACR4 (15, 31), were not retained.

ACR4 interacts with PP2A-3.

Taking the results of *SI Appendix* into account allowed us to impose additional criteria to select candidates for functional analyses. Among the candidates selected by at least two approaches and with a high score in the priority list (*SI Appendix*), we retrieved sequences that match PP2A-3 and/or PP2A-4, which are isoforms of catalytic PP2A C subunits and that form a subclade in the family of 5 *Arabidopsis* PP2A C subunits (32). In general, the PP2A heterotrimeric holoenzyme, which is a major, highly conserved eukaryotic serine/threonine phosphatase, consists of a catalytic C subunit, a type A scaffolding/regulatory subunit, and a type B regulatory subunit (33). In *Arabidopsis*, PP2A phosphatases have been implicated in various hormone-regulated, cellular and developmental processes, including spatial control of cell division and columella organization, and in innate immunity, but little is known about their dynamic and highly regulated function (34-37). In the context of our focus on formative cell division, we selected PP2A-3 (and PP2A-4) for subsequent in depth functional characterization. First, an overlay assay indicated that PP2A-3 can specifically interact with both the naïve ACR4 intracellular domain ($ACR4^{ICD}$) (endogenously phosphorylated at a limited number of residues in *E. coli* through an unknown mechanism) and fully *in vitro* auto phosphorylated $ACR4^{ICD}$ (26) (Figure. S3 and *SI Supplemental Notes*). Second, gel-filtration analyses further confirmed the interaction between the ACR4 intracellular domain ($ACR4^{ICD}$) and PP2A-3 (Figure. S3 and *SI Supplemental Notes*). Subsequently, the purified recombinant MBP: $ACR4^{ICD}$ was effectively pulled down with GST: PP2A-3 *in vitro* (Figure. 1 *B*).

Moreover, in *Nicotiana benthamiana* transient expression assays, ACR4: YFP: HA was able to co-immunoprecipitate FLAG: PP2A-3 *in planta* (Fig. 1 *C*). Taken together, these data strongly indicate that ACR4 and PP2A-3 interact with each other.

ACR4 and PP2A-3 are co-expressed.

As mentioned above, *Arabidopsis* eFP Browser data suggested that *PP2A-3* is weakly expressed in columella stem cells and in the root apical meristem (Figure. S2). To confirm this, we analyzed seedlings expressing a *pPP2A-3::n3xGFP* fusion and assessed expression in the root tip. In 5 independent transformants we indeed observed *pPP2A-3:n3xGFP* expression in the root tip, but *PP2A-3* was more broadly expressed than *ACR4* (5) (Figure. 2 *A* and Figure. S1). In addition, we observed *PP2A-3* expression during early lateral root initiation (Figure. S1), which also overlapped with *ACR4* expression at this stage (5) (Figure. S1). Taken together, these results show that *ACR4* and *PP2A-3* are expressed in overlapping domains, further supporting that they can physically interact.

PP2A-3 is involved in columella stem cell differentiation.

To test genetically if PP2A-3 plays a role in ACR4-mediated stem cell regulation, we analyzed primary root length and columella stem cell differentiation in a previously characterized *pp2a-3* mutant (36). The primary root of *pp2a-3* is slightly longer than wild type (Figure. 2 *B-C*). With respect to columella stem cell differentiation, we observed less differentiation in *pp2a-3* compared to wild type, which is similar to *acr4* (Figure. 2 *D-E*). However, since such a columella phenotype can also be explained by altered auxin distribution, levels or response (11), the similarity between the *pp2a-3* and *acr4* mutants does not provide conclusive support for a genetic and/or physical interaction. This is especially relevant since PP2A-3 has been shown to play a role in auxin transport (38). We

therefore tested to what extent *acr4* and *pp2a-3* are affected in their sensitivity to NPA with respect to primary root length and columella differentiation. In these assays, *acr4* and *pp2a-3* appeared equally sensitive to NPA treatment as Col-0 (Fig. S4), suggesting that there is no apparent auxin transport-mediated effect in this case. The genetic interaction between ACR4 and PP2A-3 was further supported by the *acr4 pp2a-3* double mutant, where we could not record an additive effect arguing both are active in the same pathway (Figure. 2 *D-E*). Although we cannot rule out cell-specific changes, we have excluded that the similarities in phenotype are due to a broad differential regulation of *ACR4* or *PP2A-3* expression in *pp2a-3* and *acr4* mutants, respectively (Figure. S5). Taken together, our observations indicate a role for PP2A-3 in cellular patterning during primary root development that overlaps with ACR4 function, and further suggest that this is possibly independent of an affected auxin transport capacity.

PP2A-3 and PP2A-4 redundantly affect primary root growth.

Given that PP2A-4 is closely related to PP2A-3, we explored possible redundancy with respect to primary root growth. Indeed, a double *pp2a-3 pp2a-4* mutant displayed a short primary root, further reduced columella differentiation and severely disrupted cell organization in the root tip compared to wild type (Figure. 2 *B-E*) (36). However, this double mutant phenotype appeared to be less severe than the one obtained by Ballesteros and co-workers (38), which is possibly due to the use of different T-DNA lines. Short root phenotypes associated with disrupted cell division and/or cellular patterning in the root tip are often associated with a loss of quiescent center cell identity (39, 40). To assess if the quiescent center was absent in the disrupted root tip of *pp2a-3 pp2a-4,* we analyzed the expression of the quiescent center marker *QC184* (7). Surprisingly, notwithstanding the

dramatic impact on the regular cellular pattern in the root tip, *QC184* expression was not abolished, and even appeared to expand into the columella (Figure. 2 *F*). The latter might suggest that the stemness gradient in *pp2a-3 pp2a-4* is perturbed. Furthermore, we applied cantharidin – an inhibitor of PP2A and PP2A-related phosphatases (*SI Supplemental Notes*) – to the *QC184* and *pWOX5::GUS* markers (7), demonstrating that quiescent center identity is not lost when interfering with PP2A activity (Figure. 2 *G* and Figure. S6). Interestingly, *WOX5* expression was shown to be similarly affected in the *clavata3/embryo surrounding region 40* (*cle40*) mutant, and ACR4 was identified as a target of CLE40 signaling (15, 22), further corroborating the potential connection between PP2A and ACR4. Next, evaluating sensitivity to cantharidin with respect to primary root growth revealed that *acr4* is equally sensitive to cantharidin treatment as *pp2a-3*, and both are not significantly more sensitive than the control (Figure. S7). We furthermore established that cantharidin does not negatively affect *ACR4* expression levels, and observed a similar (minor) up-regulation as in *pp2a-3 pp2a-4* (Fig. S5). Taken together, these results further suggest that ACR4 and PP2A-3 act in the same pathway.

ACR4 phosphorylates PP2A-3.

PP2A activity and function in eukaryotic cells is regulated via post-translational modification of PP2A subunits (41). For example, PP2A complex assembly depends on the phosphorylation status of the catalytic subunit and phosphorylation of protein phosphatases has been shown to inactivate the enzyme (41, 42), but this has not been demonstrated in plants. To evaluate if ACR4 affects the phosphorylation status of PP2A-3, we compared the phospho-proteomes of Col-0 and *acr4* seedlings. However, although we could detect a peptide (NH_3-GAGYTFGQDISEQFNHTNNLK-COOH) for PP2A-3 (or

PP2A-4) in all samples, we did not observe any (differential) phosphorylation. Since PP2A holoenzymes act in various pathways (37, 38, 43, 44) and since ACR4 only acts in a few cells, it is likely that subtle differences mediated by ACR4 could be masked. Therefore, we explored if PP2A-3 could be phosphorylated by ACR4 *in vitro*. Indeed, *in vitro* kinase assays demonstrated that purified recombinant auto phosphorylated SUMO: $ACR4^{ICD}$, but not a mutant inactive version of $ACR4^{ICD}$ with K540A and D641A amino acid exchanges ($mACR4^{ICD}$), could phosphorylate purified recombinant PP2A-3 (PP2A-3::6xHIS) (Figure. 3 *A*). Subsequently, we identified the ACR4-dependent PP2A-3 phosphosites from the *in vitro* kinase assay using high resolution mass spectrometry analyses. This revealed a total of 9 – so far unknown – phosphorylated residues of which five are at Ser, three are at Thr and one is at Tyr (Figure. S8 and *SI Appendix*). Mapping these sites on a three-dimensional homology model of *Arabidopsis* PP2A-3, based on the structure of the catalytic chain within the trimeric human PP2A enzyme, showed that these residues were predominantly solvent exposed even in the trimer structure and, therefore, quite likely accessible for phosphorylation by ACR4 (Figure. S8 and *SI Appendix*). Taken together, our results pinpoint PP2A-3 as a substrate for ACR4 kinase activity. Phosphorylation of the tail of the PP2A catalytic subunit plays an important role in regulating the assembly – and thus activity – of PP2A holoenzymes (41). We therefore explored PP2A activity in cellular extracts prepared from *acr4* seedlings using a PP2A phosphatase assay system (37, 45, 46). In our hands, this revealed a decrease in PP2A activity of about 19% in *acr4* compared to wild type, which was similar to that associated with the PP2A regulatory subunit mutant *rcn1* (22%) and the catalytic subunit mutant *pp2a-3* (16%) (Figure. 3 *B*). Although the results did not achieve statistical significance (p-value for *acr4* = 0.083), likely because the

ACR4 impact on PP2A activity is diluted, they are reproducible and suggestive of ACR4 being required for some of the cellular PP2A activity.

PP2A-3 dephosphorylates ACR4.

With respect to receptor kinases, PP2A has been shown to modulate the phosphostatus of BRI1 and the co-receptor BAK1 (37, 47, 48), so we also evaluated if PP2A-3 is capable to dephosphorylate ACR4. First, using *E. coli*-expressed PP2A-3 in a phosphatase assay did not yield a convincing difference with respect to dephosphorylation of $ACR4^{ICD}$ (Figure. S8 and *SI Supplemental Notes*). Therefore, to determine whether ACR4 could be a substrate of PP2A, we used – in accordance with Wu and colleagues (47) – a purified, active human PP2A to dephosphorylate the $ACR4^{ICD}$ that had been phosphorylated *in vitro*. This demonstrated PP2A-mediated dephosphorylation of the phosphorylated $ACR4^{ICD}$ (Figure. 4 *A*), and pinpoints ACR4 as a substrate for PP2A phosphatase activity. To assess the biological importance of altering the PP2A-mediated phosphorylation status of ACR4, we analyzed ACR4: GFP in the root of the *pp2a-3 pp2a-4* double mutant. This revealed a weak GFP signal in *pp2a-3 pp2a-4*, with reduced membrane localization, as compared to the control (Figure. 4 *B*), which is likely not due to a change in *ACR4: GFP* expression levels (Figure. S5). To explore this, further, we investigated ACR4: GFP in the presence of the PP2A inhibitor cantharidin. This revealed a reduced membrane association of ACR4: GFP upon inhibiting PP2A activity within 5 hours, while the membrane localization of the routinely used membrane marker FORMIN HOMOLOG 6 (FH6): GFP (49), was largely unaffected (Figure. 4 *C-D* and Figure. S9). Overall, these results suggest that membrane localization of ACR4 is dependent on PP2A-3 (and potentially PP2A-4).

Conclusions

Interactions between membrane-associated proteins and soluble proteins are essential for signal transduction and for regulating plant growth and development. Here, we used various approaches to generate a prioritized list of potential ACR4-interacting proteins that are possibly involved in formative cell division, cell-to-cell communication and root development. Taking all our interaction data together and since there is limited to no overlap between the different approaches, it seems that to study protein-protein interactions the use of multiple approaches is preferred as each technique seems to expose a distinct subset of potential interactors and can increase confidence in some potential interactors that would otherwise be discarded. Starting from the prioritized, potential ACR4-interacting candidates, we identified PP2A-3 as the first described ACR4 substrate and showed that PP2A-3 plays an important role in the control of columella stem cell divisions and/or differentiation. Previously, it was shown that PP2A complexes associate with membranes in growing seedlings and that PP2A may interact with plasma membrane components (35, 43). Similar to the PP2A effect on BRI1 where dephosphorylated BRI1 is internalized (47, 48) and on BAK1 (37), we showed that PP2A can dephosphorylate ACR4. In this context, we also showed that PP2A activity affects the membrane localization of ACR4. The resemblance of the *acr4* and *pp2a-3* columella stem cell phenotype, together with the cell biological data, suggest that PP2A acts as a positive regulator of ACR4 function and that it is the dephosphorylated form of the ACR4 protein that is localized to the plasma membrane and functional. On the basis of the available data, we propose a tentative model whereby on the one hand ACR4 phosphorylates the PP2A-3 catalytic subunit of the PP2A holoenzyme, possible facilitating complex assembly, and on

the other hand, PP2A dephosphorylates ACR4, regulating its membrane localization and possibly activity (Figure. S10). The balance between these two likely affects formative cell divisions and cell differentiation in the root, and as such ACR4 and/or PP2A appear to control their own activity. In future, it will be important to characterize the importance of the individual ACR4 and PP2A-3 phosphosites, and evaluate these in the context of ACR4 localization and/or activity and PP2A activity and/or complex assembly, respectively. Here, it should be taken into account that, for example in brassinosteroid signaling, PP2A type B subunits usually recruit substrates and regulate their activity (44, 50) and that membrane localization of PP2A C subunits is regulated by methylation and in turn impacts target dephosphorylation (47).

Acknowledgements

We thank Jelle Van Leene, Remco Sprangers, Debbie Rombaut and Dominique Eeckhout for experimental assistance and useful suggestions, Hyun-Sook Pai for the FLAG: PP2A-3 construct, Dr. Yasufumi Yamamoto for constructing the random 21-amino acid phage-peptide library, and R. Reid Townsend and the Proteomics Core Lab at Washington University for mass spectrometry analysis. This work was supported by a BBSRC David Phillips Fellowship (BB_BB/H022457/1) and a Marie Curie European Reintegration Grant (PERG06-GA-2009-256354) to I.D.S., a BBSRC CASE Studentship co-funded by Bayer Crop Science to N.C., and a BBSRC funded position (BB/I001875/1) to M.I. We thank the School of Biosciences for studentship funding and acknowledge the University of Nottingham research committee. The VIB Bio Imaging Core acquired the Zeiss LSM780 through a CLEM-grant from Minister Lieten. Work in the laboratory of T.B. was financed by the Interuniversity Attraction Poles Programme IUAP P7/29

‘MARS’ from the Belgian Federal Science Policy Office and by a grant of the Research Foundation Flanders (FWO G027313N). E.S. is a Postdoctoral Fellow of the Research Foundation-Flanders (FWO13/PDO/144).

References

1. De Smet I & Beeckman T (2011) Asymmetric cell division in land plants and algae: the driving force for differentiation. *Nat Rev Mol Cell Biol* 12(3):177-188.
2. Scheres B (2007) Stem-cell niches: nursery rhymes across kingdoms. *Nat Rev Mol Cell Biol* 8(5):345-354.
3. Aida M*, et al.* (2004) The PLETHORA genes mediate patterning of the Arabidopsis root stem cell niche. *Cell* 119(1):109-120.
4. Wildwater M*, et al.* (2005) The RETINOBLASTOMA-RELATED gene regulates stem cell maintenance in Arabidopsis roots. *Cell* 123(7):1337-1349.
5. De Smet I*, et al.* (2008) Receptor-like kinase ACR4 restricts formative cell divisions in the Arabidopsis root. *Science* 322(5901):594-597.
6. Stahl Y*, et al.* (2013) Moderation of Arabidopsis Root Sternness by CLAVATA1 and ARABIDOPSIS CRINKLY4 Receptor Kinase Complexes. *Curr Biol* 23(5):362-371.
7. Sarkar AK*, et al.* (2007) Conserved factors regulate signalling in Arabidopsis thaliana shoot and root stem cell organizers. *Nature* 446(7137):811-814.
8. Stahl Y, Wink RH, Ingram GC, & Simon R (2009) A signaling module controlling the stem cell niche in Arabidopsis root meristems. *Curr Biol* 19(11):909-914.
9. Zhang H*, et al.* (2010) ABA promotes quiescence of the quiescent centre and suppresses stem cell differentiation in the Arabidopsis primary root meristem. *Plant J* 64(5):764-774.
10. Azpeitia E, Weinstein N, Benitez M, Mendoza L, & Alvarez-Buylla ER (2013) Finding Missing Interactions of the Arabidopsis thaliana Root Stem Cell Niche Gene Regulatory Network. *Front Plant Sci* 4:110.
11. Ding Z & Friml J (2010) Auxin regulates distal stem cell differentiation in Arabidopsis roots. *Proc Natl Acad Sci USA* 107(26):12046-12051.
12. Kajala K*, et al.* (2014) Omics and modelling approaches for understanding regulation of asymmetric cell divisions in arabidopsis and other angiosperm plants. *Ann Bot* 113(7):1083-1105.
13. Choudhary C & Mann M (2010) Decoding signalling networks by mass spectrometry-based proteomics. *Nat Rev Mol Cell Biol* 11(6):427-439.
14. Van Damme D*, et al.* (2011) Arabidopsis alpha Aurora kinases function in formative cell division plane orientation. *Plant Cell* 23(11):4013-4024.
15. Stahl Y*, et al.* (2013) Moderation of Arabidopsis root stemness by CLAVATA1 and ARABIDOPSIS CRINKLY4 receptor kinase complexes. *Curr Biol* 23(5):362-371.
16. Nikonorova N, Vu LD, Czyzewicz N, Gevaert K, & De Smet I (2015) A phylogenetic approach to study the origin and evolution of the CRINKLY4 family. *Front Plant Sci* 6:880.

17. Jones RB, Gordus A, Krall JA, & MacBeath G (2006) A quantitative protein interaction network for the ErbB receptors using protein microarrays. *Nature* 439(7073):168-174.
18. Schulze WX, Deng L, & Mann M (2005) Phosphotyrosine interactome of the ErbB-receptor kinase family. *Mol Syst Biol* 1:2005.0008.
19. Gifford ML, Dean S, & Ingram GC (2003) The Arabidopsis ACR4 gene plays a role in cell layer organisation during ovule integument and sepal margin development. *Development* 130(18):4249-4258.
20. Tanaka H*, et al.* (2002) ACR4, a putative receptor kinase gene of Arabidopsis thaliana, that is expressed in the outer cell layers of embryos and plants, is involved in proper embryogenesis. *Plant Cell Physiol* 43(4):419-428.
21. Watanabe M, Tanaka H, Watanabe D, Machida C, & Machida Y (2004) The ACR4 receptor-like kinase is required for surface formation of epidermis-related tissues in Arabidopsis thaliana. *Plant J* 39(3):298-308.
22. Stahl Y, Wink RH, Ingram GC, & Simon R (2009) A signaling module controlling the stem cell niche in Arabidopsis root meristems. *Curr Biol* 19(11):909-914.
23. Bassel GW*, et al.* (2012) Systems analysis of plant functional, transcriptional, physical interaction, and metabolic networks. *Plant Cell* 24(10):3859-3875.
24. Jones AM*, et al.* (2014) Border control--a membrane-linked interactome of Arabidopsis. *Science* 344(6185):711-716.
25. De Bodt S, Hollunder J, Nelissen H, Meulemeester N, & Inze D (2012) CORNET 2.0: integrating plant coexpression, protein-protein interactions, regulatory interactions, gene associations and functional annotations. *New Phytol* 195(3):707-720.
26. Meyer MR, Lichti CF, Townsend RR, & Rao AG (2011) Identification of in vitro autophosphorylation sites and effects of phosphorylation on the Arabidopsis CRINKLY4 (ACR4) receptor-like kinase intracellular domain: insights into conformation, oligomerization, and activity. *Biochemistry* 50(12):2170-2186.
27. Meyer MR, Shah S, & Rao AG (2013) Insights into molecular interactions between the juxtamembrane and kinase subdomains of the Arabidopsis Crinkly-4 receptor-like kinase. *Arch Biochem Biophys*535(2):101-110.
28. Wolfe CJ, Kohane IS, & Butte AJ (2005) Systematic survey reveals general applicability of "guilt-by-association" within gene coexpression networks. *BMC Bioinformatics* 6:227.
29. Brady SM*, et al.* (2007) A high-resolution root spatiotemporal map reveals dominant expression patterns. *Science* 318(5851):801-806.
30. Winter D*, et al.* (2007) An "Electronic Fluorescent Pictograph" Browser for Exploring and Analyzing Large-Scale Biological Data Sets. *PLoS One* 2(8).
31. Meyer MR, Shah S, Zhang J, Rohrs H, & Rao AG (2015) Evidence for intermolecular interactions between the intracellular domains of the arabidopsis receptor-like kinase ACR4, its homologs and the Wox5 transcription factor. *PloS One* 10(3):e0118861.
32. Farkas I, Dombradi V, Miskei M, Szabados L, & Koncz C (2007) Arabidopsis PPP family of serine/threonine phosphatases. *Trends Plant Sci* 12(4):169-176.
33. Terol J, Bargues M, Carrasco P, Perez-Alonso M, & Paricio N (2002) Molecular characterization and evolution of the protein phosphatase 2A B' regulatory subunit family in plants. *Plant Physiol* 129(2):808-822.

34. Uhrig RG, Labandera AM, & Moorhead GB (2013) Arabidopsis PPP family of serine/threonine protein phosphatases: many targets but few engines. *Trends Plant Sci* 18(9):505-513.
35. Blakeslee JJ*, et al.* (2008) Specificity of RCN1-mediated protein phosphatase 2A regulation in meristem organization and stress response in roots. *Plant Physiol* 146(2):539-553.
36. Spinner L*, et al.* (2013) A protein phosphatase 2A complex spatially controls plant cell division. *Nat Commun* 4:1863.
37. Segonzac C*, et al.* (2014) Negative control of BAK1 by protein phosphatase 2A during plant innate immunity. *EMBO J* 33(18):2069-2079.
38. Ballesteros I*, et al.* (2013) Specialized functions of the PP2A subfamily II catalytic subunits PP2A-C3 and PP2A-C4 in the distribution of auxin fluxes and development in Arabidopsis. *Plant J* 73(5):862-872.
39. Sabatini S, Heidstra R, Wildwater M, & Scheres B (2003) SCARECROW is involved in positioning the stem cell niche in the Arabidopsis root meristem. *Genes Dev* 17(3):354-358.
40. Ueda M*, et al.* (2004) The HALTED ROOT gene encoding the 26S proteasome subunit RPT2a is essential for the maintenance of Arabidopsis meristems. *Development* 131(9):2101-2111.
41. Janssens V, Longin S, & Goris J (2008) PP2A holoenzyme assembly: in cauda venenum (the sting is in the tail). *Trends Biochem Sci* 33(3):113-121.
42. Janssens V & Goris J (2001) Protein phosphatase 2A: a highly regulated family of serine/threonine phosphatases implicated in cell growth and signalling. *Biochem J* 353(Pt 3):417-439.
43. Michniewicz M*, et al.* (2007) Antagonistic regulation of PIN phosphorylation by PP2A and PINOID directs auxin flux. *Cell* 130(6):1044-1056.
44. Tang W*, et al.* (2011) PP2A activates brassinosteroid-responsive gene expression and plant growth by dephosphorylating BZR1. *Nat Cell Biol* 13(2):124-131.
45. Chen J, Hu R, Zhu Y, Shen G, & Zhang H (2014) Arabidopsis PHOSPHOTYROSYL PHOSPHATASE ACTIVATOR is essential for PROTEIN PHOSPHATASE 2A holoenzyme assembly and plays important roles in hormone signaling, salt stress response, and plant development. *Plant Physiol* 166(3):1519-1534.
46. Gao HB, Chu YJ, & Xue HW (2013) Phosphatidic acid (PA) binds PP2AA1 to regulate PP2A activity and PIN1 polar localization. *Mol Plant* 6(5):1692-1702.
47. Wu G*, et al.* (2011) Methylation of a phosphatase specifies dephosphorylation and degradation of activated brassinosteroid receptors. *Sci Signal* 4(172):ra29.
48. Di Rubbo S, Irani NG, & Russinova E (2011) PP2A phosphatases: the "on-off" regulatory switches of brassinosteroid signaling. *Sci Signal* 4(172):pe25.
49. Van Damme D, Bouget FY, Van Poucke K, Inze D, & Geelen D (2004) Molecular dissection of plant cytokinesis and phragmoplast structure: a survey of GFP-tagged proteins. *Plant J* 40(3):386-398.
50. Wang R*, et al.* (2015) The brassinosteroid-activated BRI1 receptor kinase is switched off by dephosphorylation mediated by cytoplasm-localized PP2A B' subunits. *Mol Plant (in press)*

Figures

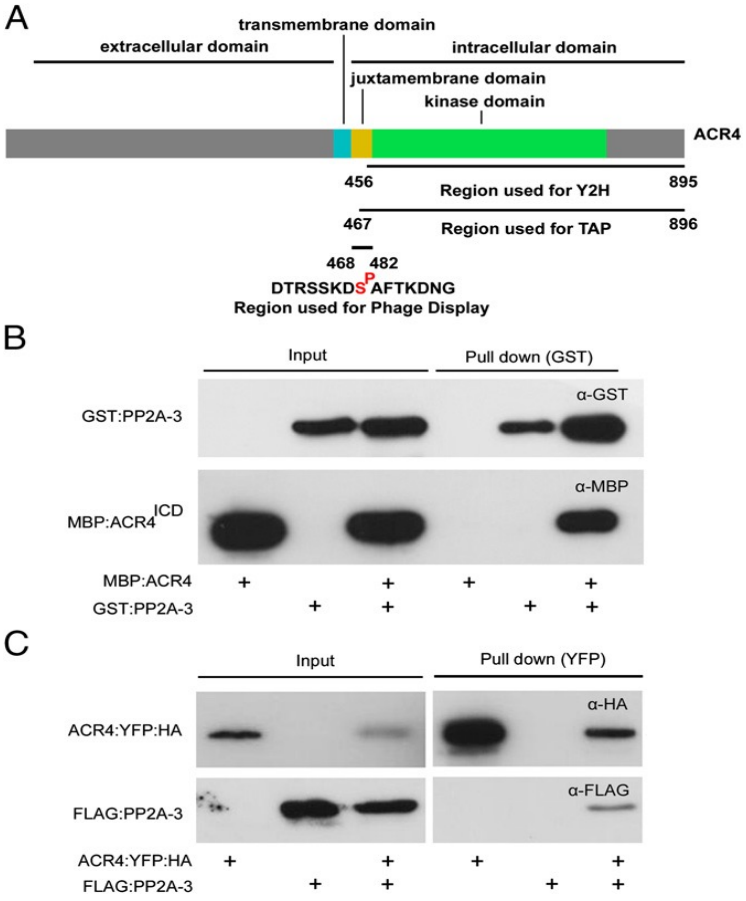

Figure 1: ACR4 interacts with PP2A-3. (A) Schematic representation of ACR4 with key domains and regions used for protein–protein interaction studies. **(B)** *In vitro* GST pull-down experiment using GST: PP2A-3 and MBP: ACR4^{ICD} according to indicated combinations (+). PP2A-3 and ACR4^{ICD} were detected by Western blotting with anti-GST and anti-MBP antibodies, respectively. **(C)** In planta YFP pull-down experiment using ACR4: YFP: HA and FLAG:PP2A-3 transiently coexpressed in tobacco leaves by Agrobacterium infiltration according to indicated combinations (+). PP2A-3 and ACR4 were detected by Western blotting with anti-FLAG and anti-HA antibodies, respectively.

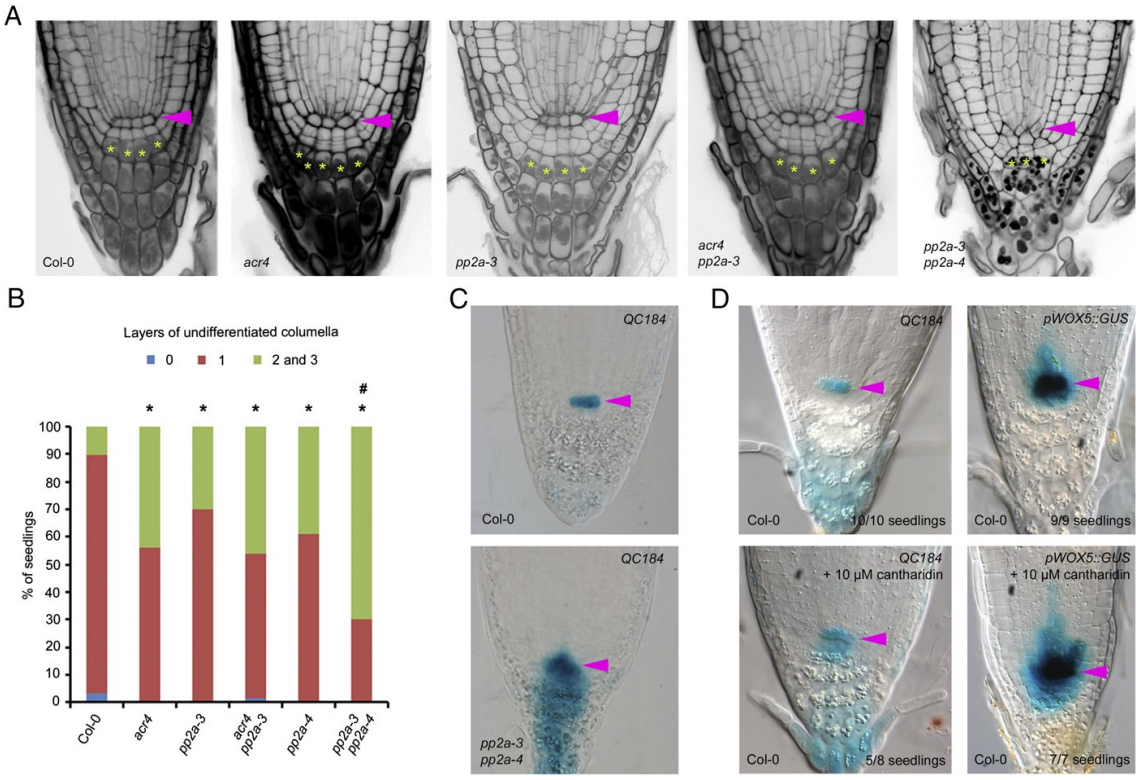

Figure 2. PP2A-3 mediates columella stem cell divisions. (A and B) Representative images (A) and quantification (B) of columella stem cell daughter cell differentiation ($20 \leq n \geq 96$) and irregular cellular pattern in pp2a-3 pp2a-4 (A, Right). Statistical significance (Z Test Calculator for 2 Population Proportions, $P < 0.05$) compared with Col-0 (*) or acr4 (#) is indicated. **(C and D)** Expression of QC184 and pWOX5::GUS in 5-d-old pp2a-3 pp2a-4 seedlings (C) or in 5-d-old seedlings grown on 10 µM cantharidin (D). Representative pictures with number of seedlings with similar expression pattern indicated. Pink arrowhead, quiescent center. Yellow asterisk, first columella cell layer with starch granules.

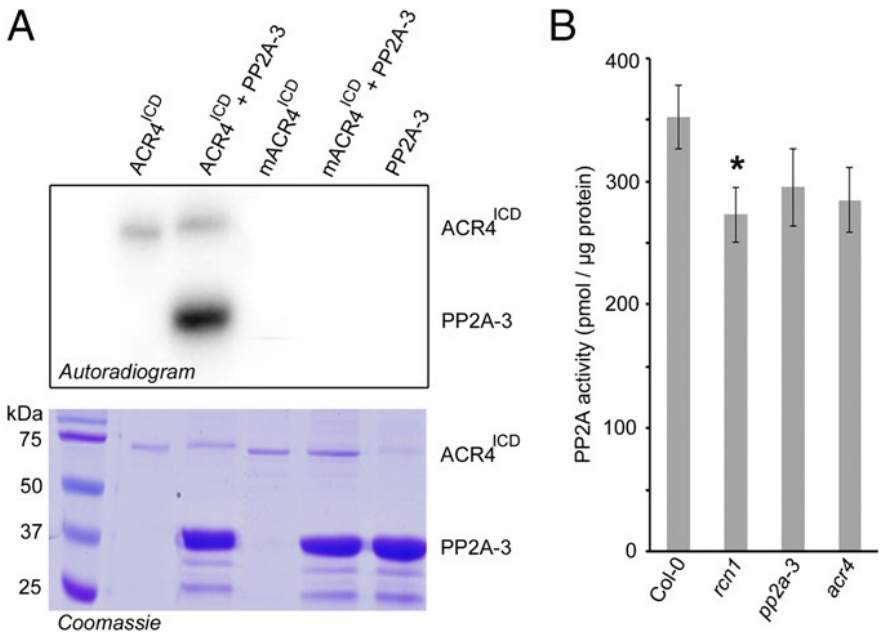

Figure 3. PP2A-3 is phosphorylated by ACR4 kinase. (A) Autoradiogram for co-incubated E. coli-expressed PP2A-3 and ACR4 kinase ($ACR4^{ICD}$) or mutant inactive kinase m $ACR4^{ICD}$ as indicated (Upper). The lanes in A are, from left to right, molecular weight standards, 1 µg of auto phosphorylated $ACR4^{ICD}$, 1 µg of auto phosphorylated $ACR4^{ICD}$ incubated with 10 µg PP2A-3, 1 µg of mutant inactive kinase $mACR4^{ICD}$, 1 µg of mutant inactive kinase $mACR4^{ICD}$ incubated with 10 µg PP2A-3, and 10 µg PP2A-3. Corresponding Coomassie blue-stained gel (Lower) was used as loading control. **(B)** Bar diagram for PP2A activity detected in whole 12-d-old seedling protein extracts as average of three bi- ological repeats (with three technical repeats each) ± SE. Statistical significance (Student's t test) compared with Col-0 is indicated: *P value < 0.05.

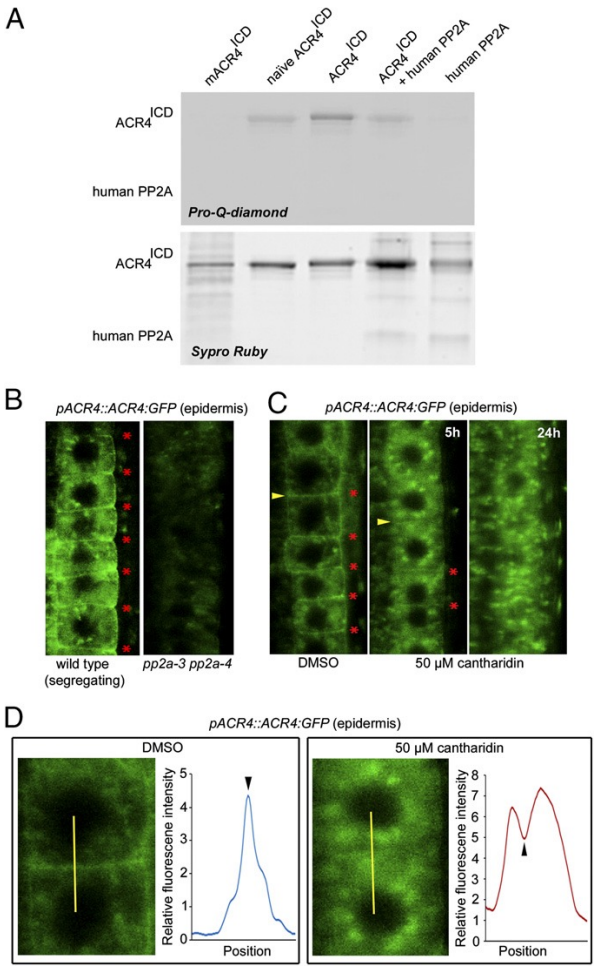

Figure. 4. PP2A-3 dephosphorylates ACR4. (A) Pro-Q-diamond stained gel showing the phosphorylation status of $ACR4^{ICD}$ coincubated without or with PP2A-3 as indicated (Upper). The same gel stained with Sypro Ruby (Lower) as loading control. **(B–D)** Localization of ACR4: GFP in pp2a-3 pp2a-4 background (B) and following treatment with DMSO or 50 µM cantharidin for indicated hours (C and D). Red asterisk, plasma membrane with ACR4 localization; arrowhead, plasma membrane analyzed in D. (D) Detail of indicated membrane in C (yellow arrowhead) and quantification of GFP signal across the yellow line as smooth average graph. Black arrowhead, position of plasma membrane.

Supplementary Information (SI)

Supplemental note on cantharidin

Cantharidin has been used extensively to inhibit PP2A (and PP2A-related) phosphatases (1-5). We have addressed the (potential) PP2A specificity by growing seedlings on 50 μM cantharidin and evaluating primary root growth (Figure. S7). Our results suggested that Col-0, *acr4* and *pp2a-3* are equally sensitive to cantharidin, while the *pp2a-4* mutant is more sensitive. In addition, the *pp2a-3 pp2a-4* double mutant still presented some sensitivity to cantharidin, suggesting additional PP2A and/or PP2A-related phosphatases are targeted in the absence of PP2A-3 and PP2A-4. Furthermore, primary root length of the *pp2a-4* mutants approached the root length of *pp2a-3 pp2a-4* double mutants. Interestingly, this suggests cantharidin, at least in the context of PP2A-3 and PP2A-4, preferentially targets PP2A-3 (see additive effect on primary root length in the absence of PP2A-4), making this a suitable chemical for our cell biological analyses, where we largely want to affect PP2A-3. Nevertheless, we cannot fully exclude that there are other cantharidin targets (as indicated by the still mildly sensitive *pp2a-3 pp2a-4* double mutant).

Supplemental note on protein overlay assay

The overlay assay, also known as the far-western blot, is a widely-used technique to detect and quantitate protein-protein interactions (6-9). The technique is dependent on the separation of target proteins by SDS-PAGE, blotting to polyvinylidene fluoride (PVDF) or nylon membranes, renaturation, probing the immobilized target with the bait protein followed by appropriate detection. Intrinsic to the technique is proper refolding of the protein upon renaturation and reconfiguration of binding sites. Consequently, non-

specific interactions are also often observed in this technique. Indeed, in our experiment, we have not been able to completely eliminate non-specific interactions particularly with control proteins GST-PTB and BSA (Figure. S3). It should, however, be noted that the negative control bait protein, SUMO (Figure. S3) also shows similar non-specific binding. The non-specific binding may therefore be attributed to the binding of the SUMO tag to the negative control proteins. Importantly, however, the SUMO protein shows no binding to PP2A-3 (Figure. S3).

Supplemental note on gel-filtration analysis

Interestingly, PP2A-3 alone, which has a calculated molecular weight of ~37 kDa, elutes in the void volume of the column (~ 8 ml) as a higher order oligomer (Figure. S3, solid double-headed arrow (*F*) and corresponding SDS-PAGE of this fraction (G). On the other hand, as demonstrated in an earlier publication (10), $ACR4^{ICD}$ elutes predominantly in later fractions (Figure. S3, dashed double-headed arrow (*H*) and corresponding SDS-PAGE of this fraction (*I*)) and has no detectable protein in the void volume fraction peak that could be attributed to the formation of an oligomer (Figure. S3, solid double headed arrow (*H*) and corresponding SDS-PAGE (*I*)). In contrast, when the two proteins are mixed and subjected to gel filtration, $ACR4^{ICD}$ now co-elutes with PP2A-3 in the void volume peak (Figure. S3, solid double-headed arrow (*J*) and corresponding SDS-PAGE of this fraction (*K*) unambiguously establishing the interaction between the two proteins.

Supplemental note on dephosphorylation assay – *E. coli* PP2A-3

We examined the ability of *E. coli*-expressed PP2A-3 to dephosphorylate $ACR4^{ICD}$ in a dephosphorylation assay using two approaches, as described in *SI Materials and Methods*. In the approach using radiolabeled $ACR4^{ICD}$ as substrate, when the protein was

incubated with PP2A-3, a slight reduction in the intensity of the P^{32}labeled $ACR4^{ICD}$ was observed (Figure. S8) in comparison with the intensity of the control protein without incubation with PP2A-3 (Figure. S8). In the corollary approach, dephosphorylation of $ACR4^{ICD}$ (phosphorylated with cold ATP) by PP2A-3 was monitored by staining with Pro Q Diamond stain. However, no discernible difference could be observed in intensities of the control protein (Figure. S8) and the protein treated with PP2A-3 (Figure. S8). These experiments suggested that the *E. coli*-expressed PP2A-3 with a C-terminal His-tag may have little or no phosphatase activity, presumably because of the requirement of a free C-terminal Leu residue and/or its carboxymethylated form for optimal activity as well as phosphorylation of specific sites that have been reported to inhibit activity (11-13). This shortcoming could be overcome when using a purified, active human PP2A that was expressed in baculovirus and post-translationally modified at the C-terminal Leu and consisted of the catalytic subunit PP2Ac and the scaffold subunit PP2Aa (Figure. 4 A)

SI Materials and Methods

Plant materials, constructs and growth conditions

T-DNA lines were previously described: *pp2a-3*, *pp2a-4* and *pp2a-3pp2a-4* (14), *acr4-2* (15), *rcn1-6* (3). The FLAG: PP2A-3 construct was previously published (16). For phenotyping and expression studies, seeds were surface sterilized and stratified at 4 ℃ in the dark for 2 days. Seeds were germinated on vertically positioned Petri dishes in a growth chamber at 21°C under continuous light (100 μmol m^{-2} s^{-1} photosynthetically active radiation).

Primary and lateral root phenotyping

Photographs of each plate were taken and measurements of primary root lengths were performed using ImageJ. Lateral roots were counted and lateral root density was calculated. For columella phenotyping, seedlings were stained with lugol and mounted in Hoyer's solution as previously described (15) (REF).

Statistics

The Z Test Calculator for 2 Population Proportions (two tailed - 0,05) (www.socscistatistics.com/tests/ztest/Default2.aspx) was used when we wanted to know whether two populations or groups differ significantly on some single characteristic. In other cases, either two-way ANOVA or Student's t-test were performed as indicated. For two-way ANOVA, analysis of variances was performed in R statistics program, using R studio (version 0.99.486).

Light microscopy

Olympus BX51 stereomicroscope or a differential interference contrast (DIC) microscope (Leica) was used for observations of the root tip (Olympus BX51 with a digital camera).

GUS Assay

Seedlings were stained in multi-well plates (Falcon 3043; Becton Dickinson). GUS assay were performed as described previsouly (17). Samples were mounted in 90% lactic acid.

mSP-PI staining

Whole seedlings were fixed in fixative (50% methanol and 10% acetic acid) at 4°C for at least 2 days. Next, seedlings were rinsed with water and incubated in 1% periodic

acid at room temperature for 40 min. The seedlings were rinsed again with water and incubated in Schiff reagent with propidium iodide (100 mM sodium metabisulphite and 0.15 N HCl; propidium iodide to a final concentration of 100 µg/mL was freshly added) for 1 to 2 h or until plants were visibly stained. The samples were then transferred into chloral hydrate solution (4 g chloral hydrate, 1 mL glycerol, and 2 mL water) overnight at room temperature. Then removed chloral hydrate and transferred seedlings onto microscope slides and mounted seedlings with Hoyer's solution (30 g gum arabic, 200 g chloral hydrate, 20 g glycerol, and 50 mL water). Slides were left undisturbed for a minimum of 3 d to allow the mounting solution to set (18).

Cantharidin treatments

pWOX5: GUS, *QC184::GUS* and *QC184::GUS x pp2a-3pp2a-4* seedlings were grown vertically on ½ MS media supplemented with and without 10 µM catharidin. The plants were submerged in 90% (v/v) acetone at 4°C for 1 hour and transferred to a GUS-staining solution of 2 mM 5-bromo-4-chloro-3-indolyl-β-D-glucuronide and 0.5 mM $K_3Fe(CN)_6$ in buffer containing 100 mM Tris and 50 mM NaCl (pH 7.0) (TBS buffer). After 1 hour of incubation at 37°C in the dark, the tissue was transferred to TBS buffer and stored at 4°C. For microscopic analysis, samples were cleared by mounting in 90% (v/v) lactic acid (Acros Organics). All samples were analyzed by differential interference contrast microscopy (BX51, Olympus). In other cases, seedlings were grown on vertical square plates containing 1/2 MS for 5 days, then transferred to plates containing cantharidin or DMSO, put back to the growth chamber vertically and kept for corresponding time.

Confocal microscopy

Zeiss LSM Zeiss LSM710 Laser Scanning Microscope and the LSM Brower software (Zeiss) were used for confocal microscopy. GFP fluorescence was imaged with 488-nm excitation of Argon laser in the frame-scanning mode alternating GFP fluorescence via a 500-/550-nm band pass emission filter. For Figure S2, seedlings have been grown under day/light conditions (16h/8h respectively) on 1/2MS media. 5-day-old roots have been stained with a 20-30 μM propidium iodide (PI) solution and inspected in the following 30 min. An inverted confocal microscope (Zeiss LSM780, objective: Plan-Apochromat 40X (1.4 oil DIC M27) has been used to excite PI with an Argon laser at 488nm and the emission was captured between 565 and 650 nm. For the signal of pACR4::ACR4: GFP a multiphoton unit excited the GFP with 910 nm and the emission has been collected between 515 and 545 nm.

pACR4::ACR4: GFP analyses and quantification

To analyze membrane localization of ACR4: GFP we processed images in ImageJ using the Plot Profile option across a selected line. Subsequently, the plot data were processed according to a moving average calculation of 5 values to smoothen the graph. Multiple cells ($n > 4$) in multiple seedlings ($n > 2$) were measured and showed similar results.

qPCR.

Seeds of Col-0 were sterilized using gas sterilization and then sown on 1/2 MS medium without (5 hours) or with nylon mesh (6, 24, 48 hours). Seeds were vernalized at + 4°C overnight (in the dark) and placed in the growth chamber. Seedlings were grown vertically until 5 days after germination and then transferred on 1/2 MS medium with 50

μM cantharidin (in DMSO) and on 1/2 MS with the same volume of DMSO as a control. Roots of seedlings were collected at 5, 6, 24 and 48 hours after transfer. RNA was extracted using RNeasy Mini Kit (Qiagen) according to the protocol provided by manufacturer and eluted in 30 μL of RNAse-free water. The RNA concentration was measured on NanoDrop ND-1000. cDNA was synthesized using iScript™ cDNA Synthesis Kit (BIO-RAD) according to the protocol provided by manufacturer and diluted 8 times. Samples for qPCR were prepared by JANUS® Automated Workstation (PerkinElmer) and qPCR was performed on LightCycler® 480 (Roche). All samples include 2-3 biological and 2-3 technical repeats. Gene-specific primers for refererence genes *ACTIN* (ACTCTTCCTGATGGACAGGTG and CTCAACGATTCCATGCTCCT) and *EEF* (CTGGAGGTTTTGAGGCTGGTAT and CCAAGGGTGAAAGCAAGAAGA), *GFP* (GAAGCGCGATCACATGGT and CCATGCCGAGAGTGATCC), *PP2A-3* (GAACCACACCTTCATCCAGTTT and TGAGATGAGTCTGTGTCCAGTGA), *PP2A-4* (TCTGCGAAAGTATGGCAATG and CCACCGTGAAGGCAGAATA), and *ACR4* (ATAAACGCACTCTTGGACCCG and TTCCCTCTCATTCTCACGCAT) were used. Calculations were done in qbase+ 2.5.

pPP2A-3::n3xGFP expressing plants

A 2000 bp promoter of *PP2A-3* upstream of the start codon was amplified from the genomic DNA (Ecotype: Col-0) using the high-fidelity DNA polymerase Phusion (New England BioLabs), and a pair of primers [PP2A-3PF (GCGAATTCCGACTGGATTTGTCACTT) and PP2A-3PR (CGGGATCCTTTCGTTAATTCGTCT)]. Previous to cloning into the intermediate vector pGem-T-easy, the blunt end PCR products were gel purified and A-tailed with dATP and

Taq DNA polymerase. After sequencing confirmation, the correct *pPP2A-3* 2Kb promoter was released from the pGem-T-easy vector with restriction enzymes EcoRI and BamHI, and then cloned into the *pGII-n3xGFP* vector. After sequencing confirmation, the correct construct was designated as *pPP2A-3::n3xGFP* and used for floral dip transformation of *A. thaliana* Col-0 plants.

Phage Display

Phage panning experiments were performed as described earlier (19). Briefly, a random 21-amino acid phage-displayed library was panned against biotinylated synthetic 15-mer peptides derived from the juxtamembrane domain containing the two phosphorylation sites Ser475 and Thr478. After four rounds of panning against both the phosphorylated and unphosphorylated peptides, consensus peptide motifs were queried against the *Arabidopsis* protein database using the Sequence Pattern search function Scansite 2.0 (http://scansite.mit.edu) (20) to identify proteins containing the identical motif.

Yeast two-hybrid screen

Yeast two-hybrid screening was performed by Hybrigenics Services, S.A.S., Paris, France (http://www.hybrigenics-services.com). The coding sequence for the *Arabidopsis thaliana* intracellular ACR4 domain (aa 456-895) (GenBank accession number gi:30694994) was PCR-amplified and cloned into pB27 as a C-terminal fusion to LexA (N-LexA-ACR4$_{ICD}$-C). The construct was checked by sequencing the entire insert and used as a bait to screen a random-primed *Arabidopsis thaliana* seedlings cDNA library constructed into pP6. pB27 and pP6 derive from the original pBTM116 (21) and pGADGH (22) plasmids, respectively. 76 million clones (8-fold the complexity of the library) were

screened using a mating approach with YHGX13 (Y187 ade2-101:loxP-kanMX-loxP, matα) and L40ΔGal4 (mata) yeast strains as previously described (23). 50 His+ colonies were selected on a medium lacking tryptophan, leucine and histidine, and supplemented with 0.5 mM 3-aminotriazole to handle bait autoactivation. The prey fragments of the positive clones were amplified by PCR and sequenced at their 5' and 3' junctions. The resulting sequences were used to identify the corresponding interacting proteins in the GenBank database (NCBI) using a fully automated procedure. A confidence score (PBS, for Predicted Biological Score) was attributed to each interaction as previously described (24). The PBS relies on two different levels of analysis. Firstly, a local score takes into account the redundancy and independency of prey fragments, as well as the distribution of reading frames and stop codons in overlapping fragments. Secondly, a global score takes into account the interactions found in all the screens performed at Hybrigenics using the same library. This global score represents the probability of an interaction being nonspecific. For practical use, the scores were divided into four categories, from A (highest confidence) to D (lowest confidence). A fifth category (E) specifically flags interactions involving highly connected prey domains previously found several times in screens performed on libraries derived from the same organism. Finally, several of these highly-connected domains have been confirmed as false-positives of the technique and are now tagged as F. The PBS scores have been shown to positively correlate with the biological significance of interactions (25, 26).

Gene ontology analysis

A Fisher exact test was used to test for enrichment of GO categories within the 657 proteins when compared to the TAIR reference set (34274 proteins). P-values were

corrected for multiple testing using the false discovery rate (FDR) controlling procedure of Benjamini and Hochberg. A P-value < 0.05 and a cutoff of FDR < 0.02 was used to score significantly over- or under-represented GO terms.

Protein expression and purification

Vectors encoding the 6X His fused to PP2A-3 were transformed into Rosetta2 (DE3) pLysS (Novagen) cells and plated on Kanamycin containing plates. Luria Broth cultures supplemented with 50 μg/ml Kanamycin were initiated by standard procedures. Cultures were grown with shaking at 37 °C for ~3 h until an OD600 = 0.6-0.8 was reached. The temperature was reduced to 20°C and cultures were induced with 0.5 mM IPTG. The cultures were incubated overnight, harvested by centrifugation, and stored at -80°C until needed. The 6X His tagged PP2A3 was purified as follows. Frozen pellets from 250 ml cultures were thawed on ice and resuspended in 10 ml Lysis Buffer (50 mM Tris-HCl pH 7.4, 150 mM NaCl, 10 mM imidazole, 0.1% Triton X-100, 8M urea, 1 mM DTT, and 1 mM AEBSF). Cells were lysed by sonication on ice and the resulting lysate was centrifuged at 13,200 rpm for 15 min at 4 °C. Supernatants were then transferred to a 10-ml column containing 250 μl of Ni-NTA Superflow resin (Qiagen) equilibrated with Lysis Buffer. The resin/lysate mixture was incubated on a rocker at 4 °C for 1 h. After incubation, the unbound proteins were allowed to flow through the column. The resin was washed with 10 ml of Wash Buffer (50 mM Tris-HCl pH 7.4, 150 mM NaCl, 20 mM imidazole, 6M urea, 1 mM DTT). Bound proteins were eluted with three successive 250 μl aliquots of Elution Buffer (50 mM Bis-Tris pH 7.2, 50 mM NaCl, 250 mM imidazole, 6M urea, 1 mM DTT) on ice. Urea was removed by three rounds of dialysis against buffer and protein amount

was determined by the Bradford method. This showed that PP2A-3 could be expressed in *E. coli* with ~90% purity ~ and a yield of ~0.8 mg/ml (Figure S11).

Circular Dichroism (CD) Measurements.

The conformation of PP2A-3 was examined by Circular Dichroism. The protein sample was dialyzed overnight against 10mM Tris HCl, pH 7.4 and 0.1mM TCEP and concentrated to an A280 value of approximately 1.0. Far-UV spectra of protein at varied concentrations, were obtained on a Jasco J-710 spectropolarimeter, in a 0.1cm path-length cuvette with excitation wavelengths ranging from 190 nm-260 nm. Scans were performed at an excitation wavelength of 280 nm, a bandwidth of 5 nm and a scan speed of 120 nm/min. The CD profile indicated a highly α-helical conformation indicating that the protein was folded correctly, in keeping with the crystal structure of the holoenzyme, which shows the C subunit to be predominantly α-helical (Figure S12).

Phosphopeptide analyses

The data-dependent tandem mass spectrometric analysis of the tryptic peptides revealed several phosphopeptides. Determination of the exact site of phosphorylation within the phosphopeptides was performed by inspection of their fragmentation pattern for specific diagnostic site-determining yn and bn ions (27). As an example, the collisional induced tandem mass spectrum for the phosphopeptide ^{299}RGEPGVpTR^{305} is shown in Figure S13 *A*. The most prominent ion is the doubly charged $[M+2H-H_3PO_4]^{2+}$ species at a m/z of 456.24. This is characteristic of a neutral loss of phosphoric acid by which phosphorylation sites are identified. An unambiguous confirmation of Thr304 as the phosphorylated residue was afforded by the presence of the site-determining non-phosphorylated and phosphorylated ions b_6, b_7, y_1 and y_2 (*SI Appendix*). Similarly, the

collision-induced high resolution mass spectrum of the peptide ^{260}VVTIFSAPNYCYR^{272} before and after phosphorylation (Figure S13 *B-C*) clearly identified the presence of phosphorylated y-series fragment ions y_2-y_5 with the expected mass shift of 80 m/z units, confirming a phosphorylated Tyr271 as the phosphorylated residue (Figure S13 *C*).

Protein overlay assays

To demonstrate interaction between PP2A-3 and naïve SUMO: ACR4^{ICD} protein (naïve and auto phosphorylated), 1 µg of 6X-Histidine tagged PP2A-3, GST fused Polypyrimidine-Tract Binding protein (PTB) and BSA protein were separated by 12 % SDS-PAGE and blotted to PVDF membrane. Blots were then blocked with 5 % milk protein in PBS + 0.1 % Tween 20 overnight. They were then incubated with purified bait proteins, naïve and auto phosphorylated ACR4^{ICD} in the protein-binding buffer to a final concentration of 10 nM. To demonstrate specific interaction between PP2A-3 and ACR4^{ICD}, blotted proteins were also incubated with SUMO protein as a control on shaker platform for about 1.5 h at room temperature, followed by three washes with PBS + 0.1% Tween (PBST) at 10 min intervals. To detect protein binding, blots were first incubated with 1:1000 diluted anti-SUMO primary antibody (Rockland Immunochemical) for 1hr at RT in 3% milk in PBST followed by three washes with PBST, each for 10min, followed by incubation with polyclonal anti-rabbit secondary antibody conjugated to Alkaline Phosphatase (AP) (Sigma, 1: 3,000) for 1hr at room temperature. Specific protein binding was calorimetrically detected by using AP Substrate kit (Bio-Rad).

Protein extraction and Phosphatase Assay

Arabidopsis lines for *acr4-2*, *rcn-1-6*, *pp2a-3,* and Col-0 were gas-sterilized (3mL 100% HCL + 97mL thin bleach solution) for 4 hours then stratified for 2 days at 4°C. Seeds

were sown on ½ Murashige-Skoog medium (including myoinositol and MES) and 1% bacteriological agar. Approximately 5g of seedlings, grown until 12 days post germination, were ground whole in liquid nitrogen. Fresh phosphatase storage buffer [50mM Tris-HCl pH 7.5, 0.05% (v/v) Triton X-100, 100uM EDTA, 500uM PMSF, 0.05% (v/v) β-mercaptoethanol, 10% (v/v) glycerol, 0.5% (v/v) protease inhibitor cocktail (Sigma)] was added (½ volume/weight) directly to the frozen tissues and ground to a fine paste, then filtered through miracloth (in a cold room) to remove cell debris. The resultant cell lysate was centrifuged for 10 min at 4°C at 13,000 *g*. Endogenous phosphate was removed using the supplied Sephadex G-25 columns (Promega) according to the manufacturer's instructions. Protein levels were quantified using the Bradford assay. PP2A phosphatase activity was measured using a molybdate dye-based phosphatase assay kit according to the manufacturer's instructions. The reactions were incubated at 37°C for 30 mins before being stopped by the addition of the molybdate dye and additive mixture. The glass bottomed 96-well plate was read on a Tecan Infinite M200 Pro spectrophotometer at 30°C, utilizing 25 flashes at 600 nm, with 4 reads per well (within a well-border of 1,700μm). The phosphate released by samples was determined by comparing the protein samples to the standard curves using Magellan v7.0 software. The experiment was performed in three independent biological repeats.

Tandem Affinity Purification

For the TAP approach, transformation of *Arabidopsis* cell suspension cultures was carried out as previously described (28, 29). Tandem affinity purification of protein complexes was done using the GStag (30) followed by protein precipitation and separation, according to a previously described protocol (29). The protocols of proteolysis and peptide

isolation, acquisition of mass spectra by a 4800 MALDI TOF/TOF Proteomics Analyzer (AB SCIEX), and MS-based protein homology identification based on the TAIR genomic database have also been described previously (31). Experimental background proteins were subtracted based on approximately 40 TAP experiments on wild type cultures and cultures expressing TAP-tagged mock proteins GUS, RFP and GFP (31).

Kinase and Phosphatase Assay

To demonstrate phosphorylation of *E. coli*-expressed PP2A-3 by the ACR4 kinase and dephosphorylation of $ACR4^{ICD}$ by PP2A-3, we used the following approaches. The kinase assay was performed as described previously (32). Briefly, SUMO fused $ACR4^{ICD}$ was first auto phosphorylated using 2μCi of [γ^{P32}] ATP as reported previously (32). 10 μg of PP2A-3 was subsequently added to 20 μl reaction volume, containing 1 μg of auto phosphorylated $ACR4^{ICD}$ in kinase buffer. The reaction was incubated for 1 hour at RT and subsequently terminated by the addition of 6 μL of 4X Laemmli buffer and boiling for 5 min. Proteins were resolved by 12% SDS-PAGE, stained with Coomassie Brilliant Blue R-250, and then analyzed by exposure to a phosphorimaging screen. To test the phosphatase activity of PP2A against phosphorylated $ACR4^{ICD}$, two approaches were utilized: (1) Pro-Q Diamond phospho-protein staining technique and (2) Radioactive assay. In the Pro-Q Diamond staining protocol, ~125 μg of $ACR4^{ICD}$ was first auto phosphorylated with 100 μM cATP in a 200 μl reaction volume of kinase buffer for 1hr at RT. The free ATP was then removed by affinity purification of the phosphorylated protein using Ni-NTA resin and multiple washing steps with wash buffer (1X TBS, 30 mM Imidazole, 1 mM DTT). The protein was subsequently eluted from the resin and used in the phosphatase assay as follows. 1μg of phosphorylated $ACR4^{ICD}$ was

incubated with 10 µg of PP2A-3 in a 40 µl reaction volume in phosphatase buffer (50mM Tris, pH 7.4, 5 mM $MnCl_2$ and 10 mM $MgCl_2$) for 1hour at room temperature. The reaction was terminated by 4X SDS buffer/heating followed by SDS-PAGE. The control proteins for comparative phosphorylation state measurement were 1µg of mutant ACR4 ($mACR4^{ICD}$) and 10 µg of PP2A in phosphatase buffer. The gel was stained with Pro-Q-diamond stain (as described in the next section) and analyzed by typhoon imaging. The destained gel was then stained with SyPro Ruby protein stain (Invitrogen) to determine the total protein. For the radioactive assay, γ^{32P} labeled $ACR4^{ICD}$ was first prepared using a mix of 25 µM cold ATP and 2 µCi of [γ^{32P}] ATP in a 200 µl reaction volume in kinase buffer. The removal of ATP and the phosphatase assay was performed as described above. The proteins were resolved on a 12% SDS PAGE and further analyzed by exposure to a phosphoimaging screen. Coomassie Blue staining determined the total protein.

Dephosphorylation of auto phosphorylated $ACR4^{ICD}$ by human PP2A

Human PP2A, consisting of both the catalytic C chain and the scaffolding A chain was obtained from Millipore. Phosphorylation status of the proteins was determined using a phospho-protein stain, Pro-Q Diamond (Invitrogen). Naïve $ACR4^{ICD}$ was first auto-phosphorylated with cold ATP as described elsewhere. Subsequently, 1 µg of auto-phosphorylated $ACR4^{ICD}$ was incubated with 0.4 units of human PP2A in 20 µl reaction volume of 50 mM Tris HCl, pH 7.4, 5 mM $MnCl_2$ and 10 mM $MgCl_2$ (phosphatase buffer) for 1 hour. The reaction was then terminated by boiling in 4X SDS sample buffer. To compare the phosphorylation status, 1 µg of inactive $mACR4^{ICD}$, naïve $ACR4^{ICD}$ and auto phosphorylated $ACR4^{ICD}$ were also separated on 12% SDS gel along with the phosphatase-treated auto-phosphorylated $ACR4^{ICD}$. The gel was then fixed for 2x30 min with solution

containing 50% methanol and 10% acetic acid followed by three washes with deionized water. Staining with Pro Q diamond stain was achieved for 90 min in the dark and then de-stained with 50 mM sodium acetate buffer pH 4.0 containing 20% acetonitrile. Images of the stained gel were acquired on a Molecular Dynamics Typhoon scanner (GE healthcare) with an excitation source of 532 nm laser and a 580-nm bandpass emission filter.

Gel Filtration.

Interaction between $sACR4^{ICD}$ and 6X His-PP2A-3 was also analyzed by gel-filtration on an AKTA FPLC system. An equimolar mixture (5 μM) of purified naïve SUMO: $ACR4^{ICD}$ and PP2A-3 was incubated in 500 μl column buffer (50 mM Tris pH 7.2, 100 mM NaCl, 1 mM DTT and 100 μM $MnCl_2$) for 1 hour at room temperature and subsequently loaded onto a Global 10/300 Superdex G-200 Column (GE healthcare, bed volume 24 ml) equilibrated with column buffer. The column was developed at a flow rate of 0.3ml/min and 0.5ml fractions were collected. Fractions corresponding to the peak were analyzed by SDS-PAGE. Gel filtration was also performed on the individual proteins $sACR4^{ICD}$ and 6X His-PP2A-3.

High-Resolution Mass Spectrometry

The endoprotease (trypsin) digests were analyzed by using nano-LC-MS with a linear ion trap orbitrap mass spectrometer (Orbitrap ELITE) (33) (Thermo Fisher Scientific). Chromatographic separations were performed by using a nano-LC 2D Plus (Eksigent, Dublin, CA) for gradient delivery and a cHiPLC-Nanoflex system (15-cm × 75-μm C18 packing (ChromXP C18-CL, 3 μm, 120 Å; Eksigent). The liquid chromatograph was interfaced to the mass spectrometer with a nanospray source (PicoView PV550; New Objective, Woburn, MA). Mobile-phase components were 1% FA in water (solvent A) and

1% FA in 99% ACN (solvent B). After equilibration of the column in 98% solvent A/2% solvent B, the samples were injected (10 µl) by using an AS2 autosampler (Eksigent), at a flow rate of 800 nl/min. The peptides were separated by using an AcN gradient at 800 nl/min, as follows: isocratic elution at 2% solvent B, 0 to 3 min; 2% solvent B to 40% solvent B, 3 to 240 min; 40% solvent B to 80% solvent B, 240 to 250 min; 80% solvent B to 2% solvent B, 250 to 255 min; isocratic elution at 2% solvent B, 255 to 275 min. The total cycle time, including column equilibration, sample loading, and gradient elution of peptides, was 305 min. The survey scans (m/z 350-2000) (MS1) were acquired at 120,000 resolution at m/z 400) in the Orbitrap in profile mode, and the product-ion mass spectrometry spectra (MS2) were acquired at 15,000 resolution in profile mode, after high energy collision-induced dissociation. The maximal injection times for the LTQ and Orbitrap were 50 ms and 200 ms, respectively. The automatic gain-control targets for the LTQ and the Orbitrap were and 3 × 104 and 1 × 106 respectively. The MS1 scans were followed by 20 MS2 events in the linear ion trap with collision activation in the ion trap (parent threshold, 15,000; isolation width, 2.5 Th; normalized collision energy, 30%; activation Q, 0.250; activation time, 30 ms). Dynamic exclusion was activated for 60 s after MS2 acquisition. A repeat count of 3, a repeat duration of 15 s, and a maximal exclusion list size of 500 were used. The following ion source parameters were used: capillary temperature, 200°C; source voltage, 4.0 kV; source current, 100 µA; tube lens, 79 V. The data were acquired by using Xcalibur 2.2.48 (Thermo Fisher).

In-vitro pull down assay

15 µl packed volume GST-Sepharose 4B (GE Healthcare) was washed 3X with 1ml HEPES/NaCl (100mM HEPES, 25 mM NaCl, pH 8) buffer. Beads were pre-blocked with

1% BSA for 10min at 4°C with rotation. 1µg of each protein was added to binding buffer (100mM HEPES, 25 mM NaCl, pH8, 10 mM $MgCl_2$, 0.2 mM $CaCl_2$, 300 µM ATP, 5mM DTT, 1% BSA (v/v)) in a total volume of 400 µl. Pre-blocked beads were added to the pull down mix and incubated for 1h at 4°C with rotation. After incubation supernatant was removed and beads washed 3X with HEPES/NaCl buffer. Bound proteins were eluted using 50 µl sample loading buffer (100 mM Tris-HCl pH 6.8, 20% glycerol (v/v), 0.2% bromophenol blue (w/v), 4% SDS (w/v), 0.2M DTT), heated at 95°C for 5 min and centrifuged for 1 min at 14000 x g. Eluted proteins and their respective inputs were separated on a 10% SDS-PAGE gel and blotted onto PVDF membrane (GE Healthcare). Membranes were probed using using anti-MBP (Abcam) 1:12000 and anti-GST 1:10000 (Abcam) and visualised using ECL prime chemiluminescence (GE Healthcare) prior to exposure on film (GE Healthcare).

In planta co-immunoprecipitation

Nicotiana benthamiana transient transformation was performed as previously described. Protein extraction and co-immunoprecipitation were performed as previously described (34) with modifications (extraction buffer at pH 9.5). GFP Trap was used for the co-immunoprecipitation. Co-immunoprecipitated proteins were detected using mouse anti-flag 1:2000 (Sigma) and rabbit anti-HA 1:5000 (Sigma), secondary antibodies used were HRP conjugated anti-mouse IgG 1:50000 (Sigma) and HRP conjugated anti-rabbit IgG 1:20000 (Sigma). Western blot transfer was performed using pH 9.5 transfer buffer.

In silico analyses

CORNET (COrelationNETworks) is online software that utilizes gene expression and protein-protein interaction databases to create potential functional associations for any

number of query genes and putative interacting partners (https://cornet.psb.ugent.be). Co-expression between pairs of query genes, and between query genes with neighbours (directly interacting partners) was determined using the Pearson correlation coefficient (PCC) (35). The output of this analysis was then analyzed using Microsoft Excel database software. For the initial ACR4 PPIs, all databases and interactions were included for the CORNET analyses, and focusing ACR4 and interactions with/between neighbors. Cytoscape software (36) was used to visualize protein–protein interaction networks. To identify similarities in possible biological processes and molecular functions of the genes in our networks we used the Cytoscape add-on BiNGO. BiNGO analyses the Gene Ontology (GO) identifiers of specified genes and categorises them into a list of either biological processes or molecular functions (among others). Through this approach an entire network, or a subset, can be selected to observe the overall trend of gene function and process. Interactome databases were individually analyzed by BiNGO to observe if there were any similarities in gene function.

Homology Modeling of PP2A-3 catalytic chain.

The MODELER program (37) in Discovery Studio v4.0 (BIOVIA, formerly Accelrys) was used to build a model for the catalytic chain of the Arabidopsis protein based on the 74% amino acid sequence identity and 83% similarity with the C chain of the human phosphatase holoenzyme. The homology model was built using the C chain coordinates within the context of the crystal structure of the trimeric human enzyme (PDB identification 2IAE) (38). Ten energy minimized models were generated and one model with the lowest value of the objective function was selected for further refinement. The compatibility of the modeled structure with its amino acid sequence was validated using

the Verify Protein (Profiles 3D) program (39). Percent side-chain solvent accessibility of the phosphorylation sites was computed based on the solvent accessibility of the corresponding residues in the catalytic chain of the human holoenzyme trimeric structure. Phosphorylation sites at Ser 5 and Thr 305 are not seen as the first 5 residues at the N-terminus and the last 15 residues at the C-terminus are not included in the homology model.

(Phospho)proteomics

For (phospho)proteomics 50 mg of seeds of *Arabidopsis thaliana* (Columbia-0) and *acr4-2* plants were surface sterilized and sown in 100 ml liquid half-strength Murashige and Skoog (MS) medium containing 1% (w/v) sucrose. Seeds were vernalized for 2 days at 4°C, after which they were grown for 5 days at 21°C in a day/night regime (16h light/8h dark) while mixing at 90 rpm. Three biological repeats were done.

The phosphoproteome pipeline was based on a previously published protocol (40), except that we opted for label free quantitation instead of the proposed ^{15}N metabolic labeling. Other than that, only minor adjustments were implemented. In brief, Arabidopsis five-day-old seedlings were ground in a mortar under liquid nitrogen. Proteins were extracted in a buffer consisting of 250 mM triethylammonium bicarbonate (TEAB) pH 8, 290 mM sucrose, 25 mM EDTA, 1 mM DTT and the appropriate amount of the Complete protease inhibitor mixture and the PhosSTOP phosphatase inhibitor mixture (both from Roche, Basel, Switzerland). After centrifugation, the proteins in the supernatant were precipitated via chloroform/methanol precipitation. The protein pellets were washed with 80% acetone and solubilized with 8 M urea. Before digestion, the samples were diluted to 1 M urea with 50 mM TEAB buffer (pH 8). *S*-reduction and *S*-alkylation were performed with DTT and iodoacetamide, as described by Minkoff et al., 2013. 1 mg of the proteins

was digested with trypsin overnight at 37 °C (Promega Trypsin Gold, mass spectrometry grade) at an enzyme-to-substrate ratio of 1:100 (w:w). The digest was acidified to pH ≤ 3 with trifluoroacetic acid (TFA) and desalted with SampliQ C18 SPE cartridges (Agilent, Waldbronn, Germany). The elutions were dried down in a vacuum centrifuge and re-dissolved in 100 µl of 80% acetonitrile, 6% TFA. The peptides were loaded on house-made chromatographic columns packed with 500 µg Sachtopore-NP TiO2 beads (5 µm, 300 Å; ZirChrom, Minnesota, USA), washed twice with 50 µl of 80% acetonitrile, 0.1% TFA and eluted with 30 µl of 1% ammonium hydroxide solution. Before drying down, the eluate was acidified with formic acid to pH < 3.

Each phosphopeptide sample was re-dissolved in 50 µl of 2% acetonitrile with 0.1% TFA. A 15 µL aliquot of each sample was subjected to LC-MS/MS analysis using an Ultimate 3000 RSLC nano LC (Thermo Fisher Scientific, Bremen, Germany) system coupled to an Q Exactive mass spectrometer (Thermo Fisher Scientific, Bremen, Germany). The sample mixture was first loaded on a trapping column (made in-house, 100 µm internal diameter (I.D.) × 20 mm, 5 µm beads C18 Reprosil-HD, Dr. Maisch, Ammerbuch-Entringen, Germany). After flushing from the trapping column, the sample was loaded on an analytical column (made in-house, 75 µm I.D. × 150 mm, 3 µm beads C18 Reprosil-HD, Dr. Maisch). Peptides were loaded with loading solvent (0.1% TFA in water) and separated with a linear gradient from 98% solvent A’ (0.1% formic acid in water) to 55% solvent B′ (0.1% formic acid in water/acetonitrile, 20/80 (v/v)) in 170 min at a flow rate of 300 nL/min. This is followed by a 5 min wash reaching 99% solvent B’. The mass spectrometer was operated in data-dependent, positive ionization mode, automatically switching between MS and MS/MS acquisition for the 10 most abundant

peaks in a given MS spectrum. The source voltage was 3.4 kV, and the capillary temperature was 275°C. One MS1 scan (m/z 400−2000, AGC target 3 × 106 ions, maximum ion injection time 80 ms) acquired at a resolution of 70000 (at 200 m/z) was followed by up to 10 tandem MS scans (resolution 17500 at 200 m/z) of the most intense ions fulfilling predefined selection criteria (AGC target 5 × 104 ions , maximum ion injection time 60 ms, isolation window 2 Da, fixed first mass 140 m/z, spectrum data type: centroid, underfill ratio 2%, intensity threshold 1.7xE4, exclusion of unassigned, 1, 5-8, >8 charged precursors, peptide match preferred, exclude isotopes on, dynamic exclusion time 20 s). The HCD collision energy was set to 25% Normalized Collision Energy and the polydimethylcyclosiloxane background ion at 445.120025 Da was used for internal calibration (lock mass).

MS/MS spectra were searched against the TAIR10 database (35,386 entries, version January 2012) with the MaxQuant software (version 1.5.0.30) with a precursor mass tolerance set to 20 ppm for the first search (used for nonlinear mass re-calibration) and set to 4.5 ppm for the main search. Trypsin was selected as enzyme setting. Cleavages between lysine/arginine-proline residues and up to two missed cleavages were allowed. Carbamidomethylation of cysteine residues was selected as a fixed modification, and phosphorylation of serine, threonine and tyrosine residues and oxidation of methionine residues were selected as variable modifications. The false discovery rate for peptide and protein was set to 1%, and the minimum peptide length was set to 7. The MaxLFQ algorithm allowing label free quantification (41) and the ‘Matching Between Runs’ feature were enabled.

References

1. Hu R, Zhu Y, Shen G, & Zhang H (2014) TAP46 plays a positive role in the ABSCISIC ACID INSENSITIVE5-regulated gene expression in Arabidopsis. *Plant Physiol* 164(2):721-734.
2. Chen J, Hu R, Zhu Y, Shen G, & Zhang H (2014) Arabidopsis PHOSPHOTYROSYL PHOSPHATASE ACTIVATOR is essential for PROTEIN PHOSPHATASE 2A holoenzyme assembly and plays important roles in hormone signaling, salt stress response, and plant development. *Plant Physiol* 166(3):1519-1534.
3. Blakeslee JJ*, et al.* (2008) Specificity of RCN1-mediated protein phosphatase 2A regulation in meristem organization and stress response in roots. *Plant Physiol* 146(2):539-553.
4. Li W*, et al.* (2010) Cantharidin, a potent and selective PP2A inhibitor, induces an oxidative stress-independent growth inhibition of pancreatic cancer cells through G2/M cell-cycle arrest and apoptosis. *Cancer Sci* 101(5):1226-1233.
5. Li YM & Casida JE (1992) Cantharidin-binding protein: identification as protein phosphatase 2A. *Proc Natl Acad Sci USA* 89(24):11867-11870.
6. Wu Y, Li Q, & Chen XZ (2007) Detecting protein-protein interactions by Far western blotting. *Nature Protoc* 2(12):3278-3284.
7. Hall RA (2015) Studying protein-protein interactions via blot overlay/far western blot. *Methods Mol Biol* 1278:371-379.
8. Jadwin JA, Mayer BJ, & Machida K (2015) Detection and quantification of protein-protein interactions by far-western blotting. *Methods Mol Biol* 1312:379-398.
9. Gromov PS & Celis JE (2001) Protein Identification: Overlay Procedures. In: eLS. John Wiley & Sons Ltd, Chichester.
10. Meyer MR, Shah S, Zhang J, Rohrs H, & Rao AG (2015) Evidence for intermolecular interactions between the intracellular domains of the arabidopsis receptor-like kinase ACR4, its homologs and the Wox5 transcription factor. *PloS One* 10(3):e0118861.
11. Janssens V & Goris J (2001) Protein phosphatase 2A: a highly regulated family of serine/threonine phosphatases implicated in cell growth and signalling. *The Biochem J* 353(Pt 3):417-439.
12. Shi Y (2009) Serine/threonine phosphatases: mechanism through structure. *Cell* 139(3):468-484.
13. Wu G*, et al.* (2011) Methylation of a phosphatase specifies dephosphorylation and degradation of activated brassinosteroid receptors. *Sci Signal* 4(172):ra29.
14. Spinner L*, et al.* (2013) A protein phosphatase 2A complex spatially controls plant cell division. *Nat Commun* 4:1863.
15. De Smet I*, et al.* (2008) Receptor-like kinase ACR4 restricts formative cell divisions in the Arabidopsis root. *Science* 322(5901):594-597.
16. Ahn CS, Han JA, Lee HS, Lee S, & Pai HS (2011) The PP2A regulatory subunit Tap46, a component of the TOR signaling pathway, modulates growth and metabolism in plants. *Plant Cell* 23(1):185-209.
17. Beeckman T & Viane R (2000) Embedding thin plant specimens for oriented sectioning. *Biotech Histochem* 75(1):23-26.

18. Truernit E*, et al.* (2008) High-resolution whole-mount imaging of three-dimensional tissue organization and gene expression enables the study of Phloem development and structure in Arabidopsis. *Plant Cell* 20(6):1494-1503.
19. Meyer MR, Shah S, & Rao AG (2013) Insights into molecular interactions between the juxtamembrane and kinase subdomains of the Arabidopsis Crinkly-4 receptor-like kinase. *Arch Biochem Biophys*535(2):101-110.
20. Obenauer JC, Cantley LC, & Yaffe MB (2003) Scansite 2.0: proteome-wide prediction of cell signaling interactions using short sequence motifs. *Nucleic Acids Res* 31(13):3635-3641.
21. Vojtek AB & Hollenberg SM (1995) Ras-Raf interaction: two-hybrid analysis. *Methods Enzymol* 255:331-342.
22. Bartel PL, Chien C-TS, R., & Fields S (1993) Using the two-hybrid system to detect protein-protein interactions. In: Hartley DA, editor. Cellular Interactions in Development: A Practical Approach. Oxford University Press; Oxford, England.pp. 153–179.
23. Fromont-Racine M, Rain JC, & Legrain P (1997) Toward a functional analysis of the yeast genome through exhaustive two-hybrid screens. *Nat Genet* 16(3):277-282.
24. Formstecher E*, et al.* (2005) Protein interaction mapping: a Drosophila case study. *Genome Res* 15(3):376-384.
25. Rain JC*, et al.* (2001) The protein-protein interaction map of Helicobacter pylori. *Nature* 409(6817):211-215.
26. Wojcik J, Boneca IG, & Legrain P (2002) Prediction, assessment and validation of protein interaction maps in bacteria. *J Mol Biol* 323(4):763-770.
27. Beausoleil SA, Villen J, Gerber SA, Rush J, & Gygi SP (2006) A probability-based approach for high-throughput protein phosphorylation analysis and site localization. *Nat Biotechnol* 24(10):1285-1292.
28. Van Leene J*, et al.* (2007) A tandem affinity purification-based technology platform to study the cell cycle interactome in Arabidopsis thaliana. *Mol Cell Proteomics* 6(7):1226-1238.
29. Van Leene J, Witters E, Inze D, & De Jaeger G (2008) Boosting tandem affinity purification of plant protein complexes. *Trends Plant Sci* 13(10):517-520.
30. Burckstummer T*, et al.* (2006) An efficient tandem affinity purification procedure for interaction proteomics in mammalian cells. *Nat Methods* 3(12):1013-1019.
31. Van Leene J*, et al.* (2010) Targeted interactomics reveals a complex core cell cycle machinery in Arabidopsis thaliana. *Mol Syst Biol* 6:397.
32. Meyer MR, Lichti CF, Townsend RR, & Rao AG (2011) Identification of in vitro autophosphorylation sites and effects of phosphorylation on the Arabidopsis CRINKLY4 (ACR4) receptor-like kinase intracellular domain: insights into conformation, oligomerization, and activity. *Biochemistry* 50(12):2170-2186.
33. Michalski A*, et al.* (2012) Ultra high resolution linear ion trap Orbitrap mass spectrometer (Orbitrap Elite) facilitates top down LC MS/MS and versatile peptide fragmentation modes. *Mol Cell Proteomics* 11(3):O111 013698.
34. Holton N, Nekrasov V, Ronald PC, & Zipfel C (2015) The phylogenetically-related pattern recognition receptors EFR and XA21 recruit similar immune signaling components in monocots and dicots. *PLoS Pathog* 11(1):e1004602.
35. Aoki K, Ogata Y, & Shibata D (2007) Approaches for extracting practical information from gene co-expression networks in plant biology. *Plant Cell Physiol* 48(3):381-390.

36. Shannon P*, et al.* (2003) Cytoscape: a software environment for integrated models of biomolecular interaction networks. *Genome Res* 13(11):2498-2504.
37. Sali A, Potterton L, Yuan F, van Vlijmen H, & Karplus M (1995) Evaluation of comparative protein modeling by MODELLER. *Proteins* 23(3):318-326.
38. Cho US & Xu W (2007) Crystal structure of a protein phosphatase 2A heterotrimeric holoenzyme. *Nature* 445(7123):53-57.
39. Eisenberg D, Luthy R, & Bowie JU (1997) VERIFY3D: assessment of protein models with three-dimensional profiles. *Methods Enzymol* 277:396-404.
40. Minkoff BB, Burch HL, & Sussman MR (2014) A pipeline for 15N metabolic labeling and phosphoproteome analysis in Arabidopsis thaliana. *Methods Mol Biol* 1062:353-379.
41. Cox J*, et al.* (2014) Accurate proteome-wide label-free quantification by delayed normalization and maximal peptide ratio extraction, termed MaxLFQ. *Mol Cell Proteomics* 13(9):2513-2526

Supplemental Figures

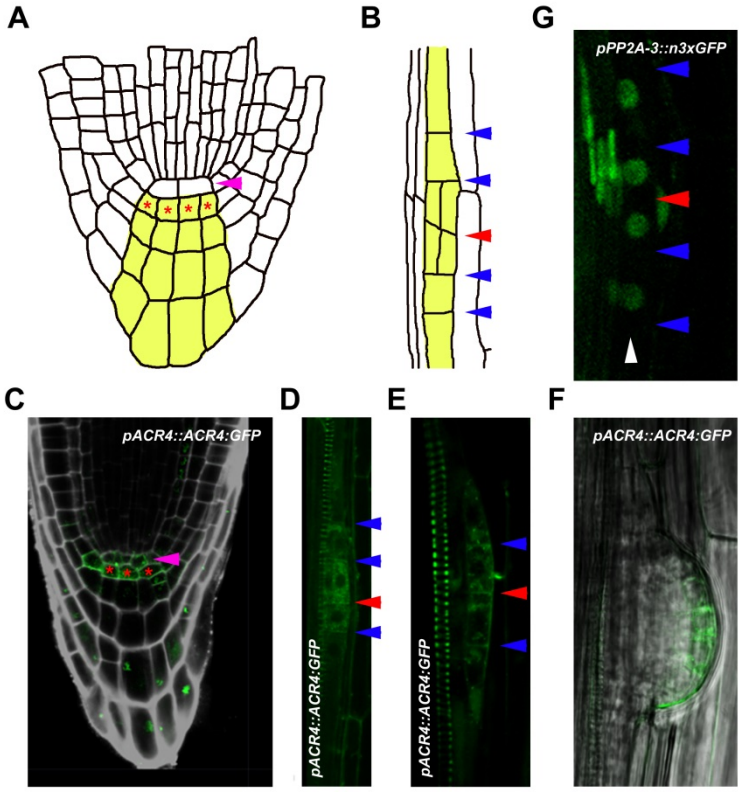

Figure S1. (A-B) Tracing of primary root tip (A) and lateral root initiation site (B). Yellow indicates region of interest, namely columella (A) and dividing pericycle (B). **(C-F)** *pACR4::ACR4:GFP* in the primary root tip stem cell / columella region (C), during lateral root initiation (D-E) and in a lateral root primordium (F). Overlay with propidium iodide staining (C) and differential interference contrast image (F) to outline the primary root tip and lateral root, respectively. **(G)** Representative image of *pPP2A-3::n3xGFP* during lateral root initiation of 4 day old seedlings. *, columella stem cells; pink arrowhead, quiescent center; red arrowhead, boundary between position of two adjacent pericycle cells before asymmetric cell division; blue arrowhead, subsequent asymmetric cell divisions; white arrowhead, pericycle.

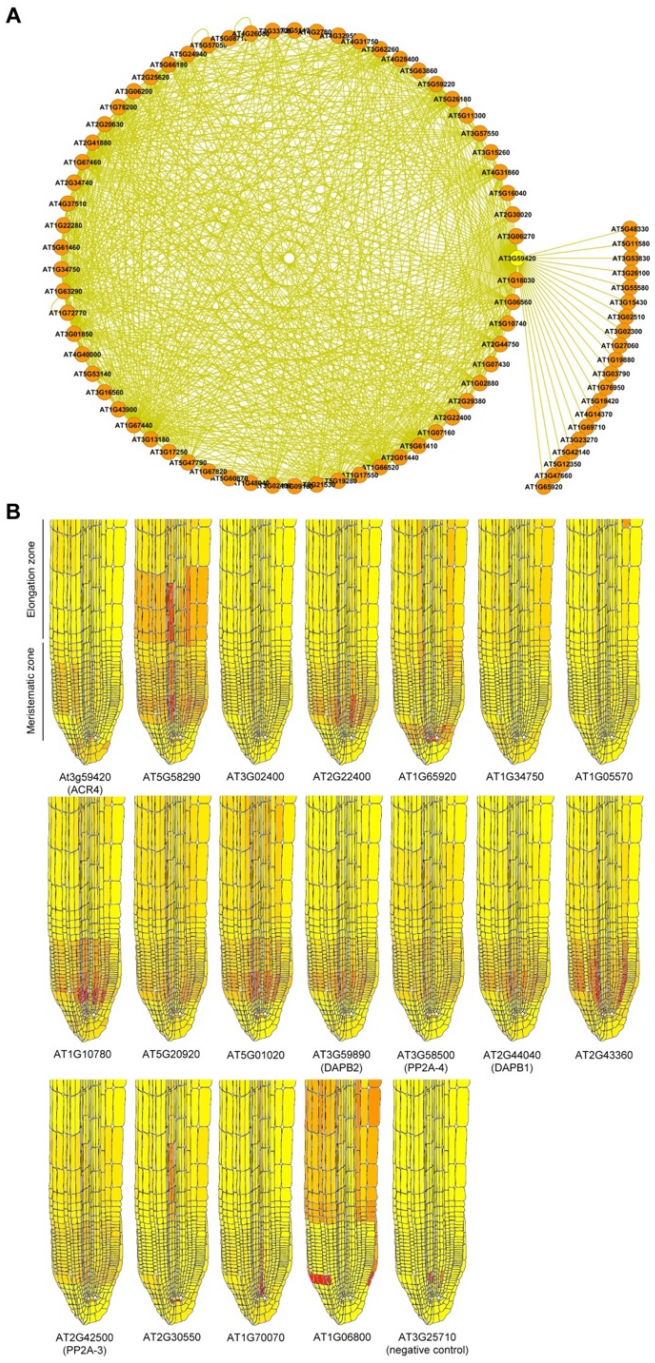

Figure S2. (A) CORNET-based interactions. ACR4 (AT3G59420) highlighted in yellow. **(B)** Root tip expression based on *Arabidopsis* eFP Browser data (absolute values – orange to red indicates gradation of increased expression.

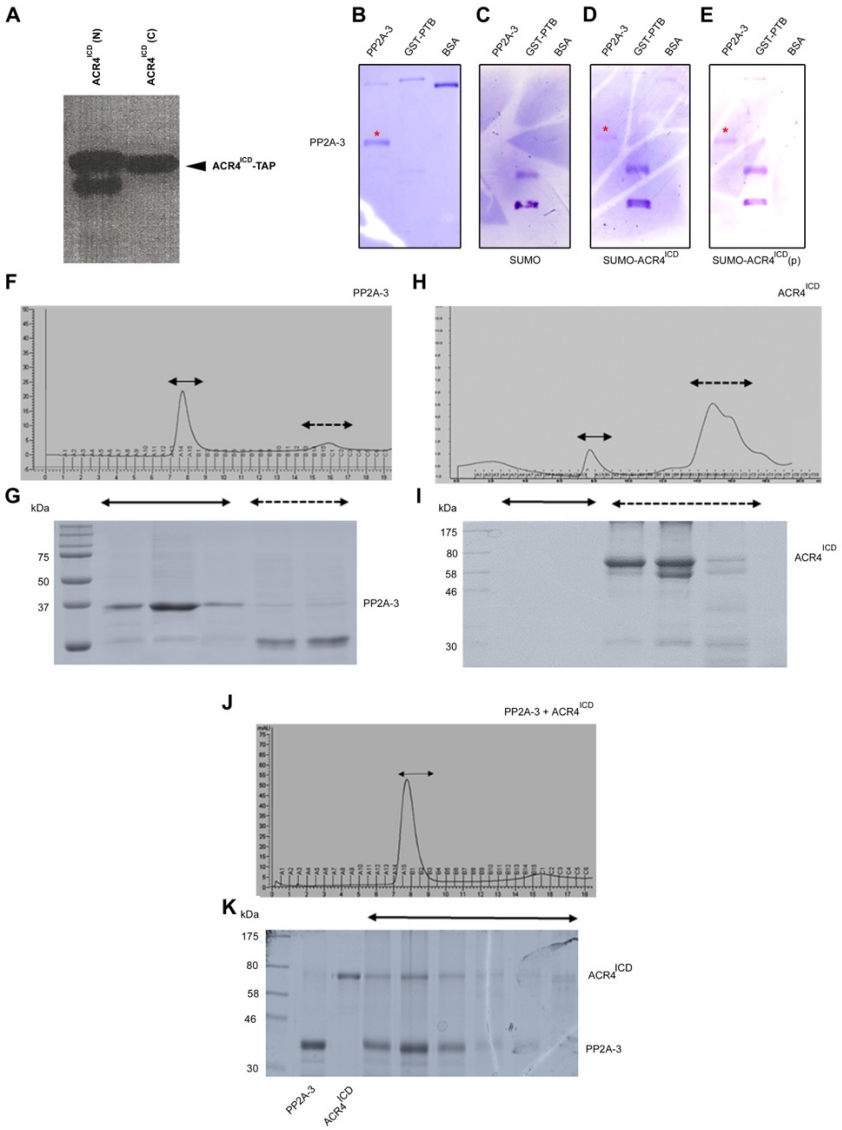

Figure S3. (A) Detection by western blot of ACR4^{ICD} fused to an N or C-terminal TAP tag produced in transgenic *Arabidopsis* cell suspension cultures. Detection was achieved with PAP antibody binding to the protein G domain in the GS-tag. **(B-E)** Protein overlay assay (see ***SI Supplemental Note*** below for further details.) showing that PP2A-3 can interact with naïve and phosphorylated ACR4^{ICD}. (B) *Lane* 1, ~1 µg of PP2A-3. *Lane*s 2 and 3 GST-fused POLYPYRIMIDINE-TRACT-BINDING PROTEIN (PTB) and *BOVINE* SERUM ALBUMINE (BSA) as negative controls. (C) Blot probed with SUMO

protein shows no specificity towards PP2A-3. (D) Blot probed with SUMO- ACR4^{ICD} shows specific binding to PP2A-3 (*Lane* 1, *). (E) Blot probed with phosphorylated SUMO- ACR4^{ICD} also shows specific binding to PP2A-3 (*Lane* 1, *). The results shown here are representative of experiments performed at least 3 times. **(F-K)** Gel filtration analysis (see ***SI Supplemental Note*** below for additional details) of the interaction between PP2A-3 and ACR4^{ICD} on a Superdex G-200 Column. (F-G) Elution profile of PP2A-3 (5 μM) at a flow rate of 0.5 ml/min. 0.3 ml fractions were collected and the fractions indicated by double-headed arrows were analyzed by SDS-PAGE (F). SDS-PAGE of fractions indicated by double-headed arrows (G). Note that PP2A-3 with a MW of ~37 kDa elutes as an oligomer (full line double headed arrow) in gel filtration and that the lower band is a PP2A-3 degradation product. (H-I) Elution profile of ACR4^{ICD} (5 μM) under the same conditions as A (H). SDS-PAGE of fractions indicated by double-headed arrows (I). Note that ACR4^{ICD} with a MW of ~62 kDa elutes closer towards the end of the bed volume (dashed line double headed arrow) and that there is no evidence of a higher order oligomer (full line double headed arrow). (J-K) Elution profile of a mixture of PP2A-3 and ACR4^{ICD} (5 μM each) under the same conditions as A (J). SDS-PAGE of fractions indicated by double-headed arrows (K). Note that the band for ACR4^{ICD} now appears along with PP2A-3 in the peak fraction, indicative of the interaction between the two proteins.

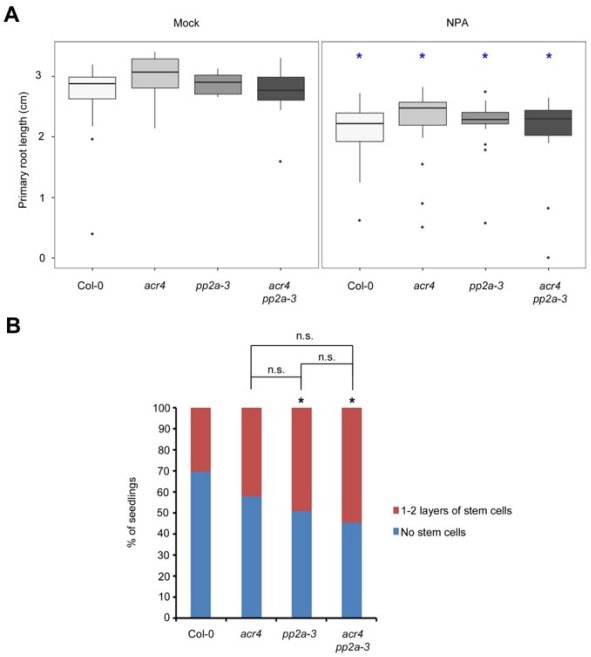

Factors	Degrees of freedom	Sum Sq	Mean Sq	F value	Pr(>F)
Line	3	1.23	0.411	1.557	0.203
Treatment	1	15.51	15.51	58.758	3.23e-12
Line:Treatment (interaction)	3	0.12	0.039	0.147	0.931
Residuals	134	35.37	0.264		

Figure S4. (A) Impact of NPA on Col-0, *acr4*, *pp2a-3* and *acr4 pp2a-3* primary root length at 7 days after germination (seedlings continuously grown on 1 µM NPA). *, p-value < 0.05 according to Student's *t*-Test compared to mock. Boxplots with outliers are shown. Table indicates two-way ANOVA analysis for A ($n \geq 15$). **(B)** Impact of NPA on Col-0, *acr4*, *pp2a-3* and *acr4 pp2a-3* columella stem cell differentiation at 4 days after germination (seedlings continuously grown on 1 µM NPA) ($n \geq 33$). Statistical significance (Z Test Calculator for 2 Population Proportions) compared to Col-0 (*, $p < 0.05$) or through connected lines (n.s., not significant at $p > 0.05$) is indicated.

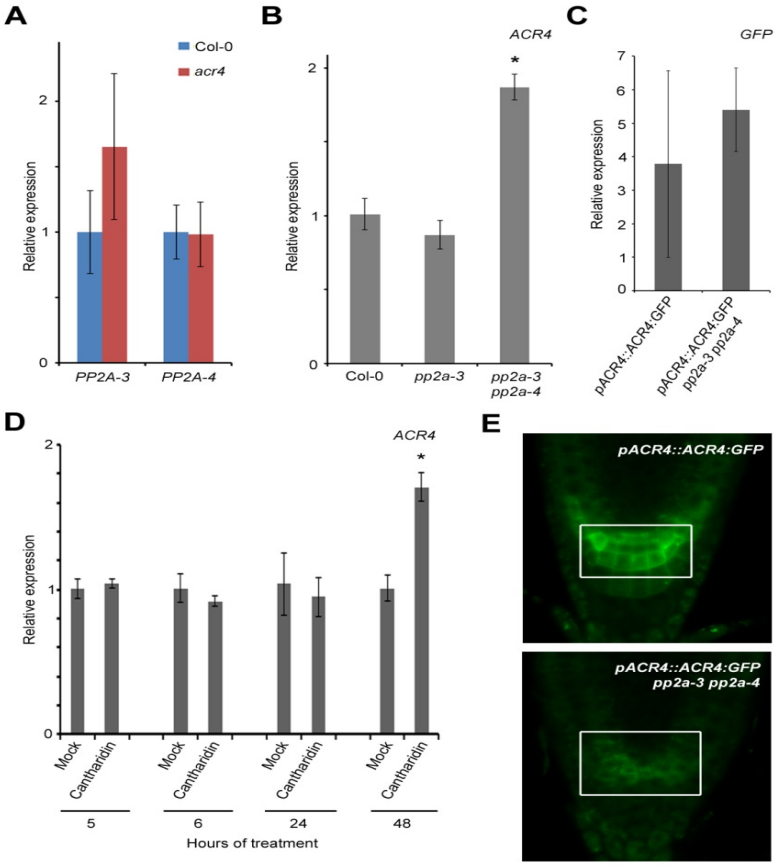

Figure S5. (A) *PP2A-3* and *PP2A-4* expression in Col-0 and *acr4* roots of 7-8 day old seedlings. **(B)** *ACR4* expression in Col-0, *pp2a-3* and *pp2a-3 pp2a-4* root tips of 6 day old seedlings. **(C)** *ACR4: GFP* expression levels (monitored through *GFP* levels) in control and *pp2a-3 pp2a-4* of root tips of 6 day old seedlings. Student's *t*-test compared to control revealed no significant difference at $p > 0.05$. **(D)** *ACR4* expression in 5 day old -0 seedling roots upon cantharidin treatment for indicated periods. **(E)** *pACR4::ACR4:GFP* in 5 day old root tips of a control line and in *pp2a-3 pp2a-4*. Although not as discrete as in the control, the *pp2a-3 pp2a-4* double mutant still displays higher GFP (white box), and some membrane localization. Graphs show average ± standard error of 2 or 3 biological repeats. Statistical significance (Student's *t*-test) compared to Col-0 is indicated: *, *p*-value < 0.05

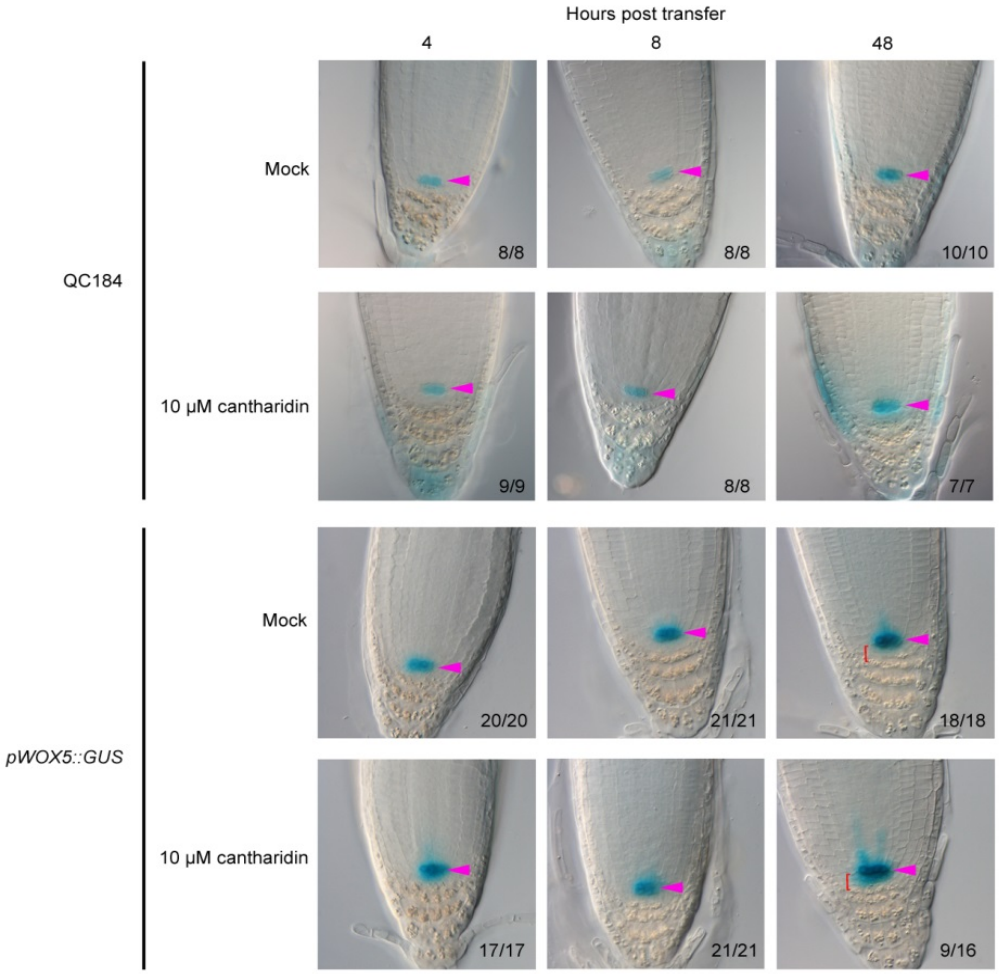

Figure S6. Expression of *QC184* and *pWOX5::GUS* in 5-day-old transferred to 10 µM cantharidin for indicated times (hrs). Representative pictures with number of seedlings with similar expression pattern indicated. The *WOX5* expression domain appears to expand quickly, but more significantly at 48 hours after transfer.

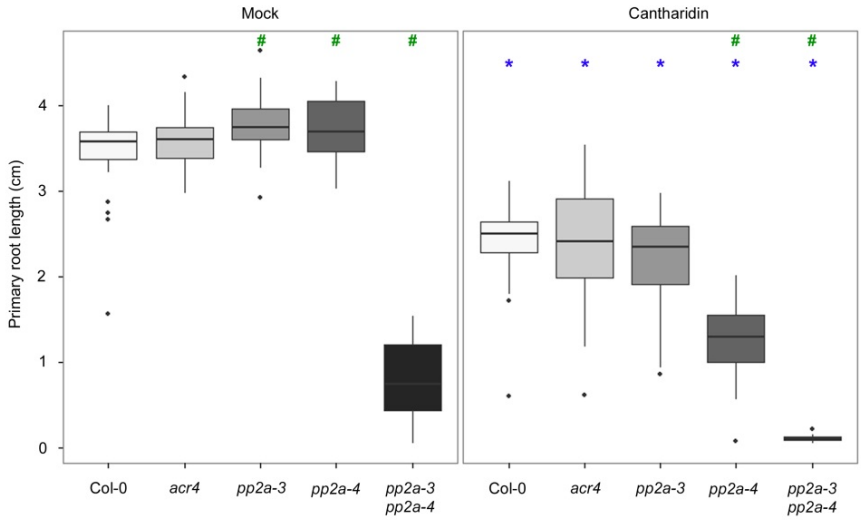

Factors	Degrees of freedom	Sum Sq	Mean Sq	F value	Pr(>F)
Line	5	233.71	46.74	123.87	< 2e-16
Treatment	1	163.14	163.14	432.34	< 2e-16
Line: Treatment (interaction)	5	23.43	4.69	12.42	6.36e-11
Residuals	288	108.67	0.38		

Figure S7. Impact of cantharidin on Col-0, *acr4*, *pp2a-3, pp2a-4* and *pp2a-3 pp2a-4* primary root length at 7 days after germination (seedlings continuously grown on cantharidin 50 µM). * or #, p-value < 0.05 according to Student's *t*-Test compared to mock or Col-0 (within mock or cantharidin treated), respectively. Boxplots with outliers are shown. Table indicates two-way ANOVA analysi

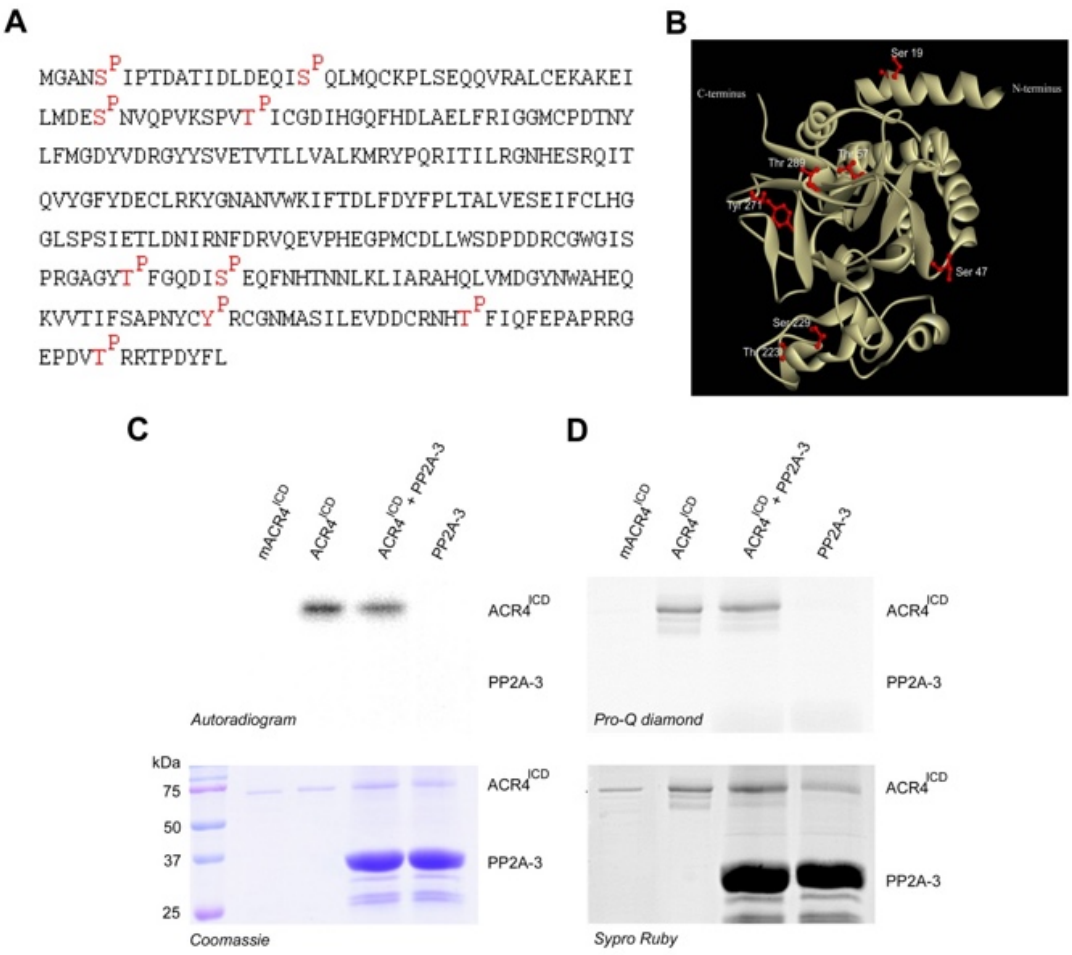

Figure S8. (A-B) ACR4-mediated phosphosites on PP2A-3. (A) Summary of ACR4-mediated phosphosites as determined by mass spectrometry of *in vitro* phosphorylated PP2A-3 and mapped on PP2A-3 protein sequence from TAIR. (B) Homology model of PP2A-3 showing 7 of the 9 phosphorylated residues (red ball and stick). **(C-D)** *E. coli*-expressed PP2A-3 does not dephosphorylate ACR4^{ICD}. (C) Phosphatase assay using [γ^{32P}] labeled ACR4^{ICD} and autoradiogram. Lower panel, Coomassie stained gel; upper panel, corresponding autoradiogram. From left to right, molecular weight standards; 1 µg of mutant inactive kinase mACR4^{ICD} (*lane* 1); 1 µg of auto phosphorylated [γ^{32P}] ACR4^{ICD} (with free ATP removed) (*lane* 2); 1 µg of auto phosphorylated [γ^{32P}] ACR4^{ICD} (with free ATP removed) incubated with 10 µg PP2A-3 in phosphatase buffer *(lane 3*); 10 µg PP2A-

3 in phosphatase buffer (*lane 4*). (D) Phosphatase assay using ACR4^{ICD} phosphorylated with cold ATP and phosphoprotein Pro-Q Diamond staining. Lower panel, Sypro Ruby stained gel; upper panel, corresponding Pro-Q Diamond stained gel. From left to right, 1 µg of mutant inactive kinase mACR4^{ICD} (*lane* 1); 1 µg of auto phosphorylated ACR4^{ICD} (with free ATP removed) (*lane* 2); 1 µg of auto phosphorylated ACR4^{ICD} (with free ATP removed) incubated with 10 µg PP2A-3 in phosphatase buffer (*lane* 3); 10 µg PP2A-3 in phosphatase buffer (*lane* 4).

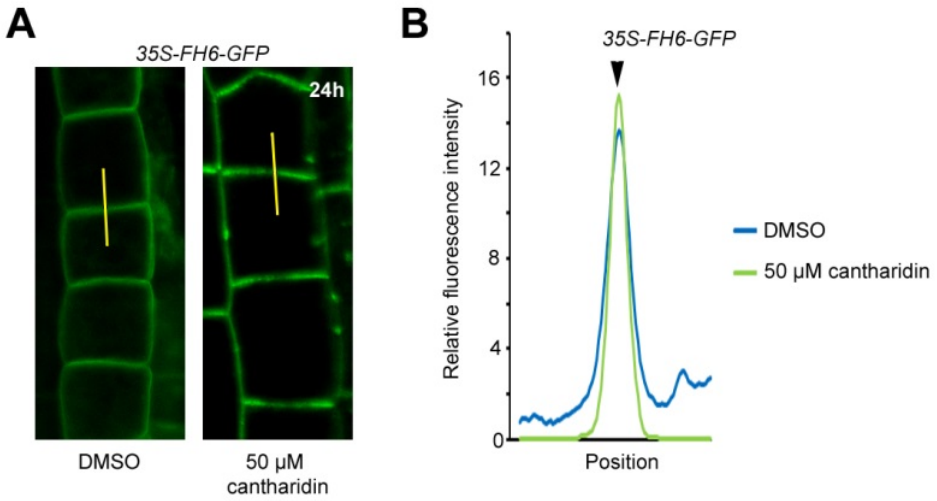

Figure S9. Localization of membrane marker FH6: GFP following treatment with DMSO or 50 µM cantharidin for 24 hours. **(A)** Localization of FH6: GFP. **(B)** Quantification of GFP signal across the yellow line in (A) as smooth average graph. Arrowhead, position of plasma membrane.

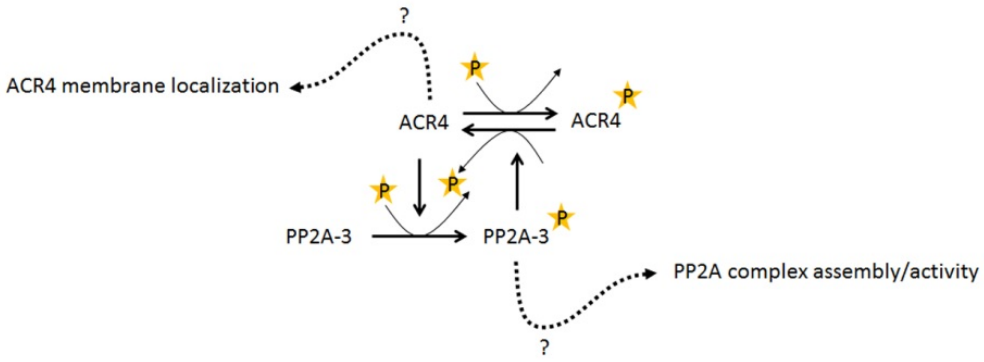

Figure S10. Tentative model for the interactions between ACR4 and PP2A-3.

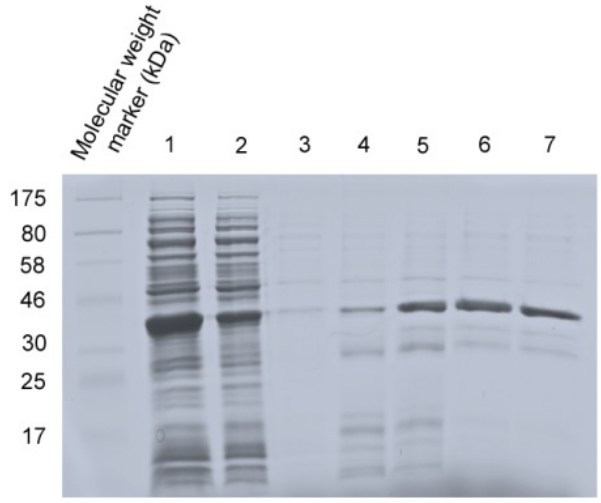

Figure S11. Analysis of PP2A-3 protein purification by SDS-PAGE. *Lane 1*, total protein from *E. coli* lysate; *Lane* 2, flow-through after incubation of lysate with Ni-NTA resin; *Lane 3,* fraction collected after washing the resin with buffer containing 6M urea; *Lanes 4-7*, four fractions collected with elution buffer containing 250 mM imidazole and 6 M urea.

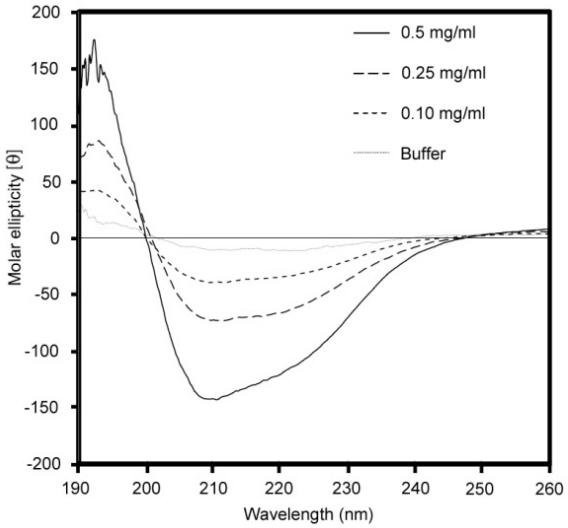

Figure S12. Conformational analysis of PP2A-3. Far UV CD spectra in 10 mM Tris (pH 7.4) and 0.1 mM TCEP at concentrations of 0.5 mg/ml, 0.25 mg/ml and 0.10 mg/ml. Minima are observed at ~208 and 222 nm, indicating a dominant α-helical structure.

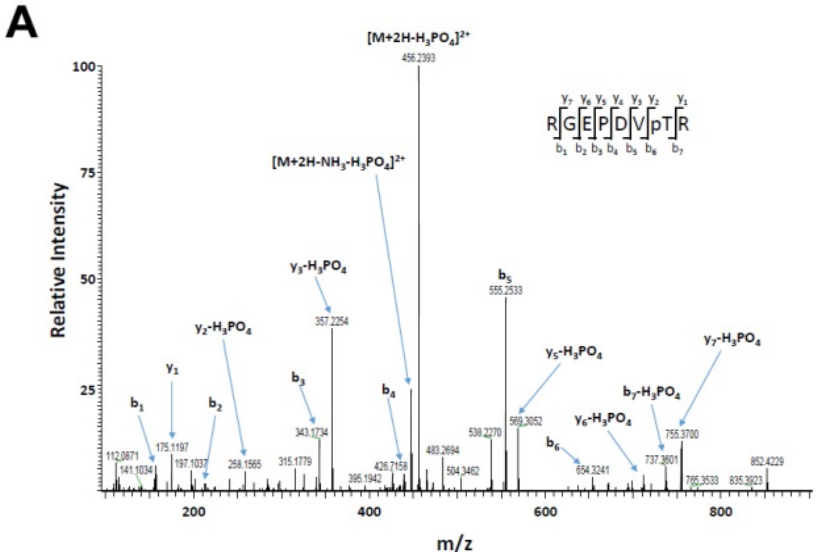

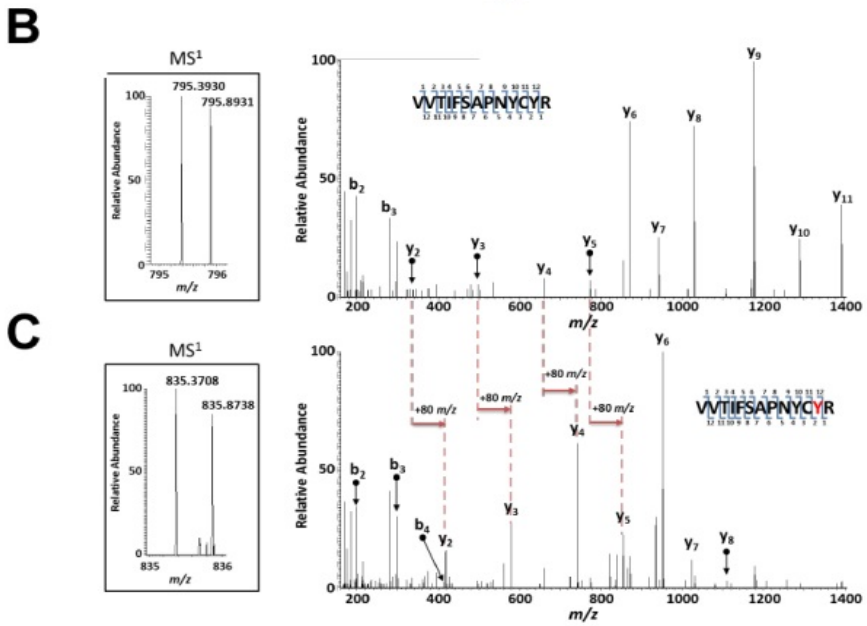

Figure S13. Examples of phosphopeptide determination. **(A)** Collision-induced high resolution fragmentation spectrum of the phosphopeptide RGEPDVpTR encompassing residues 299-305 (underlined). The presence of phosphorylated y-series fragment ions y2-y7 confirms T305 as the site of phosphorylation. **(B-C)** Collision-induced high resolution fragmentation spectrum of the peptide VVTIFSAPNYCYR (Mascot ion score 65) (B) and the phosphorylated VVTIFSAPNYCpYR (Mascot ion score 62) (C), encompassing residues 260-272 of the PP2A3c sequence (underlines). The MS1 panels show the MS spectrum of the doubly charged protonated molecular ion [M+2H]2+ for each peptide (B-C). Isotope clusters are separated by 0.50 Da, confirming the charge state of each peptide. The MS/MS spectrum demonstrates the presence of the phosphorylated y-series fragment ions, y2-y8, confirms Y271as the site of phosphorylation (C). As an example, the nominal mass shift of a 80 m/z units is represented for the phosphorylated y2-y5 fragments ions is shown.

Additional Experiments

Pull down assay

The MBP fused intracellular domain of ACR4 kinase (20 μg per reaction) was used as bait to pull out 6XHis-tagged PP2A3c (30 μg per reaction). Depending on the assay conditions, MBP-ACR4(ICD) was auto phosphorylated in 200 μl Kinase Buffer (20 mM Bis-Tris pH 7.2, 25 mM NaCl, 5mM $MnCl_2$, 1 mM DTT) and 100 μM ATP, 1 h prior to pull-down experiments[1]. Separate reactions with phosphorylated and naïve ACR4-ICD were incubated with 25 μl bed volume of amylose resin. Binding buffer was added (50 mM Tris-HCl pH 7.4, 150 mM NaCl, 1 mM DTT, 0.02% NP-40) to a final reaction volume of 500 μl and the proteins were allowed to bind to resin for 1h on a rotator at room temperature. Subsequently, 30 μg of PP2A3c was added and the reactions were further incubated for 1h at room temperature on rotator. Reactions were spun down at 1,000 rpm for 30 sec to pellet the resin. The resin was washed three times with binding buffer to remove unbound protein. After the third wash, the supernatant was removed and 100 μl of 1X SDS buffer was added to the resin. The resin/protein mixture was boiled at 95ºC for 5 min, and then centrifuged at max speed to pellet resin. 50 μl of supernatant from each reaction was separated by 12% SDS-PAGE and proteins were analyzed by Coomassie staining.

Kinase Assay between PP2A3c and ACR4 kinase phospho mutants.

1 μg SUMO fused ACR4 ICD (wild type, inactive SUMO-ACR4- 2m mutant, and alanine mutants of ACR4 phosphorylation sites) were first auto phosphorylated using 2 μCi of [γ-^{32}P] ATP in kinase buffer for 1 h at room temperature as reported previously. Sixteen sites of phosphorylation were determined and the non-phosphorylated alanine for

each phospho-site mutant were prepared as described in [2]. Subsequently, 10 µg of purified PP2A3c was added to 20 µl reaction volume containing 1 µg of the auto phosphorylated sACR4 protein(s) in kinase buffer for 1 h at RT. Reactions were terminated by the addition of 6µL of 4X Lammeli buffer and boiling for 5 min at 95°C. Proteins were resolved by 12% SDS-PAGE, stained with Coomassie Brilliant Blue R-250, and then analyzed by exposure to an autoradiograph film or a phosphor imaging screen.

Analytical ultracentrifugation

Sedimentation velocity analysis of PP2A3-6H, was performed on an XL-A analytical ultracentrifuge (Beckman Coulter). The purified protein was dialyzed overnight at 4 °C in 10 mM Tris- HCl (pH 7.4), 50 mM NaCl, and 0.1 mM TCEP. The protein sample was concentrated to an A_{280} of 0.5; 300 µL of the sample was loaded into a preassembled flow-through assembly housing an Epon, two-channel centerpiece and quartz windows. The rotor and sample cell temperatures were allowed to equilibrate to 20°C for 2h. The sample was spun at 30000 rpm and 20°C for a total of 300 scans with a scan rate of one scan per minute. Boundaries were monitored by recording the absorbance at 280 nm. Scan analysis was performed using Van Holde-Weischet analysis [3] as implemented in Ultrascan II. Sedimentation coefficients ($S_{20,w}$) were corrected for 20 °C and water.

Results & Discussion

ACR4 interacts with PP2A3c

In addition to the pull-down assay performed by our collaborators (Figure 1 C), and previously described gel filtration and overlay assays which established the interaction between ACR4 and PP2A3c (Figure. S3 and SI Supplemental Notes), we provide evidence of interaction between PP2A3c and ICD of ACR4 independent of the phosphorylation state

of ACR4-ICD by means of a pull-down assay (Figure A1), where both naïve and auto phosphorylated MBP-fused ACR4 (ICD) interact with PP2A3c (*Lane 3* and *Lane 4*)

Oligomeric state of PP2A3c

The denatured and renatured PP2A3c purified through affinity chromatography and a secondary size exclusion chromatography was predominantly produced as an oligomer (FigureS3, F-G). To eliminate unordered aggregates caused due to possibility of any unaccounted disulfide bonds in the purified fractions, the affinity enriched PP2A3c-6H (in an elution buffer (described previously) containing 1mM DTT), was further dialyzed under high reducing conditions into a buffer with 10mM DTT and purified through a G200 size exclusion chromatography superdex column in a buffer containing 50 mM Tris pH 7.2, 100 mM NaCl, 10 mM DTT and 100 μM $MnCl_2$ (data not shown). We also attempted to break open the oligomer by running the affinity enriched sample under high salt conditions in a buffer containing 50 mM Tris pH 7.2, 1M NaCl, 10 mM DTT and 100 μM $MnCl_2$. (data not shown). Under both these conditions, the protein solely eluted in the void volume fraction of G200 column, suggesting the oligomer is not a disordered aggregate but a high molecular weight ordered aggregate. We performed sedimentation velocity to determine the self-association property of PP2A3c-6H. The homogenous non-interacting molecules sediment with discrete sedimentation coefficients (S) values, whereas the higher ordered oligomers formed by interacting molecules exhibit a broad range of sedimenting species. Figure A2(*top*) represents the sedimentation velocity analysis of PP2A3-6H where the percent distribution of species is plotted as diffusion –corrected sedimentation coefficients along the sedimentation boundary. Figure A2 (*bottom*) represents the Van Holde – Weischet analysis of the same data, where the sedimenting boundary is divided into

numerous segments and the data is fit by linear least-square analysis to the apparent sedimentation coefficient of each boundary segment. Figure A2 (*top*) shows about 25% of sedimenting species exists as homogenous non-interacting monomeric species with $S_{20, w}$ value of 4 and the rest 75% show a considerably wider range of much higher S values, representing heterogeneous mix of polymeric species. The sedimentation coefficient of non-interacting homogenous samples yield a same sedimentation coefficient as a function of time in all the parts of the sedimenting boundary and the extrapolated lines for the various segments converge to a single value at the y-axis [3,4] but PP2A3c-6H, (Figure A2, *bottom*) show different sedimentation coefficients when the different parts of the sedimenting boundary are extrapolated, indicating the heterogeneous nature of PP2A3c-6H. Together these results suggest the high ordered oligomeric nature of PP2A3c-6H.

Phosphorylation of PP2A3c is independent of the phosphorylation state of ACR4.

To further analyze the nature of substrate (PP2A3c) phosphorylation by intracellular domain of ACR4, we utilized non-phosphorylated alanine mutants of sixteen phosphorylated residues of ACR4 ICD and performed kinase assay against PP2A3c. Clearly, we did not observe any phospho- mutant to inhibit or enhance the phosphorylation state of PP2A3c qualitatively, suggesting the phosphorylation of PP2A3c is independent of the specified phosphorylated state of ACR4 or it is also reasonable to speculate these phosphorylated residues are not important for the interaction between ACR4 and PP2A3c.

References

1. Meyer MR, Lichti CF, Townsend RR, Rao AG (2011) Identification of in vitro autophosphorylation sites and effects of phosphorylation on the Arabidopsis CRINKLY4 (ACR4) receptor-like kinase intracellular domain: insights into conformation, oligomerization, and activity. Biochemistry 50: 2170-2186.
2. Meyer MR, Shah S, Rao AG (2013) Insights into molecular interactions between the juxtamembrane and kinase subdomains of the Arabidopsis Crinkly-4 receptor-like kinase. Arch Biochem Biophys 535: 101-110.
3. Holde KEV (1978) Boundary analysis of sedimentation-velocity experiments with monodisperse and paucidisperse solutes. Biopolymers 17,: 1387–1403.
4. Hansen JC, Lebowitz J, Demeler B (1994) Analytical Ultracentrifugation of Complex Macromolecular Systems. Biochemistry 33: 13155-13163

Figures

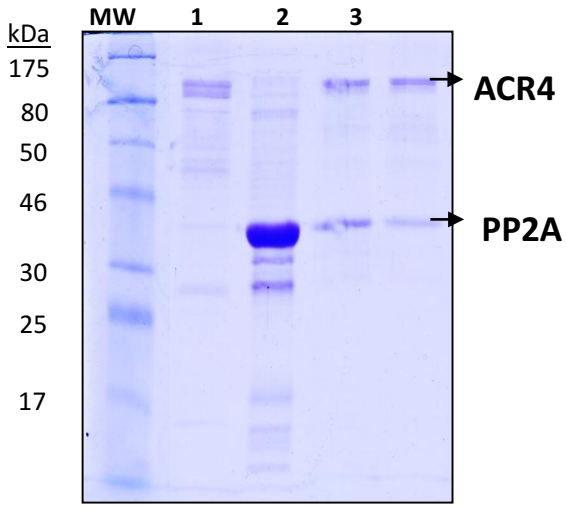

Figure A1: Pull-down assays were performed to determine the interaction between MBP-fused ACD4-ICD and PP2A3c as described in Materials & Methods. Supernatants from pull-down reactions were separated by 12% SDS-PAGE. *Lane 1,* MBP-ACR4; *Lane 2,* His-tagged PP2A3c; *Lane 3,* auto phosphorylated ICD of ACR4 (pACR4) and His-tagged PP2A3c; *Lane 4,* naïve ACR4 and His-tagged PP2A3c. *Lanes 3 and 4* demonstrate that PP2A3c interacts with both naïve and auto phosphorylated ACR4.

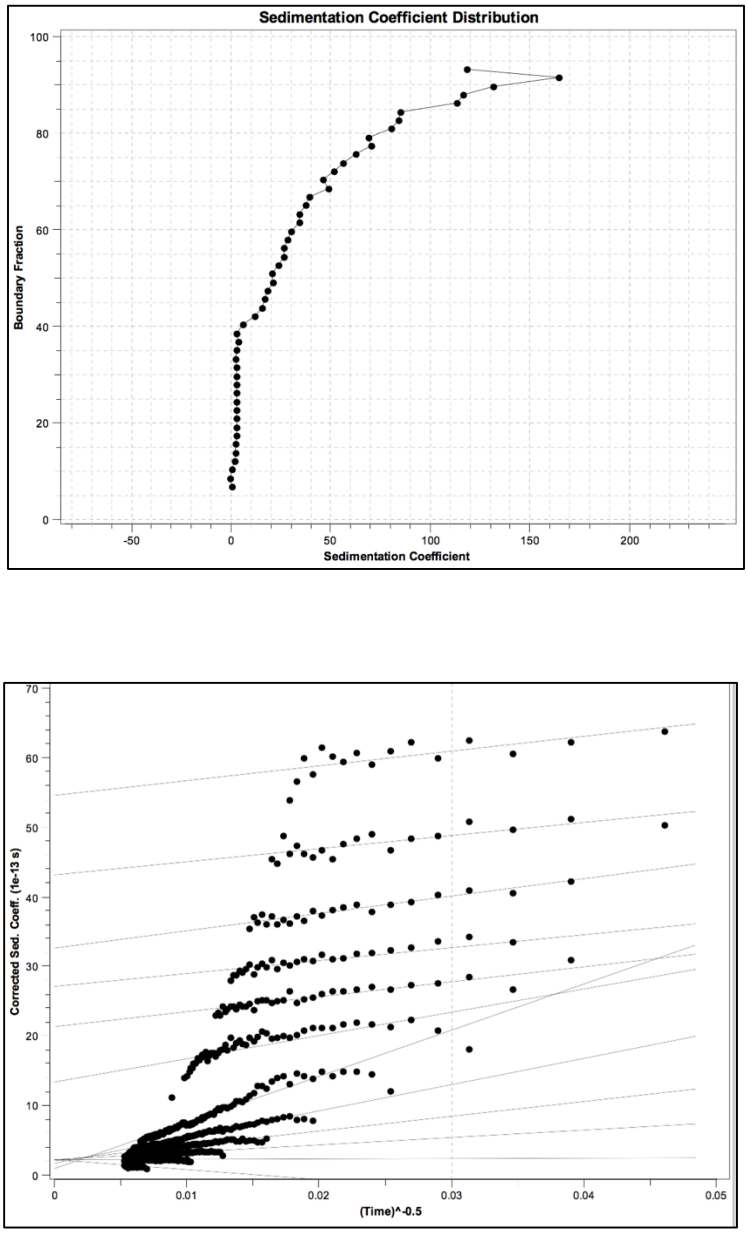

Figure A2: Top: Sedimentation velocity analysis of PP2A3-6H performed on an XL-A analytical ultracentrifuge using a protein sample with an A_{280} of 0.4. The sample was spun at 30000 rpm and 20 °C for a total of 300 scans with a scan rate of one scan per minute; (Bottom) Van Holde-Weischet analysis of PP2A3c.

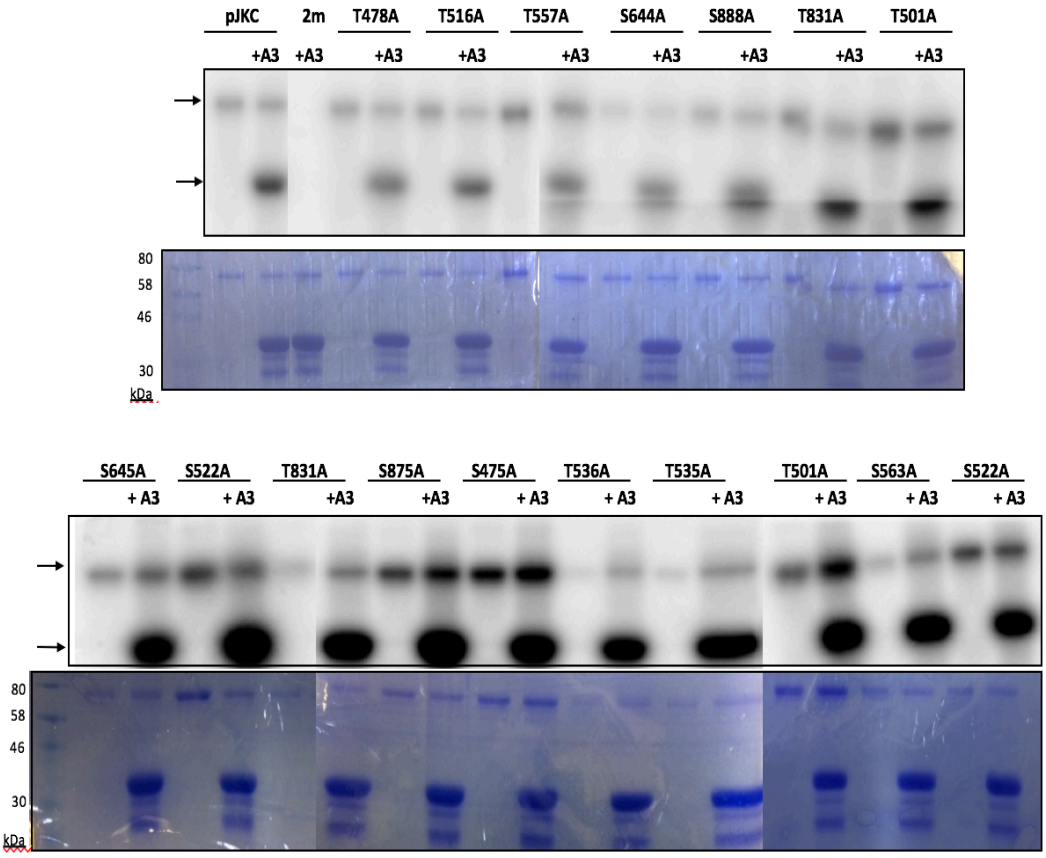

Figure A3: PP2A3c is phosphorylated by alanine mutants of ACR4 kinase phospho-sites. The assay was performed as described in Materials & Methods. 1 µg ACR4 protein (wild type, inactive mutant and described alanine phospho-mutants) were incubated in the kinase reaction with 10 µg of PP2A3c-6H. Proteins were resolved on a 12% SDS-PAGE gel, coomassie stained (*Bottom*) and, analyzed by phosphor-imaging (*Top).*

CHAPTER 3: TOWARDS THE *IN VITRO* ACTIVATION OF *ARABIDOPSIS* PHOSPHATASE PP2A3 CATALYTIC SUBUNIT EXPRESSED IN *ESCHERICHIA COLI*

A manuscript prepared for submission to PLOS one

Priyanka Sandal, Shweta Shah, Matthew R. Meyer, A. Gururaj Rao

Abstract

Protein Phosphatase 2A (PP2A) is a serine/threonine phosphatase that exists as a hetero-trimeric complex composed of the Scaffold A subunit, the catalytic C subunit and the substrate specific variable B subunit. PP2A-3 and PP2A-4 are the two isoforms of the C subunit in *Arabidopsis*. We have previously demonstrated that one of the key steps in the regulation of formative cell division in the root is the interaction between the catalytic subunit of PP2A3 (PP2A3c) and the kinase domain of the receptor like kinase Arabidopsis CRINKLY4 (ACR4). Importantly, PP2A3c is phosphorylated by ACR4 and the phosphatase is the first described novel substrate for the receptor kinase. *In vivo*, the catalytic activity of PP2Ac and its interaction with other proteins is regulated by a variety of post-translational modifications and, owing to the intrinsic availability of all necessary regulatory proteins necessary for differential regulation and activation, expression in eukaryotic systems such as insect cell or mammalian cell cultures has been the preferred method for obtaining catalytically active human PP2Ac. Here, we describe an alternative expression system in *Escherichia coli.* Although the protein is initially expressed in an inactive form, distinct but measurable activity can be detected over time at room temperature suggesting a slow conformational change to an active state. Importantly, we demonstrate the ability to recover phosphatase activity *in vitro* in the presence of the

protein PP2A PHOSPHATASE ACTIVATOR also referred to as phosphotyrosyl phosphatase activator (PTPA).

Abbreviations

PP2A, protein phosphatase 2A; PP2A3c, catalytic subunit of PP2A3 isoform; ACR4, *Arabidopsis* CRINKLY 4; PTPA, phospho-tyrosyl phosphatase activator; LCMT-1, leucine carboxyl methyl transferase-1; PME-1, phospho methylesterase-1; MBP, maltose binding protein; MBP-PP2A3c, MBP-fused PP2A3c subunit; PP2A3c-Tr, MBP fused PP2A3c missing the C terminal residues RTPDYFL; LIC, ligation independent cloning; IPTG, isopropyl β-D-1-thiogalactopyranoside; DTT, dithiothreitol; AEBSF, 4-(2-aminoethyl) benzene sulfonyl fluoride hydrochloride; IMAC, immobilized metal ion affinity chromatography; TBS, Tris buffered saline; FBS, fetal bovine serum; AP, alkaline phosphatase; SD, standard deviation; TCEP, [tris(2-carboxyethyl)phosphine]; F-PP2A3c, FLAG tagged PP2A3c; PP2A3c-6H, C-terminal 6xHistidine tagged PP2A3c.

Introduction

Protein phosphorylation is an important regulatory mechanism in eukaryotic cell signaling. Reversible phosphorylation is coordinated by kinases and phosphatases. PP2A is a major phosphatase that belongs to the Phosphoprotein Phosphatase (PPP) family of phosphatase enzymes and is highly conserved among eukaryotes. It regulates diverse physiological and cellular processes in humans [1] and is implicated in diseases such as cancer [2] and Alzheimer's [3]. In plants, PP2A is one of the major plant serine/threonine phosphatases with important roles in growth and development [4,5], cytoskeleton structure formation [6], auxin transport [7,8], biotic and abiotic stress signaling [9], abscisic acid and ethylene signaling [10,11,12]. In a previous study [13], we have demonstrated that PP2A3c

is a substrate for ACR4 and that a signaling pathway mediated by this interaction could be a key determinant in the regulation of formative cell division in the *Arabidopsis* root.he core PP2A enzyme exists as a heterodimer composed of the catalytic subunit (PP2A-C) and a scaffolding/regulatory subunit (PP2A-A). Specificity of phosphatase activity is provided via a combinatorial array of holoenzymes from an assembly of the core enzyme with different isoforms of the B subunit[14]. *Arabidopsis* has five genes encoding PP2A-C (C1-5), three genes encoding 'A' subunit (A1-3) and seventeen genes encoding 'B' subunits[15]. *In vivo*, the biogenesis, assembly and activity of the enzymatic complex is regulated by a variety of post-translational modifications and protein-protein interactions. These include activation of inactive PP2A-C by PTPA through interaction with both active site residues and the conserved C-terminal tail of PP2A-C [16,17], the carboxy-methylation of the C-terminal leucine by Leucine Carboxy-Methyl Transferase LCMT-1 that is required for binding to 'B' subunit and holoenzyme assembly [14], the subtle interplay with the PP2A specific phospho-methylesterase PME-1 that modulates holoenzyme interactions by reversing the C-terminal methylation [18,19] and, phosphorylation of Thr 304 and Tyr 307 in the catalytic subunit that inhibit catalytic activity [20]. Significant insights into PP2A function have been obtained from biochemical investigations of the protein in different organisms and structural investigations of the core and holoenzyme have advanced our mechanistic understanding of catalysis. Notwithstanding these studies, the molecular basis of what appears to be a tightly controlled linear process *in vivo* may be better understood through parallel structure-function studies *in vitro* with individual recombinantly produced proteins that can be used to query the biochemical context of specific interactions through biochemical, biophysical and mutagenesis experiments.

Owing to the intrinsic availability of all necessary regulatory proteins necessary for differential regulation and activation, hitherto, our understanding of the role of post-translational modifications in the structure and function of PP2A-C has been developed predominantly through studies on protein expressed in mammalian cell cultures [21], insect cell cultures [22] and yeast cells [23] or direct extraction from animal (bovine) or plant cell extracts [24,25,26]. Given the expense and laboriousness of these systems, we now report on the expression of the catalytic chain of the isoform PP2A-3 from *Arabidopsis* (PP2A3c) in *E. coli,* to produce a platform for *in vitro* structural and functional investigations of PP2A assembly and regulation and, further delineate the important role of specific post-translational modifications in a more facile manner. To this end, in this study we describe the properties of MBP tagged PP2A3c and its mutants and demonstrate the ability to generate phosphatase activity *in vitro* in the presence of PTPA, also expressed in *E. coli.*

Material and methods

Construction of expression plasmids

The catalytic subunit of PP2A3 (TAIR, The Arabidopsis Information Resource; AT2G42500). Full length catalytic subunit of PP2A3c (PP2A3c, residues 1-313) and the truncated form (missing the C terminal residues RTPDYFL) PP2A3c-Tr [(residues 1-306) were cloned as C terminal fusions to Maltose binding protein (MBP) in pMAL-C2E vector (Addgene) using the same forward primer 5’GCGGGCGCGGCCTTAATGGGCGCGAATTCTATTCC 3’ for both clones with the reverse primer 5’CCAACCGCGGCCTCATCACAGGAAATAGTCTGGAGTCCT 3’ for the full length clone and 5’CCAACCGCGGCCTCATCGGGTGACGTCTGGTTCT 3’ for the truncated form producing MBP-PP2A3c and MBP-PP2A3c-Tr respectively. The PCR

amplified product was cloned by ligation independent cloning (LIC) [27] into an in-house modified pMAL–C2E vector containing the inserted LIC site 'CGGCCTTA' and, verified by DNA sequencing. Preparation of the mutant protein containing an Ala substitution at Tyr 311 (MBP-PP2A3c-Y311A) was completed using the Quick Change Multi Site-Directed Mutagenesis Kit (Stratagene) with the primer 5' CGAAGGACACCTGACGCTTTCCTTTGAGGC 3' and mutation was verified by DNA sequencing.

PP2A phosphatase activator (also referred to as phosphotyrosyl phosphatase activator, PTPA). (TAIR; AT4G08960) was cloned as a N-terminus fusion to 6x His tag (PTPA-6H) in a pET-28c vector (Novagen) using forward primer 5' GCAGCGGCACCATGGAACCTCCAAAGGAACAACAAAAC 3'and reverse primer 5' GCAGCGCTCGAGGCCCTGAAAATACAGGTTTTCCTCTTCCCATTTGATGAGCC AG with NcoI and XhoI restriction sites respectively.

Intracellular domain of ACR4. N-terminus SUMO fused ACR4 ICD was produced as described by Meyer et al. [28]

Cloning of PP2A3c for Baculovirus Insect cell expression. PP2A3c was PCR amplified using forward primer 5'CACCATGGACTACAAAGACGATGACGACAAGATGGGCGCGAATTCTATTCC GACG 3'and reverse primer 5'TCACAGGAAATAGTCTGGAGTCC3'as a C-terminal fusion to FLAG epitope tag. The amplified gene (F-PP2A3c) was cloned into pENTR/D-TOPO vector using pENTR directional TOPO cloning kit (Invitrogen). In-frame cloning was verified by DNA sequencing. LR clonase II enzyme (Invitrogen) was used to

recombine pENTR vector containing the PP2A3c subunit *in vitro* with BaculoDirect C-Term Linear DNA (Invitrogen) according to the manufacturer's instructions (Invitrogen).

Protein Expression and Purification

MBP-PP2A3c, MBP-PP2A3c-Tr and MBP-PP2A3c-Y311A. Respective plasmids were transformed into chemically competent T7 express cells (NEB). A 500-ml culture supplemented with ampicillin (50 µg/ml) was grown at 37 °C until O. D_{600} of 0.6 before inducing for 5 h at 20 °C with 0.5 mM IPTG. Cell pellets were harvested by centrifugation, resuspended in 20 ml of lysis buffer (1x TBS pH 7.4, 0.5% Triton, 1mM DTT and 1 mM AEBSF). Cells were sonicated on ice and clarified lysate was prepared after centrifugation at 24470 x g for 20 min at 4 °C. Supernatant was incubated with 250 µl of amylose resin (NEB) equilibrated with lysis buffer for 1 h at 4 °C. Unbound protein was removed with 1x TBS pH 7.4 and 1mM DTT. Bound protein was eluted from the amylose resin using freshly prepared elution buffer 1x TBS pH 7.4, 1 mM DTT and 10 mM Maltose. A secondary purification was performed on an ÄKTA FPLC system (Amersham) using Global 10/300 Superdex G200 column (GE Healthcare) equilibrated with column buffer (50 mM Tris-HCl pH 7.4, 100 mM NaCl, 1 mM DTT, 100 µM $MnCl_2$ and 100 µM $MgCl_2$). Protein was eluted at a rate of 0.4 ml/min and 300 µl fractions of appropriate peaks collected and pooled to be used for further study. Approximately 1 mg of purified protein is obtained from 2.5 L of culture as determined by Bradford assay [29].

The C-terminal of MBP protein includes a ‘DDDK’ motif, a cleavage site for enterokinase protease which specifically cleaves after the lysine residue. Enterokinase protease (NEB) was used to cleave the tag from the fusion protein (MBP-free). Briefly, 25 µg of Maltose free MBP-PP2A proteins were incubated in 20mM Tris pH 8, 50 mM NaCl

and 2 mM $CaCl_2$, with 1unit of enterokinase protease in a 100 µl reaction volume overnight at 23 °C in a temperature controlled water bath. Cleaved MBP protein was removed by incubation with amylose resin (NEB) equilibrated with 1x TBS pH7.4, 1mM DTT and 1mM AEBSF, and the MBP- free protein present in the supernatant was carefully pipetted out. However, we were unsuccessful in obtaining enriched tag less PP2A3c after the enterokinase cleavage.

PTPA-6H. Briefly, PTPA-6H was expressed in Rosetta (DE3) pLysS (Novagen) expression cells. A 500ml culture was grown to $O.D_{600}$ of 0.6 at 37 °C and, expression was induced with 0.25 mM IPTG at 23 °C for 4 h. Protein was purified by resuspending 100 ml culture pellet in lysis buffer 1x TBS pH 7.4, 30 mM Imidazole, 0.5% Triton, 1 mM DTT & 1 mM AEBSF. Clarified lysate obtained after sonication and centrifugation was incubated with 250 µl of Ni^{2+} IMAC Sepharose High Performance resin (GE Healthcare) equilibrated with lysis buffer. Unbound protein was removed using wash buffer 1x TBS pH 7.4, 40 mM Imidazole and 1 mM DTT. Protein was eluted with 50 mM Bis-Tris pH 7.2, 50 mM NaCl, 200 mM Imidazole and 1 mM DTT (Figure. 9D). Concentration of eluted protein was determined by Bradford assay [29].

Expression of PP2A3c in Baculovirus. The recombined baculovirus DNA (N-terminus FLAG tagged PP2A3c; F-PP2A3c) produced using the gateway technology was transfected into Sf9 cells using Cellfectin II according to the Invitrogen's Manual. Sf9 cells (Invitrogen B825-01) were maintained as adherent culture at density of $4X10^5$ cells/ml in 10% FBS (Invitrogen) supplemented Sf900III SFM (1x) medium (Gibco). Four rounds of viral selection and amplifications were carried out as described by the manufacturer (Invitrogen). Cells were maintained at 27 °C and sub-cultured every 36 h. Recombinant

Baculovirus/viral stocks were produced and amplified in Sf9 cells and stored at 4 ºC/dark until further infection of Sf9/High-five cells. Small scale expression of F-PP2A3c was tested using viral stocks (50 µl to 1ml per 16 ml of adherent culture plate) and was compared with uninfected control adherent Sf9 cells. High five cells (Invitrogen) were grown in suspension culture in Express Five serum-free medium (Gibco Life) supplemented with 1x of Antibiotic Antimycotic Solution (Corning) and 10x of L-Glutamine (Gibco). Appropriate amount of fourth round of amplified Baculovirus stock (F-PP2A3c) determined from small scale test expression was used to infect $1X10^6$ cells/ml in suspension (20 ml of phage per 500 ml of High-five suspension cells). Cells were harvested after 36 h, resuspended in 1x TBS, pH 7.4, 1% Triton and 1 x of complete protease inhibitor cocktail tablet (Sigma). After sonication on ice, cells were centrifuged at 13,000 rpm for 1h at 4 °C. The supernatant was filtered through a 0.45 µm (corning) filter and loaded onto 1x TBS pH7.4 equilibrated ANTI-FLAG-M2 affinity resin (Sigma) for 2 h at 4 ºC. Unbound proteins were removed with 1x TBS pH7.4 and the bound protein was eluted under native conditions using a competitive 1x Flag-peptide (Sigma). Secondary purification was performed on an anion exchange Hi-trap Q (GE healthcare) column using Buffer A- 30 mM ethanolamine pH 9 & Buffer B -30 mM ethanolamine pH 9, 1 M NaCl. Approximately 80-100 µg of F-PP2A3c is recovered from 500 ml of suspension culture. Protein was detected by Western blot analysis using primary antibody: Anti-PP2A3c monoclonal antibody (Millipore); Anti-FLAG monoclonal antibody (Sigma) and Anti-methyl-PP2A antibody (Millipore) and Alkaline phosphatase (AP) conjugated Anti-mouse IgG secondary antibody (Sigma). The detection was completed using AP Conjugate Substrate Kit (Bio-Rad).

Functional Analysis of PP2A3c proteins

Phosphatase Activity assay. Protein samples (MBP-PP2A3c, MBP-PP2A3c-Tr & MBP-PP2A3c-Y311A) were prepared by incubation at 4 °C and 23 °C for 16 h in a temperature-controlled water bath and protein concentrations were determined by the Bradford assay [29]. A non-radioactive colorimetric phosphatase assay was performed in a 96 well (Costar Cat. # 3690) plate as follows. In each microtiter well, 100 µM (5 µl of 1 mM stock) of the supplied synthetic phospho-threonine peptide (RRApTVA) was incubated with 1x phosphatase assay buffer (50 mM Tris pH 7.4, 5 mM $MnCl_2$, 10 mM $MgCl_2$ and 1 mM DTT) for 3-5 min at room temperature and shaken prior to addition of enzyme. Reactions were initiated by addition of varying concentrations (0.5 µM-5 µM) of proteins in a total reaction volume of 50 µl for 20 mins at 30 °C. Negative controls without enzyme and without substrate were also set up. Reactions were terminated by addition of 50 µl of Molybdate dye/Additive mixture (as described in the manufacturer's protocol manual). The release of free phosphate from the phosphopeptide was detected after 15 min of stable color development at 23 °C. The optical density of the samples was read on a Spectramax 190 spectrophotometer (Molecular devices) at 630 nm. Each reaction was performed in triplicate. Absorbance readings were corrected for blank and data fitted by linear regression.

Phosphatase activity of the proteins was also performed using [γ^{32}P] labeled ACR4-ICD (pACR4) as a substrate. Briefly, auto phosphorylation of ACR4 (pACR4) was performed for 1 h as described by Meyer et al. [30] and the excess of unbound ATP was removed on a Ni-NTA column with multiple washes using 1x TBS/1 mM DTT followed by elution of bound pACR4 with elution buffer. 1 µg of the pACR4 was incubated for 1 h

at room temperature with 1 µg of PP2A3c protein in a 20 µl reaction volume containing 1x phosphatase buffer. Control reaction contained 1µg of pACR4 in phosphatase buffer with no PP2A3c protein. Reactions were stopped by addition of 4x SDS buffer and boiling for 5 min at 95 °C. Proteins were resolved by 12 % SDS-PAGE, stained with Coomassie Brilliant Blue R-250, and the radioactive bands were analyzed by phosphor imaging.

Potentiation of phosphatase activity by PTPA. Activation of the PP2A3c phosphatase activity was performed using PTPA-6H protein *in vitro* in the presence of ATP and $MgCl_2$. In the first step, 0.8 µM of MBP-PP2A3c was incubated with 0.8 µM of PTPA in phosphatase buffer in 40 µl reaction volume with 0.2 µM or 1 mM ATP for 1 h at 30 °C. Subsequently, phosphatase activity assay was performed by addition of 0.8 µM of pACR4 to the PTPA-PP2A3c samples and incubating for various time periods. Reactions were stopped by addition of 4x SDS buffer and boiling for 5 min at 95 °C. Control reactions were performed under similar condition but in absence of PTPA activator. Proteins were resolved by 12 % SDS-PAGE, stained with Coomassie Brilliant Blue R-250, and then analyzed by exposure to a phosphor imaging screen. The gel bands corresponding to radioactive pACR4 at varying time points were excised, incubated in 5 ml of scintillation cocktail and amount of radioactive [γ^{32}P] incorporation was quantified by liquid scintillation counting. Each condition was tested at least three times and all results are presented as mean (SD). Error bars were calculated for each data point using the standard deviation from the mean.

Conformational studies

The conformational difference between MBP-PP2A3c at 23 °C and 4 °C was probed by intrinsic fluorescence measurements and limited proteolysis by trypsin.

Intrinsic fluorescence: MBP-PP2A3c was first dialyzed against 10 mM Tris-HCl pH 7.4 and 0.1 mM TCEP and incubated at 23 ºC and 4 ºC overnight. Fluorescence scans were then performed on protein samples adjusted to an A_{280} of 0.1. Measurements were made in a 1 cm cuvette at room temperature with a Cary Eclipse spectrofluorometer (Varian). Scans were executed at an excitation wavelength of 280 nm, a bandwidth of 5 nm, and a scan speed of 120 nm/min.

Limited proteolysis*:* 125 µg of the overnight incubated MBP-PP2A3c at 23 °C and 4 °C was diluted into a 200 µl solution containing 50 mM Tris-HCl pH 8.0, 1 mM $CaCl_2$, and 1 mM DTT. Proteolysis by trypsin (Promega) at a 1:1000 (w/w) protease: substrate ratio was initiated at room temperature for defined time-points. Aliquots (25 µl) removed at predetermined time points, were stopped by the addition of 6 µl of 4xSDS sample buffer and boiling at 95 °C for 5 min. Samples were separated on a 10 % SDS-PAGE, and stained by Coomassie Blue staining.

Mass Spectrometry

Identification of phosphorylated residues in naïve PP2A3c by mass spectrometry was performed as described previously [13]. Briefly, peptides were generated from the reduced-alkylated protein by digestion with sequencing grade modified trypsin (Promega, Cat. # V511A) overnight at 37 °C, desalted on a reversed-phase column and phosphopeptides subsequently enriched using the PHOS-Select Ga^{3+} Silica Spin Column kit (Supelco) according to the kit instructions. The endoprotease (trypsin) digests were analyzed by using nano-LC-MS with a linear ion trap orbitrap mass spectrometer (Orbitrap ELITE) (Thermo Fisher Scientific) as described in [13]. The data-dependent tandem mass spectrometric analysis of the tryptic peptides revealed at least 3 phosphorylation sites.

Determination of the exact site of phosphorylation within the phosphopeptides was performed by inspection of their fragmentation pattern for specific diagnostic site-determining yn and bn ions [31].

Results

Expression, Purification, and Phosphatase activity of PP2A3c

In a recent paper [13] we described the expression of PP2A3c with a C-terminal Histidine tag in *E. coli* and subsequent purification and solubilization of the protein from inclusion bodies using urea. Here, we report expression of PP2A3c in *E. coli* as a C-terminal fusion to Maltose binding protein (MBP-PP2A3c) in a soluble form. An affinity (amylose resin) enriched PP2A3c preparation was purified by secondary size exclusion chromatography on a G-200 column as described in Materials and Methods (Figure. 1A). MBP-PP2A3c elutes in the void volume fraction presumably as an oligomer (*peak 1*) along with a fraction that elutes later in the chromatogram (*peak 2*). Changes in buffer composition, ionic strength and reducing conditions did not affect the elution of *peak 1* (data not shown). *Peak 1* and *2* protein fractions were resolved by SDS-PAGE (Figure. 1B) and the identity of the protein as PP2A3c was confirmed by western blot analysis using mouse monoclonal antibody against PP2A (Millipore) (Figure. 1C) and by MALDI-MS analysis of tryptic peptides of the excised protein band (data not shown). The far-UV CD spectrum of the MBP-PP2A3c indicated a predominantly α-helical structure with typical minima at 208 nm and 222 nm (Figure. 1D), in keeping with the crystal structure of PP2A [14,32,33]. Both *peak 1* and *peak 2* fractions were inactive as a phosphatase against a synthetic phospho-threonine peptide RRA(pT)VA (Promega) in a colorimetric assay measuring released phosphate and could not dephosphorylate [γ^{32}P] labeled pACR4

(Figure. 2A, *lane 3*). However, MBP-PP2A3c was a substrate for pACR4 and could be phosphorylated by pACR4 in a kinase assay using [γ^{32}P] ATP (Figure. 2B, *lanes 2* and *3*).

In a parallel effort, we also expressed PP2A3c recombinantly as C-terminal fusion to FLAG epitope tag (F-PP2A3c) in a Baculovirus insect cell expression system using High-five cells (Invitrogen) as described in Materials and Methods. Figure. 3A (*lane 1*) represents heterogeneous mix of proteins, including F-PP2A3c, obtained after an affinity enrichment with Anti-Flag M2 resin (Sigma) and anion exchange chromatography. The identity of F-PP2A3c was confirmed by mass spectrometry (data not shown) and none of the other proteins were identified as phosphatases. Importantly, this fraction containing F-PP2A3c, showed phosphatase activity using the synthetic phosphopeptide (data not shown) activity and was also able to dephosphorylate [γ^{32}P] labeled pACR4 (Figure. 3B, *lane 2*, autoradiogram). This may be attributed to an active PP2A3c with the methylated C-terminal Leucine, an important post-translational modification influencing both phosphatase activity and PP2A complex formation *in vivo* and, presence of endogenous activation chaperones such as PTPA. Indeed, western blot analysis using anti-methyl PP2Ac antibody (Millipore) confirmed the expression of methylated F-PP2A3c in the cell-lysate (Figure. 3C, last panel, *lane 1*) and enriched F-PP2A3c (Figure. 3C, last panel, *lane 2*). Western blots were also performed with anti-PP2A3c (Millipore) and anti-Flag (Sigma) antibodies (Figure. 3C).

Phosphorylated state of PP2A3c

In mammalian systems, the inactivity in PP2Ac has been attributed in part to phosphorylation of conserved residues Tyr 307 and Thr 304 in the C-terminal tail [34,35]. To determine the phosphorylation state of MBP-PP2A3c expressed in *E. coli* (naïve

protein), we performed tandem-mass spectrometric analysis of tryptic peptides from MBP-PP2A3c as well as the previously expressed PP2A3c-6H [13]. The conserved C terminal peptide containing the regulatory phosphorylation Tyr and Thr residues was not enriched in MBP-PP2A3c but was enriched in the PP2A3c-6H protein probably due to the presence of a basic histidine residues at the C terminus. We identified Tyr 311 to be phosphorylated as well as three other phosphorylated residues, Tyr 222, Thr 223 and Ser 265 (Figure. 4A and 4B). Tyr 311 corresponds to the conserved Tyr 307 residue in mammalian PP2Ac that is implicated in the phosphorylation dependent inhibition of phosphatase activity in mammalian system. Therefore, to verify this possibility in MBP-PP2A3c, we mutated Tyr 311 to Ala (PP2A3c-Y311A) and created a truncated version of MBP-PP2A3c missing the C-terminal residues TRRTPDYFL (PP2A3c-Tr). However, the mutant proteins did not show any phosphatase activity in the colorimetric phospho-peptide assay and nor were they able to dephosphorylate [γ^{32}P] pACR4 (Figure. 5A and 5B). This suggests that the observed lack of phosphatase activity of MBP-PP2A3c is unlikely to be due to the phosphorylation of Tyr 311.

MBP-PP2A3c shows measurable phosphatase activity after incubation at 23 °C for 16 h

To determine if the MBP-tag was inhibiting phosphatase activity, MBP-PP2A3c was incubated with enterokinase (NEB) at 23 °C for 16 h as described in Materials & Methods, to remove the tag. In parallel, a control reaction of MBP-PP2A3c without enterokinase was also prepared. Unfortunately, adequate amount of untagged PP2A3c could not be recovered to test for phosphatase activity after the cleavage reaction. Interestingly, however, the similarly incubated control displayed measurable phosphatase

activity against the synthetic phosphopeptide substrate in comparison with the protein incubated at 4 °C for 16 h which showed no discernible activity. This is shown in Figure. 6A as a function of MBP-PP2A3c concentration. Figure. 6B demonstrates that the Y311A mutant behaves similarly to the wildtype protein.

Activation of phosphatase activity is accompanied by a conformational change

To address whether the phosphatase activity was influenced by conformational changes, we used fluorescence spectroscopy and limited proteolysis, both versatile techniques that are sensitive to perturbations in conformation [36,37,38,39]. Fluorescence spectroscopy is a particularly sensitive probe of protein folding and is significantly influenced by the microenvironment of tyrosine and tryptophan residues. At 280 nm both these aromatic residues absorb and contribute to the emission spectra. When excited at 280 nm, the intrinsic fluorescence spectra of MBP-PP2A3c incubated at 4 °C and 23 °C showed an emission λ_{max} around 342 nm. However, the quantum yield of fluorescence was significantly higher for the protein kept at 23 °C for 16 h, suggesting a distinct conformational difference (Figure. 7).

Limited proteolysis is also a widely used reporter of structural changes in proteins and a sensitive probe for detecting changes in protein flexibility as measured by the susceptibility of peptide bonds to proteolysis in the context of the local structure and interactions [37]. The digestive patterns of proteins at 4 °C (Figure. 8A) and 23 °C (Figure. 8C) show a distinct difference in the proteolytic fragments generated on digestion with trypsin as a function of time. The fragment(s), indicated with an *, was identified as MBP by mass spectrometry and appears as two fragments in the 4 °C sample (Figure. 8A) but just one in the 23 °C protein (Figure. 8C). Fragments labeled ***a***, ***b*** and ***c*** are derived from

PP2A3c as analyzed by mass spectrometry and western blot analysis using Anti-PP2Ac antibody (Figure. 8B and 8D). Whereas the appearance of fragment ***a*** is similar in both samples, it is worth noting that fragment ***b*** has a significantly stronger presence in the 4 °C sample (Figure. 8A and B) compared to the 23 °C sample (Figure. 8C and D). Fragment **c** appears in both the 4 °C and 23 °C protein samples (Figure. 8A and C) but is less detectable in the Western blot of the 23 °C sample (Figure. 8D).

MBP-PP2A3c can be activated by PTPA

PTPA is an ATP-dependent activation chaperone, known to play a key role in the biogenesis of active PP2A in eukaryotes [16,40,41,42]. It is also reported to have isomerization activity on the conserved Pro 190 of PP2Ac [43]. We therefore examined the potential ability of recombinantly expressed PTPA (Figure. 9A) to activate PP2A3c *in vitro* in the presence of $MgCl_2$ and ATP, as described in Materials & Methods. We tested the phosphatase activity on both *Peak 1* and *Peak 2* protein fractions from gel filtration. When activated with equimolar amount of PTPA (0.8 μM) in the presence of 0.2 μM ATP as a function of time in hours (Figure. 9B, *top*), there was clear evidence of dephosphorylation of [γ^{32}P] pACR4 in the autoradiogram (Figure. 9B, *bottom*). A quantitative assessment of the radioactivity in the band indicated ~35% decrease in [γ^{32}P] pACR4 after 5 h (Figure. 9C). Measurable PTPA activated phosphatase activity was observed in both *peaks 1* and *2* in replicate experiments. Interestingly, the rate of reaction increased five-fold when the same reaction was performed in presence of 1 mM ATP. The autoradiogram (Figure. 10A, *bottom*) shows the progressive decrease in intensity of the [γ^{32}P] pACR4 band from 0 to 60 mins in contrast to the control without the PTPA (Figure. 10B). A quantitative assessment of the radioactivity in the [γ^{32}P] pACR4 band indicated ~35% decrease in

intensity after 60 mins (Figure. 10C). These experiments suggest that PTPA is able to activate PP2A3c phosphatase activity *in trans*, albeit to a modest extent.

Discussion

In this study, we describe the properties of an N-terminally tagged catalytic subunit of *Arabidopsis* PP2A3 (MBP-PP2A3c) expressed in *E. coli*. Previous attempts to over-express human PP2Ac in *E.coli* cells have met with limited success [44]. Typically, biochemical and structural investigations of biologically active PP2Ac have been performed either by direct extraction from host tissues [45] or by recombinant expression in yeast [23,46], mammalian cells [21] or insect cells [47,48,49] However, mammalian cell culturing is time consuming and expensive, and optimal expression and yields in insect cells until now were achieved only with active-site mutants with an attempt to overcome the auto-regulatory mechanism exerted by endogenous PP2Ac which depresses the expression of the transgenic protein but a recent study by Ikehara et al. [47,48,49] reported increase in expression of one of the two human PP2A isoforms (PP2B and not PP2Cα) in insect cells cultured at low temperature of 19 °C instead of 23 °C.

Herein, we report yields ~1 mg of purified protein from a 2.5 L of *E. coli* culture that can be substantially scaled up to rapidly obtain high milligram quantities of protein without undertaking the intensive and expensive insect cell or mammalian cell culturing. However, the protein lacks phosphatase activity. Although plausible, it is unlikely that the inactivity is due to the MBP tag at the N-terminus since the addition of the nine-amino acid hemagglutinin-peptide at the amino terminal end of PP2A does not inhibit the activity of the protein expressed in mammalian and insect cells [21]. Furthermore, the solubility of the protein and the predominantly α-helical conformation indicated by the CD analysis, are

indicative of a properly folded protein. The elution of the protein in gel filtration (Figure. 1) suggests that it forms native-like aggregates (from a normally folded protein) that is unlikely to be mediated by the MBP tag which is known to not dimerize [50]. Importantly, neither changes in salt concentration, reducing agent or low concentrations of urea were effective in disrupting the oligomeric fraction and the precise nature of the oligomer needs to be further investigated by other biophysical methods. It is worth noting, however, that there was little or no difference in the PTPA-mediated activation of the two peaks (Figure. 10C). We were also unsuccessful in cleaving the MBP-tag to obtain tag free protein but in ongoing and future experiments we will examine expression in E. coli using other fusion partners, varying various parameters that are known to affect expression as well as targeting the expression to the periplasm.

Since it is known that phosphorylation of Tyr 311 and Thr 304 can inhibit and regulate PP2A activity *in vivo and in vitro* [20,35], and that *E. coli* possess Tyr/ Ser/ Thr kinase activity [51,52], we speculated that the inactivity may be due to phosphorylation of these sites. We therefore investigated potential phosphorylation sites in naïve PP2A3c and, although we did not find evidence of Thr 304 phosphorylation, we clearly identified a phosphopeptide containing Tyr 311 phosphorylation and, interestingly, three other phosphorylation sites at Tyr 222, Thr 223 and Ser 265. There has been no previous report of phosphorylation at these sites and there is also no evidence of any associated inhibitory activity. Our future studies will examine the role of these sites in the activity of PP2A3c. Importantly, mutation of Tyr 311 to alanine did not restore phosphatase activity, suggesting that at least in the *Arabidopsis* PP2A3c homolog, phosphorylation of Tyr 311 may not be a regulatory step, although it remains to be verified *in planta.*

A particularly crucial step in the regulation of PP2Ac and its activity is its non-covalent interaction with the activator protein, PP2A phosphatase activator, PTPA. Structural studies [16] indicate that the PP2A-PTPA interaction stabilizes the active site of the catalytic subunit and forms a joint ATP-binding pocket that properly orients the γ-phosphate to chelate catalytic metal ions (Mg^{++}) and facilitates a conformational change in PP2A to acquire phosphatase activity. Subsequently, ATP hydrolysis is achieved by the activated PP2A phosphatase. Significantly, the molecular mechanism of activation, correlates with the peptidyl-prolyl isomerization activity of PTPA and the isomerization of the conserved Pro 190 in PP2Ac is believed to underpin the activation of the catalytic subunit [14]. Furthermore, the ATP-dependent activation of PP2Ac by PTPA also enhances phosphotyrosine phosphatase activity [53] and promotes the essential steps of association with the 'A' subunit, carboxymethylation of the C-terminal Leucine, and subsequent interaction with the 'B' subunit driving the formation of the whole heterotrimeric complex [2,16,17,32,54]. Interestingly, using chemically inactivated PP2Ac, Guo et al [16] also demonstrated that PTPA was crucial to restoring and stabilizing a proper protein fold of the catalytic chain required for activity and other studies [41,42,43] attest to the ability of PTPA to activate the inactive form of PP2Ac. We therefore examined the ability of recombinantly expressed PTPA to activate PP2A3c *in vitro* in the presence of ATP and Mg^{++} and observed significant activation of phosphatase activity against [γ^{32}P] labeled ACR4-ICD phosphorylated ACR4 (Figure.10A) Approximately 40% activation of PP2A3c phosphatase activity was observed at both low (0.2 μM) and high concentrations (1 mM -5 mM) of ATP, but the activation was more rapid at 1 mM ATP (minutes vs hours). Thus, in accordance with the structural studies of PTPA [16,53], we attribute the activation

of PP2A3c to the PTPA catalyzed prolyl isomerization along with composite ATPase activity of PTPA-PP2Ac complex. It is important to also contextualize the catalytic function of PP2Ac vis-à-vis other protein-protein interactions. Thus, using knockout strains of yeast, Hombauer et al [55] have shown that a functional interaction between the A subunit (TPD3) and PTPA (RRD2) can generate catalytically active C subunit. Therefore, in our future experiments we will examine the co-expression of PTPA A and C subunits in E. coli to obtain maximally active PP2A3c.

The modest but measurable phosphatase activity of MBP-PPA3c after overnight incubation at 23 °C is intriguing. We hypothesize that the purified protein exists in a near-native conformational state and undergoes a slow conformational change to a more "activated state". Although the exact structural difference between the two states is not obvious and remains to be determined, the observed change in the fluorescence spectrum and the difference in lability to proteolysis are indicative of significant differences in conformation. However, we do not have a clear understanding of the molecular basis of this activation. Importantly, even though prolyl *cis*/*trans* isomerization can be an enzymatically catalyzed process, it can also be an intrinsic mechanism in protein folding in native structures and regulate subtle conformational changes [56]. Therefore, in the absence of an isomerase, it may not unreasonable to propose that *cis*-*trans* isomerization of the peptide bond at Pro 190 could be one of the rate-limiting steps in protein folding to an "activated state". One must also consider the possibility of isomerization of non-prolyl *cis* peptide bonds in the slow activation of MBP-PP2A3c. Indeed, non-prolyl *cis* peptide bonds are not uncommon in the native structures of proteins [57] and can potentially affect folding kinetics time scale [58]. Another consideration is the role of the proline residue in

the SAPNYC sequence of PP2A3c (residues 265-270, Figure. 4B). This motif is highly conserved in the Ser/Thr PPP phosphatase family [43,59] and, in the case of calcineurin, the peptidyl-Pro undergoes isomerization from the *trans* to *cis* conformation, catalyzed by FKBP12 and cyclophilin A [43,59]. Although, there does not appear to be any structural evidence of a similar conformational state for peptidyl-Pro in PP2A3c [14,32], its potential role in the slow activation of MBP-PP2A3c may need further investigation. Sufficient to say, we do not presently, have a clear understanding of the molecular basis of this activation. Protein folding is a complex multistate process and proline residues play a particularly critical role in transitions to functionally different states [60,61]. Interestingly, slow structural transitions of proteins towards the native state have been observed in other proteins and a particularly interesting example is provided by rat muscle phosphoglycerate kinase that *in vivo* "ages" slowly to a different conformational state over time.

In summary, we offer the following perspectives. Within cells, protein-protein interactions are fundamental to assembly of protein complexes and are dictated by specific binding partners, binding sites and affinity of interaction (high and low). Clearly, important molecular understanding of the structure and function of PP2A has come from biochemical analysis in eukaryotic systems including mammalian, yeast and insect cells [21,23,45,46,47,48,49]. However, these systems are not ideal for producing adequate amounts of protein for more robust biochemical/biophysical investigations that can enhance our understanding of the PP2A complex and PP2A controlled signaling *in vivo*. To this end, to better understand the molecular interactions between the component chains and the molecular architecture of the PP2A complex, we have developed a facile system in *E. coli* to express and purify adequate quantities of the catalytic chain of PP2A as a fusion

protein with MBP. Although the initially expressed protein is *inactive* as a phosphatase, it displays the ability to be activated by PTPA, in *trans*. The system provides an excellent platform for reconstituting the complex with component proteins and dissecting and delineating the individual roles of the different modulators, both quantitative and qualitative, using diverse biochemical and biophysical approaches. Thus*, in vitro* studies using purified proteins can provide greater clarity on our molecular understanding of the important but conflicting role of methylation at the C-terminus in PP2Ac catalytic activity, its interaction with 'B' subunits in holoenzyme assembly *in vivo* versus *in vitro* [33,62], and subtle synergistic interactions between PTPA and reversible carboxy-methylation mediated by PME1[63,64]. While *in vivo* studies using the tools of genetics and cell biology are necessary to understand physiological function and evaluate phenotypic responses, a more holistic understanding of biological processes can be derived through a mechanistic understanding of the role of individual genes at the protein level. To this end, the E. coli system offers a low cost *in vitro* platform to interrogate the specific function of each of the players in the biogenesis of PP2A and conditionally examine the importance of posttranslational modifications on PP2A function. Our on-going studies are directed towards recapitulating a maximally active PP2A3c by co-expression of PP2A core enzyme along with PTPA in *E. coli*. Although our initial attempts to obtain a stoichiometric complex of the AC dimer in *E. coli* was not successful, the crude lysate containing the AC dimer showed significantly enhanced phosphatase activity upon activation by PTPA as measured by dephosphorylation of radio-labeled pACR4 (data not shown).

Acknowledgements

We thank Dr. Raji Joseph at the Roy. J- Carver Department of Biochemistry, Biophysics and Molecular Biology, Iowa State University, for providing valuable guidance and technical expertise in cloning and expression of FLAG tagged PP2A3c in Baculovirus insect cell culture expression system. We also thank R. Reid Townsend and the Proteomics Core Lab at Washington University in St. Louis, MO, for the mass spectrometry analysis of the naïve PP2A3c subunit.

References

1. Wlodarchak N, Xing Y (2016) PP2A as a master regulator of the cell cycle. Crit Rev Biochem Mol Biol 51: 162-184.
2. Janssens V, Goris J, Van Hoof C (2005) PP2A: the expected tumor suppressor. Curr Opin Genet Dev 15: 34-41.
3. Sontag E, Nunbhakdi-Craig V, Sontag JM, Diaz-Arrastia R, Ogris E, et al. (2007) Protein phosphatase 2A methyltransferase links homocysteine metabolism with tau and amyloid precursor protein regulation. J Neurosci 27: 2751-2759.
4. Zhou HW, Nussbaumer C, Chao Y, DeLong A (2004) Disparate roles for the regulatory A subunit isoforms in Arabidopsis protein phosphatase 2A. Plant Cell 16: 709-722.
5. Blakeslee JJ, Zhou HW, Heath JT, Skottke KR, Barrios JA, et al. (2008) Specificity of RCN1-mediated protein phosphatase 2A regulation in meristem organization and stress response in roots. Plant Physiol 146: 539-553.
6. Camilleri C, Azimzadeh J, Pastuglia M, Bellini C, Grandjean O, et al. (2002) The Arabidopsis TONNEAU2 gene encodes a putative novel protein phosphatase 2A regulatory subunit essential for the control of the cortical cytoskeleton. Plant Cell 14: 833-845.
7. Garbers C, DeLong A, Deruere J, Bernasconi P, Soll D (1996) A mutation in protein phosphatase 2A regulatory subunit A affects auxin transport in Arabidopsis. EMBO J 15: 2115-2124.
8. Michniewicz M, Zago MK, Abas L, Weijers D, Schweighofer A, et al. (2007) Antagonistic regulation of PIN phosphorylation by PP2A and PINOID directs auxin flux. Cell 130: 1044-1056.
9. Pais SM, Tellez-Inon MT, Capiati DA (2009) Serine/threonine protein phosphatases type 2A and their roles in stress signaling. Plant Signal Behav 4: 1013-1015.
10. Kwak JM, Moon JH, Murata Y, Kuchitsu K, Leonhardt N, et al. (2002) Disruption of a guard cell-expressed protein phosphatase 2A regulatory subunit, RCN1, confers abscisic acid insensitivity in Arabidopsis. Plant Cell 14: 2849-2861.
11. Larsen PB, Cancel JD (2003) Enhanced ethylene responsiveness in the Arabidopsis eer1 mutant results from a loss-of-function mutation in the protein phosphatase 2A A regulatory subunit, RCN1. Plant J 34: 709-718.

12. Pernas M, Garcia-Casado G, Rojo E, Solano R, Sanchez-Serrano JJ (2007) A protein phosphatase 2A catalytic subunit is a negative regulator of abscisic acid signalling. Plant J 51: 763-778.
13. Yue K, Sandal P, Williams EL, Murphy E, Stes E, et al. (2016) PP2A-3 interacts with ACR4 and regulates formative cell division in the Arabidopsis root. Proc Natl Acad Sci U S A 113: 1447-1452.
14. Cho US, Xu W (2007) Crystal structure of a protein phosphatase 2A heterotrimeric holoenzyme. Nature 445: 53-57.
15. Farkas I, Dombradi V, Miskei M, Szabados L, Koncz C (2007) Arabidopsis PPP family of serine/threonine phosphatases. Trends Plant Sci 12: 169-176.
16. Guo F, Stanevich V, Wlodarchak N, Sengupta R, Jiang L, et al. (2014) Structural basis of PP2A activation by PTPA, an ATP-dependent activation chaperone. Cell Res 24: 190-203.
17. Low C, Quistgaard EM, Kovermann M, Anandapadamanaban M, Balbach J, et al. (2014) Structural basis for PTPA interaction with the invariant C-terminal tail of PP2A. Biol Chem 395: 881-889.
18. Ogris E, Du X, Nelson KC, Mak EK, Yu XX, et al. (1999) A protein phosphatase methylesterase (PME-1) is one of several novel proteins stably associating with two inactive mutants of protein phosphatase 2A. J Biol Chem 274: 14382-14391.
19. Lee J, Chen Y, Tolstykh T, Stock J (1996) A specific protein carboxyl methylesterase that demethylates phosphoprotein phosphatase 2A in bovine brain. Proc Natl Acad Sci U S A 93: 6043-6047.
20. Luo Y, Nie YJ, Shi HR, Ni ZF, Wang Q, et al. (2013) PTPA activates protein phosphatase-2A through reducing its phosphorylation at tyrosine-307 with upregulation of protein tyrosine phosphatase 1B. Biochim Biophys Acta 1833: 1235-1243.
21. Wadzinski BE, Eisfelder BJ, Peruski LF, Jr., Mumby MC, Johnson GL (1992) NH2-terminal modification of the phosphatase 2A catalytic subunit allows functional expression in mammalian cells. J Biol Chem 267: 16883-16888.
22. Kamibayashi C, Estes R, Lickteig RL, Yang SI, Craft C, et al. (1994) Comparison of heterotrimeric protein phosphatase 2A containing different B subunits. J Biol Chem 269: 20139-20148.
23. Evans DR, Myles T, Hofsteenge J, Hemmings BA (1999) Functional expression of human PP2Ac in yeast permits the identification of novel C-terminal and dominant-negative mutant forms. J Biol Chem 274: 24038-24046.
24. Chen J, Hu R, Zhu Y, Shen G, Zhang H (2014) Arabidopsis PHOSPHOTYROSYL PHOSPHATASE ACTIVATOR is essential for PROTEIN PHOSPHATASE 2A holoenzyme assembly and plays important roles in hormone signaling, salt stress response, and plant development. Plant Physiol 166: 1519-1534.
25. Muniz Garcia MN, Muro MC, Mazzocchi LC, Pais SM, Stritzler M, et al. (2017) The protein phosphatase 2A catalytic subunit StPP2Ac2b acts as a positive regulator of tuberization induction in Solanum tuberosum L. Plant Mol Biol 93: 227-245.
26. Hu R, Zhu Y, Wei J, Chen J, Shi H, et al. (2017) Overexpression of PP2A-C5 that encodes the catalytic subunit 5 of protein phosphatase 2A in Arabidopsis confers better root and shoot development under salt conditions. Plant Cell Environ 40: 150-164.

27. Tonikian R, Zhang Y, Boone C, Sidhu SS (2007) Identifying specificity profiles for peptide recognition modules from phage-displayed peptide libraries. Nat Protoc 2: 1368-1386.
28. Meyer MR, Shah S, Rao AG (2013) Insights into molecular interactions between the juxtamembrane and kinase subdomains of the Arabidopsis Crinkly-4 receptor-like kinase. Arch Biochem Biophys 535: 101-110.
29. Bradford MM (1976) A rapid and sensitive method for the quantitation of microgram quantities of protein utilizing the principle of protein-dye binding. Anal Biochem 72: 248-254.
30. Meyer MR, Lichti CF, Townsend RR, Rao AG (2011) Identification of in vitro autophosphorylation sites and effects of phosphorylation on the Arabidopsis CRINKLY4 (ACR4) receptor-like kinase intracellular domain: insights into conformation, oligomerization, and activity. Biochemistry 50: 2170-2186.
31. Beausoleil SA, Villen J, Gerber SA, Rush J, Gygi SP (2006) A probability-based approach for high-throughput protein phosphorylation analysis and site localization. Nat Biotechnol 24: 1285-1292.
32. Xing Y, Xu Y, Chen Y, Jeffrey PD, Chao Y, et al. (2006) Structure of protein phosphatase 2A core enzyme bound to tumor-inducing toxins. Cell 127: 341-353.
33. Xu Y, Xing Y, Chen Y, Chao Y, Lin Z, et al. (2006) Structure of the protein phosphatase 2A holoenzyme. Cell 127: 1239-1251.
34. Cristobal I, Manso R, Rincon R, Carames C, Zazo S, et al. (2014) Phosphorylated protein phosphatase 2A determines poor outcome in patients with metastatic colorectal cancer. Br J Cancer 111: 756-762.
35. Liu R, Zhou XW, Tanila H, Bjorkdahl C, Wang JZ, et al. (2008) Phosphorylated PP2A (tyrosine 307) is associated with Alzheimer neurofibrillary pathology. J Cell Mol Med 12: 241-257.
36. Laskowicz JR (1986) Principles of Fluorescence Spectroscopy. Plenum Press, New York.
37. Fontana A, Fassina G, Vita C, Dalzoppo D, Zamai M, et al. (1986) Correlation between sites of limited proteolysis and segmental mobility in thermolysin. Biochemistry 25: 1847-1851.
38. Polverino de Laureto P, Frare E, Gottardo R, Van Dael H, Fontana A (2002) Partly folded states of members of the lysozyme/lactalbumin superfamily: a comparative study by circular dichroism spectroscopy and limited proteolysis. Protein Sci 11: 2932-2946.
39. Kamath N, Karwowska-Desaulniers P, Pflum MK (2006) Limited proteolysis of human histone deacetylase 1. BMC Biochem 7: 22.
40. Fellner T, Lackner DH, Hombauer H, Piribauer P, Mudrak I, et al. (2003) A novel and essential mechanism determining specificity and activity of protein phosphatase 2A (PP2A) in vivo. Genes Dev 17: 2138-2150.
41. Longin S, Jordens J, Martens E, Stevens I, Janssens V, et al. (2004) An inactive protein phosphatase 2A population is associated with methylesterase and can be re-activated by the phosphotyrosyl phosphatase activator. Biochem J 380: 111-119.
42. Van Hoof C, Janssens V, Dinishiotu A, Merlevede W, Goris J (1998) Functional analysis of conserved domains in the phosphotyrosyl phosphatase activator. Molecular cloning of the homologues from Drosophila melanogaster and Saccharomyces cerevisiae. Biochemistry 37: 12899-12908.

43. Jordens J, Janssens V, Longin S, Stevens I, Martens E, et al. (2006) The protein phosphatase 2A phosphatase activator is a novel peptidyl-prolyl cis/trans-isomerase. J Biol Chem 281: 6349-6357.
44. Magnúsdóttir A (2008) Structural studies on PP2A and Methods in Protein Production
45. Tubaro A, Florio C, Luxich E, Sosa S, Della Loggia R, et al. (1996) A protein phosphatase 2A inhibition assay for a fast and sensitive assessment of okadaic acid contamination in mussels. Toxicon 34: 743-752.
46. Evans DR, Hemmings BA (2000) Important role for phylogenetically invariant PP2Acalpha active site and C-terminal residues revealed by mutational analysis in Saccharomyces cerevisiae. Genetics 156: 21-29.
47. Ikehara T, Shinjo F, Ikehara S, Imamura S, Yasumoto T (2006) Baculovirus expression, purification, and characterization of human protein phosphatase 2A catalytic subunits alpha and beta. Protein Expr Purif 45: 150-156.
48. Ikehara T, Nakashima S, Nakashima J, Kinoshita T, Yasumoto T (2016) Efficient production of recombinant PP2A at a low temperature using a baculovirus expression system. Biotechnol Rep (Amst) 11: 86-89.
49. Myles T, Schmidt K, Evans DR, Cron P, Hemmings BA (2001) Active-site mutations impairing the catalytic function of the catalytic subunit of human protein phosphatase 2A permit baculovirus-mediated overexpression in insect cells. Biochem J 357: 225-232.
50. Reuten R, Nikodemus D, Oliveira MB, Patel TR, Brachvogel B, et al. (2016) Maltose-Binding Protein (MBP), a Secretion-Enhancing Tag for Mammalian Protein Expression Systems. PLoS One 11: e0152386.
51. Shi L, Ji B, Kolar-Znika L, Boskovic A, Jadeau F, et al. (2014) Evolution of bacterial protein-tyrosine kinases and their relaxed specificity toward substrates. Genome Biol Evol 6: 800-817.
52. Vincent C, Doublet P, Grangeasse C, Vaganay E, Cozzone AJ, et al. (1999) Cells of Escherichia coli contain a protein-tyrosine kinase, Wzc, and a phosphotyrosine-protein phosphatase, Wzb. J Bacteriol 181: 3472-3477.
53. Chao Y, Xing Y, Chen Y, Xu Y, Lin Z, et al. (2006) Structure and mechanism of the phosphotyrosyl phosphatase activator. Mol Cell 23: 535-546.
54. Stanevich V, Jiang L, Satyshur KA, Li Y, Jeffrey PD, et al. (2011) The structural basis for tight control of PP2A methylation and function by LCMT-1. Mol Cell 41: 331-342.
55. Hombauer H, Weismann D, Mudrak I, Stanzel C, Fellner T, et al. (2007) Generation of active protein phosphatase 2A is coupled to holoenzyme assembly. PLoS Biol 5: e155.
56. Andreotti AH (2003) Native state proline isomerization: an intrinsic molecular switch. Biochemistry 42: 9515-9524.
57. Jabs A, Weiss MS, Hilgenfeld R (1999) Non-proline cis peptide bonds in proteins. J Mol Biol 286: 291-304.
58. Pappenberger G, Aygun H, Engels JW, Reimer U, Fischer G, et al. (2001) Nonprolyl cis peptide bonds in unfolded proteins cause complex folding kinetics. Nat Struct Biol 8: 452-458.
59. Guasch A, Aranguren-Ibanez A, Perez-Luque R, Aparicio D, Martinez-Hoyer S, et al. (2015) Calcineurin Undergoes a Conformational Switch Evoked via Peptidyl-Prolyl Isomerization. PLoS One 10: e0134569.
60. Wedemeyer WJ, Welker E, Scheraga HA (2002) Proline cis-trans isomerization and protein folding. Biochemistry 41: 14637-14644.

61. Englander SW, Mayne L (2014) The nature of protein folding pathways. Proc Natl Acad Sci U S A 111: 15873-15880.
62. Ikehara T, Ikehara S, Imamura S, Shinjo F, Yasumoto T (2007) Methylation of the C-terminal leucine residue of the PP2A catalytic subunit is unnecessary for the catalytic activity and the binding of regulatory subunit (PR55/B). Biochem Biophys Res Commun 354: 1052-1057.
63. Maud Martin RKFD (2010) Recent insights into Protein Phosphatase 2A structure and regulation: the reasons why PP2A is no longer considered as a lazy passive housekeeping enzyme. Biotechnol Agron Soc Environ 14: : 243-252.
64. Sents W, Ivanova E, Lambrecht C, Haesen D, Janssens V (2013) The biogenesis of active protein phosphatase 2A holoenzymes: a tightly regulated process creating phosphatase specificity. FEBS J 280: 644-661.

Figures

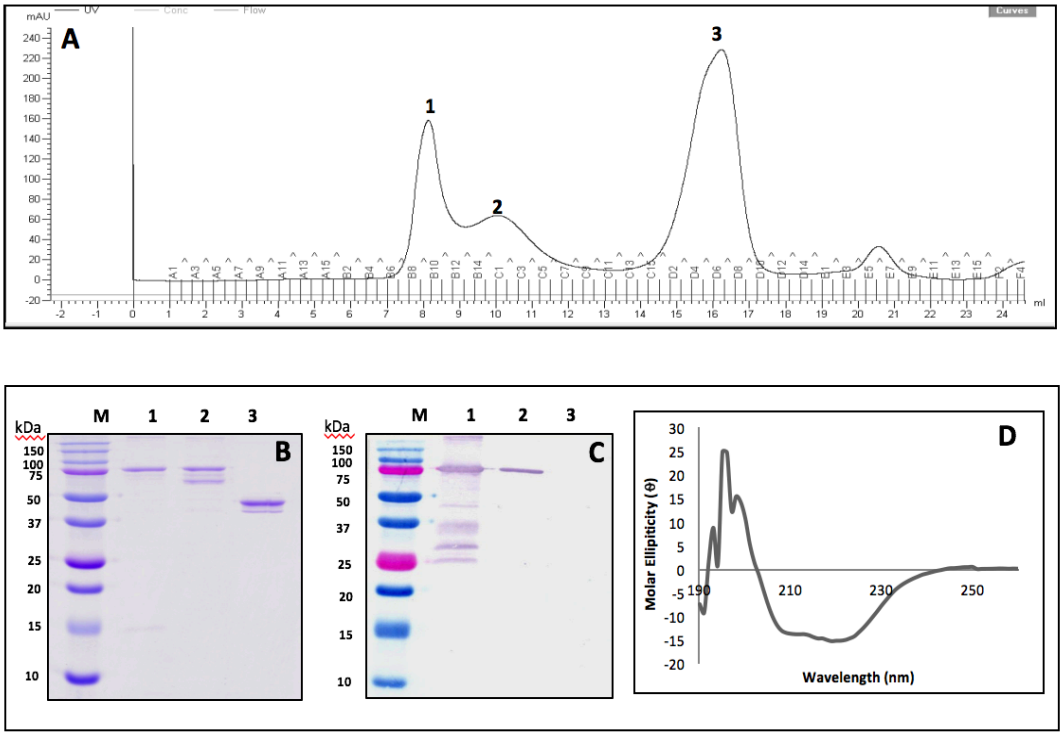

Figure 1: **Purification of MBP-PP2A3c from *E. coli*.** **(A)** Gel filtration profile of affinity-enriched MBP-PP2A3c in 50 mM Tris, pH 7.4, 100 mM NaCl, 1 mM DTT, 100 µM $MnCl_2$ and 200 µM $MgCl_2$. The protein elutes as an oligomeric fraction (*Peak 1*) and as a smaller fraction (*Peak 2*). *Peak 3* contains cleaved MBP protein. **(B)** 1 µg of protein from *Peaks 1-3* separated on 12 % SDS-PAGE: *Lane 1*, *Peak 1; Lane 2*, *Peak 2; Lane 3*, MBP **(C)**

Western blot analysis using monoclonal antibody against PP2A (Millipore) (**D)** Far UV CD spectra in 10mM Tris pH 7.4 and 0.1mM TCEP at concentration of 0.25mg/ml. Minima are observed at ~208 and 222 nm, indicating a dominant α-helical structure.

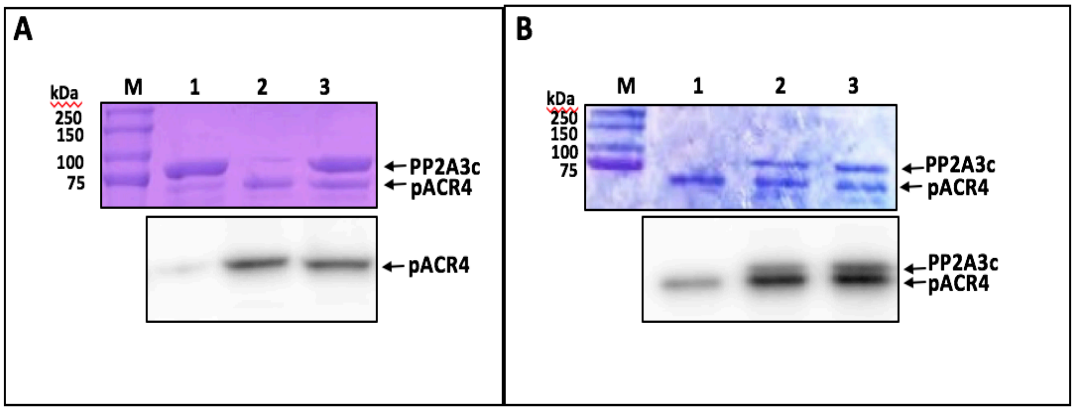

Figure 2: (A) Functional regulation between MBP-PP2A3c and phosphorylated ACR4 kinase (pACR4) labeled with [γ^{32}P] ATP. (A) Activity of M-PP2A3c determined by phosphatase assay against pACR4; **(***Top)* Coomassie Blue stained 12 % SDS-PAGE showing *Lane 1,* 5 µg of PP2A3c control; *Lane 2*, 1µg of pACR4 and *Lane 3* represents the phosphatase reaction between 1µg of pACR4 with 5µg of PP2A3c as described in Materials and Methods. (*Bottom)* corresponding autoradiogram. **(B)** pACR4 can phosphorylate PP2A3c in a kinase assay. (*Top*) Coomassie Blue stained 12 % SDS-PAGE showing *Lane 1,* 1µg of control pACR4, *lanes 2* and *3* represent kinase reactions using 1µg of pACR4 with 1µg and 2µg of PP2A3c respectively. (*Bottom*) corresponding autoradiogram.

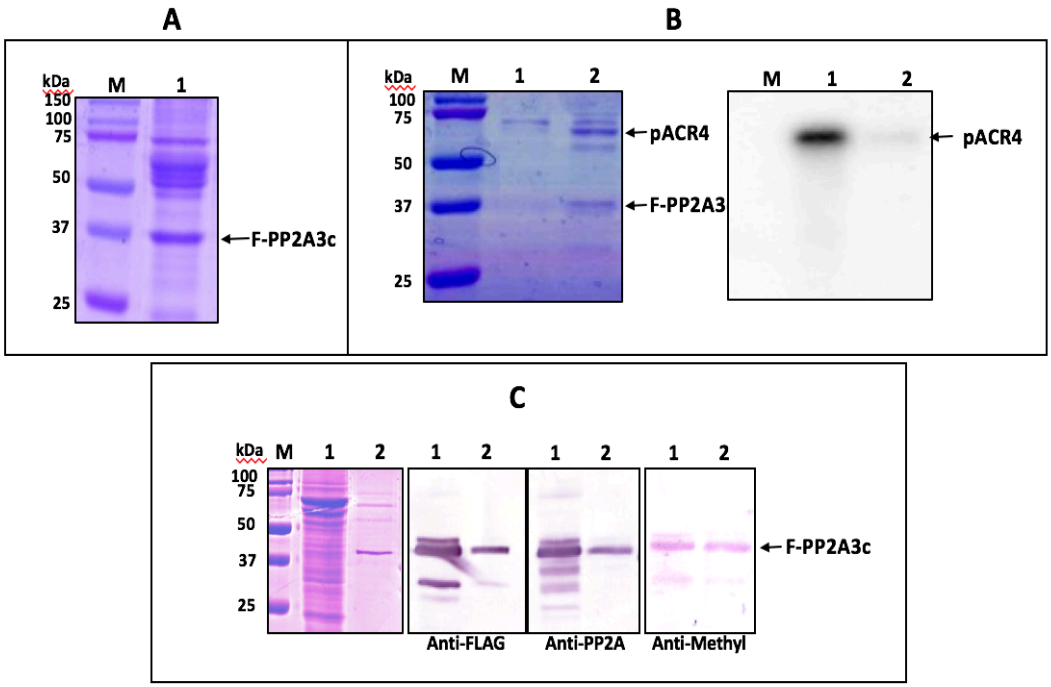

Figure 3: Purification and functional analysis of FLAG tagged PP2A3c (F-PP2A3c) expressed in *Baculovirus insect cells*. (A) Two-step purified (Amylose enriched and anion exchange purified) F-PP2A3c, separated on a 12 % SDS-PAGE gel stained with Coomassie Blue stain. **(B)** Phosphatase activity of F-PP2A3c. *Lane 1,* 1µg of Control [γ^{32}P] labeled ACR4 (pACR4); *Lane 2***,** phosphatase reaction between 1µg of pACR4 and 1µg of F-PP2A3c protein separated on 12% SDS PAGE gel (*Left*) and analyzed by phosphor-imaging (*Right*). **(C)** Western blot analysis of F-PP2A3c confirms a carboxymethylated C-terminal residue. (*Left*) Coomassie Blue Stained SDS-PAGE gel showing *Lane 1***,** soluble lysate fraction of Baculovirus cells expressing F-PP2A3c and *Lane 2*, 1 µg of two step purified F-PP2A3c protein sample. (*Right*) Western blot of individual gels probed with Monoclonal Anti-Flag M2 Ab (Sigma), Monoclonal Anti-PP2A, C subunit Ab (Millipore) and Anti-Methyl –PP2A, C subunit (Millipore) respectively.

A

Enriched Peptide	b ion	Phosphorylated b ion	y ion	Phosphorylated y ion
(R)GAGyTFGQDISEQFNHTNNLK(L)	b3 (+1, 22.2)	b4 (+1, 69.1)	y17 (+2, 54.3)	y18 (--)
(R)GAGYtFGQDISEQFNHTNNLK(L)	b4 (+1, 19.4)	b5 (+1, 32.8)	y16 (+2, 19.4)	y17 (+2, 25.4)
(R)RTPDyFLGHHHHHH(-)	b4 (+1, 100.0)	b5 (+1, 6.5)	y9 (+2, 3.7)	y10 (--)
(K)VVTIFsAPNYCYR(C)	b5 (--)	b6 (+1, 0.13)	y7(+1,100.0)	y8 (+1, 0.15)

B

```
1          10         20         30         40
MGANSIPTDATIDLDEQISQLMQCKPLSEQQVRALCEKAKEILM
      50         60         70         80
DESNVQPVKSPVTICGDIHGQFHDLAELFRIGGMCPDTNYLFMG
  90         100        110        120        130
DYVDRGYYSVETVTLLVALKMRYPQRITILRGNHESRQITQVYG
      140        150        160        170
FYDECLRKYGNANVWKIFTDLFDYFPLTALVESEIFCLHGGLSP
   180        190        200        210        220
SIETLDNIRNFDRVQEVPHEGPMCDLLWSDPDDRCGWGISPRGA
          230        240        250        260
GYTFGQDISEQFNHTNNLKLIARAHQLVMDGYNWAHEQKVVTIF
      270        280        290        300
SAPNYCYRCGNMASILEVDDCRNHTFIQFEPAPRRGEPDVTRRT
 310
PDYFL
```

Figure 4: Identification of endogenous phosphorylation sites in *E. coli* expressed MBP-PP2A3c. (A) Site-determining ions in MBP-PP2A3c (the percentage of maximal intensity for each site-determining ion in the averaged spectrum is shown in parenthesis **(B)** The sequence of PP2A3c is shown. The phosphopeptide identified by mass spectrometry are underlined and phosphorylated residues are colored red. The doubly-underlined RTPDYFL motif represents the conserved C–terminal tail of the PP2A3c family of proteins. *In vivo*, the activity of PP2Ac is regulated by methylation-demethylation of the conserved C-terminal Leucine (in green) and phosphorylation-dephosphorylation of Y311 (corresponds to mammalian Y307).

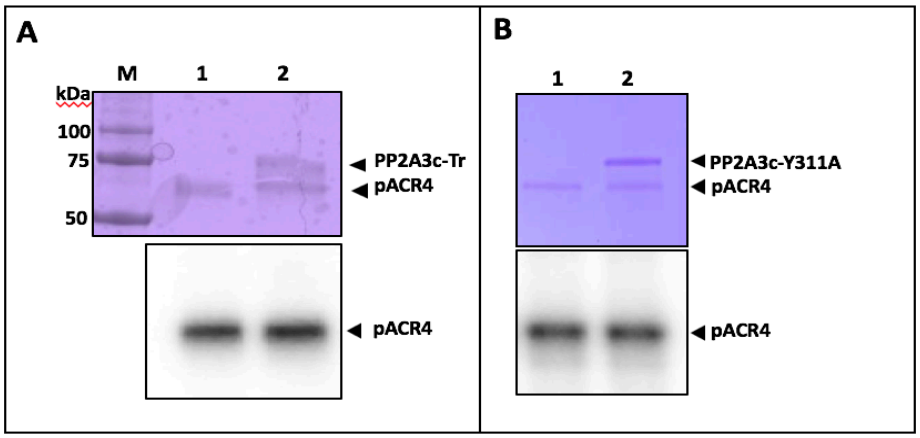

Figure 5: Phosphatase activity of PP2A3c mutants against [γ^{32}P] labeled ACR4-ICD. (*Top*) Coomassie blue stained 12 % SDS –PAGE gel, (*Bottom*) corresponding autoradiogram. **(A)** Assay with truncated MBP-PP2A3c missing the conserved C-terminal tail (PP2A3c-Tr). M, mol. wt standards, *Lane 1*, 1µg of control pACR4*, Lane 2*, 1 µg of pACR4 with 2 µg of PP2A3c-Tr. **(B)** Assay with the mutant PP2A3c-Y311A. *Lane 1,* 1 µg of control pACR4, *Lane 2*, 1 µg of pACR4 with 2 µg of PP2A3c –Y311A.

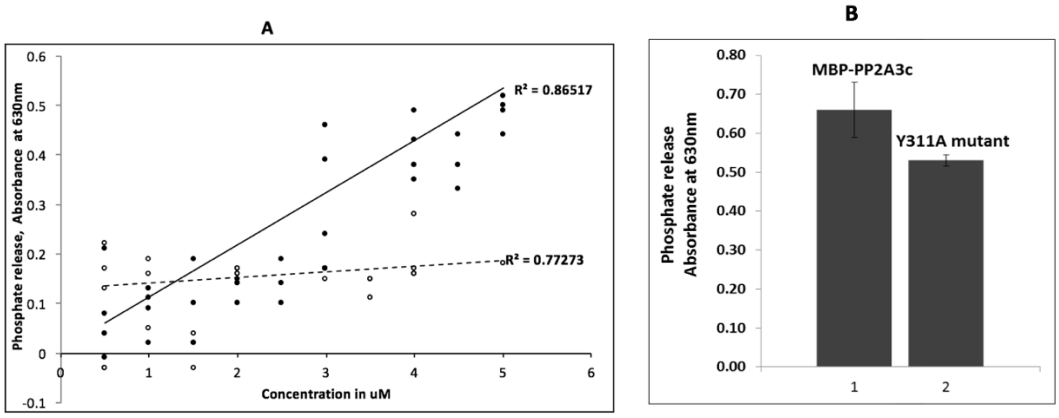

Figure 6: Phosphatase activity of MBP-PP2A3c after overnight incubation. MBP-PP2A3c incubated overnight at 23 °C and 4 °C was tested for phosphatase activity against a synthetic phospho-peptide substrate (Promega) as described in Materials & Methods. **(A)** Multiple replicates of increasing concentrations (0.5 to 5 µM) of protein incubated at 23

°C (●) and 4 °C (○) were assayed for phosphatase activity against a synthetic phospho-peptide in a phosphatase reaction buffer at room temperature. Molybdate/additive dye mixture was used to stop the reaction and the absorbance of released free phosphate was determined at 630 nm on a plate reader. **(B)** Bar diagram showing the activity of 5 µM amounts of MBP-PP2A3c and the PP2A3c-Y311A mutant after overnight incubation at 23 °C using the synthetic phosphopeptide. Data sets are means ± Standard deviation.

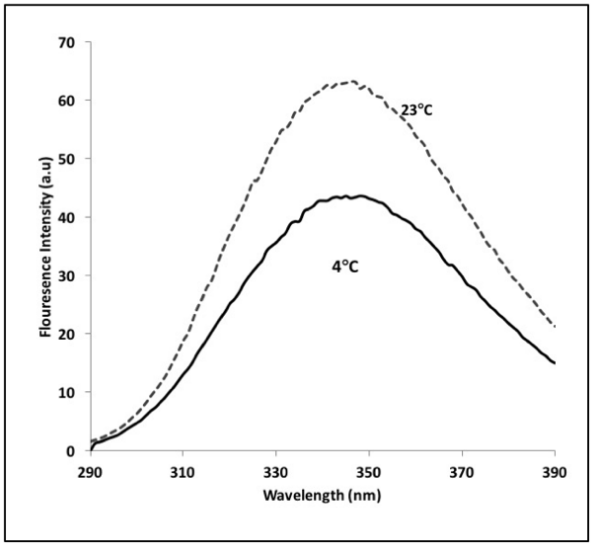

Figure 7: Intrinsic fluorescence of overnight incubated MBP-PP2A3c at 4 °C and 23 °C Intrinsic fluorescence spectra in 10 mM Tris pH 7.4 and 0.1mM TCEP with an A_{280} of 0.1. Measurements were taken in a 1 cm cuvette at room temperature with a Cary Eclipse spectrofluorimeter (Varian) at an excitation wavelength of 280 nm.

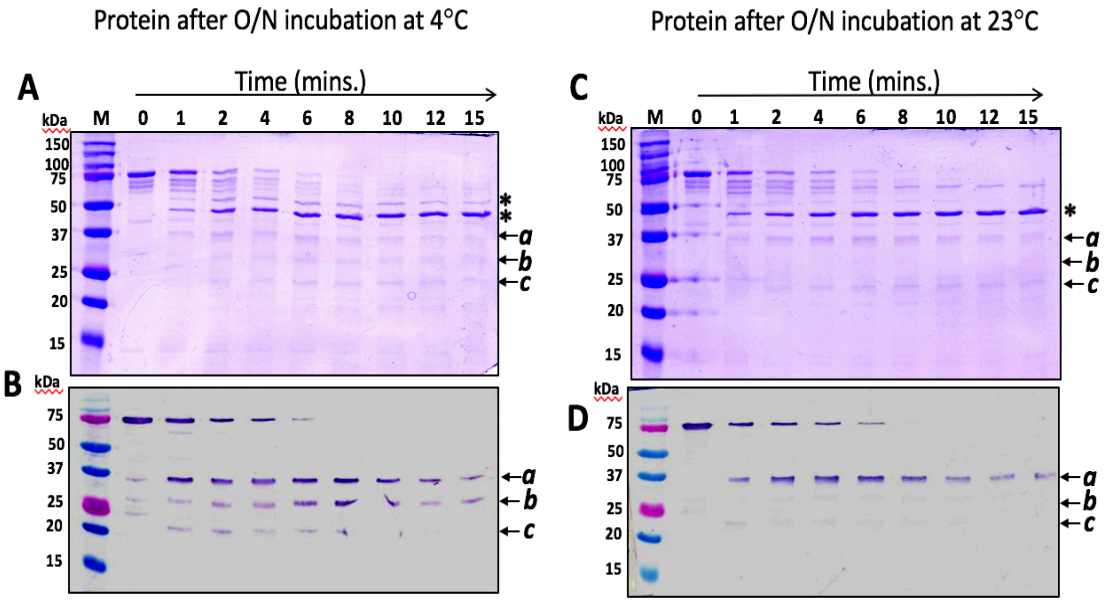

Figure 8: Conformational analysis of MBP-PP2A3c by limited proteolysis. Time course of the tryptic digest of overnight incubated protein at 4 °C and at 23 °C. Proteins were incubated at room temperature for the indicated times with a 1:1000 (w/w) ratio of enzyme to substrate followed by SDS-PAGE analysis **(A & C)** and corresponding western blot using a monoclonal antibody against PP2A 'C 'subunit **(B & D)**. A-B depicts the digestion pattern of protein that was incubated overnight at 4 °C and C-D depicts the digestion pattern of protein that was incubated overnight at 23 °C. Bands from cleaved MBP are indicated by * (confirmed by mass spectrometry) in the SDS-PAGE. Differences in digestion pattern are indicated by bands ***a, b*** and ***c*** in the SDS-PAGE (*top*) and the western blot (*bottom*)

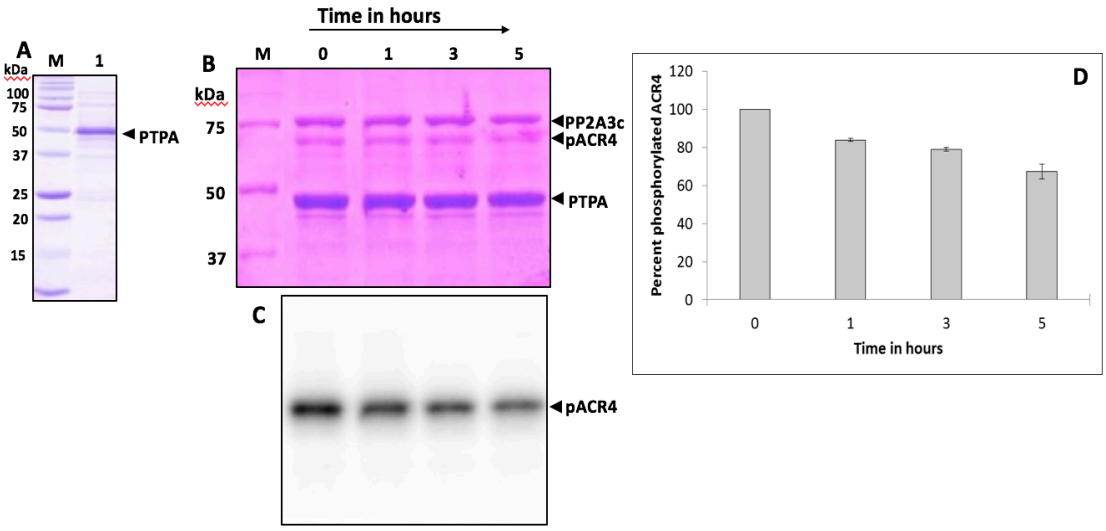

Figure 9: (A) 12% SDS-PAGE of purified PTPA-6H. **(B)** Activation of PP2A3c phosphatase activity by the activator protein PTPA at µM concentrations of ATP. In separate reactions, 0.8 µM MBP-PP2A3c (*Peak 1* from gel filtration) was incubated for 1, 3 and 5 hours with equimolar concentration of PTPA-6H protein in the presence of 0.2 µM ATP. Subsequently, all reactions were further incubated with [γ^{32}P] labeled pACR4 for 1h in a phosphatase reaction buffer. Reaction were stopped and separated on a 12 % SDS-PAGE gel. *Top*, Coomassie Blue stained gel; *Bottom* corresponding autoradiogram **(C)** Bar diagram showing dephosphorylation of pACR4-ICD by activated PP2A3c in presence of 0.2 µM ATP as a function of time. Data sets are means ± Standard deviation.

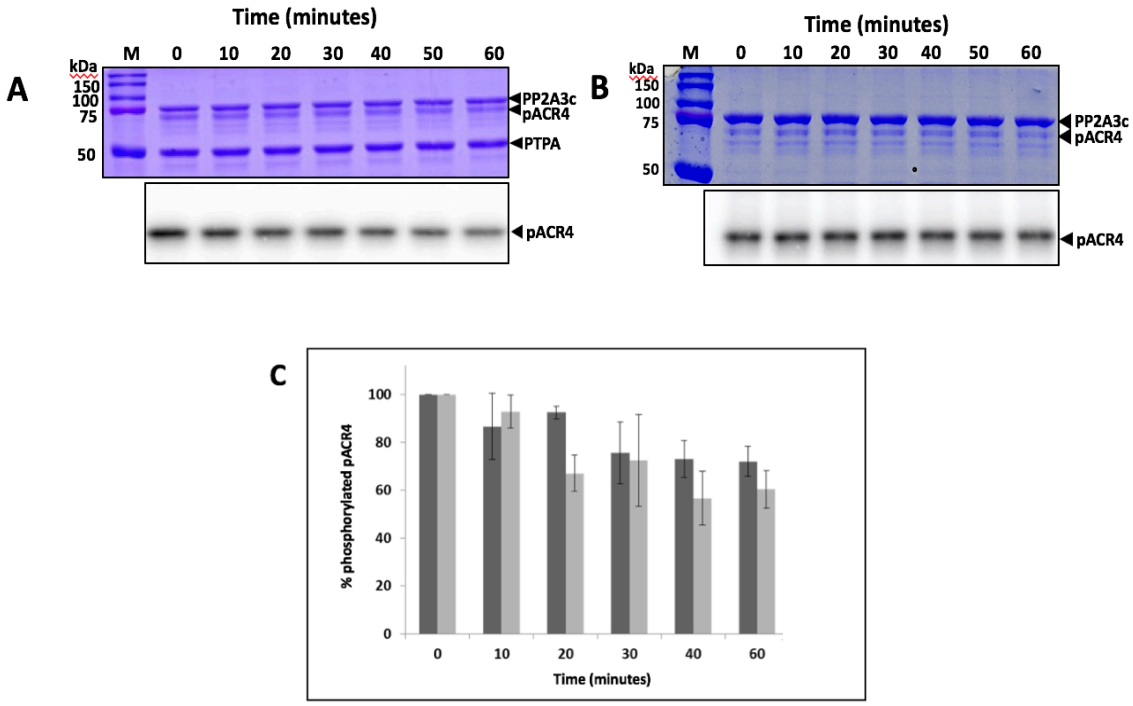

Figure 10: Activation of PP2A3c phosphatase activity by the activator protein PTPA at mM concentrations of ATP. In separate reactions, 0.8 µM MBP-PP2A3c (*Peak 1* from gel filtration) was incubated from 0 to 60 minutes with equimolar concentration of PTPA-6H protein in the presence of 1 mM ATP. Subsequently, all reactions were further incubated with [γ^{32}P] labeled pACR4 for 1h in a phosphatase reaction buffer. Reaction were stopped and separated on a 12 % SDS-PAGE gel **(A)** Coomassie Blue stained gel (*top*) and corresponding autoradiogram (*bottom*) **(B)** Control phosphatase reaction with 0.8 µM MBP-PP2A3c under similar conditions but in absence of PTPA and ATP. Coomassie Blue stained gel (*top*) and corresponding autoradiogram (*bottom*) **(C)** Bar diagram showing % phosphorylated pACR4 remaining after dephosphorylation by activated MBP-PP2A3c (*Peak 1* from gel filtration, *dark grey bars*; *Peak 2* from gel filtration, *light grey bars*) at various time points. Data sets are mean ± Standard Deviation.

CHAPTER 4: BIOCHEMICAL PROPERTIES OF THE RECEPTOR-LIKE KINASE ATCRK1, AND ITS INTERACTION WITH THE CATALYTIC SUBUNIT OF PP2A3 (PP2A3c) PHOSPHATASE.

A manuscript to be submitted for publication in ACS Biochemistry.

Priyanka Sandal, Mathew R. Meyer, Petra Gilmore, Reid R. Townsend, and A. Gururaj Rao

Abstract

In addition to ACR4, the *Arabidopsis* genome encodes four other members of the ACR4 receptor-–like kinase family high sequence similarity and conserved structural features. Among these, AtCRK1 and At CRR3 are the two homologs of ACR4 with a functional kinase domain. Genetic, cell biology and *in vitro* biochemical studies have provided a robust understanding of the biochemistry of ACR4, its regulation by PP2A phosphatase and compelling evidence for *in vitro* heteromeric interaction within the ACR4 family. In this study, we build on this foundation of reported interactions of ACR4 with CRK1 and ACR4 with PP2A3c and demonstrate that PP2A3c is also a substrate for CRK1. Furthermore, we characterize the basic kinetics of the kinase activity of the recombinantly expressed intracellular domain of CRK1 including its auto phosphorylation and mass spectrometric mapping of auto phosphorylation sites. Quantitative mass spectrometry analysis using isobaric TMT labeling indicates that the naïve CRK1 and the auto phosphorylated CRK1 are similarly phosphorylated but the extent of phosphorylation is greater in the auto phosphorylated CRK1. We anticipate that this study will catalyze in planta studies to understand the relationship between PP2A and the family of ACR4 RLK.

Abbreviations

ACR4, *Arabidopsis* CRINKLY4; ALE2, ABNORMAL LEAF SHAPE 2; ACN, Acetonitrile; ATP, adenosine triphosphate; BAK1, BRASSINOSTEROID INSENSITIVE 1-associated receptor kinase 1; BRI1, Brassinosteroid insensitive 1; CORNET 2.0, **cor**relation **net**work; CR4, maize CRINKLY4; CD, circular dichroism; AtCRR, *Arabidopsis* CRINKLY4 related; CRK1m, inactive mutant; DTT, dithiothreitol; EGFR, epidermal growth factor receptor; Eph, ephrin binding receptor; FA, formic acid; FLS2, flagellin-sensitive 2; FHA, Fork Head-Associated domains; ICD, intracellular domain; MBP, maltose binding protein, PDGF, platelet derived growth factor; POL; POLTERGEIST; PLL1, POLTERGEIST-LIKE1; PP2A3c, Protein phosphatase -3 catalytic subunit; RLK, receptor-like kinase; RTK, receptor tyrosine kinase; SERK, somatic embryogenesis receptor-like kinase; SYMRK, symbiosis receptor kinase; TCEP, Tris (2-carboxyethyl) phosphine hydrochloride; TMT, tandem mass tag; UV, ultraviolet.

Introduction

Mammalian systems utilize receptor tyrosine kinases (RTK) to perceive and transmit the extracellular signals to mediate diverse downstream signaling cascades affecting proliferation, migration, differentiation and cell cycle control [1]. Similarly, plants utilize receptor-like kinases (RLK) to mediate various plant signaling processes responsive to a plethora of stimuli [2,3,4,5]. RTKs and RLKs have comparable architectural features which drive similar activation processes. Ligand binding on the extracellular domain transmits the signal via a trans membrane domain and activates the intracellular kinase domain by means of reversible phosphorylation which elicits differential downstream signaling cascade mediated by diverse yet specific signaling molecules. Structural, biophysical,

biochemical and functional studies of several RTKs such as the Epidermal Growth Factor Receptor (EGFR) family [6,7,8,9], Insulin-like Growth Factor Receptor [10], Platelet-derived Growth Factor (PDGF) [11] Somatostatin and Opioid receptors [12], and RLKs such as FLS2 and BAK1 [13], CLAVATA2 [14], and BRI1[15,16] have demonstrated their ability to assemble as homo- or hetero-dimeric complexes with distinct ligand specificity/affinities and downstream signaling activity.

The *Arabidopsis* genome encodes a receptor kinase *Arabidopsis* CRINKLY4 (AT3G59420), as well as four homologs, termed *Arabidopsis* CRINKLY 4 related proteins or AtCRRs which share sequence and architectural similarity [17]. These are CRINKLY 4 RELATED 1 (CCR1 or CRR1, AT3G09780), CCR2 (or CRR2, AT2G39180), CCR3 (or CRR3, AT3G55950), and CCR4/CRINKLY 4-RELATED KINASE 1 (CRK1, AT5G47850). ACR4 is a plasma-membrane localized RLK, which is part of a mechanism that controls formative cell divisions in *Arabidopsis* root [18,19,20]. Genetic, cell biology and *in-vitro* studies suggest potential interactions within the members of ACR4 family with functional redundancy towards a specific genetic pathway [17,18,21,22]. RT-PCR studies of ACR4 and CRR transcript levels and in-silico gene expression analysis by CORNET 2.0 [18,22], demonstrate overlapping yet comparable levels of expression in the quiescent center, lateral root cap, root tip, root cortex and columella root cap cell, for all members of ACR4 family. Furthermore*, in vitro* studies provide evidence of heteromeric interactions between the intracellular domains of ACR4 and the CRRs in a phosphorylation independent manner along with the ability of ACR4 to phosphorylate inactive CRRs [22]*,* also advocating the co-functionality of these spatio-temporally co-expressed proteins within the ACR4 family members [17]. Besides ACR4, CRK1 and CRR3 are the other two

RLKs in the ACR4 family that possess kinase activity and the interaction between the kinase domain of ACR4 and CRK1/CRR3 is mediated through a conserved KDSAF motif in the helix C of CRK1/CRR3 as demonstrated by peptide binding assays and H-D exchange studies [22] (Fig. 2B). Precedence for such heteromeric interaction exists within the members of AtSERK family [23] and members of brassinosteroid receptor kinases (BRI-1), known to mediate multiple signaling pathways and modulate the kinase activity of their partner RLK through phosphorylation [15,16].

Regulation of kinase activity is mediated by specific phosphatases, such as POLTERGEIST (POL) and POLTERGEIST-LIKE1 (PLL1) and KINASE ASSOCIATED PROTEIN PHOSPHATASE (KAPP) interact with CLAVATA-1/ CLAVATA2 and regulate cell proliferation and differentiation in shoot and root meristems [24,25]. We previously reported the catalytic subunit of PP2A3 (PP2A3c) phosphatase, as the first known substrate for ACR4 kinase [26]. With compelling evidence of co-expression and functional interaction of ACR4 with CRK1 in root meristem, and the established regulatory interaction of ACR4 with PP2A3c, we propose PP2A3c to be a common downstream interacting protein for ACR4 and CRK1. In this study, we provide evidence of an *in-vitro* interaction between intracellular domain of CRK1 and catalytic subunit of PP2A3c and further characterize the kinase properties of the recombinantly produced intracellular domain of CRK1 kinase, including mass spectrometric mapping of auto phosphorylation sites and the importance of phosphorylation sites within the activation loop.

Material and Methods

Vector construction and mutagenesis

Constructs of SUMO-fused CRK1 (sCRK1) and SUMO-fused CRK1m (inactive) mutant (sCRK1m) were prepared as described in [22]. MBP-fused catalytic subunit of PP2A3 (M-PP2A3c) was cloned as C terminal fusion to Maltose Binding Protein (MBP) in pMAL-C2E vector (Addgene) using the forward primer 5'GCGGGCGCGGCCTTAATGGGCGCGAATTCTATTCC 3' and the reverse primer 5'CCAACCGCGGCCTCATCACAGGAAATAGTCTGGAGTCCT 3'. The PCR amplified gene was cloned by standard ligation independent cloning (LIC) procedures into an in-house modified pMAL-C2E vector generated for LIC, containing a 6X His tag at N-terminus of MBP. DNA sequencing confirmed correct insertion of the PP2A3c gene into the pMAL-C2E vector. Mutagenesis to create non-phospho and phospho-mimetic mutants of the phosphorylation sites in and around the activation loop was carried out using the QuickChange Lightning Multi Site-Directed Mutagenesis Kit (Stratagene) using mutagenic primers listed in Table 1.

Protein Expression and Purification of SUMO-tagged and tag-less CRK1 Proteins

Expression and purification of SUMO-tagged CRK1 protein was performed as described by Meyer et al [27]. The cleavage reaction to remove SUMO tag was performed by incubating SUMO protease (gift from Nelson Lab, Iowa State University) with the affinity-enriched SUMO-CRK1 at 1:100 concentration in 50 mM Tris, pH 8, 0.2% NP40, 150 mM NaCl and 1 mM DTT overnight at 4°C while dialyzing the cleavage reaction against 50 mM Tris, pH 8, 150 mM NaCl and 1 mM DTT. The cleaved SUMO protein was removed by affinity enrichment of the dialyzed cleavage reaction to obtain tag-less CRK1

Circular Dichroism (CD) measurements

CRK1 purified from *E. coli* (naïve CRK1) and auto phosphorylated CRK1 (pCRK1) were dialyzed overnight at 4°C in 10 mM Tris-HCl, pH 7.4 and 0.1 mM TCEP and concentrated to an A_{280} value of approximately 0.4. Far-UV spectrum of each protein was obtained on a Jasco J-710 spectropolarimeter, in a 0.1cm path-length cuvette with excitation wavelengths ranging from 190 nm-260 nm.

Fluorescence Measurements

Naïve CRK1 and pCRK1 were dialyzed in 10 mM Tris-HCl, pH 7.4 and 0.1 mM TCEP and brought to a concentration of A_{280} = 0.1 prior to fluorescence scans. Measurements were made in a 1 cm cuvette at room temperature with a Cary Eclipse spectrofluorometric (Varian). Scans were executed at an excitation wavelength of 280 nm and a band width of 5 nm and a scan speed of 120 nm/min.

Kinase Activity Assays.

Auto phosphorylated cold pCRK1 was produced by incubating 1 μg of sCRK1 in 1ml reaction buffer containing 20 mM Bis-Tris pH 7.2, 25 mM NaCl, 5 mM $MnCl_2$, 1 mM DTT, 100 μM ATP at a temperature of 30℃.

Phosphorylation of MBP- fused PP2A3c was performed in two separate reactions with sCRK1 and sACR4. 1 μM of kinase protein was incubated with 1 μM PP2A3c protein in 20 μl of Kinase Buffer (20 mM Bis-Tris pH 7.2, 25 mM NaCl, 5 mM $MnCl_2$,1 mM DTT, 25 μM ATP) supplemented with 2 μCi of [γ-^{32}P] ATP (Perkin Elmer, 6,000 Ci/mmol). Proteins were incubated at room temperature for 1 h. Reactions were terminated with the addition of 4X SDS sample buffer and boiled. Proteins were separated by 12% SDS-PAGE and radioactive bands were analyzed by phosphor imaging.

Assays to determine the auto phosphorylation mechanism were performed using the SUMO-CRK1 (sCRK1) and SUMO free CRK1 (CRK1) proteins. A series of reactions were carried out containing increasing concentrations of sCRK1 and CRK1 in the range 0.1-15μM (17.5 μM in case of sCRK1). The protein was incubated in 20 μl reactions of optimized kinase buffer containing 2.5 μCi of [γ-^{32}P] ATP. Reactions were initiated with the addition of the enzyme and incubated for 15 min at room temperature. They were then terminated and separated by 12% SDS-PAGE and radioactive bands were analyzed by phosphorimaging. Protein bands were excised from the gel and radioactivity was determined by scintillation counting. Phosphate incorporation for each sample was calculated based on the radioactive counts and the use of a [γ-^{32}P] ATP standard curve. The data was then used to generate a Van't Hoff plot (log of enzyme activity vs log of enzyme concentration) and the intramolecular nature of the mechanism inferred from the slope of this plot.

Initial velocity for CRK1 auto phosphorylation was determined at varying ATP concentration (0.1μM -50 μM) in a 40 μl kinase reaction volume containing 4 μCi of γ-^{32}P labeled ATP. Kinase reaction at each ATP concentration was carried out at increasing time points from 0-50 mins at room temperature. Amount of phosphate incorporation was determined as described above. The initial velocity at each substrate (ATP) concentration was calculated by plotting the pmole of phosphate incorporation v/s time. The rate of the reaction was then calculated by plotting the initial velocities v/s substrate concentration using the Sigma Plot 11.2 (Systat Software Inc., San Jose, CA) Enzyme Kinetics module (version 1.3) and Michaelis-Menten constants were determined by non- linear regression analysis.

Pull down Assay

The MBP fused PP2A3c (20 µg per reaction) was used as bait to pull out naïve CRK1 kinase and auto phosphorylated CRK1 kinase (50 µg per reaction), devoid of SUMO tag. Bait proteins (MBP-PP2A3c and MBP protein) were incubated with 25 µl bed volume of amylose resin in 1X binding Buffer (50 mM Tris-HCl pH 7.4, 150 mM NaCl, 1 mM DTT, 0.02% NP-40) in a 500µl volume for 1 h at room temperature. To remove unbound MBP proteins, the resin was washed three times with binding buffer by spinning the protein bound resin at 1000 rpm for 30 secs and carefully discarding the supernatant containing unbound protein at each wash step. CRK1 proteins were added to the amylose bound MBP proteins in separate reaction, in 500 µl of binding buffer and incubation for 1 h at room temperature on a rotator. Unbound proteins were washed off in a similar fashion as described. Bound complex protein was eluted from resin by addition of 100 µl of Laemmli buffer and boiling the protein complex/resin mixture at 95°C for 5 min followed by centrifuging at max speed to pellet resin. 40 µl of supernatant from each reaction was separated by 12% SDS-PAGE and proteins were analyzed by coomassie staining and by western blots with polyclonal anti-ACR4 (cross reactive within ACR4 family) at 1:3000 dilution and anti-mouse alkaline phosphatase (AP) conjugated secondary antibody at 1:20000 dilution.

Gel – filtration studies

Purified CRK1 protein was incubated with MBP-PP2A3c protein at equimolar concentrations to determine possible interaction. 5 µM CRK1 was incubated with 5 µM of MBP-PP2A3c in 500 µl of Column Buffer (50 mM Tris pH 7.4, 100 mM NaCl, 100 µM $MnCl_2$, 100 µM $MgCl_2$ and 1mM DTT) for 1 h at room temperature. Protein mixtures were

then loaded onto a Global 10/300 Superdex G- 200 Column (GE Healthcare) coupled to an AKTA FPLC system. Proteins were passed through the column at a flow rate of 0.4 ml/min and 0.3 ml fractions were collected. Fractions corresponding to protein peaks were analyzed by 12% SDS-PAGE and western blot analysis using polyclonal anti-ACR4 primary antibody and AP conjugated Anti-mouse IgG secondary antibody.

Sample Preparation for Liquid Chromatography-Tandem Mass Spectrometry (LC-MS/MS) Analysis.

To prepare peptides, proteins were concentrated by lyophilization. The lyophilized protein was dissolved in SDT buffer (4% SDS, 100mM Tris-HCl pH 8) containing 50mM DTT. Protein samples were heat denatured at 95°C for 5min, alkylated in 50mM Iodoacetamide for 45mins in dark, followed by addition of 600 µl of urea to each sample. The sample were loaded onto a YM-30 filter unit and SDS buffer was exchanged by washing twice with 200µl of Urea and one time wash with 200µl of 100mM Tris, pH 8. The protein(s) were digested in two steps, with 1µg of trypsin digestion carried out for 2hours, followed by a second dose of overnight trypsinization. The digested peptide samples were cleaned using Sep-Pak (Waters, part# WAT054960). 120 µg of peptide sample were dissolved in 200µl of HEPES, pH 8.0 and TMT (Pierce, part # 90060) labelled by addition of 1.6 mg of TMT-126 and TMT-127 (dissolved in 41µl of 100% acetonitrile) to phosphorylated and naïve CRK1 proteins with 1h of incubation at Room temperature. The reaction was quenched using 16µl of 5% hydroxylamine for 15 mins. The labeled sample was dried down in vaccum centrifuge and excess of unbound TMT reagent was removed by Sep-Pak. Phosphopeptides were enriched using $FeCl_3$ activated Ni-NTA beads. Briefly, $FeCl_3$ activated Ni-NTA beads were prepared by using 100ul of 5% metal activated Ni-NTA bead suspension. The beads were washed with Nano-pure water and

treated with 100mM EDTA, pH 8 for 30 min with end-over-end rotation in Invitrogen Hula Mixer. Excess EDTA by washed off the beads three times with nano-pure water. Metal free washed beads were then activated with 10mM $FeCl_3$ in aqueous metal ion solution for 30 min with end-over-end rotation in Invitrogen Hula Mixer. Excess metal ions were washed with nano-pure water as described. Aliquoted beads were washed with of 80% acetonitrile with 0.1% TFA. Phospho-peptides were enriched by resuspending dried peptide samples(100ug) in 200ul of resuspension/wash buffer containing 80% acetonitrile and 0.1% TFA. Suspended samples were incubated with activated beads for 30 minutes with end-over-end rotation in Invitrogen hula mixer. Unbound sample was washed with 80% acetonitrile, 0.1% TFA, three times with each wash performed for a min. Phospho-peptides were eluted with 1:1 5% ammonia water (Sigma 35% NH_4OH to make 5% Ammonia) in 5mM pH 8 phosphate buffer, pH ~10. The phospho-sample were immediately acidified to pH 3.4-4 with $1/10^{th}$ volume of 50% TFA. SPE with 1 set of C4+PGC tips without further drying in speedvac. Wet SPE tips with 60% Acetonitrile containing 0.1%TFA 10 times by aspirating 25µL and dispensing to waste. Equilibrate tips to loading conditions 10 times with 0.1%TFA by aspirating 25 µL and dispensing to waste. Load samples by aspirating and dispensing 65 µL 50 times. Wash loaded tips by aspirating 65 µL of 0.1% TFA and dispensing to waste 10 times. Elute peptides with 60% Acetonitrile containing 0.1%TFA with 35 µL, aspirating and dispensing into elution vial 25 times. Rinse tip with an additional 25 µL of 60% Acetonitrile containing 0.1%TFA. Combine C4 and PGC tip eluate, dry in speed vac. Solubilize dried peptides in 1%TFA to approximate concentration of 0.6µg/µL and transfer to AS vial.

Nano-LC-MS/MS Analysis of TMT-labeled Phosphopeptides

The samples were loaded (2.5 µL) onto a 75 µm i.d. × 50 cm Acclaim® PepMap 100 C18 RSLC column (Thermo-Fisher Scientific) on an EASY nanoLC (Thermo Fisher Scientific) at a constant pressure of 700 bar at 100% A (0.1%FA). Before sample loading the column was equilibrated to 100%A for a total of 20µL at 700 bar pressure. Peptide chromatography was initiated with mobile phase A (0.1% FA) containing 5%B (100% ACN, 0.1% FA) for 1 min, then increased to 15% B over 102 min, to 25% B over 87 min, to 35% B over 40min, to 70% B over 6 min, hold for 6 min, then increased to 95% B over 2 min and held at 95% B for 18 min, with a flow rate of 300 nL/min. The data were acquired in data-dependent acquisition (DDA) mode. The full-scan mass spectra were acquired by the Orbitrap mass analyzer with a scan range of *m/z* = 375 to 1500 and a mass resolving power set to 70,000. Twelve data-dependent high-energy collisional dissociations were performed with a mass resolving power set to 35000, a fixed lower value of *m/z* 100, an isolation width of1. 2 Da, and the normalized collision energy setting of 32. The maximum injection time was 60 ms for parent-ion analysis and 120 ms for product-ion analysis. The target ions that were selected for MS/MS were dynamically excluded for 40 sec. The automatic gain control (AGC) was set at a target value of 3e6 ions for full MS scans and 1e5 ions for MS2. Peptide ions with charge states of one or ≥ 7 were excluded for CID acquisition.

Phosphopeptide site identification and quantification.

The unprocessed instrument data were converted to peak lists using Proteome Discoverer (version 2.1.0.81, Thermo-Fisher Scientific) with integration of reporter ion intensities from the TMT two-plex (TMT-126 and 127N) using a mass tolerance of ± 3.15

mDa. The Mascot software (Matrix Science, London, UK; version 2.5.1) was used to search against a database of SwissProt (species: *Arabidopsis thaliana*; 13,315 entries; version 2017_07), containing common laboratory contaminant proteins (cRAP, version 2012_01; 116 entries) using "trypsin allows P" enzyme specificity with up to 4 missed cleavages. Phosphorylation of serine, threonine and tyrosine, deamidation of asparagine, formation of pyro-glutamic acid from any N-terminal glutamine, acetylation of protein N-terminus, oxidation of methionine, iodoacetamide derivatization of any cysteine and pyro-carbamidomethylation at any N-terminal cysteine were specified in Mascot as variable modifications. Isobaric labeling with TMT was required for Lys residues and the N-terminal residue for these peptides and not specified for label-free experiments. The peptide spectral matches (PSM) were filtered at 1% false-discovery rate (FDR) by searching against a decoy database and the ascribed peptide identities were accepted. The FDR of peptides was estimated using the approximated formula $N_{decoy\ pep}/N_{ARA\ pep}$ where $N_{decoy\ pep}$ and $N_{ARA\ pep}$ denotes the number of decoy and and forward-*Arabidopsis* peptides, respectively. Using the principal of parsimony, protein identities containing ≥ 2 unique or Occam's razor peptides were accepted. The FDR of the proteins was estimated using the approximated formula $N_{decoy\ prn,n\geq 2}/N_{ARA\ prn,n\geq 2}$ where $N_{decoy\ prn,n\geq 2}$ and $N_{ARA\ prn,n\geq 2}$ denotes the number of decoy proteins and *Arabidopsis* proteins, respectively, containing ≥ 2 peptides (Table 3). Intensities of the reporter ions from the two TMT channels were obtained from Mascot. The mean intensity of PSMs that can be assigned to a same peptide was taken to represent the intensity of the incumbent peptide. Peptide ratios between TMT channels were obtained with intensity normalization at the basis of equal summed intensity under each TMT channel.

Results

Characterization of CRK1 and its kinase activity.

The intra-cellular domain of CRK1 (residues 364-75) was expressed as a C-terminal fusion to yeast SUMO protein and, the expression and purification of CRK1 was performed as described by [22]. SUMO-fused CRK1 and SUMO-free CRK1 protein both exist as monomeric proteins as described by size-exclusion chromatography (Figure 1A). Figure 2A shows the far-UV CD spectrum of naive CRK1 with minima at 208 nm and 222 nm, similar to the CD spectrum of its homolog ACR4 [27] and consistent with an α helical conformation observed in the CD spectra many receptor tyrosine kinases [28,29].

The optimal condition for maximal kinase activity of CRK1 was reported in [22]. The auto phosphorylation assay of CRK1 was performed in 20 mM Bis Tris, pH 7.2, 25 mM NaCl, 5 mM $MnCl_2$, 1 mM DTT in presence of 100 μM cold ATP at room temperature. The time course of auto phosphorylation indicate maximal phosphorylation is achieved in 1 h (Figure 3A). The enzyme displays typical Michaelis- Menten kinetics with respect to ATP (Figure 3B). The Km and Vmax of ~3 μM and ~24.9 pmol $min^{-1}mg^{-1}$ was identified for ATP dependent auto phosphorylation of CRK1. The values were obtained by fitting the data to the Michaelis - Menten equation (using the Enzyme Kinetics Module on SigmaPlot 11.2). The Km for ATP, in case of ACR4 was twofold higher than CRK1, suggesting CRK1 to be better kinase enzymatically.

Intra-molecular mechanism of auto phosphorylation.

Kinases can undergo auto phosphorylation either through intra molecular (first-order with respect to enzyme concentration) or inter molecular mechanism (second-order with respect to enzyme concentration). In separate reactions, increasing concentration of

SUMO fused CRK1 (0.1 μM -17.5 μM) and tag less CRK1 (0.1 μM -15 μM) were incubated in series of kinase reactions. Rate of auto phosphorylation was linear with respect to enzyme concentration (Figure 4A & 4D) and, the specific activity defined as the amount of phosphate incorporation per molecule remained constant over increasing enzyme concentration indicating a first order of reaction (Figure 4B & 4E). The Van't hoff analysis is a plot of logarithm of the phosphorylation rate over the logarithm of the enzyme concentration, the slope of 1.09 and 0.98 and linear regression coefficient of 0.99 and 0.98 for sCRK1 and CRK1 respectively was obtained, suggesting intra-molecular mechanism of auto phosphorylation in case of both proteins. It is likely that the SUMO tag adds to the stability of the protein, as suggested by the reduced specific activity observed in tag-less CRK1 in comparison to sCRK1.

Mapping of auto phosphorylation sites.

Approximately forty phospho-sites (comprised of twenty serines, twelve threonines and eight tyrosines) were determined by performing tandem mass spectrometric analysis on tryptic digests of CRK1 kinase. The identified phospho-peptides span the intracellular domain (ICD) of CRK1 kinase (Figure 5A). The precise phosphorylated residue in the sequence was confirmed by inspection of the fragmentation pattern for specific site-determining y and b ions. As an example, the collision induced tandem mass spectrum for ^{579}DIKpSSNILLDATWTAK^{594,} is shown in Figure 5B. The difference in the theoretical m/z and the observed m/z of the precursor ion is 80 Da, which is indicative of the presence of one phosphorylated residue in the peptide. Further, the presence of doubly charged $[M+2H-H_3PO_4]^{2+}$ species at m/z of 879.47, a characteristic peak for neutral loss of phosphoric acid, indicates the presence of one phosphorylation site within the peptide. The

ambiguity of which Serine residue (Ser^{582} or Ser^{583}) is phosphorylated was solved by the presence of site determining y and b ions in the CID spectrum. Phosphorylated b4 (theoretical m/z 524.21, observed m/z 524.21) and y13 (theoretical m/z 1499.71, observed m/z 1499.72), along with non-phosphorylated b3 (theoretical m/z 351.21 and observed m/z 351.21) and y12 (theoretical m/z 1332.71 and observed m/z 1332.72 confirm the identity of the phosphorylated $Ser^{582.}$ The tryptic peptide ^{595}VSDFGLSQMGPTEEDDVSHLSLHAAGTLGYIDPEYYK^{631} harbors the activation loop has with nine probable phosphorylation sites, including six serine/threonine –Ser^{596}, Ser^{601}, Thr^{606}, Ser^{612}, Ser^{615}, Thr^{621}; and three tyrosines- Try^{624}, Try^{629} and Try^{630}. We identified the presence of site-determining b and y ions for Ser^{601} and Thr^{621}. Figure 5C represents MS2 spectrum reported for one of the enriched phosphopeptide spanning the activation loop. The theoretical m/z of non-phosphorylated peptide with +5 charge is 811.17 and the observed m/z of $[M+5H]^{5+}$ is 844.56. The difference of 32 Da mass supports the presence of two phosphorylated residues within this peptide. We looked for peaks representing phosphorylated and/or non-phosphorylated b and y ions scanning through the peptide from N & C terminal end. Represented MS2 spectrum shows the presence of non-phosphorylated b3 (m/z 302.11), b6 (m/z 619.31) and b13 (m/z 1365.599) ions and y12 (m/z 1418.68) and y13 (1489.72) ions, which eliminated phosphorylation at sites Ser^{596}, Ser^{601} and Thr^{606}at the N terminus end and Thr^{621}, Try^{624}, Try^{629} and Try^{630} at the C terminus end of the peptide. The expected set of diagnostic ions were not identified for Ser^{612} and Ser^{615} in this MS2 spectrum, but we were able to narrow down possible phosphorylation sites to Ser^{612} and/or Ser^{615}. The tyrosines in the activation loop were also analyzed separately using another MS2 spectrum. We analyzed the difference in the theoretical m/z

of activation loop for of a non-phosphorylated $[M+4H]^{4+}$ (m/z 1015.22) and the observed m/z of 1095.20. This is indicative of four phosphorylation sites within this peptide. The presence of tyrosine phosphorylation was confirmed with the presence of a peak at m/z of 216.04, which represents the peak for immonium ion, generated on internal fragmentation of peptide containing phosphorylated tyrosine. However, the exact phosphorylation site at Try^{630} was confirmed by the presence of site-determining y ions. Non-phosphorylated y1 (observed m/z 147.11 and theoretical m/z 147.11) and, phosphorylated y2 (observed m/z 390.15 and theoretical m/z 390.143) was identified in the MS2 spectrum under study. We narrowed down four potential phosphorylation sites in the activation loop with confirmed Ser^{601}, Thr^{621}, Try^{630} and either Ser^{612} or Ser^{615} by manually analyzing the various MS spectrums of enriched tryptic peptide containing activation loop. Table 2 shows the complete list of identified phosphopeptides and their site-determining ions.

We also performed quantitative mass spectrometry analysis to detect the difference in phosphorylation states between naïve (as isolated from *E. coli*) and auto phosphorylated CRK1 by utilizing isobaric Tandem Mass tag (TMT) labeling on the digested peptides (as described in Materials and Methods). Using a cut-off of >2-fold intensity change (normalized intensity) for phosphopeptides derived from the phosphorylated protein compared with the corresponding phosphopeptides from the control naïve protein, we identified 16 peptides (Table 3) that correlated with the phosphosites in Table 2. This study indicates that the peptide LCTLASLGNPGQLMEFSIDELALATDGFSVR, for example, is phosphorylated in both the naïve and phosphorylated CRK1 but the extent of phosphorylation is much greater in the latter as evidenced by a 6.5-fold higher intensity in the phosphopeptide derived from the phosphorylated protein relative to non-

phosphorylated CRK1. This analysis parallels our observation of minimal change in phosphorylation state between naïve and auto phosphorylated CRK1 on a qualitative Pro-Q-Diamond phospho-proteome analysis (data not shown).

Auto phosphorylation induces a conformational change

Phosphorylation and dephosphorylation induce conformational changes and structural modifications within proteins [30,31,32]. To address whether phosphorylation of CRK1 causes any structural perturbations, we used circular dichroism (CD) and fluorescent spectroscopy, both techniques that are sensitive to changes in secondary structure and t microenvironment of proteins respectively [33,34,35,36]. The CD spectrum (Figure 2A) of auto phosphorylated CRK1 is similar to that of the naïve CRK1 but is indicative of slight perturbation in the secondary structure on phosphorylation of CRK1. Figure 2B represents the emission spectra of naïve CRK1 and pCRK1. Fluorescence spectroscopy is a sensitive probe of protein folding and tertiary structure and reveals variations in the microenvironment of tyrosine and tryptophan residues. At 280 nm both these aromatic residues absorb and contribute to the emission spectra [33,37]. While the λ_{max} of emission, 334 nm, is the same for both proteins, there is a substantial decrease in the quantum yield of fluorescence of pCRK1, indicating a distinct conformational shift.

Auto phosphorylation of activation loop important for CRK1 kinase activity

The activation loop in kinases is a key regulatory element. Phosphorylation of specific residues within the activation loop critically regulates the overall kinase activity amongst receptor like kinases. Conserved residues within the activation loop are often indicative of conserved function of these residues throughout the RLK family of receptors. The activation loop, comprising ~ 25-30 residues, spans from residues “DFG” in

subdomain VII to residues "XPE" in subdomain VIII, which serve as hinge points for activation loop movement. The aspartate in DFG motif functions towards chelation of a Mg^{2+} ion and stabilization of β and γ phosphates of incoming ATP molecule, where XPE motif stabilizes the C lobe of kinase structurally. Figure 6 represents a sequence alignment of activation loop within the plant Ser/thr RLK and indicates evolutionary conservation of specific residues (black box). Note that some of these conserved sites are also conserved phosphorylation sites amongst plant RLKs (Red). We report four confirmed phosphorylation sites (S^{601}, $S^{612}/^{615}$, T^{621}, Y^{624}) within the activation loop (Figure 6). We also tested the role of phosphorylation at a conserved tyrosine (Try 566) upstream to catalytic loop in CRK1. The phosphorylation of this conserved tyrosine was identified *in vitro* in trans-membrane bound ICD of ACR4 (unpublished data). Site-directed mutagenesis of these residues differentially altered kinase activity (Figure 7). We replaced each of these phosphorylation sites within CRK1 with either an alanine or phenylalanine (in case of tyrosine), or a glutamic acid which mimics phosphorylation. Mutation of S601 to S601A abolished the kinase activity completely which was regained to some extent in S601E mutation, suggesting the requirement of negative charge at this position 601 for kinase activity, which suggests that it is most likely candidate for phosphorylation. The kinase activity of S612A was knocked down in comparison to S612E, hinting towards the necessity of negative charge at this position for maximum activity, which is fulfilled by phosphorylation. It also suggests that phosphorylation at S601 and S612 positively regulates the kinase activity of CRK1 kinase. Kinase activity of S615E was minimally knocked down relative to S615A mutant suggesting potential negative regulation by phosphorylation at this site. The kinase activity of both Y566E and Y566F were

comparable, but substantially less than wild type CRK1. Interestingly, the mutants T621E and Y624E/F indicate loss of activity, suggesting that T621 and Y624 are essential residues for kinase activity and that the kinase activity is not linked with the property of the introduced amino acid. The conservation of T621 and Y624 residues across many RLKs, and the fact that we do not observe any restoration of kinase activity on mutation to a phospho-mimetic or a non-mimetic residue, strongly supports a structurally important role for these residues. [38,39,40].

CRK1 interacts with PP2A3c

In silico analysis of mRNA expression data provides strong evidence of co-expression of ACR4, PP2A3c and CRK1 in the same cellular environment. Co-expression of proteins is a strong indicator of interaction between proteins. We have previously reported the interaction of ACR4 with PP2A3c [26] and Meyer et al have demonstrated the interaction between ACR4 and CRK1[22].On this basis, we have rationalized that PP2A3c may be a common substrate and interaction partner for RLKs within the ACR4 family. We therefore investigated the ability of PP2A3c and CRK1 to interact with each other by gel-filtration analysis (Figure 1 C & D) and pull down assay (Figure 8). For gel-filtration studies, we incubated tag-less CRK1 in equimolar concentration with MBP-PP2A3c (5 μM each) prior to loading on a Superdex G-200 column. It is evident that CRK1 by itself elutes as a monomeric protein (Figure 1A, Peak 3) and M-PP2A3c elutes as an oligomer protein (Figure 1B, Peak 1). When the proteins are incubated together, the gel-filtration profile clearly indicates co-elution of MBP-PP2A3c with CRK1 in the void volume fraction (Figure 1C, Peak 1), suggesting that majority of the monomeric CRK1 protein formed a complex with MBP-PP2A3c, with very little of monomeric CRK1 eluting by itself as seen

in the SDS-PAGE analysis (Insets). The presence of CRK1 in the eluted fractions from was confirmed using polyclonal Anti-ACR4 (cross reactive with CRK1) (Figure 1D)

The interaction between CRK1 and PP2A3c was further confirmed by pull down experiment. The MBP-fused PP2A3c was used as bait and tag-less CRK1 was used as a prey. Our results indicate that MBP-PP2A3c can interact with both naïve (Figure 9A, *Lane* 1) and auto-phosphorylated (Figure 9A, *Lane* 2). Control reactions between MBP protein and CRK1 showed that the interaction specifically occurred between ICD of CRK1 and PP2A3 catalytic domain and discounted any nonspecific interaction of CRK1 with the fused MBP-tag protein. The presence of CRK1 in each reaction was confirmed using polyclonal Anti-ACR4 (cross reactive with CRK1) (Figure 9B).

PP2A3c is a substrate for CRK1

We have previously reported the catalytic subunit of PP2A3 as a substrate for ACR4 kinase activity [26]. Here we used both MBP-PP2A3c and PP2A3c-6H as a substrate and assessed the kinase activity of CRK1 and ACR4. Figure 10A and 10B shows the difference in phosphorylation of PP2A3c mediated by sCRK1 and sACR4. Clearly, the ability of ACR4 to phosphorylate PP2A3c (both MBP fused and 6XHis fused) is much higher than the ability of CRK1 to phosphorylate PP2A3c (*Lane* 1 & 2, 9A- 9B). This difference notwithstanding, that PP2A3c is a common substrate for both ACR4 and CRK1 phosphorylation. Note that MBP-PP2A3c (Figure 9A & B, *Lane* 1) was phosphorylated to a lesser extent than PP2A3-6H (Figure 9A & B, *Lane* 2). This could be attributed to conformational differences between MBP-PP2A3c and PP2A3-6H. The presence of 42 kDa MBP tag could also block the accessibility of residues for phosphorylation by kinase.

Discussion

The model of single ligand–single receptor mediating downstream signaling is challenged by the growing evidence of multiple receptor interactions and signal perception and transduction in both RTKs and RLKs such as EFGR [6,7,9], Insulin–like Growth Factor Receptor [10], CLAVATA2 [14], BRI1 [15,16], FLS2 and BAK1 [13]. Specifically, in roots, a heterodimer/homodimer assembly of CLAVATA1 and ACR4 is known to moderate root stemness in *Arabidopsis* [20]. In this study, we have characterized the kinase activity of CRK1 and further build on the potential of heteromeric interactions within the ACR4 family of receptors and regulation by PP2A3c.

Phosphatases regulate plant RLK activity and examples include regulation of CLAVATA 1 by kinase-associated protein phosphatase (KAPP), together with its co-receptors CLAVATA 2 (CLV2) and CORYNE, striking a balance between cell proliferation and differentiation in the shoot meristem [52]. POL and PLL1 phosphatases, also act as signaling intermediates of CLV1 signaling, positively regulating stem cell specification. In-silico assessment for co-expression of proteins in root apical meristem was analyzed using Arabidopsis "electronic fluorescent pictograph" (eFP) browser (http://bar.utoronto.ca) [41], which described over-lapping expression patterns for ACR4 and CRK1 [22] and weak overlap between ACR4 and PP2A3c in columella cells and lateral roots [26]. However, strong experimental evidence of co-expression of ACR4 and PP2A3 in columella cells in root meristem has been obtained using GFP-fused proteins [26]. Similarly, although in silico analysis with the eFP browser shows weak overlap between CRK1 and PP2A3c expression patterns (data not shown) in roots, it does not preclude the possibility of their interaction *in vivo*. Certainly, a case may be made for more

confirmatory spatio-temporal genetic analysis of the co-expression patterns of CRK1 and PP2A3c. However, sequence similarity, co-expression and interaction between ACR4 and CRK1 provided a compelling reason to examine the interaction of CRK1 and PP2A3c. Thus, we performed *in vitro* investigations and report interaction of PP2A3c with both naïve and auto phosphorylated intracellular domain of CRK1 kinase, via gel-filtration and pull down experiments. *In vitro* kinase assay further indicates phosphorylation of PP2A3c by CRK1 (similar to ACR4 mediated phosphorylation) and, in conjunction with the known interaction between ACR4 and CRK 1 [22] is strongly suggestive of PP2A3c acting as a common substrate for both homologs and together or separately mediating the signaling pathway(s). It is not unreasonable to speculate that multiple related kinases share a common phosphatase. For example, recent studies in BRI1 signaling have reported the role of PP2A phosphatase to both positively and negatively regulate BR signaling cascades. Auto regulated inactive BRI1-BAK inhibits plant growth by phosphorylation of downstream BZR1 transcription factor, which in presence of low BR is dephosphorylated by PP2A, in-turn activating BR signaling[42,43]. Additionally, methylation of PP2A drives its membrane localization and its association with BRI1, leading to degradation and signal attenuation following dephosphorylation of BRI-1 [44]. Clearly these studies emphasize the importance of phosphatase mediated regulation of RLKs. and emphasize the need for further *in planta* studies to understand the significance of ACR4- CRK1- PP2A3c interactions in root meristem and lateral roots.

We further characterized the biochemical properties of CRK1 kinase and identified over forty sites of auto phosphorylation spanning the entire intracellular domain of CRK1 by means LC-MS/MS analysis. To a large extent, phosphorylation of key residues creates

binding surfaces and drive intracellular signaling via diverse phospho-amino acid binding modules such as the 14-3-3, WW and Fork Head-Associated domains (FHA) [45,46]. An example of FHA-containing module in *Arabidopsis* is the kinase-associated protein phosphatase (KAPP). KAPP binds to phosphorylated Ser/Thr residues of several plant RLKs such as CLAVATA 1 (CLV1), SERK1, HAESA, and FLS2 and acts as a negative regulator of receptor signaling [shah47,48,49,50]. These interactions could either involve stable formation of multi-meric complexes via adaptor and scaffolding proteins, or reversible interaction with phosphatases or could facilitate transient dynamic interactions. Besides phosphorylation at serines and threonines, we identified phosphorylation of 8 tyrosine residues Recent reports of tyrosine phosphorylation in multiple plant RLKs such as BRI1, HAESA, show evolution of kinases with dual specificity towards both serine/threonine and tyrosine residues [39,40,51,52]. In a separate study with transmembrane bound intracellular domain of ACR4 in nanodiscs, we identified phosphorylation at Try^{566} (unpublished) and, interestingly, is also conserved in CRK1. Both Y566E and Y566F mutation showed reduced kinase in comparison to wildtype CRK1 suggesting the structural importance of this residue in both CRK1 and ACR4. Mitra et al [53] recently reported a database of *in vitro* auto phosphorylation sites for 223 LRR-RLKs, representing ~30% of LRR-RLKs in *Arabidopsis*, with a highest of 24 sites of auto phosphorylation (At2g01820.1) and an average of 10 auto phosphorylation sites amongst the RLKs under study, with 16 and 18 *in vitro* sites of auto phosphorylation identified in ACR4 [27] and BRI1[40,43,54] respectively. The vast number of *in-vitro* auto phosphorylation sites identified in CRK1 could be attributed to a mixture of endogenous phosphorylation sites and auto-phosphorylation sites, with comparable level of

phosphorylation observed in naïve and auto phosphorylated CRK1 proteins on Pro-Q-diamond phospho-proteome analysis (data not shown). It should also be noted that *E. coli* genome possess endogenous tyrosine kinases such as Wzc and Etk kinases and serine/ threonine kinases (eSTKs) such has YihE kinase [55,56,57], which may drive phosphorylation at some sites in recombinantly expressed CRK1. However, the biological significance of the *in vitro* phosphorylation sites remains to be validated by *in planta* studies.

Auto phosphorylation induces conformational change within the intracellular domain of CRK1 as indicated by changes in CD spectrum and fluorescence measurements. Very little to no change in phosphorylation state was observed between CRK1 and pCRK1 from Pro-Q-diamond analysis and further quantitative mass spectrometry analysis, as illustrated in table 3, reveals phospho-peptides enriched with twofold (or more) change in phosphorylation relative to peptides from naïve CRK1. For example, phosphorylated peptide 'ADKDSAFVNELESMSR' enriched from auto-phosphorylated protein has 2.3-fold occurrence relative to the phosphorylated version of this peptide in non-phosphorylated protein, clearly indicating the presence of phosphorylation on Ser/Thr residues in both the naïve and auto phosphorylated peptide although to much higher extent in auto phosphorylated state. More than likely, auto phosphorylation mediates the *close to open* conformational change which is otherwise held together by the different regions of intra-cellular domain in accordance with the regulatory role of JMD and CTD regions in RTKs such as ephrin binding receptor (EpH) family, platelet-derived growth factor (PDGF) receptor family, and epidermal growth factor receptor (EGFR) family [58,59,60,61,62], and negative regulatory role of CTD in the function of BRI-1 RLK [63].

The classical paradigm of ligand mediated dimerization of receptor inducing conformational change and activation of kinase domain by *cis* (intramolecular) or *trans* (intermolecular) auto phosphorylation [64,65]. We report an intramolecular mode of auto phosphorylation of CRK1, and we speculate that *in vivo*, on binding to its ligand CRK1/ACR4 could undergo a conformational change in its intracellular domain which drives its subsequent interaction with a second kinase within/outside of the ACR4 family of RLKs, that is capable of *trans* phosphorylating at a specific site on the ACR4 intracellular domain and "activating" an intramolecular auto phosphorylation event.

Intriguingly, we identified multiple auto phosphorylation sites within the activation loop of CRK1 as opposed to just one site (T681) of phosphorylation within the activation loop of ACR4 [27]. The activation segment is a conserved region in protein kinases that occurs between subdomains VII and VIII of the kinase domain [66], harbors essential phosphorylation sites regulating the kinase activity and possesses elements important for substrate binding [32,63,67]. Phosphorylation of specific residues within the activation loop is required to attain maximal enzymatic activity. There is strict conservation of Threonine 621, Tyrosine 624 and Serine 615 (specific to CRK1) throughout RD –type RLKs. The alanine mutation of corresponding conserved threonine in BRI-1, abolishes auto phosphorylation and substrate phosphorylation *in vitro*, and does not rescue the weak bri1-5 brassinosteroid insensitive mutant *in planta* (37). Similarly, phosphorylation of the conserved Thr^{468} in AtSERK1 [50] and Thr^{769} in SYMRK activity [68] are important for both auto phosphorylation and phosphorylation of artificial substrates *in vitro*. In CRK1, non-phospho and phosphor-mimetic mutations of conserved T621 (T621A and T621E) and Y624 (Y624F and Y624E) completely abolished the kinase activity indicating the

structural importance of these residues but the S615A/E mutation did not affect the phosphorylation state of CRK1 to any extent. However, in case of the RLKs BAK1 and HAE, mutations at these congruent sites facilitate regain in phosphorylation activity, suggesting phosphorylation at these sites positively regulate the kinase activity. We also observed phosphorylation at S601 to positively regulate the kinase activity of CRK1, clearly suggesting the functional importance of additional phosphorylation sites within activation loop, that are not conserved across RD-type RLKs alignment. Recent studies on HAE RLK opened a new avenue to understand the dual specificity within RLK where the phosphor-mimetic mutation at S856 and S861 in activation loop of HAE displayed elevated auto-phosphorylation at Y724. It is possible that the tyrosine phosphorylation (Try 624) within CRK1 activation loop is a result of phosphorylation at other residues thereby imparting dual-specificity to CRK1 kinase much like HAE RLK [52].

In conclusion, we propose ACR4-CRK1-PP2A3c interactions as being important in the regulation of a common signaling pathway coordinating formative cell division in root meristems. With physiological effects reported from our prior work on PP2A3c-ACR4 interaction in roots, and the involvement of PP2A in the regulation of other RLKs [26,42,43,44], our future studies are directed towards delineating the role of CRK1 and PP2A3c interacting *in planta*. Furthermore, the biochemical characterization of the intra-cellular domain of CRK1 and the mapping of *in vitro* auto phosphorylation sites lays a strong foundation for more in-depth genetic and *in planta* analysis of heteromeric interactions in the ACR4 family and PP2A affecting the differentiation of root cells and root formation.

Acknowledgements

We would like to thank R. Reid Townsend, Petra Gilmore and the Proteomics Core Lab at Washington University in St. Louis, MO, for the mass spectrometry analysis of the auto phosphorylated CRK1 and the quantitative mass spectrometry analysis of naïve and auto phosphorylated CRK1.

References

1. Lemmon MA, Schlessinger J (2010) Cell Signaling by Receptor Tyrosine Kinases. Cell 141: 1117-1134.
2. Afzal AJ, Wood AJ, Lightfoot DA (2008) Plant receptor-like serine threonine kinases: roles in signaling and plant defense. Mol Plant Microbe Interact 21: 507-517.
3. Haffani YZ, Silva NF, Goring DR (2004) Receptor kinase signalling in plants. Canadian Journal of Botany-Revue Canadienne De Botanique 82: 1-15.
4. Kim TW, Guan S, Sun Y, Deng Z, Tang W, et al. (2009) Brassinosteroid signal transduction from cell-surface receptor kinases to nuclear transcription factors. Nature Cell Biology 11: 1254-1260.
5. Shiu SH, Bleecker AB (2001) Receptor-like kinases from Arabidopsis form a monophyletic gene family related to animal receptor kinases. Proc Natl Acad Sci U S A 98: 10763-10768.
6. Olayioye MA, Neve RM, Lane HA, Hynes NE (2000) The ErbB signaling network: receptor heterodimerization in development and cancer. EMBO J 19: 3159-3167.
7. Prenzel N, Fischer OM, Streit S, Hart S, Ullrich A (2001) The epidermal growth factor receptor family as a central element for cellular signal transduction and diversification. Endocr Relat Cancer 8: 11-31.
8. Wieduwilt MJ, Moasser MM (2008) The epidermal growth factor receptor family: biology driving targeted therapeutics. Cell Mol Life Sci 65: 1566-1584.
9. Schulze WX, Deng L, Mann M (2005) Phosphotyrosine interactome of the ErbB-receptor kinase family. Mol Syst Biol 1: 2005 0008.
10. Morgillo F, Woo JK, Kim ES, Hong WK, Lee HY (2006) Heterodimerization of insulin-like growth factor receptor/epidermal growth factor receptor and induction of survivin expression counteract the antitumor action of erlotinib. Cancer Res 66: 10100-10111.
11. Saito Y, Haendeler J, Hojo Y, Yamamoto K, Berk BC (2001) Receptor heterodimerization: essential mechanism for platelet-derived growth factor-induced epidermal growth factor receptor transactivation. Mol Cell Biol 21: 6387-6394.
12. Pfeiffer M, Koch T, Schroder H, Laugsch M, Hollt V, et al. (2002) Heterodimerization of somatostatin and opioid receptors cross-modulates phosphorylation, internalization, and desensitization. J Biol Chem 277: 19762-19772.
13. Chinchilla D, Zipfel C, Robatzek S, Kemmerling B, Nurnberger T, et al. (2007) A flagellin-induced complex of the receptor FLS2 and BAK1 initiates plant defence. Nature 448: 497-500.

14. Guo Y, Han L, Hymes M, Denver R, Clark SE (2010) CLAVATA2 forms a distinct CLE-binding receptor complex regulating Arabidopsis stem cell specification. Plant J 63: 889-900.
15. Clouse SD (2011) Brassinosteroid signal transduction: from receptor kinase activation to transcriptional networks regulating plant development. Plant Cell 23: 1219-1230.
16. Ye H, Li L, Yin Y (2011) Recent advances in the regulation of brassinosteroid signaling and biosynthesis pathways. J Integr Plant Biol 53: 455-468.
17. Cao X, Li K, Suh SG, Guo T, Becraft PW (2005) Molecular analysis of the CRINKLY4 gene family in Arabidopsis thaliana. Planta 220: 645-657.
18. De Smet I, Vassileva V, De Rybel B, Levesque MP, Grunewald W, et al. (2008) Receptor-like kinase ACR4 restricts formative cell divisions in the Arabidopsis root. Science 322: 594-597.
19. Nikonorova N, Vu LD, Czyzewicz N, Gevaert K, De Smet I (2015) A phylogenetic approach to study the origin and evolution of the CRINKLY4 family. Front Plant Sci 6: 880.
20. Stahl Y, Grabowski S, Bleckmann A, Kuhnemuth R, Weidtkamp-Peters S, et al. (2013) Moderation of Arabidopsis root stemness by CLAVATA1 and ARABIDOPSIS CRINKLY4 receptor kinase complexes. Curr Biol 23: 362-371.
21. Gifford ML, Robertson FC, Soares DC, Ingram GC (2005) ARABIDOPSIS CRINKLY4 function, internalization, and turnover are dependent on the extracellular crinkly repeat domain. Plant Cell 17: 1154-1166.
22. Meyer MR, Shah S, Zhang J, Rohrs H, Rao AG (2015) Evidence for intermolecular interactions between the intracellular domains of the arabidopsis receptor-like kinase ACR4, its homologs and the Wox5 transcription factor. PLoS One 10: e0118861.
23. Albrecht C, Russinova E, Kemmerling B, Kwaaitaal M, de Vries SC (2008) Arabidopsis SOMATIC EMBRYOGENESIS RECEPTOR KINASE proteins serve brassinosteroid-dependent and -independent signaling pathways. Plant Physiol 148: 611-619.
24. Boyer F, Simon R (2015) Asymmetric cell divisions constructing Arabidopsis stem cell niches: the emerging role of protein phosphatases. Plant Biol (Stuttg) 17: 935-945.
25. Wang Y, Li Z, Liu D, Xu J, Wei X, et al. (2014) Assessment of BAK1 activity in different plant receptor-like kinase complexes by quantitative profiling of phosphorylation patterns. J Proteomics 108: 484-493.
26. Yue K, Sandal P, Williams EL, Murphy E, Stes E, et al. (2016) PP2A-3 interacts with ACR4 and regulates formative cell division in the Arabidopsis root. Proc Natl Acad Sci U S A 113: 1447-1452.
27. Meyer MR, Lichti CF, Townsend RR, Rao AG (2011) Identification of in vitro autophosphorylation sites and effects of phosphorylation on the Arabidopsis CRINKLY4 (ACR4) receptor-like kinase intracellular domain: insights into conformation, oligomerization, and activity. Biochemistry 50: 2170-2186.
28. Sierke SL, Cheng K, Kim HH, Koland JG (1997) Biochemical characterization of the protein tyrosine kinase homology domain of the ErbB3 (HER3) receptor protein. Biochem J 322 (Pt 3): 757-763.
29. Wente SR, Villalba M, Schramm VL, Rosen OM (1990) Mn2(+)-binding properties of a recombinant protein-tyrosine kinase derived from the human insulin receptor. Proc Natl Acad Sci U S A 87: 2805-2809.

30. Groban ES, Narayanan A, Jacobson MP (2006) Conformational changes in protein loops and helices induced by post-translational phosphorylation. Plos Computational Biology 2: 238-250.
31. Huse M, Kuriyan J (2002) The conformational plasticity of protein kinases. Cell 109: 275-282.
32. Nolen B, Taylor S, Ghosh G (2004) Regulation of protein kinases: Controlling activity through activation segment conformation. Molecular Cell 15: 661-675.
33. Laskowicz JR (1986) Principles of Fluorescence Spectroscopy. Plenum Press, New York.
34. Fontana A, Fassina G, Vita C, Dalzoppo D, Zamai M, et al. (1986) Correlation between sites of limited proteolysis and segmental mobility in thermolysin. Biochemistry 25: 1847-1851.
35. Polverino de Laureto P, Frare E, Gottardo R, Van Dael H, Fontana A (2002) Partly folded states of members of the lysozyme/lactalbumin superfamily: a comparative study by circular dichroism spectroscopy and limited proteolysis. Protein Sci 11: 2932-2946.
36. Kamath N, Karwowska-Desaulniers P, Pflum MK (2006) Limited proteolysis of human histone deacetylase 1. BMC Biochem 7: 22.
37. Barry JK, Selinger DA, Wang C, Olsen OA, Rao AG (2006) Biochemical characterization of a truncated penta-EF-hand Ca2+ binding protein from maize. Biochim Biophys Acta 1764: 239-245.
38. Jaillais Y, Hothorn M, Belkhadir Y, Dabi T, Nimchuk ZL, et al. (2011) Tyrosine phosphorylation controls brassinosteroid receptor activation by triggering membrane release of its kinase inhibitor. Genes & Development 25: 232-237.
39. Lin W, Li B, Lu D, Chen S, Zhu N, et al. (2014) Tyrosine phosphorylation of protein kinase complex BAK1/BIK1 mediates Arabidopsis innate immunity. Proc Natl Acad Sci U S A 111: 3632-3637.
40. Oh MH, Wang XF, Kota U, Goshe MB, Clouse SD, et al. (2009) Tyrosine phosphorylation of the BRI1 receptor kinase emerges as a component of brassinosteroid signaling in Arabidopsis. Proceedings of the National Academy of Sciences of the United States of America 106: 658-663.
41. Winter D, Vinegar B, Nahal H, Ammar R, Wilson GV, et al. (2007) An "Electronic Fluorescent Pictograph" browser for exploring and analyzing large-scale biological data sets. PLoS One 2: e718.
42. Tang W, Yuan M, Wang R, Yang Y, Wang C, et al. (2011) PP2A activates brassinosteroid-responsive gene expression and plant growth by dephosphorylating BZR1. Nature Cell Biology 13: 124-131.
43. Wu G, Wang X, Li X, Kamiya Y, Otegui MS, et al. (2011) Methylation of a phosphatase specifies dephosphorylation and degradation of activated brassinosteroid receptors. Sci Signal 4: ra29.
44. Di Rubbo S, Irani NG, Russinova E (2011) PP2A phosphatases: the "on-off" regulatory switches of brassinosteroid signaling. Sci Signal 4: pe25.
45. Chevalier D, Morris ER, Walker JC (2009) 14-3-3 and FHA domains mediate phosphoprotein interactions. Annu Rev Plant Biol 60: 67-91.
46. Yaffe MB, Elia AE (2001) Phosphoserine/threonine-binding domains. Curr Opin Cell Biol 13: 131-138.

47. Gomez-Gomez L, Bauer Z, Boller T (2001) Both the extracellular leucine-rich repeat domain and the kinase activity of FLS2 are required for flagellin binding and signaling in arabidopsis. Plant Cell 13: 1155-1163.
48. Stone JM, Collinge MA, Smith RD, Horn MA, Walker JC (1994) Interaction of a Protein Phosphatase with an Arabidopsis Serine-Threonine Receptor Kinase. Science 266: 793-795.
49. Williams RW, Wilson JM, Meyerowitz EM (1997) A possible role for kinase-associated protein phosphatase in the Arabidopsis CLAVATA1 signaling pathway. Proc Natl Acad Sci U S A 94: 10467-10472.
50. Shah K, Vervoort J, de Vries SC (2001) Role of threonines in the Arabidopsis thaliana somatic embryogenesis receptor kinase 1 activation loop in phosphorylation. J Biol Chem 276: 41263-41269.
51. Gish LA, Clark SE (2011) The RLK/Pelle family of kinases. Plant J 66: 117-127.
52. Taylor I, Wang Y, Seitz K, Baer J, Bennewitz S, et al. (2016) Analysis of Phosphorylation of the Receptor-Like Protein Kinase HAESA during Arabidopsis Floral Abscission. PLoS One 11: e0147203.
53. Mitra SK, Chen R, Dhandaydham M, Wang X, Blackburn RK, et al. (2015) An autophosphorylation site database for leucine-rich repeat receptor-like kinases in Arabidopsis thaliana. Plant J 82: 1042-1060.
54. Wang XL, Chory J (2006) Brassinosteroids regulate dissociation of BKI1, a negative regulator of BRI1 signaling, from the plasma membrane. Science 313: 1118-1122.
55. Lee DC, Zheng J, She YM, Jia Z (2008) Structure of Escherichia coli tyrosine kinase Etk reveals a novel activation mechanism. EMBO J 27: 1758-1766.
56. Vincent C, Doublet P, Grangeasse C, Vaganay E, Cozzone AJ, et al. (1999) Cells of Escherichia coli contain a protein-tyrosine kinase, Wzc, and a phosphotyrosine-protein phosphatase, Wzb. J Bacteriol 181: 3472-3477.
57. Zheng J, He C, Singh VK, Martin NL, Jia Z (2007) Crystal structure of a novel prokaryotic Ser/Thr kinase and its implication in the Cpx stress response pathway. Mol Microbiol 63: 1360-1371.
58. Griffith J, Black J, Faerman C, Swenson L, Wynn M, et al. (2004) The structural basis for autoinhibition of FLT3 by the juxtamembrane domain. Molecular Cell 13: 169-178.
59. Hubbard SR (2004) Juxtamembrane autoinhibition in receptor tyrosine kinases. Nature Reviews Molecular Cell Biology 5: 464-470.
60. Lee NY, Koland JG (2005) Conformational changes accompany phosphorylation of the epidermal growth factor receptor C-terminal domain. Protein Science 14: 2793-2803.
61. Niu XL, Peters KG, Kontos CD (2002) Deletion of the carboxyl terminus of Tie2 enhances kinase activity, signaling, and function. Evidence for an autoinhibitory mechanism. J Biol Chem 277: 31768-31773.
62. Thiel KW, Carpenter G (2007) Epidermal growth factor receptor juxtamembrane region regulates allosteric tyrosine kinase activation. Proceedings of the National Academy of Sciences of the United States of America 104: 19238-19243.
63. Wang XL, Li XQ, Meisenhelder J, Hunter T, Yoshida S, et al. (2005) Autoregulation and homodimerization are involved in the activation of the plant steroid receptor BRI1. Developmental Cell 8: 855-865.
64. Jiang.G (1995) Protein kinases and phosphatases: the yin and yang of protein phosphorylation and signaling. Cell 80: 225-236.

65. Schlessinger J (2000) Cell signaling by receptor tyrosine kinases. Cell 103: 211-225.
66. Hanks SK, Hunter T (1995) Protein kinases 6. The eukaryotic protein kinase superfamily: kinase (catalytic) domain structure and classification. FASEB J 9: 576-596.
67. Taylor SS, Kornev AP (2011) Protein kinases: evolution of dynamic regulatory proteins. Trends in Biochemical Sciences 36: 65-77.
68. Yoshida S, Parniske M (2005) Regulation of plant symbiosis receptor kinase through serine and threonine phosphorylation. Journal of Biological Chemistry 280: 9203-9209.

Figures

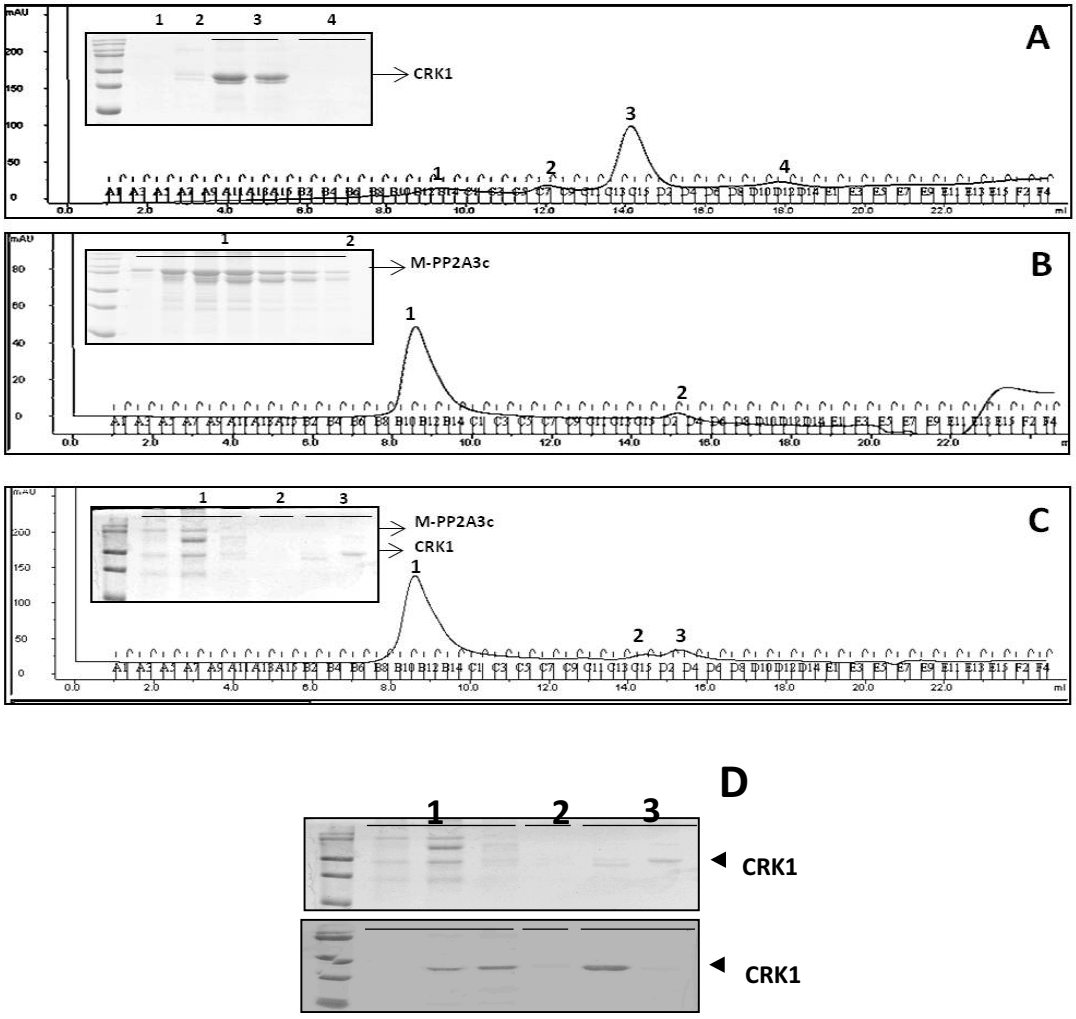

Figure 1: Gel filtration analysis of M-PP2A3c and CRK1 interaction on a Superdex G-200 column. A, B and C represents individual elution profiles of CRK1 (5µM), M-PP2A3c (5uM) and, CRK1(5uM) with M-PP2A3c (5uM) respectively. Insets show the

corresponding SDS-PAGE of the proteins present in peak fractions 1, 2, 3 and 4. **(A)** CRK1 (~47kDa) elutes as a monomer in *peak 3* as indicated in SDS-PAGE (Inset). **(B)** M-PP2A3c (~80kDa) elutes as an oligomer in void volume of the column represented in *peak 1* and as identified in SDS-PAGE gel (Inset). **(C)** CRK1 co-elutes with M-PP2A3c in *peak 1*, with now CRK1 predominantly appears with M-PP2A3c as seen in corresponding SDS-PAGE (inset), indicative of the interaction between the two proteins. **(D)** A western blot analysis with Anti-ACR4 antibody on the eluted fractions from C, confirms the presence of CRK1 elution in complex with M-PP2A3c.

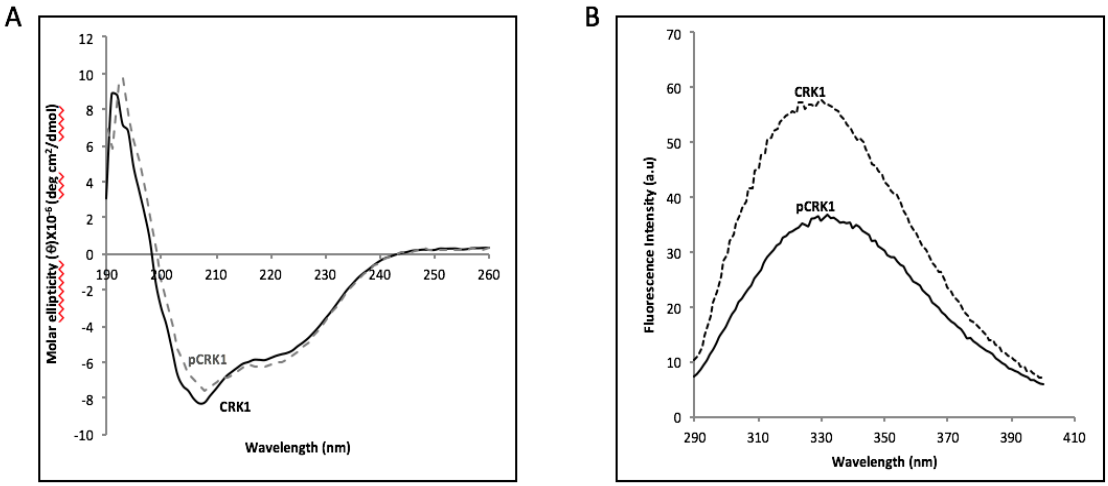

Figure 2: Conformational analysis of CRK1 proteins. (A) Far-UV CD spectra of naïve CRK1, and auto phosphorylated pCRK1 in 10 mM Tris, pH 7.4 and 0.1 mM TCEP with an A_{280} value of ~0.4. **(B)** Intrinsic fluorescence spectra of CRK1, and pCRK1 in the same buffer with an A_{280} of 0.1. Measurements were made in a 1cm cuvette at room temperature with a Cary Eclipse spectrofluorometer (Varian) at an excitation wavelength of 280 nm.

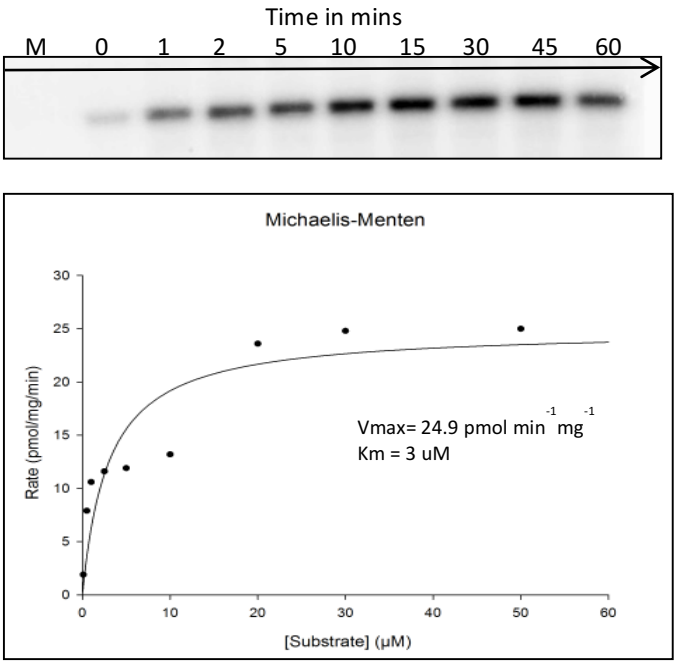

Figure 3: Auto phosphorylation of CRK1. (A) Time course of auto phosphorylation for CRK1. **(B)** Plot of enzyme velocity vs ATP concentration. Data were fitted directly to the Michaelis-Menten equation using SigmaPlot 11.2 and the Enzyme Kinetics 1.3 module. The Km value for ATP was 3µM and the Vmax value was 24.9pmol/min/mg.

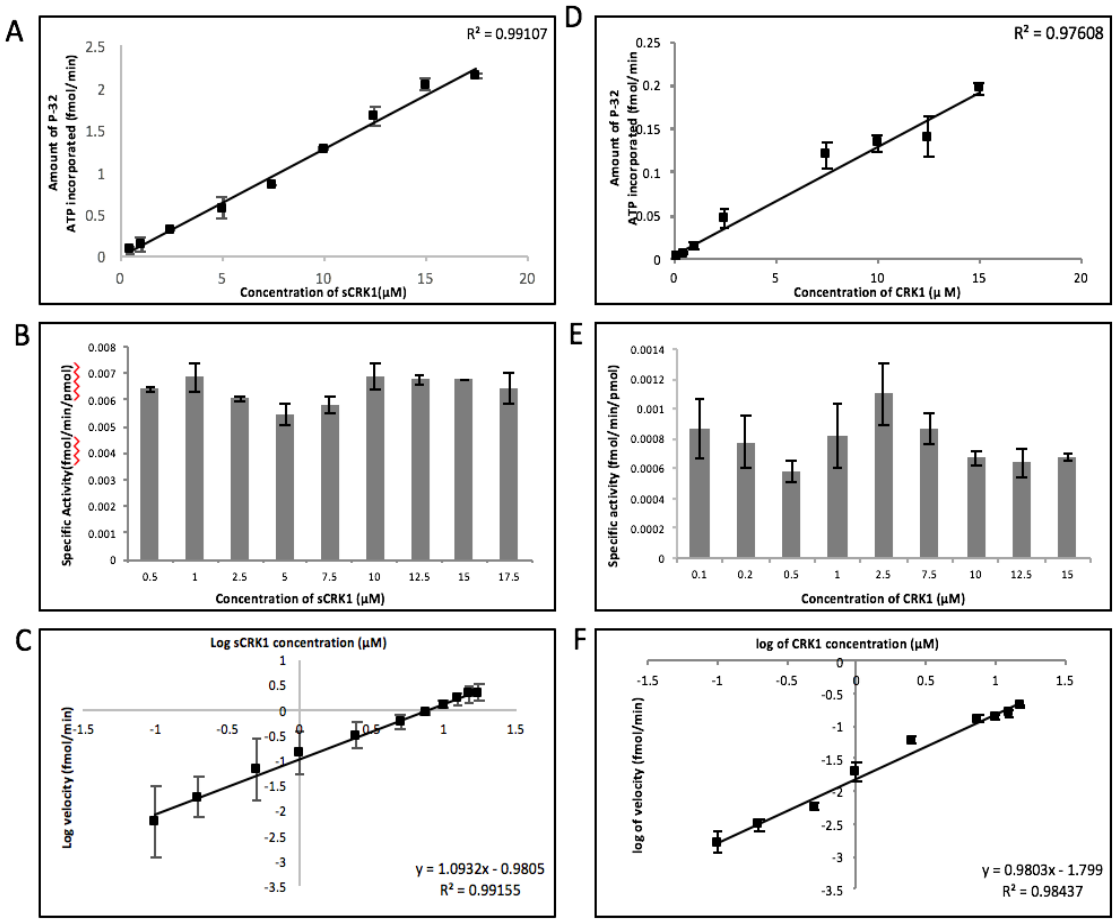

Figure 4: CRK1 auto phosphorylates via an intramolecular mechanism. SUMO: CRK1 **(A-C)** and CRK1 **(D-F)** were incubated at increasing enzyme concentrations in an auto phosphorylation assay**. (A and D)** Plot of velocity vs enzyme concentration. **(B and E)** Plot of specific activity vs enzyme concentration. **(C and F)** Van't Hoff plot of the logarithm of the enzyme velocity vs the logarithm of the enzyme concentration. Linear regression of the data in panels C and F estimates a slope of 1.09 for SUMO: CRK1 and a slope of 0.98 for CRK1. All data are means ± standard deviation.

A

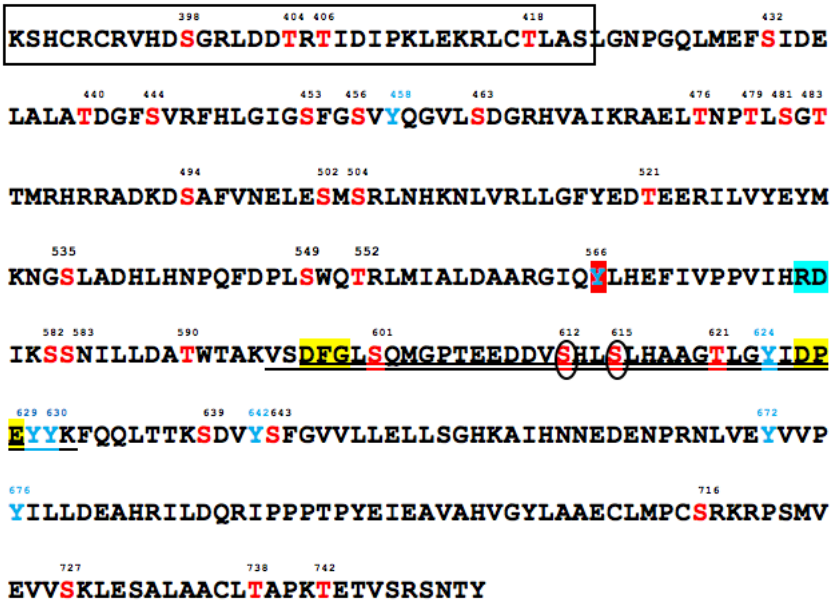
KSHCRCRVHDSGRLDDTRTIDIPKLEKRLCTLASLGNPGQLMEFSIDE
LALATDGFSVRFHLGIGSFGSVYQGVLSDGRHVAIKRAELTNPTLSGT
TMRHRRADKDSAFVNELESMSRLNHKNLVRLLGFYEDTEERILVYEYM
KNGSLADHLHNPQFDPLSWQTRLMIALDAARGIQYLHEFIVPPVIHRD
IKSSNILLDATWTAKVSDFGLSQMGPTEEDDVSHLSLHAAGTLGYIDP
EYYKFQQLTTKSDVYSFGVVLLELLSGHKAIHNNEDENPRNLVEYVVP
YILLDEAHRILDQRIPPPTPYEIEAVAHVGYLAAECLMPCSRKRPSMV
EVVSKLESALAACLTAPKTETVSRSNTY

B

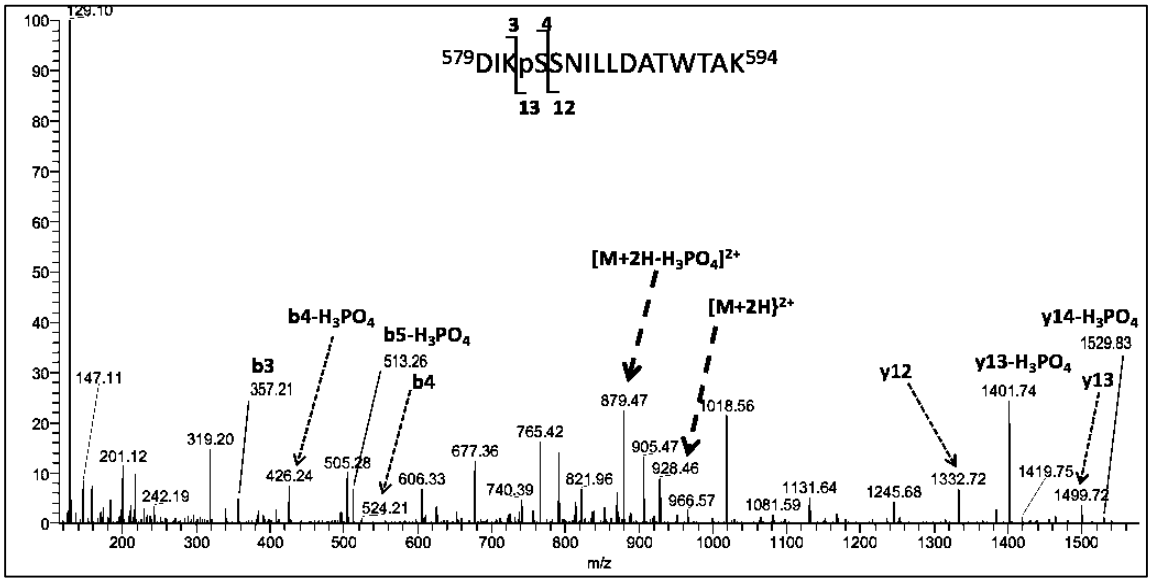
579DIKpSSNILLDATWTAK594
3 4
13 12
[M+2H-H3PO4]2+
[M+2H]2+
b4-H3PO4
b5-H3PO4
b3
b4
y14-H3PO4
y13-H3PO4
y12
y13
m/z

C

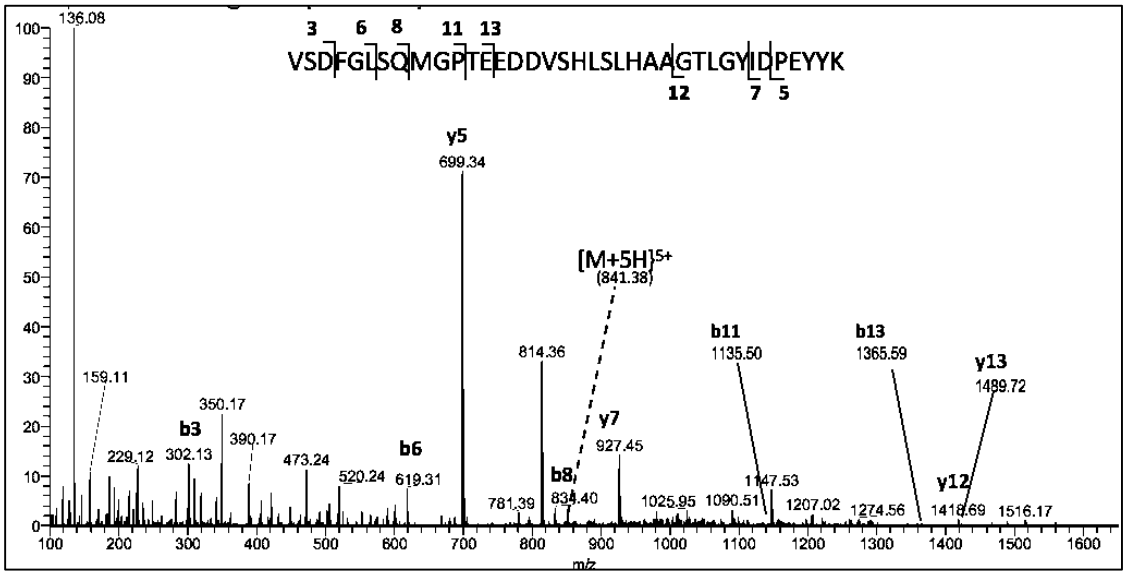

Figure 5: (A) Diagram showing the identified phosphorylation sites in the intracellular domain of CRK1. Solid boxed region corresponds to juxta membrane (JMD) domain. Confirmed phosphorylated Serine and threonine residues (red) and tyrosine residues (Blue). Phosphorylation on S612 and S615 residues (oval circle) are potential phosphorylation sites with the absence of site determining ions. The central kinase domain (KD) with a 37 amino-acid long tryptic peptide (underlined), and the activation loop (double underline) spanning between DFG and DPE residues (yellow highlight), the "RD" motif characteristic of RD-type kinases (blue) **(B)** Collision-induced low resolution fragmentation spectrum of phosphopeptides (Ranging from amino acids 579 - 594) DIKpSSNILLDATWTAK (mascot score 112) The presence of phosphorylated b4 (theoretical m/z 524.24 and observed m/z 524.24) and non-phosphorylated b3 (theoretical m/z 357.21 and observed m/z 357.21), along with site determining phosphorylated y12 (theoretical m/z 1332.72 and observed m/z 1332.72) and nonphosphorylated y13 (theoretical m/z 1529.83 and observed m/z 1529.83) confirmed the phosphorylation at

Ser582. **(C)** CID MS/MS spectrum for tryptic peptide 595VSDFGLSQMGPTEEDDVSHLSHAAGTLGYIDPEYYK[631] containing the activation loop. The presence of $[M+5H]^{5+}$ (m/z 841.38) indicate the mass of doubly phosphorylated peptide with +5 charge.

Figure 6: Alignment of the activation loop sequences of select plant RLKs belonging to the RD kinase family with the activation loop sequence between "DFG" in subdomain VII (green) and "XPE" in subdomain VIII (green). Conserved residues are highlighted in red. Conserved residues (Ser/ Thr /Try) throughout the activation loop of plant RLK (black box).

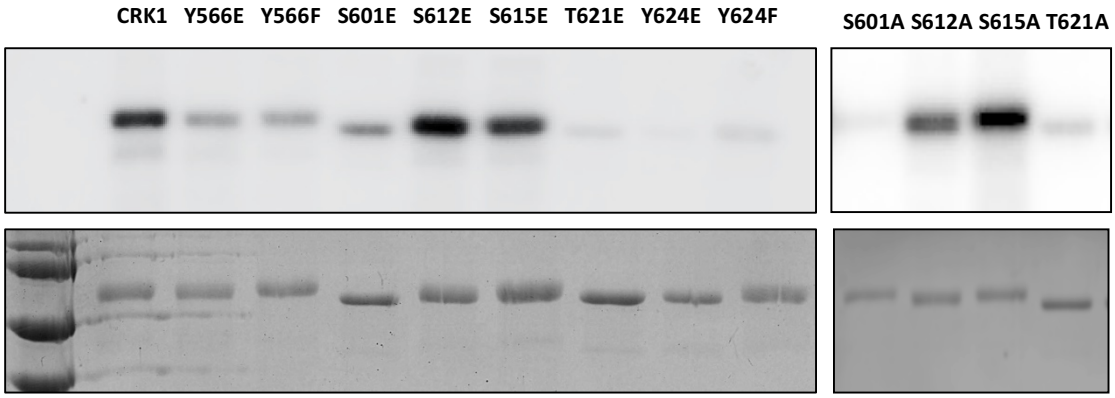

Figure 7: Effect of mutating activation loop phosphorylation sites on kinase activity. Non-phospho mutations to Y566 (conserved phosphorylated tyrosine between ACR4 and CRK1 beyond the activation loop), S601, S612, S515, T621 and Y624 to Ala. Try566 and 624 were mutated to Phe and Glutamic acid representing non-phospho and phospho-mimetic mutations respectively, along with phospho-mimetic mutations of S601, S612, S515, T621 to Glu. *In vitro* kinase assay on each purified protein was performed as described in material and methods. Equal amounts of recombinant proteins were loaded and separated by SDS-PAGE followed by autoradiography. In panels A and B, the top panel shows the autoradiogram and the bottom panel is the corresponding Coomassie Blue-stained gel. Wild-type CRK1 and mutant CRK1m (inactive) were used as controls

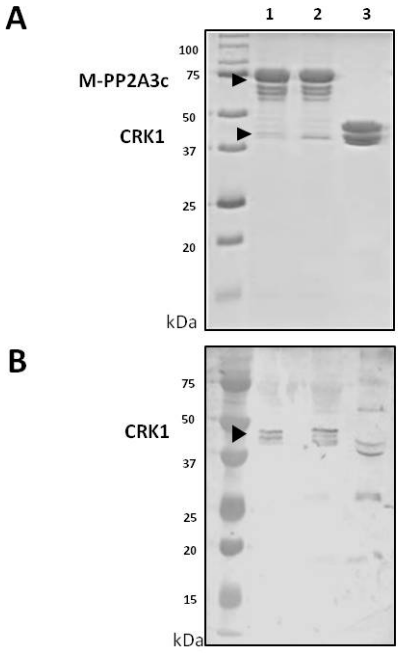

Figure 8: CRK1 ICD interaction with M-PP2A3c. M-PP2A3c was incubated with naïve and auto phosphorylated CRK1 in an *in vitro* pull-down assay. (A) Pull down reactions were separated on a 12% SDS-PAGE and Commassie blue stained reactions. M-PP2A3 specifically bind and pull-down naïve CRK1 (*Lane 1*) and autophosphorylated CRK1 (*Lane 2)*. Control pull down reaction between MBP protein and CRK1. **(B)** A corresponding western blot analysis confirms the identity of CRK1 in the pull-down reactions. An anti-ACR4 (cross reactive with CRK1) polyclonal antibody confirmed CRK1 binding in *Lane 1* & *Lane 2* (lower panel, arrow) and, no binding to MBP tag alone in *Lane* 3.

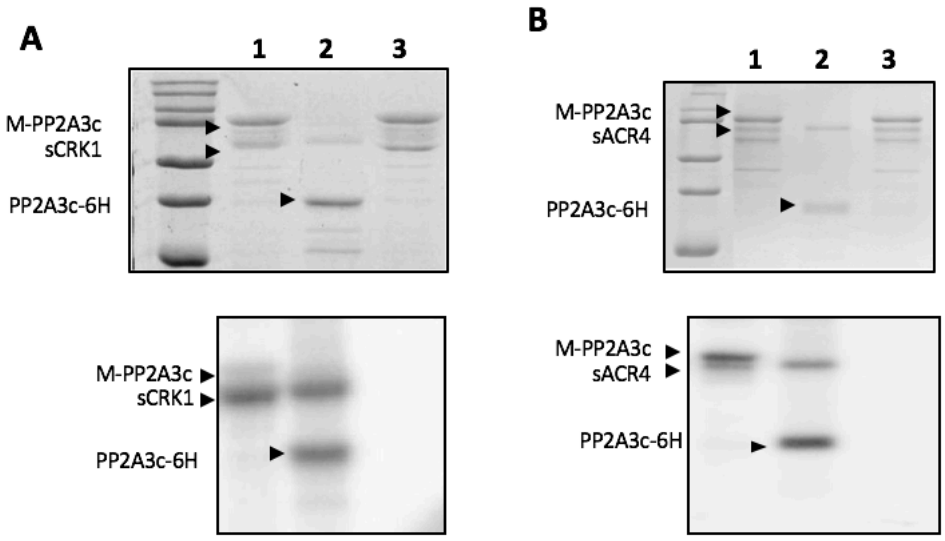

Figure 9: PP2A3c is a substrate for both CRK1 and ACR4. (A) 1µM of sCRK1 incubated with 1µM MBP-PP2A3c (*Lane 1*) and 1µM PP2A3c-6H (*Lane 2*) in an *in vitro* kinase assay respectively; control 1µM of M-PP2A3c protein (*Lane 3*). **(B)** *In vitro* kinase assay between 1µM sACR4 and 1µM MBP-PP2A3c (*Lane 1*) and 1µM of PP2A3c-6H (*Lane 2*) respectively; control 1µM of M-PP2A3c protein (*Lane 3*). Proteins were separated on an SDS-PAGE gel. *Top* panel presents commassie stained gel and *bottom* panel represents the corresponding autoradiogram. Both MBP fused and 6XHis fused PP2A3c are phosphorylated to a larger extend by ACR4 in comparison to CRK1, suggesting it to be a favored substrate for ACR4 over CRK1

Table 1: Primers used to mutate phosphorylation residues in the activation loop of CRK1 protein.

	Mutation	Sequence (5'-3')
Non-phospho mutant	Y566F	CGTGGGATCCAATTCCTTCATGAGTTTATCGTG
	S601A	GATTTCGGCCTAGCTCAAATGGGTCCAACG
	S612A	GAAGATGACGTCGCACATCTCTCTTTACACG
	S615A	GTCTCACATCTCGCTTTACACGCTGCC
	T621A	CACGCTGCCGGTGCATTGGGATATATC
	Y624F	CGTGGGATCCAAGCCCTTCATGAGTTTATCGTG
Phospho-mimetic mutant	Y566E	CGTGGGATCCAAGAACTTCATGAGTTTATCGTGCC
	S601E	TCAGATTTCGGCCTAGAGCAAATGGGTCCAACGGAAG
	S612E	GAAGAAGATGACGTCGAACATCTCTCTTTACACGCTGCC
	S615E	GATGACGTCTCACATCTCGAATTACACGCTGCCGG
	T621E	TTACACGCTGCCGGTGAATTGGGATATATCGACCCG
	Y624E	GCCGGTACATTGGGAGAAATCGACCCGGAGTAC

Table 2. Site-discriminating ions for phosphorylated Serine, threonine and tyrosine residues (in red) identified in the enriched phosphopeptides. The percentage of maximum intensity for each site-discriminating ion in the averaged high resolution CID spectrum are shown in parenthesis (supporting ion information is available for underlined peptide sequences).

Peptide	b ion	Phosphorylated b ion	y ion	Phosphorylated y ion
SERINE & THREONINE				
^{395}VHDSGRLDDTRTIDIPKLEKR^{415} ^{401}LDDTRTIDIPKLEK^{414}	b3 (+1, 12.38) b4 (-)	b4 (+1, 2.16) b5 (+1, 2.91)	y17 (-) y10 (-)	y18 (-) y11 (-)
^{401}LDDTRTIDIPKLEK^{414}	b5 (+1, 2.73)	b6 (+1, 2.63)	y8 (+1, 2.07)	y9 (-)
^{415}RLCTLASLGNPGQLMEFSIDELALATDGFSVR^{446}	b17 (-)	b18 (-)	y14 (+1, 3.88)	y15 (+1, 2.84)
^{416}LCTLASLGNPGQLMEFSIDELALATDGFSVR^{446}	b5 (+1, 0.17)	b6 (+1, 0.24)	y25 (-)	y26 (-)
^{416}LCTLASLGNPGQLMEFSIDELALATDGFSVR^{446}	b24 (-)	b25 (-)	y6 (+1, 32.86)	y7 (+1, 13.44)
^{416}LCTLASLGNPGQLMEFSIDELALATDGFSVR ^{446}	b28 (-)	b29 (-)	y2 (+1, 35.75)	y3 (+1, 17.61)
^{447}FHLGIGSFGSVYQGVLSDGR^{466}	b6 (+1, 6.92)	b7 (-)	y13 (+1, 5.48)	y14 (+1, 1.06)
^{447}FHLGIGSFGSVYQGVLSDGR^{466}	b16 (+2, 2.32)	b17 (-)	y3 (+1, 7.2)	y4 (+1, 2.54)
^{447}FHLGIGSFGSVYQGVLSDGR^{466}	b9 (+1, 4.61)	b10 (+1, 0.39)	y10 (+1, 0.87)	y11 (-)
^{472}RAELTNPTLSGTTMR^{486}	b11 (-)	b12 (-)	y3 (+2, 11.59)	y4 (+1, 0.21)
^{472}RAELTNPTLSGTTMR^{486}	b7 (-)	b8 (-)	y7 (+1, 2.71)	y8 (+1, 0.31)
^{472}RAELTNPTLSGTTMR^{486}	b19 (+1, 0.24)	b10 (-)	y5 (+1, 20.54)	y6 (+1, 13.18)
^{473}AELTNPTLSGTTMR^{486}	b3 (+2, 0.95)	b4 (-)	y11 (-)	y12 (-)
^{490}ADKDSAFVNELESMSR^{505}	b4 (+1, 23.29)	b5 (+1, 1.12)	y11 (+1,18.51)	y12 (+1, 6.71)
^{493}DSAFVNELESMSR^{505}	b9 (-)	b10 (-)	y3 (+1, 8.01)	y4 (+2, 10.7)
^{490}ADKDSAFVNELESMSR^{505}	b14 (-)	b15 (-)	y1 (+1, 23.4)	y2 (+1, 1.86)
^{514}LLGFYEDTEER^{524}	b7 (-)	b8 (-)	y3 (+1, 19.57)	y4 (-)
^{533}NGSLADHLHNPQFDPLSWQTR^{553}	b2(+2, 6.21)	b3 (+1, 9.72)	y18 (-)	y19 (-)
^{533}NGSLADHLHNPQFDPLSWQTR^{553}	b19 (-)	b20 (-)	y1 (+1, 24.45)	y2 (+1, 0.94)
^{533}NGSLADHLHNPQFDPLSWQTR^{553}	b16 (-)	b17(-)	y4 (+1, 20.93)	y5 (+1, 68.58)
^{579}DIKSSNILLDATWTAK^{594}	b3(+1, 4.99)	b4 (+1, 1.04)	y12 (+1, 7.21)	y13 (+1, 3.51)
^{579}DIKSSNILLDATWTAK^{594}	b4 (+1, 0.32)	b5 (+1, 3.28)	y11 (-)	y12 (-)
^{582}SSNILLDATWTAK^{594}	b8 (-)	b9 (-)	y4 (+1, 38.22)	y5 (+1, 3.76)
^{595}VSDFGLSQMGPTEEDDVSHLSHAAGTLGYIDPEYYK^{631}	b6(+1, 10.95)	b7 (-)	y29 (-)	y30 (-)
^{595}VSDFGLSQMGPTEEDDVSHLSHAAGTLGYIDPEYYK^{631}	b25 (-)	b26 (-)	y10 (-)	y11 (+1, 2.06)
^{632}FQQLTTKSDVYSFGVVLLELLSGHK^{656}	b7 (+1, 0.31)	b8 (+1, 1.01)	y17 (-)	y18 (-)
^{632}FQQLTTKSDVYSFGVVLLELLSGHK^{656}	b21 (-)	b22 (-)	y3 (+1, 17.71)	y4 (+1, 19.83)
^{632}FQQLTTKSDVYSFGVVLLELLSGHK^{656}	b5 (+1, 8.79)	b6 (-)	y19 (-)	y20 (-)

Table 2 continued:

^{639}SDVYSFGVVLLELLSGHK^{656}	b4(+1, 5.52)	b5(-)	y13 (+1, 4.49)	y14 (-)
^{690}IPPTPYEIEAVAHVGYLAAECLMPCSR^{716}	b24 (-)	b25 (-)	y1 (+2, 7.1)	y2 (+1, 3.95)
^{718}KRPSMEVVSK^{728}	b8 (-)	b9 (-)	y1 (+1, 2.92)	y2 (+1, 7.24)
^{718}KRPSMVEVVSKLESALAACLTAPK^{741}	b20(-)	b21 (-)	y3 (+1, 20.3)	y4 (+1, 5.42)
^{729}LESALAACLTAPKTETVSR^{747}	b12 (-)	b13 (-)	y5 (+1, 5.1)	y6 (+1, 2.34)
TYROSINE				
^{447}FHLGIGSFGSVYQGVLSDGR^{466} ^{563}GIQYLHEFIVPPVIHR^{578}	b11 (+1, 1.17) b3 (+1, 3.07)	b12 (+1, 1.21) b4 (+2, 3.23)	y8 (+1, 1.36) y12 (-)	y9 (+1, 12.75) y13 (-)
^{595}VSDFGLSQMGPTEEDDVSHLSHAAGTLGYIDPEYYK^{631}	b28 (-)	b29 (-)	y7 (+1, 7.65)	y8 (+1,2.52)
^{595}VSDFGLSQMGPTEEDDVSHLSHAAGTLGYIDPEYYK^{631}	b33 (-)	b34 (-)	y2(+1, 28.88)	y3 (+1, 15)
^{595}VSDFGLSQMGPTEEDDVSHLSHAAGTLGYIDPEYYK^{631}	b34 (-)	b35 (-)	y1 (+1, 8.35)	y2 (+1, 6.82)
^{632}FQQLTTKSDVYSFGVVLLELLSGHK^{656}	b10 (+1, 0.04)	b11 (+1, 0.41)	y14 (+1, 0.44)	y15 (-)
^{668}NLVEYVVPYILLDEAHR^{684}	b4 (+1, 7.03)	b5 (+2, 19.7)	y12 (+1, 8.1)	y13 (+1, 4.19)
^{668}NLVEYVVPYILLDEAHR^{684}	b8(+1, 1.69)	b9(-)	y8(+1, 2.41)	y9 (+1, 3.97)

Table 3: A consolidated list of phosphorylated peptides (phosphorylated at Serine, threonine and tyrosine residues) enriched from pCRK1 protein with a fold change of ≥2, with respect to same phosphorylated peptide enriched from naïve CRK1.

	Peptide sequence modified	Phosphorylated State	N_Intensity (phospho)	N_Intensity (naive)	FC
1	RLCTLASLGNPGQLMEFSIDELALATDGFSVR	Phospho (ST)	6862912.505	1205060	5.7
2	LDDTRTIDIPK	Phospho (ST)	4384665.44	833350	5.3
3	NGSLADHLHNPQFDPLSWQTR	Phospho (ST)	7274906.615	1555024.167	4.7
4	DSAFVNELESMSR	Phospho (ST)	28421954.07	7076761.917	4.0
5	DIKSSNILLDATWTAK	Phospho (ST)	12390203.6	3602000	3.4
6	AELTNPTLSGTTMRHR	Phospho (ST)	36250385.09	10735528.33	3.4
7	RADKDSAFVNELESMSR	Phospho (ST)	7000322.18	2101950	3.3
8	LLGFYEDTEER	Phospho (ST); Phospho (Y)	14905386.36	4789000	3.1
9	FHLGIGSFGSVYQGVLSDGR	Phospho (ST); Phospho (Y)	4384284.496	1439720	3.0
10	TETVSRSNTY	Phospho (ST)	1243782.16	429000	2.9
11	VSDFGLSQMGPTEEDDVSHLSLHAAGTLGYIDPEYYKF QQLTTK	Phospho (ST); Phospho (Y)	8656023.849	2962565.833	2.9
12	VHDSGRLDDTR	Phospho (ST)	2195856.452	759633.3333	2.9
13	RAELTNPTLSGTTMRHR	Phospho (ST)	38210632.14	13262927.15	2.9
14	LESALAACLTAPKTETVSRSNTY	Phospho (ST); Phospho (Y)	17484533.08	6227538.312	2.8
15	ADKDSAFVNELESMSR	Phospho (ST)	3079773.513	1318433.333	2.3

CHAPTER 5: PRODUCTION OF MONOCLONAL ANTIBODY DISPLAYING SPECIFICITY TO THE INTRACELLULAR DOMAIN OF ACR4

Abstract

Overall plant growth and development is to a large extent mediated by a diverse set of receptor-like kinases (RLK). In this regard, an important long-term goal is to better understand the role of the RLK, Arabidopsis Crinkly 4 (ACR4) in, in root differentiation. Major advances in fundamental biology, medicine and miscellaneous science disciplines have been catalyzed through the hybridoma technology and the ease of production of monoclonal antibodies. Here, we describe the production of a highly specific monoclonal antibody(5A4) towards the intracellular domain (ICD) of ACR4, with no detectable cross-reactivity with other homologs of ACR4 or the unrelated RLK CLAVATA1. The monoclonal antibody recognizes both auto-phosphorylated and naïve ACR4 and, in preliminary studies, we have identified a potential epitope within the ACR4 domain spanning amino acid residues 531-616. We anticipate that this antibody will be an invaluable reagent in furthering more comprehensive investigations on the biology biochemistry and genetics of ACR4.

Abbreviations

ACR4, Arabidopsis CRINKLY 4; BSA, bovine serum albumin; CRR, CRINKLY Related receptor; CLV1, CLAVATA; DTT, Dithiothreitol; DMEM, Dulbecco's Modified Eagle Medium; EGFR, epidermal growth factor receptor; ELISA, enzyme linked immunosorbent assay; GFP, green fluorescent protein; HAT, hypoxanthine-aminopterin-thymidine; HER2, human epidermal growth factor receptor 2; ICD, intracellular domain;

mAb, monoclonal antibody; pAb, polyclonal antibody; PEG, polyethylene glycerol; PBS, phosphate buffered saline; PBST, phosphate buffered saline with 0.05% tween; PP2A3c, protein phosphatase 2A; pNPP, p-nitro phenyl phosphate; PVDF, polyvinylidene difluoride; RLK, receptor like kinase; YFP, yellow fluorescent protein.

Introduction

Antibodies are highly specific and selective immunological proteins used as a biochemical tool in a range of applications including selection, identification, purification/immuno-precipitation [1,2,3], protein function and structure determination [4] and therapeutic targets [5,6]. Antibodies are produced by differentiated B lymphocytes, plasma cells, of higher animals in response to foreign substances (antigens). B lymphocytes differentiate into plasma cells and secrete a single specific antibody in response to one antigenic determinant.

Antibodies are classified broadly into two groups: Polyclonal and Monoclonal antibodies based on their specificity, distinguishing characteristics and applications [7]. Polyclonal antibodies (pAb) are heterogeneous mixture of antibodies directed against multiple epitopes (determinants) on the same antigen. Different B-cell clones of the animal generate the antibodies and hence are immunochemically dissimilar with respect to specificities and affinities. On the other hand, monoclonal antibodies are generated from identical B cells that are clones of a unique parent cell with monovalent affinity and specifically bind to a single epitope on the antigen. Monoclonal Antibodies (mAb) are produced from B-cell secreting cell clones, produced by fusion of myeloma cells with mouse spleen cells immunized with desired antigen [8]. The fusion generates a hybridoma cell line which has two important properties: an immortal nature coupled to expression of an antigen-specific antibody.

Production of mAbs is an expensive, elaborate and painstaking process with a much longer turn-around time in comparison to pAb Polyclonal. Nevertheless, due to their homogeneity, consistency and mono-specificity, mAbs have been a preferred tool used to evaluate molecular conformation, protein-protein interaction, post-translational modification and identification of single members with protein families. Co-immuno precipitation with specific antibodies is a routinely used method to isolate complexes of physically interacting proteins *in vivo* [1,2,3 & 9]. Many monoclonal antibodies, targeted to receptor tyrosine kinases such as EGFR and HER2, have been developed as therapeutic agents to treat human diseases [10,11,12,13,14,15]. While this is less important in the plant sciences, antibodies have still served as essential reagents in a variety of studies.

Arabidopsis genome encodes four homologs of ACR4 (AtCRRs) with high sequence similarity and conserved structural features. ACR4 is expressed throughout the plant development and is required for the overall development to plant encompassing proper cell formation and cell division in both root and shoot apical meristem [16,17]. Genetic, in-silico co-expression analysis and *in vitro* studies have identified many important interacting proteins including the AtCRRs [17,18], PP2A3c [19], unrelated RLKs [20], and the transcription factor WOX5 [21], that are implicated in the regulation of formative cell differentiation of columella stem cells in root apical meristem and lateral root formation [22,23]. However there many unanswered questions remain with regard to ACR4 mediated signaling pathways affecting developmental aspects of both root apical meristem and shoot apical meristem.

To further the mechanism of ACR4 signaling, and identify the important players in the network of interactions, we undertook the development of antibodies to the ICD of

ACR4. In this study, we report the development, purification and characterization of a monoclonal antibody highly specific to the intracellular domain of ACR4. No cross reactivity within the highly similar and related RLKs could be detected by ELISA and western blot analysis. We also narrowed down a region within ACR4 as a potential epitope for the mAb using phage-displayed domains of the RLK.

Material and Methods

Construct design, protein production and isolation of Antigen (Intracellular domain of ACR4) and other proteins.

The intracellular domain of the proteins was recombinantly cloned C-terminal to SUMO in pE-SUMO vector (life sensors). Cloning, expression and purification of SUMO-fused ACR4 (sACR4) and SUMO-fused CRRs (sCRK1, sCRR1, sCRR2, sCRR3) were prepared as described in Meyer et al [24]. Control SUMO protein was obtained by expressing the endogenous SUMO protein in the pE-SUMO (Kan) vector (Life Sensors) in a similar manner. SUMO-CLV1 was cloned in similar fashion using forward primer 5'-GCGGCAGGTCTCTAGGTATGCGTCAGATGAATAAGAAGAAGA-3' and reverse primer 5'-GCAGCAGGTCTCTCTAGATCAACGCGATCAAGTTCGCCAC-3. pSUMO tag was cleaved incubating SUMO protease (gift from Nelson Lab, Iowa State University) with the affinity-enriched SUMO-tagged proteins at 1:100 concentration in 50 mM Tris, pH 8, 0.2% NP40, 150 mM NaCl and 1 mM DTT overnight at 4°C while dialyzing the cleavage reaction against 50 mM Tris, pH 8, 150 mM NaCl and 1 mM DTT. The cleaved SUMO protein was removed by affinity enrichment of the dialyzed cleavage reaction to obtain tag-less proteins.

Production and initial screening of hybridomas

Monoclonal antibodies were produced at the Hybridoma Facility at Iowa State University as described in http://www.biotech.iastate.edu/Hybridoma/cell-fusion-and-cell-passage/. Briefly, 25µg of SUMO-fused Intracellular domain of ACR4 (Antigen) was injected per mice (4 mice used -N, R, L & RR). Three injections at an interval of 2 weeks were performed per mice. Each injection was a 1:1 volume of adjuvant Freund's Complete Adjuvant to antigen. Two weeks after the last boost, mice are bled and the sera is tested for titer by dot-blot analysis against antigen as described below. The mouse with the highest titer is sacrificed and the spleen cells used for fusion. All materials, media, solutions, equipment and apparatus used were autoclave sterilized. Four days prior to the fusion, three T-75 flasks of SP2/0's were split at 1:30 in Dulbecco's Modified Eagle Medium (DMEM) supplemented with 10%Horse Serum (D-10) to a final volume of 60 ml per flask. 60 ml of Dulbecco's Modified Eagle Medium DMEM 50/10 HAT was supplemented with 0.15 ml Gentamycin, 1.5 ml Glutamine, 1.5 ml Penn/Strep, 3 ml HAT (50X), 75 ml conditioned media, 15 ml Horse Serum in the order listed making sure the minor components are evenly dispersed. The three T-75 flasks of SP2/0's cells were pooled into one flask. 4 x 10^7 SP2/0 cells were aliquoted into three 50ml tubes. Meanwhile, 2.7ml sterile PBS was added to dissolve to 2.25 g of Polyethylene glycol (PEG) in 60°C water bath. 20ml aliquot of DMEM in 50 ml centrifuge tube and dissolved PEG, both solutions were incubated at 37°C. The mouse was carbon dioxide asphyxiated and the spleen was harvested in a sterile petri dish. The spleen cells were counted and 4 x 10^7 spleen cells were added to the SP2/0 cells, gently mixed and centrifuged at 200 x g for 8

mins. The supernatant was discarded and the pellet was gently loosened by flicking. Filter sterilized 1 ml of PBS solution was added dropwise to the pellet and swirled for 15 secs to 30 secs and left undisturbed for an additional 90 secs. 1 ml of DMEM was added very gently dropwise for 30 secs with gentle mixing for 30 secs followed by similar dropwise addition and gentle mixing of 9 ml of DMEM for 46 seconds. The mixture was set aside for 5 mins before centrifuging at 200 x g for 8 min. The supernatant was discarded and 10 ml of HAT media was added to cell pellet and resuspended by gently pipetting up and down. The entire mixture was slowly transferred to 100 ml of HAT media and incubated for 1 h at 37 °C. The contents of the bottle were gently mixed and a 25 ml aliquot of the mixture was transferred to sterile media boat. 200 µl of the mixture was aliquoted to each well of a 96 well plate using multichannel pipette with sterile filter tip. These results in 12-16, 96-well plates per mouse.

Following a color change to yellow, which signified growth, supernatant fluids from 300-800 wells were sampled and an initial pre-screening was performed by ELISA or dot-blot against the ACR4 antigen. The cells in the wells containing the positive supernatant fluid were moved up to 48-well plates and allowed to expand. At each stage, the supernatant fluids were re-screened to confirm the positive hybridomas. Positives were then expanded to 24-well plates, T25 flasks, T75 flasks and then finally frozen at -140 °C.

Pre- Screening by Dot-blot analysis.

Pre-screening of the sera from mouse bleed was performed by dot blot assay. 1 µg of sACR4 was carefully blotted to 1 cm x 1 cm cut nitrocellulose paper and allowed to adsorb. Five 1cm x 1cm blots were per prepared for each mouse serum. The blots were

blocked with 5% nonfat dry milk in PBST for 1 h at room temperature followed by three washes with PBST (0.5% tween). Serially diluted (1:300 to 1:4800) mouse sera in PBS from four mice were incubated with the blots for 1 h at room temperature followed by three washes with PBST and further incubated with 1:10000 dilution of alkaline phosphatase conjugated anti-mouse secondary Ab. The sera with highest titer were detected calorimetrically by AP Conjugate Substrate kit (Bio-Rad).

ELISA Screening assay

The screening at each step was carried out by performing ELISA against sACR4 antigen coated well. 10 µg/ml of sACR4 was immobilized per well in 100 µl of $NaHCO_3$, pH 9.6 and incubated room temperature for 2 h on a shaker. Plate was washed two times with PBST (0.05% Tween) followed by blocking with PBST containing 0.1 % BSA for 1 h at room temperature on a shaker. It was then washed three times with PBST followed by incubation with the appropriate solution of monoclonal Ab (monoclonal supernatant/purified monoclonal) for 1-2 h. Subsequently, the plate was washed three times with PBST followed by incubation with 50 µl anti-mouse alkaline phosphatase conjugated secondary antibody (Sigma) in PBST for 1 h. The plate was the again washed four times with PBST. The positives supernatants or specificity of purified mAbs was detected colorimetrically by incubating with 100 µl of a p-nitro phenyl phosphate (pNPP) solution (Sigma) to each well. The reactions were allowed to incubate for 5 mins with occasional manual shaking. Reactions were terminated with the addition of 50 µl of 2N NaOH to each well and absorbance was measured at 405 nm on a plate reader (Spectra Max 180).

Purification of monoclonal antibodies by Ammonium sulphate precipitation

Monoclonal antibodies were purified from 50 ml of selected frozen supernatants by ammonium sulphate precipitation. 100% saturated ammonium sulphate ($AmSO_4$), pH 7 was prepared. At room temperature, 50 ml of prepared 100% saturated $AmSO_4$ solution was added progressively with continuous gentle stirring with a magnetic stirrer. Stirring was continued for 20 mins after the last addition of $AmSO_4$. The mixture was centrifuged at 12000 g for 30 mins at 4°C. The supernatant was discarded and the precipitated pellet was resuspended in 15 ml of PBS solution. Any remaining $AmSO_4$ was eliminated by dialysis against PBS overnight at 4°C with three buffer changes. The dialyzed sample by further centrifuged at maximum speed for 15 mins to remove any aggregates. 15 ml of supernatant was concentrated down to 5 ml through vivaspin 20 MWCO 10000 (GE healthcare) by centrifuging at 4000 x g for 30 mins. Multiple 500 µl aliquots were prepared for long term storage at -20 °C.

Characterization of mAbs

The monoclonals (generally IgG) were isotype following manufacturer's protocol for isotype testing (Pierce Kit: Fisher # PI-26178) (Table 2). An absorbance spectrum scan was collected for each purified mAb (with appropriate dilution in PBS) in the 210-310 nm ultraviolet range and concentration was determined by using O.D at 280 nm and molar extinction coefficient of 1.36

The saturating concentration of mAbs was determined by an indirect ELISA assay. 0.1 µg of sACR4 antigen coated wells were blocked and incubated with serially diluted (1:2 to 1:64) mAbs, diluted in PBS buffer for 1 h at room temperature followed by 1 h of incubation with 1:20000 alkaline phosphatase conjugated anti- mouse secondary antibody.

Colorimetric detection was performed by using pNPP substrate kit (Sigma) as described before. Saturation curves were plotted by subtracting the background control reading from each test reading. The concentration of each antibody required to saturate the antigen is determined from the saturation curves by extrapolating the reading from constant plateau region in the plot.

Western blot Analysis and ELISA

1 μg of purified proteins (sACR4, sCRK1, sCRR1, sCRR2, sCRR3, sCLV1 and SUMO) were separated on a 12% SDS-PAGE gel and blotted onto a PVDF membrane. The membrane was blocked and probed with saturating concentration of purified monoclonal antibody, washed, and then probed with a secondary anti-mouse IgG antibody (1: 10,000) conjugated to alkaline phosphatase (Sigma). Protein detection was completed using an AP Conjugate Substrate kit (Bio-Rad).

Similarly, to test the specificity towards ACR4, and to eliminate any cross reactivity, microtiter plates were also coated with equal amount (10 μg/ml) of sCRK1, sCRR1, sCRR2, sCRR4, sCLV1 and control SUMO and ELISA was performed as described above.

Construction of Phage-displayed Overlapping Domains of ACR4 ICD.

Five overlapping domains of intracellular domain (ICD) of ACR4 (J1-J5) with five amino acid overlap were prepared as described by Shah et al [25]. The domains span amino acid residues 456- 895 within the intracellular domain. Individual domains J1, J2, J3, J4 and J5 domains consists of 80, 85, 85, 85,85, 125 amino acids respectively. PCR of the cDNA of ACR4 fused in pE-SUMO vector was used as template and amplified using the forward and reverse primers listed in table 3. The PCR fragments were then digested with

SfiI and NotI, ligated into a similarly digested pCANTAB 5E phagemid vector and subsequently transformed into *E. coli* XL1-Blue cells (Stratagene). Single colonies from each plate were inoculated into 5 ml 2YT/ carb/Amp media, grown to O.D at 600 λ ~0.2–0.3 at 37 °C and then infected with helper phage-VCSM13 (Stratagene). After 1 h the cell culture was transferred to 25 ml 2YT/Kan media and further incubated overnight at 37°C. After removing cell debris by centrifugation, phage particles were precipitated from the supernatant using 7.5 ml of 20% PEG solution containing NaCl. The precipitate was re-suspended in 1 ml of PBS and phage concentration determined by measuring absorbance at 268 nm (O.D 268 nm = 1.0 for a solution containing 5 x 10^{12} phages per ml).

Phage ELISA

1 μg of purified monoclonal Antibody (5A4) was coated in triplicates (or a total of 3 x 7 = 21 wells) on a microtiter Nunc plate (Thermo scientific) in 100 μl of 50 mM $NaHCO_3$, pH 9.6 on gentle rotation for 2 h at room temperature. Plate was then washed two times with PBST (0.05%) followed by blocking with PBST containing 0.2% BSA for 1 h. Subsequently, after three washings with PBST, wells were incubated with the 100 μl of appropriate concentration of phage domain (1 x 10^{12} phage particles) in PBST, 0.02% BSA, for 2 h at room temperature with gentle shaking followed by three time washes with PBST. Control reaction of 5A4 was against equivalent amount of the PP2A3c phage domain (prepared similarly to ACR4 domain) and helper phage. Each well was then incubated with anti-M13 HRP conjugated antibody for 1 h followed by four time washes with PBST. The bound phage in each well was detected by incubating with 50 μl of SureBlue Reserve TMB Microwell peroxidase substrate (KPL) till the blue color develops (usually 5-10mins). Thereafter, reactions were terminated by the addition of 50 μl of 1N

HCl, 0.6N Sulfuric acid and the absorbance of the developed yellow color was measured at 450 nm. Data were generated by subtracting the absorbance of the control (helper phage control) wells from the experimental wells.

Results

Screening and purification of Ten Monoclonal Antibodies (mAbs)

Pre-bleeds were obtained from four mice, injected with 25 μg of SUMO-ACR4(ICD) after 2 weeks and tested via dot-blot assay (Figure 1). One mouse was selected to isolate spleen cells for fusion with SP20 cells. Two rounds of screening against the antigen was performed by ELISA and wells with readings with an absorbance of 0.05 above background (about 30 lines) was advanced for further screening. After two further rounds of selection by the same process, 10 lines were finally selected to produce 50 ml supernatants. The selected 10 hybridoma supernatants were purified at 50% ammonium sulphate saturation, as suggested for IgG precipitation [26]. According to their general structure, antibodies are classified as IgG, IgM, IgE, IgA or IgD, with hybridomas primarily expressing the IgG type [27].

Characterization of Monoclonal Antibodies

The general structure of IgG consists of two long heavy chains (H) and two short chains light chains (L) linked by disulfide bonds. Each purified antibody was separated on an 12% SDS PAGE gel (Figure 2). The two bands corresponding to 50 kDa and 25 kDa (Figure 2) represents heavy and light chain of the IgG mAb. The other contaminating bands may correspond to lipids, albumin, transferrin, lipoproteins, endogenous IgG, other host proteins and depending on future applications, may require a secondary step of purification such as ion-exchange chromatography or size exclusion chromatography. Table 1

summarizes the concentration of diluted monoclonal antibodies calculated from A280 values from absorbance curves for obtained for each antibody and specifies the saturating concentration of each diluted mAb to be used for ELISA and western blot analysis as determined from saturation curves.

Table 2 classifies the mAbs according to their isotypes. The IgG immunoglobulins are subdivided into isotypes: IgG1, IgG2, IgG3, and IgG4 due the difference in the number of disulfide bonds linking the two heavy chains [28,29,30]. The ability to fix complement and specific response towards protein, polysaccharides and allergens vary within the members of IgG subclass [29,30]. The ten monoclonals represent different isomers of IgG immunoglobulins sub classified based on variability in the disulfide bonds within the hinge region. The kappa isomers are structural hinge isomers to IgG2 subclass. Hence, each isotype of the purified monoclonal could serve to recognize a different biomolecule within an epitope.

5A4: Specificity of mAb toACR4

The specificity of each purified mAb against the intracellular domain of ACR4 was analyzed by ELISA (Figure 5A). Preliminary ELISA indicated cross reactivity of 9 out of 10 mAb against all the SUMO fused test proteins. Test proteins comprised members of ACR4 RLK family with high sequence similarity. The antigen injected was SUMO-fused ACR4 (ICD); hence SUMO protein was included as a control. SUMO-fused CLAVATA-1 (sCLV1), an unrelated RLK, with little or no similarity to the ACR4 or its homologs, was an additional control. All Abs, except 5A4, showed cross-reactivity with SUMO. The O.D readings were obtained in triplicates and average mean values at 405 nm were plotted for

each mAb (Figure 5B), clearly indicating specificity of only one mAb (5A4) for ACR4 antigen (red arrow and red boxed O.D reading)

Further western blot analysis confirmed the specificity of 5A4 against sACR4, SUMO-free ACR4 with no indication of cross-reactivity against ACR4 homologs, sCLV1 or SUMO (Figure 6).

5A4 cross-reacts with naïve and auto phosphorylated ACR4.

Injection of naïve sACR4 generated one highly specific mAb, 5A4, against the intra-cellular domain. We analyzed the cross reactivity 5A4 against naïve and auto phosphorylated (pACR4) by Western Blot analysis (Figure 7A) and ELISA (Figure 7B). Both the assays indicate that 5A4 recognizes both ACR4 and pACR4.

Epitope mapping

To further characterize 5A4, we attempted epitope mapping of by testing binding of the antibody to specific regions of ACR4 displayed on phage particles, as described in Materials and Methods. Overlapping domains (J1-J5) spanning the entire intracellular domain ACR4 were expressed as individual antigenic regions ligated to the pIII coat gene and displayed as a part of the outer coat protein of an M13 phage particle (Figure 8A). Phage-ELISA performed with homogeneous phage particles of the individual domains showed that the J2 domain has the strongest binding affinity towards 5A4 proteins followed by J4 domain. The relative binding affinities of other domains were significantly reduced compared to J2 domain (Figure 8B). To further delineate the epitope, sub-domains within J2 domain could be used for phage ELISA and mutagenesis of residues within the sub-domains could pinpoint the important residues within the epitope.

Discussion

Arabidopsis CRINKLY4 (ACR4) is a plant receptor like kinase with critical role in the overall development of the entire plant [16,17,21,31,32]. ACR4 regulates the columella stem cell differentiation in the root apical meristem and lateral root formation in the developing root, affects the epidermal cell morphology and formation in leaves, ovules, sepal margins, seed coat development. *Arabidopsis* genome encodes more than 600 RLKs [33], with four architecturally similar homologs of ACR4 RLK with high sequence similarity [17]. Recent advances in understanding the ACR4 signaling and the interactome have come from genetic, in-silico and *in vitro* studies [19]. In an earlier report, we described its regulatory interaction with a downstream phosphatase PP2A3c [19]. It is apparent that the RLK is important in cell fate specification; however, an overall understanding at a biological level is quite limited. *In vitro* studies complemented with *in planta* and structure-function findings can provide valuable information about ACR4 signaling.

In this study, we report development of a highly specific monoclonal antibody (5A4) against the intracellular domain of ACR4 and identified its potential epitope on ACR4. Monoclonal antibodies are extremely important tool and have been widely used both *in planta* and *in vitro* studies. *In-planta*, 5A4 mAb can be utilized to dissect novel and existing protein-protein interactions by immunoprecipitation.

The cellular localization of endogenous ACR4 protein and recombinantly expressed ACR4 in transgenic lines can be visualized by fluorescently labeling the monoclonal antibody with organic dyes, fusion with fluorescent proteins such as GFP or phycobiliproteins or by quantum dots. In an earlier report, we established interaction

between ACR4 and PP2A3c *in planta*, by using fluorescently labeled epitope tagged ACR4 (ACR4: YFP: HA) to co-immuno precipitate PP2A3c (FLAG-PP2A3c) in transient expression lines in *Nicotiana benthamiana* [19]. However, the ACR4 is an over expressed version of a fluorescently tagged protein and does not represent the endogenous, native protein. With the generation of a monoclonal Ab against ACR4, with no cross-reactivity against the homologs with any other protein related (homologs) or an unrelated RLK, it is feasible to perform endogenous protein localization and immune-precipitation to identify interacting partners.

Monoclonal antibodies have been routinely used as probes to determine structure and function. Structure analysis of Na+/H+ anti-porter NhaA from *E.coli* [34] and crystal structure of cyclic AMP –dependent protein[4,35] have been reported in past which utilized monoclonal antibodies. The kinase structure of ACR4 is modeled against Interleukin-1 receptor associated kinase used as template [36]. With the availability of ACR4 specific mAb, crystallization of ACR4 kinase domain can now be attempted. Structure-function studies will provide more in-depth understanding of the mode of ACR4 activation, auto-phosphorylation mechanism and interaction with other proteins.

We mapped the potential epitope of 5A4 by means of phage ELISA assay and epitope was further narrowed down to the 531-616 amino acid sequence within the intracellular domain. However, this is 85 amino acid long region and our future studies are directed towards sub-cloning smaller sections within this region and narrowing down the epitope. A more comprehensive understanding of the binding motif will be analyzed by phage panning of the sub-domain library against a randomized peptide library. Mutagenesis of individual amino acid within the identified consensus motif (potential

epitope) will provide a better understanding of interaction between epitope and mAb at a single residue level.

In conclusion, the developed highly specific monoclonal antibody will serve as an important reagent for both *in planta* and *in vitro* studies for researchers around the globe working towards a better understanding of ACR4 mediated signaling.

Acknowledgements

We like to thank Mr. Paul Kapke and Ms. Amanda Brockman from Hybridoma Facility at Iowa State University, for the time and effort towards breeding the mouse, performing the hybridoma fusion and providing all the technical expertise in the production of Monoclonal Antibody against intracellular domain of ACR4.

References

1. Ren L, Emery D, Kaboord B, Chang E, Qoronfleh MW (2003) Improved immunomatrix methods to detect protein:protein interactions. J Biochem Biophys Methods 57: 143-157.
2. Phee BK, Shin DH, Cho JH, Kim SH, Kim JI, et al. (2006) Identification of phytochrome-interacting protein candidates in Arabidopsis thaliana by co-immunoprecipitation coupled with MALDI-TOF MS. Proteomics 6: 3671-3680.
3. Monti M, Orru S, Pagnozzi D, Pucci P (2005) Interaction proteomics. Biosci Rep 25: 45-56.
4. Miller EJ, Cohen AB (1991) Use of Antibodies in the Study of Protein-Structure and Function in Lung-Diseases. American Journal of Physiology 260: L1-L12.
5. Fauvel B, Yasri A (2014) Antibodies directed against receptor tyrosine kinases Current and future strategies to fight cancer. Mabs 6: 838-851.
6. Miglietta R, Pastori C, Venuti A, Ochsenbauer C, Lopalco L (2014) Synergy in monoclonal antibody neutralization of HIV-1 pseudoviruses and infectious molecular clones. Journal of Translational Medicine 12.
7. Lipman NS, Jackson LR, Trudel LJ, Weis-Garcia F (2005) Monoclonal versus polyclonal antibodies: distinguishing characteristics, applications, and information resources. ILAR J 46: 258-268.
8. Kohler G, Milstein C (1975) Continuous cultures of fused cells secreting antibody of predefined specificity. Nature 256: 495-497.

9. Barberini ML, Muschietti JP (2017) Expression of Plant Receptor Kinases in Yeast. Methods Mol Biol 1621: 21-27.
10. Baselga J, Swain SM (2009) Novel anticancer targets: revisiting ERBB2 and discovering ERBB3. Nat Rev Cancer 9: 463-475.
11. Giannopoulou E, Antonacopoulou A, Matsouka P, Kalofonos HP (2009) Autophagy: novel action of panitumumab in colon cancer. Anticancer Res 29: 5077-5082.
12. Goldenberg MM (1999) Trastuzumab, a recombinant DNA-derived humanized monoclonal antibody, a novel agent for the treatment of metastatic breast cancer. Clin Ther 21: 309-318.
13. Hudis CA (2007) Trastuzumab--mechanism of action and use in clinical practice. N Engl J Med 357: 39-51.
14. Patel D, Bassi R, Hooper A, Prewett M, Hicklin DJ, et al. (2009) Anti-epidermal growth factor receptor monoclonal antibody cetuximab inhibits EGFR/HER-2 heterodimerization and activation. Int J Oncol 34: 25-32.
15. Yang BB, Lum P, Chen A, Arends R, Roskos L, et al. (2010) Pharmacokinetic and pharmacodynamic perspectives on the clinical drug development of panitumumab. Clin Pharmacokinet 49: 729-740.
16. De Smet I, Vassileva V, De Rybel B, Levesque MP, Grunewald W, et al. (2008) Receptor-like kinase ACR4 restricts formative cell divisions in the Arabidopsis root. Science 322: 594-597.
17. Cao X, Li K, Suh SG, Guo T, Becraft PW (2005) Molecular analysis of the CRINKLY4 gene family in Arabidopsis thaliana. Planta 220: 645-657.
18. Meyer MR, Shah S, Zhang J, Rohrs H, Rao AG (2015) Evidence for intermolecular interactions between the intracellular domains of the arabidopsis receptor-like kinase ACR4, its homologs and the Wox5 transcription factor. PLoS One 10: e0118861.
19. Yue K, Sandal P, Williams EL, Murphy E, Stes E, et al. (2016) PP2A-3 interacts with ACR4 and regulates formative cell division in the Arabidopsis root. Proc Natl Acad Sci U S A 113: 1447-1452.
20. Stahl Y, Grabowski S, Bleckmann A, Kuhnemuth R, Weidtkamp-Peters S, et al. (2013) Moderation of Arabidopsis root stemness by CLAVATA1 and ARABIDOPSIS CRINKLY4 receptor kinase complexes. Curr Biol 23: 362-371.
21. Stahl Y, Wink RH, Ingram GC, Simon R (2009) A signaling module controlling the stem cell niche in Arabidopsis root meristems. Curr Biol 19: 909-914.
22. Guo F, Stanevich V, Wlodarchak N, Sengupta R, Jiang L, et al. (2014) Structural basis of PP2A activation by PTPA, an ATP-dependent activation chaperone. Cell Res 24: 190-203.
23. Oh MH, Wang X, Kota U, Goshe MB, Clouse SD, et al. (2009) Tyrosine phosphorylation of the BRI1 receptor kinase emerges as a component of brassinosteroid signaling in Arabidopsis. Proc Natl Acad Sci U S A 106: 658-663.
24. Meyer MR, Lichti CF, Townsend RR, Rao AG (2011) Identification of in vitro autophosphorylation sites and effects of phosphorylation on the Arabidopsis CRINKLY4 (ACR4) receptor-like kinase intracellular domain: insights into conformation, oligomerization, and activity. Biochemistry 50: 2170-2186.
25. Shah S, Butler NM, Hannapel DJ, Rao AG (2013) Mapping and characterization of the interaction interface between two polypyrimidine-tract binding proteins and a nova-type protein of Solanum tuberosum. PLoS One 8: e64783.

26. Berenstein ACGE (2009) Introduction to the Purification of Antibodies. Immunocytochemical Methods and Protocols 588: 11-13.
27. Janeway CA Jr TP, Walport M, et al. (2001) The structure of a typical antibody molecule. Immunobiology: The Immune System in Health and Disease 5th edition.
28. Shakib F (1990) The Human IgG Subclasses. Molecular Analysis of Structure, Function and Regulation.
29. Schur PH (1987) Igg Subclasses - a Review. Annals of Allergy 58: 89-&.
30. Vidarsson G, Dekkers G, Rispens T (2014) IgG subclasses and allotypes: from structure to effector functions. Frontiers in Immunology 5.
31. Gifford ML, Dean S, Ingram GC (2003) The Arabidopsis ACR4 gene plays a role in cell layer organisation during ovule integument and sepal margin development. Development 130: 4249-4258.
32. Watanabe M, Tanaka H, Watanabe D, Machida C, Machida Y (2004) The ACR4 receptor-like kinase is required for surface formation of epidermis-related tissues in Arabidopsis thaliana. Plant J 39: 298-308.
33. Shiu SH, Bleecker AB (2001) Receptor-like kinases from Arabidopsis form a monophyletic gene family related to animal receptor kinases. Proc Natl Acad Sci U S A 98: 10763-10768.
34. Venturi M, Hunte C (2003) Monoclonal antibodies for the structural analysis of the Na+/H+ antiporter NhaA from Escherichia coli. Biochim Biophys Acta 1610: 46-50.
35. Mumby MC, Weldon SL, Scott CW, Taylor SS (1985) Monoclonal-Antibodies as Probes of Structure, Function and Isoenzyme Forms of the Type-Ii Regulatory Subunit of Cyclic Amp-Dependent Protein-Kinase. Pharmacology & Therapeutics 28: 367-387.
36. Czyzewicz N, Nikonorova N, Meyer MR, Sandal P, Shah S, et al. (2016) The growing story of (ARABIDOPSIS) CRINKLY 4. J Exp Bot 67: 4835-4847.

Figures

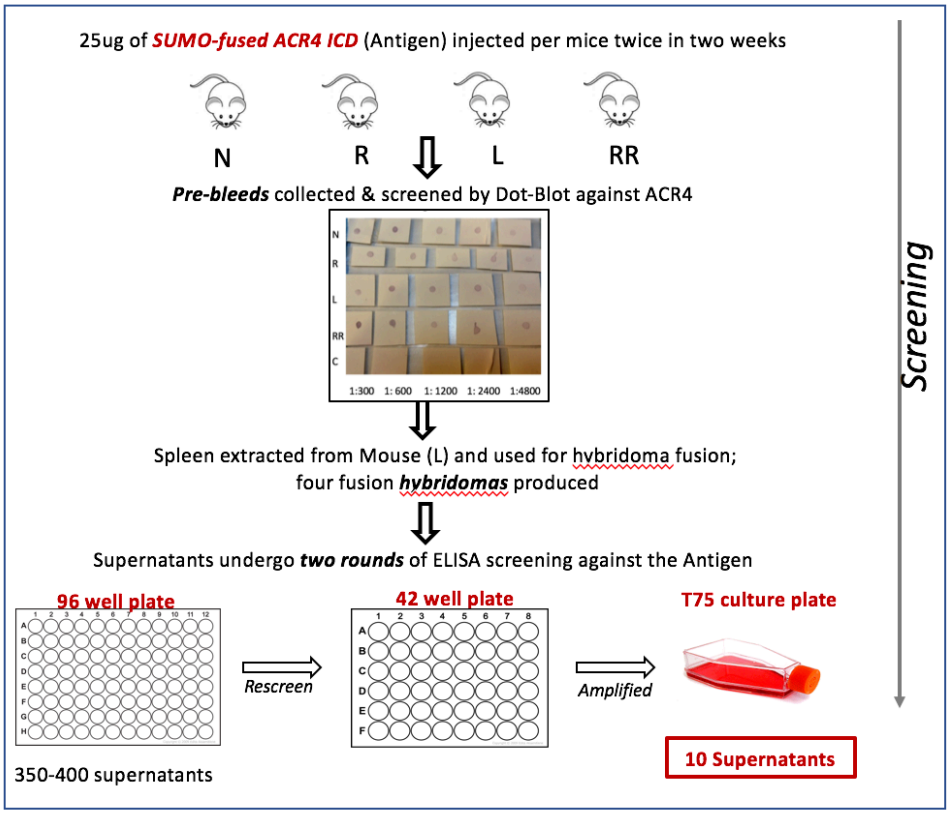

Figure 1: Schematic describing the screening and selection of the hybridoma supernatants.

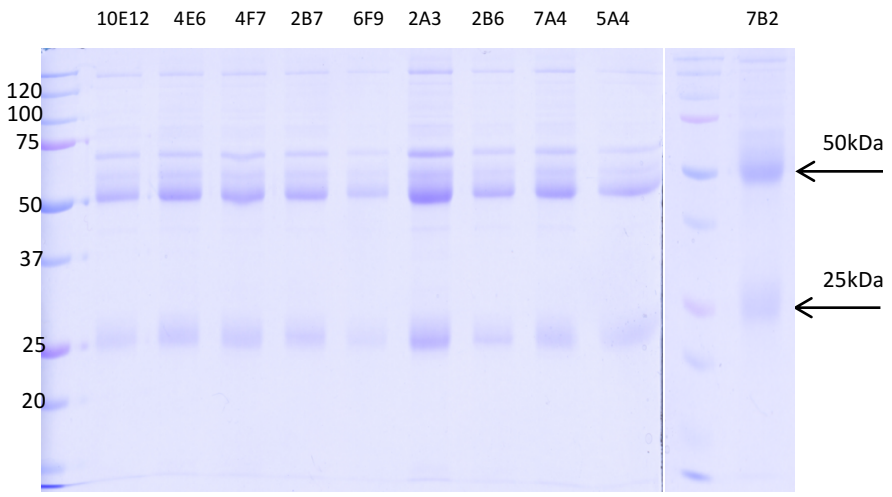

Figure 2: Purification of Monoclonal Antibodies from supernatant by Ammonium sulfate precipitation. 5 µg of purified antibodies separated on a 12 % SDS PAGE gel and Coomassie stained. The two prominent bands at 50 kDa and 25 kDa represent the heavy and light chain of IgG antibody respectively.

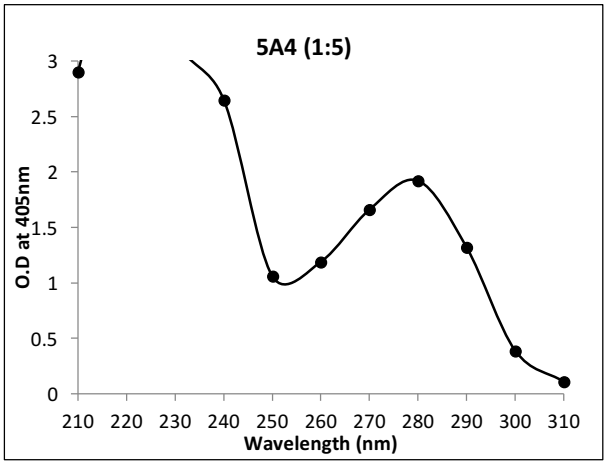

Figure 3: Absorbance spectra scan for purified 5A4 monoclonal antibody. A UV scan (210 nm- 310nm) was performed. The concentration of monoclonal was calculated from absorbance reading at 280nm subtracted out from the absorbance reading at 310 nm,

divided by % extinction coefficient of 1.36. The concentration (mg/ml) and the A280 values for each monoclonal is listed in Table 2.

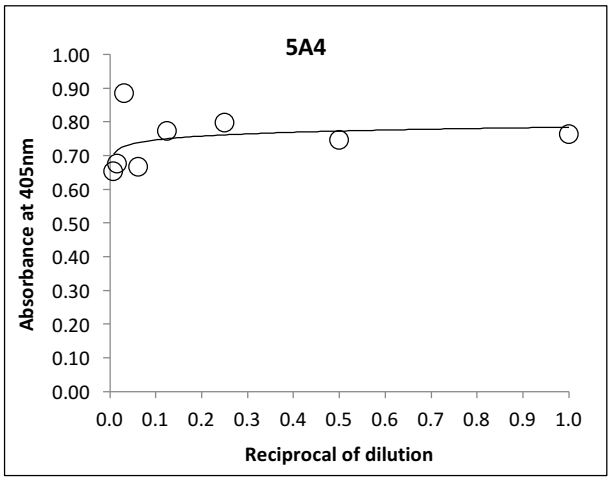

Figure 4: Saturation curve for purified 5A4 monoclonal antibody 1:5 dilution of 5A4 was further serially diluted (1:2 -1:64) in PBS buffer. The absorbance of the end-product (pNPP) obtained after ELISA was read at 405nm. O.D reading at each concentration was used to generate the scatter plot to obtain saturating dilution. Saturating concentration was obtained by extrapolating the absorbance value and the corresponding dilution from the plateau region of the curve. The saturating concentration for each mAb is listed in Table 2.

A

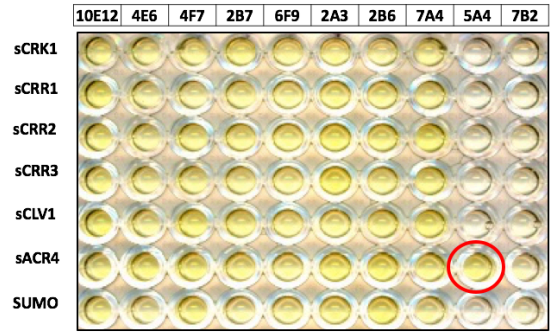

B

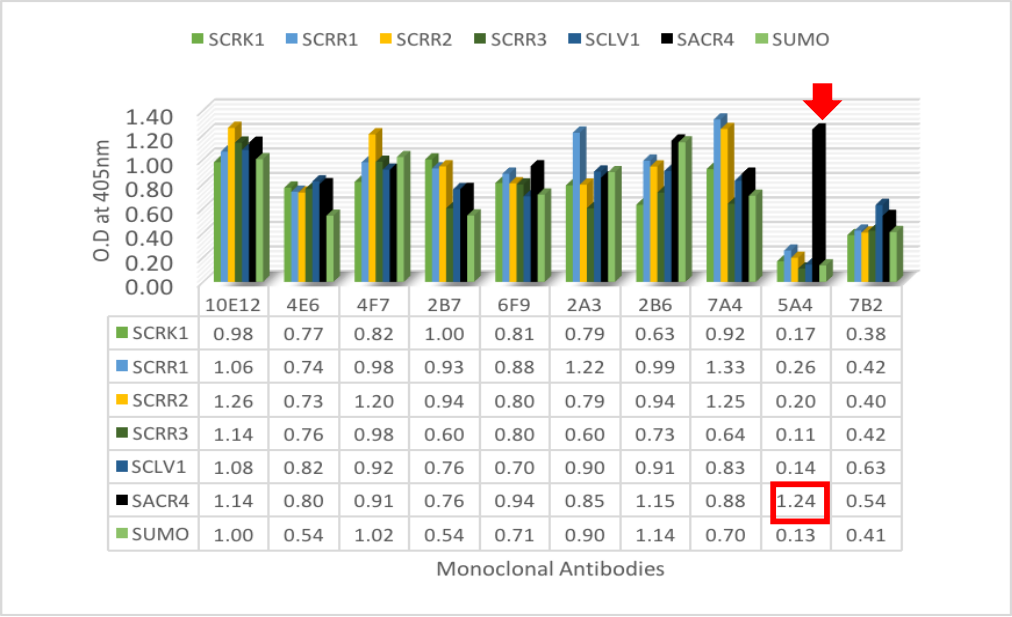

	10E12	4E6	4F7	2B7	6F9	2A3	2B6	7A4	5A4	7B2
SCRK1	0.98	0.77	0.82	1.00	0.81	0.79	0.63	0.92	0.17	0.38
SCRR1	1.06	0.74	0.98	0.93	0.88	1.22	0.99	1.33	0.26	0.42
SCRR2	1.26	0.73	1.20	0.94	0.80	0.79	0.94	1.25	0.20	0.40
SCRR3	1.14	0.76	0.98	0.60	0.80	0.60	0.73	0.64	0.11	0.42
SCLV1	1.08	0.82	0.92	0.76	0.70	0.90	0.91	0.83	0.14	0.63
SACR4	1.14	0.80	0.91	0.76	0.94	0.85	1.15	0.88	1.24	0.54
SUMO	1.00	0.54	1.02	0.54	0.71	0.90	1.14	0.70	0.13	0.41

Figure 5: Cross-reactivity of monoclonal Antibodies. Binding specificity of each monoclonal towards ICDs of SUMO fused ACR4 (sACR4), ACR4 homologs (sCRK1, sCRR1, sCRR2, sCRR3, sCLV1) and sCLV1 along with control SUMO protein was determined by ELISA. **(A)** All antibodies cross- react with SUMO protein and hence cross react with SUMO-tagged RLK, except 5A4 which binds specifically to ACR4 (red circle) and does not cross reacts with SUMO protein or any other protein**. (B)** Absorbance measurements at 405 nm plotted as bar graph. Red arrow indicates specificity of 5A4 against ACR4 Red box has its corresponding absorbance.

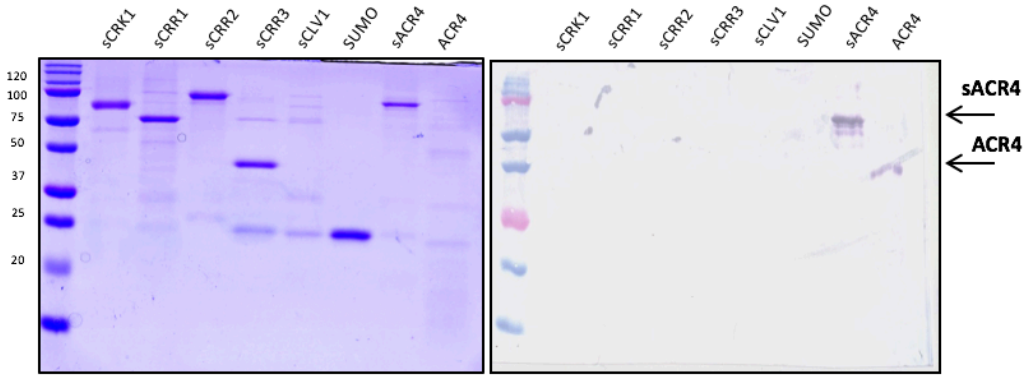

Figure 6: Specificity of 5A4 towards intracellular domain of ACR4. Ni-NTA purified SUMO fused proteins, along with SUMO-free ACR4 and control SUMO protein separated on a 12% SDS-PAGE gel (left) and the specificity of 5A4 towards ACR4 was analyzed by western blot analysis (right) using 1:400 dilution of 5A4 as primary antibody and 1: 10000 dilution of alkaline phosphatase conjugated anti-mouse IgG secondary antibody (sigma) followed by detection by AP substrate kit.

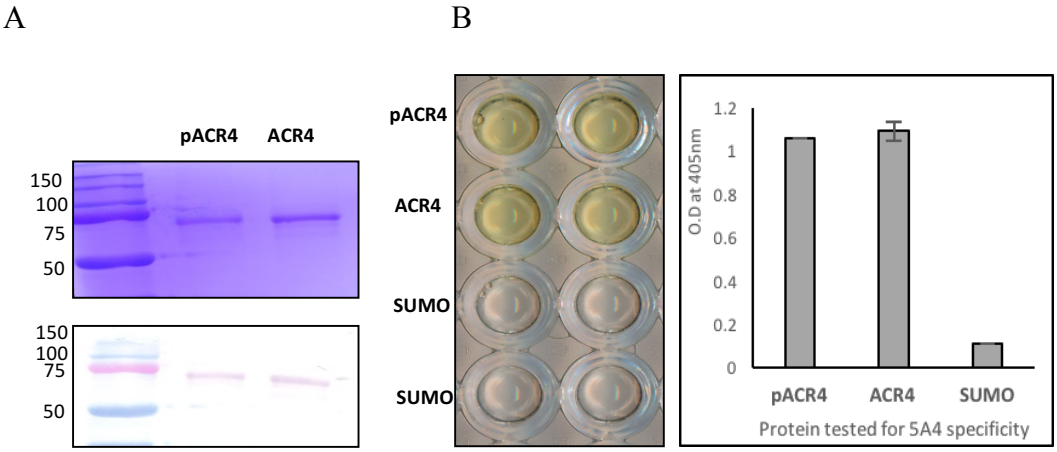

Figure 7: Cross reactivity of 5A4 against naïve ACR4 and auto phosphorylated ACR4(pACR4) demonstrated by **(A)** western blot analysis**; (B)** ELISA with control SUMO protein. Auto phosphorylated ACR4 was produced as described in Meyer et al [24]. The absorbance values at 405nm are plotted as a bar graph ± standard deviation.

A B

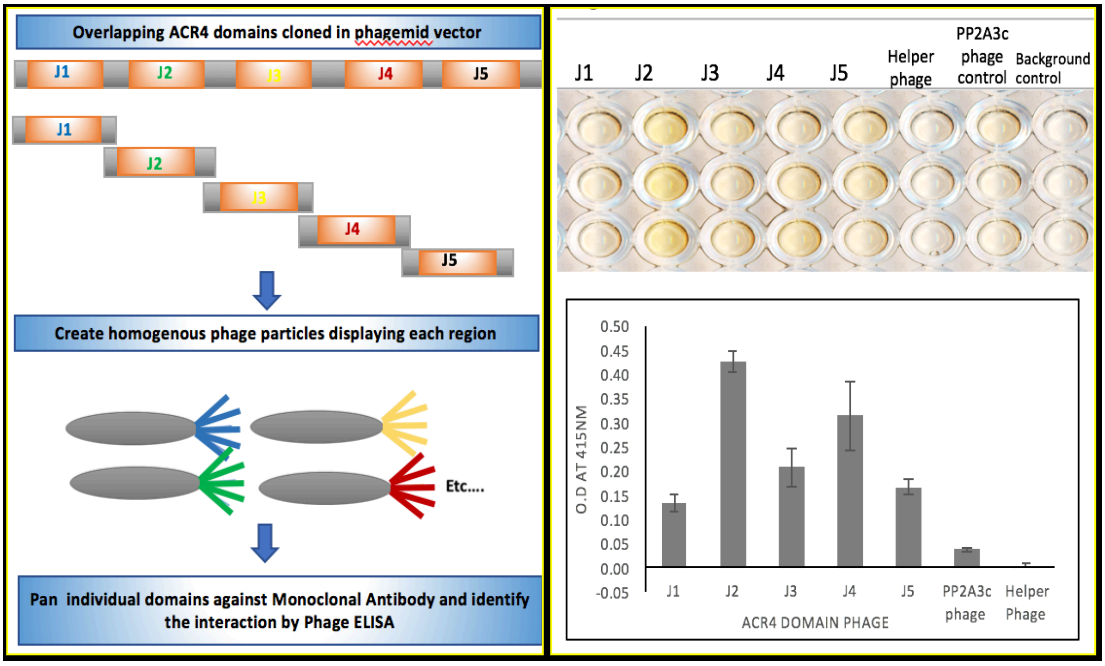

Figure 8: Epitope mapping by Phage ELISA. **(A)** Overlapping domains (J1-J5) of intracellular domain used to generate phage particles displaying each domain homogenously. **(B)** 1 µg of 5A4 was coated on microtiter plate and incubated individually with 1 X 10^{12} phage particles expressing each domain. Maximal binding of 5A4 was with J2 domain. PP2A3c (domain) phage and helper phage used as negative controls, showed no binding towards 5A4 Reactions were performed in triplicates (top); Bar diagram showing quantification of phage binding, absorbance reading corrected for negative control (helper phage) ± standard deviation.

Table 1: The concentration (mg/ml), absorbance A280, & saturation dilution of purified mAb are compiled together.

Monoclonal Ab	Dilution	A280	Concentration (mg/ml)	Saturation Dilution
10E12	1:10	0.5	3	1:200
4E6	1:30	1.5	28.5	1:600
4F7	1:15	0.57	4.75	1:200
2B7	1:10	0.69	3.45	1:200
6F9	1:5	1.45	4.5	1:50
2A3	1:10	0.85	4.7	1:200
2B6	1:5	1.65	5.45	1:200
7A4	1:15	0.82	7.6	1:100
5A4	1:5	1.92	6.65	1:200
7B2	1:10	0.78	5.14	1:10

Table 2: The isotype and subclass of each purified monoclonal antibody.

Primary Line	Isotype
10E12	G1, Kappa
4E6	G1, weak G2b, Kappa
4F7	G2a, weak G2b, Kappa
2B7	G2b, M Kappa
6F9	G1, weak G3, M Kappa
2A3	G2b, M Kappa
2B6	G2b, Kappa
7A4	G1, G2b, Kappa
5A4	G1, Kappa
7B2	G1, G2b, Kappa

Table 3: The sequence of overlapping domains of ICD of ACR4, with the respective sequence of forward and reverse primers used for PCR amplification.

J1 domain sequence **RYRLRNCRCSENDTRSSKDSAFTKDNGKIRPDLDELQKRRRARVFTYEELEKAADGFKEESIVGKGSFSCVYKGVLRDGT**	
Forward Primer	GCAGCGGCA**GGCCCAGCCGGCC**AGGTACAGATTGAGGAATTGTA
Reverse Primer	GCGGCAGCGGCCGCGGTTCCATCTCTCAGTACTC
J2 domain sequence **LRDGTTVAVKRAIMSSDKQKNSNEFRTELDLLSRLNHAHLLSLLGYCEECGERLLVYEFMAHGSLHNHLHGKNKALKEQ LDWVKR**	
Forward Primer	GCAGCGGCAGGCCCAGCCGGCCCTGAGAGATGGAACCACTGT
Reverse Primer	GCGGCAGCGGCCGCTCTTTTGACCCAATCTAGTTG
J3 domain sequence **DWVKRVTIAVQAARGIEYLHGYACPPVIHRDIKSSNILIDEEHNARVADFGLSLLGPVDSGSPLAELPAGTLGYLDPEYYRL HYL**	
Forward Primer	GCAGCGGCAGGCCCAGCCGGCCGATTGGGTCAAAAGAGTAACG
Reverse Primer	GCGGCAGCGGCCGCGAGATAGTGAAGTCGATAGTACTC
J4 domain sequence **RLHYLTTKSDVYSFGVLLLEILSGRKAIDMHYEEGNIVEWAVPLIKAGDINALLDPVLKHPSEIEALKRIVSVACKCVRMRG KDR**	
Forward Primer	GCAGCGGCAGGCCCAGCCGGCCCGACTTCACTATCTCACAAC
Reverse Primer	GCGGCAGCGGCCGCTCTATCTTTCCCTCTCATTCT
J5 domain sequence **RGKDRPSMDKVTTALERALAQLMGNPSSEQPILPTEVVLGSSRMHKKSWRIGSKRSGSENTEFRGGSWITFPSVTSSQRRK SSASEGDVAEEEDEGRKQQEALRSLEEEIGPASPGQSLFLHHNF**	
Forward Primer	GCAGCGGCAGGCCCAGCCGGCCAGAGGGAAAGATAGACCATCA
Reverse Primer	GCGGCAGCGGCCGCGAAATTATGATGCAAGAACAAG

CHAPTER 6: CONCLUSIONS AND FUTURE WORK

General Conclusion

In the past decade, studies have been increasingly directed towards mechanistic understanding of *Arabidopsis* CRINKLY 4 (ACR4) complemented by in planta studies. Collective in-silico, genetic and cell biology experiments have provided key in-sights towards the biological function of ACR4 in cell division and differentiation of root apical meristem [1,2,3,4]. Recent studies have described *in vitro* heteromeric interaction between the intracellular domains [3] (Figure 1) and potential homo dimerization interaction at the transmembrane level, within the ACR4 family members [5]. Additionally, transgenic lines with double and triple mutants within ACR4 family have displayed increased lateral root meristems suggesting functional redundancy within ACR4 family of RLKs [2,6]. Together, *in vitro* and genetic studies provide evidence of a concerted function within the ACR4 family members at the membrane level. Importantly, hetero-dimerization of ACR4 and CLAVATA1 (CLV1) has been shown to be a key interaction in the regulation of root meristem and restricting root stemness [7]. However, not much is known about the downstream signaling partners of the ACR4 family, other than interaction of ACR4 with WOX5, [3,6]. The regulation of activated auto phosphorylated ACR4 and activated ACR4 complexes is completely unknown.

In this dissertation, I have built on this foundation in collaboration with plant biologists at University of Ghent, Belgium, to further understand the biological implication of our findings. The significant findings from each study is described chapter wise as follows:

CHAPTER 2: ACR4 interacts with PP2A3c.

- Identifies the catalytic subunit of Protein Phosphatase 2A-3 (PP2A3c) as the first reported substrate of ACR4 phosphorylation regulating formative cell division in root-tip and lateral roots.
- *In vitro* studies provide strong indication of a tight reciprocal regulation between PP2A3c and ACR4, wherein active PP2A3c has the ability to dephosphorylate ACR4 *in vitro* and ACR4 in-turn mediates phosphorylation of PP2A3c.
- *In planta* studies provide evidence of co-expression of PP2A3c and ACR4 in the columella root apical meristem and propose a mechanism of membrane localization of ACR4 coupled to dephosphorylation by PP2A3c, indicating the positive regulatory role of PP2A3c in ACR4 signaling.

CHAPTER 3: Recombinant expression of PP2A3c in *E. coli* and its *in-trans* activation.

- The catalytic subunit of PP2A3c was expressed in prokaryotic (bacterial) expression system, with no known prior reports of successful expression of PP2A3c in *E. coli*. Milligram amounts of PP2A3c was obtained by expressing MBP-fused PP2A3c in *E. coli*.
- The *E. coli* produced MBP fused PP2A3c was inactive but a slow conformational change of MBP=PP2A3c is observed over a long period (16 h) of incubation at room temperature, and this is accompanied by regain in modest phosphatase activity against a synthetic phospho- peptide.
- Importantly, I provide evidence of significant *in-trans* activation of the inactive PP2A3c by the chaperone Phosphatase 2A Protein Activator (PTPA) as demonstrated by

the dephosphorylation of radiolabeled ACR4.

CHAPTER 4: Biochemical characterization of AtCRK1 and its interaction with PP2A3c

- I have characterized the biochemical properties of the intracellular domain of CRK and demonstrated the phosphorylation of Ser, Thr and even Tyr residues by mass spectrometry.
- I also demonstrate the interaction between PP2A3c and CRK1 by gel-filtration analysis and pull-down assays and suggest that there may be an analogous mechanism to that attributed to ACR4

CHAPTER 4: Monoclonal Antibody specific to ACR4 intracellular domain.

- I describe the development and characterization of a monoclonal antibody that will likely be an invaluable in the identification of novel and existing interactions of ACR4 both via in-planta and *in-vitro* studies.

Future Work

Role of post-translational modifications

The catalytic activity of PP2A3c and the assembly of the phosphatase holoenzyme is regulated through an array of post-translational modifications. In my studies, I have described a method to produce adequate quantities of PP2A3c that could provide a template for understanding the molecular basis of catalytic activity and a stepwise examination of the PTMs *in vitro. In vitro*, ACR4 phosphorylates PP2A3c at nine residues (Chapter 2). Currently, we do not know the relevance of these phosphorylation sites with respect to interaction and role of these phosphorylation sites towards phenotype of the plant. I also identified phosphorylation at Y311 in the conserved C-terminal tail of C subunit (Chapter

3), which is reported to be inhibitory in mammalian systems [8,9]. However, my mutagenesis studies were not corroborative this and thus needs to be studied in future.

The recombinant expression of PP2A3c in baculovirus insect cell expression system generated active C subunit, with methylation at the conserved C-terminal Leucine residue, although not to a large extent (Figure 3C, Chapter 3). At this point, we do not have a good understanding of whether the methylation at C-terminal leucine is driving the production of active PP2A3c in insect cells or endogenous activation chaperones or other unknown factors guide the active conformation of C subunit and needs to be further investigated. Alternatively, I propose that the role of leucine methylation can be investigated by *in-trans* methylation of inactive or partially active C subunit *in vitro,* by means of Leucine Carboxyl Methyl Transferase (LCMT-1) in presence of S-Adenosyl methionine (SAM).

Atomic level understanding of PP2A3c activation.

My studies have shown a slow conformational change accompanied by mild yet measurable phosphatase activity, in absence of PTPA (Chapter 3). It will be interesting to investigate the difference in conformation by biophysical techniques, including NMR. My studies also indicate 35-40% regain in phosphatase activity of PP2A3c by PTPA activation chaperone (Figure 10, Chapter 3). PTPA is reported to be ATP dependent [10] in addition to prolyl *cis-trans* isomerization activity [11], together coordinating the activation of inactive C subunit. I have proposed a similar mode of activation of PP2A3c by PTPA. However, at this point it is not clear if PTPA isomerizes the conserved Proline 190, as reported for mammalian PP2A or isomerization occurs at a different proline residue. Mutagenesis studies in the future can provide more in-sights towards this activation.

Role of other subunits of PP2A phosphatase

The catalytic subunit is a part of the heterotrimeric PP2A holoenzyme that includes, a conserved ~65 kDa structural scaffold 'A' subunit that forms a PP2A core enzyme, and a variable B subunit that determines substrate specificity and cellular localization of PP2A [12,13,14]. With contradictory reports explaining inactivity of C subunit and the sequential order of active holoenzyme assembly, it will be interesting to understand the biogenesis of recombinant active holoenzyme assembly in *E. coli*. Our initial attempts to co-express A and C subunit in *E. coli*, strongly imply the additive role of A subunit in stabilizing the dynamic nature of C subunit. Future studies directed towards co-expression of A, B and C subunit in presence of PTPA chaperone could invoke a better understanding of active PP2A holoenzyme assembly.

Various *in-planta* studies have pinpointed the role of different isoforms of A, B and C subunits individually [15, 16,17,18, 19, 20, 21]. With such mounting evidence of each subunit driving distinct biological function, it will be worth investigating the interaction of ACR4 kinase with other subunits of PP2A phosphatase and determine the physiological effects of these interactions. It may be possible to tailor specific combinations of heteromers influencing new signaling pathways and phenotypes.

Role of phosphorylation sites on kinase activity of CRK1.

In this dissertation, I provide evidence of intra-molecular auto phosphorylation mechanism of recombinantly produced intracellular domain (ICD) of CRK1, a homolog of ACR4, and identified several (~40) phosphorylation sites (Chapter 4). It is challenging to delineate the role of each phosphorylation site influencing ACR signaling, but it will be particularly interesting to examine the biochemical and physiological role of the four sites

of phosphorylation within the juxta membrane domain (JMD) of CRK1 vis-à-vis the reported importance of the phosphorylation sites in the JMD of ACR4 and other RLKs [22,23,24]. Intriguingly, I also identified eight phosphorylated tyrosine residues in CRK1 and the mutagenesis of these residues could be revealing of CRK1 kinase activity, its interaction with ACR4 and downstream PP2A phosphatase.

Interactions of CRK1 with ACR4 and PP2A3c.

Earlier reports have reported a potential mechanism of inter-molecular interaction of 'KDSAF' motif in CRK1/CRR3 and 'LLSLL' region of ACR4 [3]. Interestingly, PP2A3 catalytic subunit has a LLXXL motif, that is known to be a protein-protein interaction motif, and it will be interesting to investigate if ACR4 and CRK1 interact with LLXXL motif of PP2A3c. The precise role of individual residues within the interacting motifs needs to be studied *in vitro* in parallel with phenotypic consequence of these mutations *in planta*.

In chapter 4, I provide evidence of an interaction of CRK1 with PP2A3c (Figure 1 & 8) and radioactive kinase assay indicated PP2A3c as downstream substrate for CRK1 much like ACR4. However, the *in vivo* regulation of CRK1 kinase activity by PP2A3c is yet to be determined. More detailed mechanistic understanding of the interactions between PP2A3c, CRK1 and ACR4 can be provided by various biochemical and biophysical techniques such as alanine scanning, H-D exchange and NMR studies. Ultimate understanding of CRK1 activation and interaction with ACR4 and PP2A3c can be established by developing a three-dimensional structure. Additionally, much like ACR4 interactome study described in Chapter 2, a CRK1 centered interactome study using complementary proteomic approaches may identify novel interacting partners common to ACR4 and CRK1 or unique to CRK1.

Outstanding questions of ACR4 family of RLKs.

In-planta knock out studies complemented with various proteomic approaches have provided a substantial information of the biological role of ACR4 driving stem cell differentiation in root tip [6] and proper differentiation of epidermis in vegetative and reproductive tissues, but other than functional redundancy within in ACR4 family members, no biological role of CRK1 kinase has been reported yet and hence it will be interesting to explore the role(s) of CR4 family members and assess the extent of their evolutionary conservation relative to their function.

While ACR4, CRK1 and other members of the ACR4 family possess an extracellular ligand binding domain, other than a postulation by Stahl et al [6] that CLE40, a member of a class of hormone peptide, up regulates the expression of ACR4, and downstream activation of the transcription factor WOX5, there is no conclusive biochemical data supporting this hypothesis. Interestingly, expression of CRK1 is reported to be negatively regulated by the plant hormones auxin, ABA, and cytokinin [25]. Contradictory to negative regulation of CRK1 by cytokinin, cytokinin deficient plants display reduced ACR4 expression [26], with ACR4 not being a primary cytokinin response gene. It is possible that the members of ACR4 family are activated by different ligands and hence it will be interesting to determine not only the potential individual ligand(s) but also if ligand binding is mediated by singular RLK or homo/heteromeric interaction of RLKs.

The interaction of ACR4 outside of the ACR4 family members has been recently reported, with evidence of dimerization of ACR4 with CLAVATA1 (atypical RLK) [7] and a phosphorylation driven dimerization with ABNORMAL LEAF SHAPE 2 (ALE2) [27]. Such studies provide a strong basis to further investigate the potential network of

interactions of ACR4 and homologs in plant growth and development and advance knowledge-based manipulation of signaling pathways for improved crops.

References

1. Cao X, Li K, Suh SG, Guo T, Becraft PW (2005) Molecular analysis of the CRINKLY4 gene family in Arabidopsis thaliana. Planta 220: 645-657.
2. De Smet I, Vassileva V, De Rybel B, Levesque MP, Grunewald W, et al. (2008) Receptor-like kinase ACR4 restricts formative cell divisions in the Arabidopsis root. Science 322: 594-597.
3. Meyer MR, Shah S, Zhang J, Rohrs H, Rao AG (2015) Evidence for intermolecular interactions between the intracellular domains of the arabidopsis receptor-like kinase ACR4, its homologs and the Wox5 transcription factor. PLoS One 10: e0118861.
4. Yue K, Sandal P, Williams EL, Murphy E, Stes E, et al. (2016) PP2A-3 interacts with ACR4 and regulates formative cell division in the Arabidopsis root. Proc Natl Acad Sci U S A 113: 1447-1452.
5. Stokes KD, Gururaj Rao A (2008) Dimerization properties of the transmembrane domains of Arabidopsis CRINKLY4 receptor-like kinase and homologs. Arch Biochem Biophys 477: 219-226.
6. Stahl Y, Wink RH, Ingram GC, Simon R (2009) A signaling module controlling the stem cell niche in Arabidopsis root meristems. Curr Biol 19: 909-914.
7. Stahl Y, Grabowski S, Bleckmann A, Kuhnemuth R, Weidtkamp-Peters S, et al. (2013) Moderation of Arabidopsis root stemness by CLAVATA1 and ARABIDOPSIS CRINKLY4 receptor kinase complexes. Curr Biol 23: 362-371.
8. Liu R, Zhou XW, Tanila H, Bjorkdahl C, Wang JZ, et al. (2008) Phosphorylated PP2A (tyrosine 307) is associated with Alzheimer neurofibrillary pathology. J Cell Mol Med 12: 241-257.
9. Luo Y, Nie YJ, Shi HR, Ni ZF, Wang Q, et al. (2013) PTPA activates protein phosphatase-2A through reducing its phosphorylation at tyrosine-307 with upregulation of protein tyrosine phosphatase 1B. Biochim Biophys Acta 1833: 1235-1243.
10. Guo F, Stanevich V, Wlodarchak N, Sengupta R, Jiang L, et al. (2014) Structural basis of PP2A activation by PTPA, an ATP-dependent activation chaperone. Cell Res 24: 190-203.
11. Jordens J, Janssens V, Longin S, Stevens I, Martens E, et al. (2006) The protein phosphatase 2A phosphatase activator is a novel peptidyl-prolyl cis/trans-isomerase. J Biol Chem 281: 6349-6357.
12. Cho US, Xu W (2007) Crystal structure of a protein phosphatase 2A heterotrimeric holoenzyme. Nature 445: 53-57.
13. Xing Y, Xu Y, Chen Y, Jeffrey PD, Chao Y, et al. (2006) Structure of protein phosphatase 2A core enzyme bound to tumor-inducing toxins. Cell 127: 341-353.
14. Xu Y, Xing Y, Chen Y, Chao Y, Lin Z, et al. (2006) Structure of the protein phosphatase 2A holoenzyme. Cell 127: 1239-1251.

15. Blakeslee JJ, Zhou HW, Heath JT, Skottke KR, Barrios JA, et al. (2008) Specificity of RCN1-mediated protein phosphatase 2A regulation in meristem organization and stress response in roots. Plant Physiol 146: 539-553.
16. Garbers C, DeLong A, Deruere J, Bernasconi P, Soll D (1996) A mutation in protein phosphatase 2A regulatory subunit A affects auxin transport in Arabidopsis. EMBO J 15: 2115-2124.
17. Kwak JM, Moon JH, Murata Y, Kuchitsu K, Leonhardt N, et al. (2002) Disruption of a guard cell-expressed protein phosphatase 2A regulatory subunit, RCN1, confers abscisic acid insensitivity in Arabidopsis. Plant Cell 14: 2849-2861.
18. Larsen PB, Cancel JD (2003) Enhanced ethylene responsiveness in the Arabidopsis eer1 mutant results from a loss-of-function mutation in the protein phosphatase 2A A regulatory subunit, RCN1. Plant J 34: 709-718.
19. Heidari B, Nemie-Feyissa D, Kangasjarvi S, Lillo C (2013) Antagonistic regulation of flowering time through distinct regulatory subunits of protein phosphatase 2A. PLoS One 8: e67987.
20. Kleine-Vehn J, Huang F, Naramoto S, Zhang J, Michniewicz M, et al. (2009) PIN Auxin Efflux Carrier Polarity Is Regulated by PINOID Kinase-Mediated Recruitment into GNOM-Independent Trafficking in Arabidopsis. Plant Cell 21: 3839-3849.
21. Michniewicz M, Zago MK, Abas L, Weijers D, Schweighofer A, et al. (2007) Antagonistic regulation of PIN phosphorylation by PP2A and PINOID directs auxin flux. Cell 130: 1044-1056.
22. Binns KL, Taylor PP, Sicheri F, Pawson T, Holland SJ (2000) Phosphorylation of tyrosine residues in the kinase domain and juxtamembrane region regulates the biological and catalytic activities of Eph receptors. Mol Cell Biol 20: 4791-4805.
23. Chan PM, Ilangumaran S, La Rose J, Chakrabartty A, Rottapel R (2003) Autoinhibition of the kit receptor tyrosine kinase by the cytosolic juxtamembrane region. Mol Cell Biol 23: 3067-3078.
24. Davis TL, Walker JR, Loppnau P, Butler-Cole C, Allali-Hassani A, et al. (2008) Autoregulation by the juxtamembrane region of the human ephrin receptor tyrosine kinase A3 (EphA3). Structure 16: 873-884.
25. Schafer S, Schmulling T (2002) The CRK1 receptor-like kinase gene of tobacco is negatively regulated by cytokinin. Plant Mol Biol 50: 155-166.
26. Chang L, Ramireddy E, Schmulling T (2015) Cytokinin as a positional cue regulating lateral root spacing in Arabidopsis. Journal of Experimental Botany 66: 4759-4768.
27. Tanaka H, Watanabe M, Sasabe M, Hiroe T, Tanaka T, et al. (2007) Novel receptor-like kinase ALE2 controls shoot development by specifying epidermis in Arabidopsis. Development 134: 1643-1652.

Figures

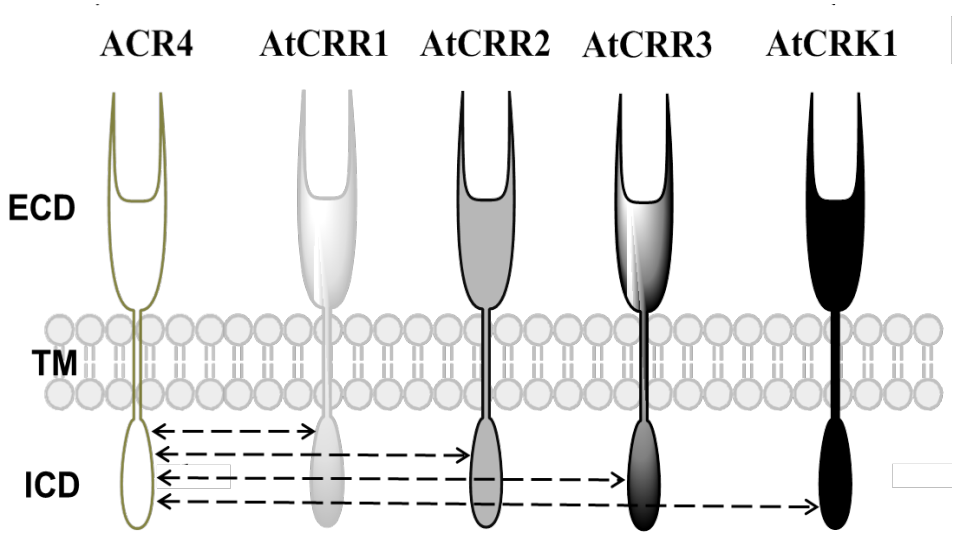

Figure 1: Heteromeric interaction within the intracellular domain of ACR4 and its homolog proteins (CRRs).